58/1/2026
ISSN 1338–3523
ISSN 0369–2086

Mineralia Slovaca

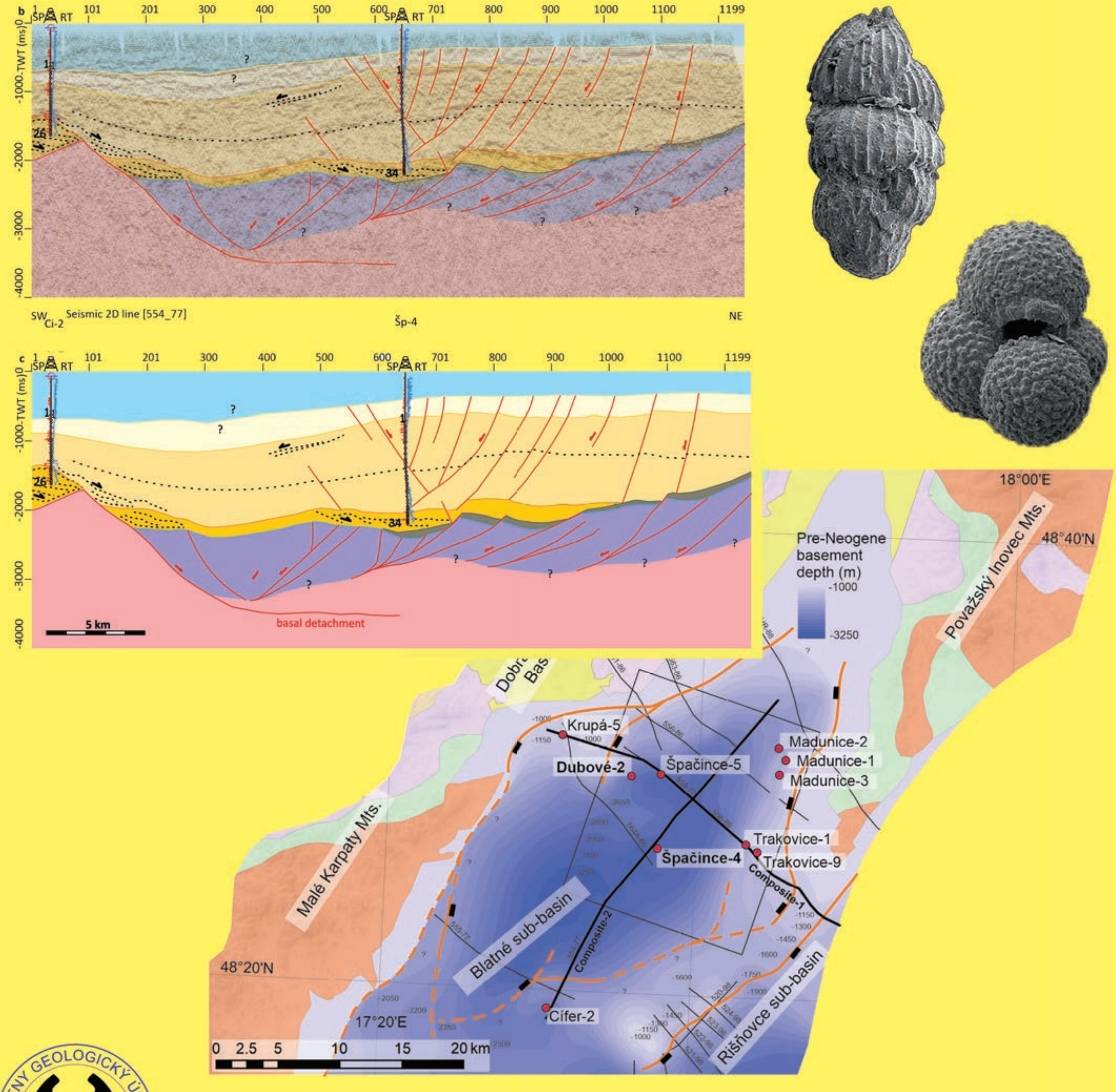

Štátny geologický ústav Dionýza Štúra Bratislava

Mineralia Slovaca

Časopis pre základné a aplikované vedy o Zemi

Journal of Basic and Applied Earth Sciences

Mineralia Slovaca (Web ISSN 1338-3523, ISSN 0369-2086), EV 3534/09, vychádza dvakrát ročne. Vydavateľ a tlač: Štátny geologický ústav Dionýza Štúra, Mlynská dolina 1, 817 04 Bratislava, IČO 31 753 604. Dátum vydania čísla 58/1/2026: august 2026.
Predplatné v roku 2026 vrátane DPH, poštovného a balného pre jednotlivcov 22,00 €, pre členov SGS a geologických asociácií 20,90 €, pre organizácie v SR 31,90 €, pre organizácie v ČR 55,00 €. Cena jednotlivého čísla pri nákupe cez e-shop alebo pri osobnom nákupe v predajni ŠGÚDŠ v RGS Košice je 6,05 € vrátane DPH. Časopis možno objednať v redakcii a v knižnici regionálnej geologickej služby v Košiciach.

Adresa redakcie:
Štátny geologický ústav D. Štúra, Mlynská dolina 1, 817 04 Bratislava. Telefón: 02/59 375 257; e-mail: mineralia.slovaca@geology.sk, e-mail knižnica: secretary.ke@geology.sk

Mineralia Slovaca (Web ISSN 1338-3523, ISSN 0369-2086) is published twice a year by the State Geological Institute of Dionýz Štúr Bratislava, Slovak Republic. The date of issuing of the number 58/1/2026: August, 2026.
Subscription for the whole 2026 calendar year (two numbers of the journal): 66.00 € (Europe), 77.00 € (besides Europe), including VAT, postage and packing cost. Claims for nonreceipt of any issue will be filled gratis.
Order of the Editorial Office: Štátny geologický ústav D. Štúra – RC Košice (Library), Jesenského 8, SK-040 01 Košice, Slovak Republic. Phone: +421/55/625 00 43; fax: +421/55/625 00 44, e-mail: mineralia.slovaca@geology.sk, library: secretary.ke@geology.sk

Obsah – Content Mineralia Slovaca 58 (2026) • 1

PÔVODNÉ ČLÁNKY – ORIGINAL PAPERS

OBÁLKA:

Hore – kompozitný seizmický rez na základe línie 554_77 s vyznačením vrtov Cífer-2 a Špačince-4, interpretovanými horizontmi a zlomami.

Stred – geologická interpretácia. Foraminifery *Uvigerina ventusa* a *Globoturborotalia druryi* z vrtu Du-2.

Dole – geologická štruktúrna schéma blatnianskej priehlbiny s vyznačením hĺbky kenozoickej výplne, zlomov, vrtov a seizmických profilov.

COVER:

Top – composite seismic profile 2, based on line 554_77 with marked wells Cífer-2 and Špačince-4, interpreted horizons and faults.

Center – geological interpretation. Foraminifers *Uvigerina ventusa* and *Globoturborotalia druryi* from Du-2 well.

Bottom – geological sketch map of the Blatné sub-basin, showing the depth of the Cenozoic sedimentary fill, faults, wells and seismic lines.

Mineralia Slovaca, Web ISSN 1338-3523, ISSN 0369-2086, https://doi.org/10.56623/ms.2026.58.1.1
58, 1 (2026), 3 – 36,

Badenian-Pannonian (Langhian-Tortonian) evolution of the Blatné sub-basin, northwestern Danube Basin (Central Paratethys): integrated biostratigraphic, facies and seismic evidence from the Špačince-4 and Dubové-2 wells

SAMUEL RYBÁR[1, 2], NATÁLIA HUDÁČKOVÁ[1,*], ĽUBOMÍR SLIVA[4], MICHAL JAMRICH[1], KATARÍNA ŠARINOVÁ[3], MARIANNA KOVÁČOVÁ[1], ANDREJ RUMAN[1] and BRANISLAV ŠÁLY[4]

[1] Comenius University Bratislava, Faculty of Natural Sciences, Department of Geology and Paleontology, Ilkovičova 6, Mlynská dolina, 842 15 Bratislava, Slovak Republic

[2] Faculty of Mining and Geology, Department of Geodesy and Mine Surveying, Technical University of Ostrava, 17. listopadu 2172/15, 708 00 Ostrava, Poruba, Czech Republic

[3] Comenius University Bratislava, Faculty of Natural Sciences, Mlynská Dolina, Department of Mineralogy, Petrology and Economic Geology, Ilkovičova 6, 842 15 Bratislava, Slovak Republic

[4] NAFTA, a. s., 900 68 Plavecký Štvrtok, Slovak Republic

* Corresponding author: natalia.hudackova@uniba.sk

Abstract: The Špačince-4 and Dubové-2 wells in the Blatné sub-basin of the Danube Basin were integrated with SP/RT logs and seismic profiles to refine Badenian-Pannonian (Langhian-Tortonian) stratigraphy and basin evolution. The study integrates core-facies, provenance, XRF, well-log and seismic interpretations with reinterpreted data from, in total, 29 foraminiferal, 41 calcareous-nannofossil and 16 palynological samples. Calcareous nannofossils document NN4–NN6 zones, while planktonic foraminifera constrain parts of the succession to CPN7–CPN8. Key markers include *Orbulina suturalis, Globorotalia bykovae, Sphenolithus heteromorphus, ?Helicosphaera ampliaperta* and *Reticulofenestra pseudoumbilicus > 7 µm*. The succession is mainly lower to upper Badenian, whereas Sarmatian-Pannonian deposits are inferred from upper log-defined and seismic intervals. The Špačince-4 borehole records basal coarse-clastic and volcaniclastic deposits passing upward into marine gravity-flow and suspension-dominated facies; Dubové-2 preserves a thinner marine succession above pre-Neogene basement. Agglutinated morphogroups are locally compatible with bathyal-equivalent conditions where preservation permits, while *Bulimina-Bolivina-Uvigerina*-rich assemblages are consistent with enhanced organic flux and locally reduced oxygen availability. Phytoclast-rich residues indicate terrestrial input. Seismic data reveal an asymmetric half-graben bounded by listric normal faults above a low-angle detachment, with Badenian growth strata overlain by Sarmatian onlap and subhorizontal Pannonian post-rift deposits. Overall, the succession records Badenian syn-rift sedimentation followed by Sarmatian-Pannonian shallowing and deltaic-lacustrine-fluvial infilling.

Key words: Neogene, Central Paratethys, biostratigraphy, sedimentology, core analysis

Introduction

The Miocene evolution of the northwestern Central Paratethys was controlled by back-arc extension associated with the Alpine-Carpathian orogenic system and the lateral extrusion of the ALCAPA mega-unit (Royden et al., 1983; Tari et al., 1992; Schmid et al., 2008). Within this framework, the Pannonian Basin System developed as a series of syn-rift depocentres characterized by rapid subsidence, high sedimentation rates (e.g. Balázs et al., 2016), and coeval volcanic activity during the Middle Miocene (Harangi et al., 2025). The Danube Basin represents one of the principal depocentres of this system (Sztanó et al., 2016). Its northwestern sector, including the Blatné sub-basin, preserves a thick Miocene succession recording the transition from syn-rift extension to post-rift thermal subsidence (Šujan et al., 2021; Rybár et al., 2025). The regional extensional evolution of the Danube

Basin, including its Middle Miocene back-arc setting, polyphase rifting and subsequent post-rift subsidence, is well established (Hók et al., 2016; Šujan et al., 2021, 2026). Previous studies also place the initial opening of the Blatné sub-basin in the lower Badenian and continued syn-rift subsidence in the upper Badenian (Šarinová et al., 2018, 2021; Rybár & Kotulová, 2023; Rybár et al., 2024, 2025). However, the local expression of this regional evolution within individual fault blocks of the Blatné sub-basin remains incompletely constrained. In particular, uncertainties concern: (1) the position and local expression of the transition from proximal coarse-clastic and volcaniclastic sedimentation to unequivocally marine deposition; and (2) the lateral correlation and fault-block-scale architecture of Badenian gravity-flow packages between the studied wells and adjacent parts of the sub-basin. This study therefore aims to refine the local chronostratigraphic and tectono-sedimentary architecture of the Blatné sub-basin rather than to revise the established regional extensional model. To address these issues, this study presents an integrated investigation of the Špačince-4 (Lat: 48°26'19.6794"N; Lon: 17°37'40.2977"E) and Dubové-2 (Lat: 48°29’20.9416"N; Lon: 17°35'52.6196"E) deep wells in the Blatné sub-basin. An unpublished technical report by Hudáčková et al. (2018) presented the original foraminiferal, calcareous-nannofossil and palynological datasets, together with preliminary core-lithology, SP/RT logs and palaeoenvironmental interpretations. In the present study, these data were reinterpreted, and selected archived residues and slides were re-examined where clarification or revision was required. The study further integrates substantially expanded core-facies and provenance analyses, new XRF measurements and new reflection-seismic interpretation. Its principal contribution is the integration of the two well successions within a fault-block-scale model of the Blatné half-graben. Published numerical ages and data from neighbouring wells were used for regional chronostratigraphic calibration; no new radiometric dating was performed.

The objectives were to: (1) refine the biostratigraphic framework of the Miocene succession using multiple microfossil groups; (2) reconstruct depositional environments and facies architecture from the core data; (3) correlate the studied well successions using SP and RT logs and integrate them with the reflection-seismic profiles; and (4) determine whether the contrasting Špačince-4 and Dubové-2 successions reflect different structural positions within the fault-controlled Blatné half-graben (Fig. 1).

Geological setting

Tectonic framework

The Danube Basin forms the northwestern segment of the Pannonian Basin System (PBS), a Miocene back-arc basin that developed during extensional collapse of the Alpine-Carpathian orogen (Royden et al., 1982, 1983; Horváth et al., 2006, 2015; Matenco & Radivojević, 2012; Tari et al., 1992, 2021). Basin formation was controlled by slab rollback beneath the Carpathian arc and lateral extrusion of the ALCAPA mega-unit (Ratschbacher et al., 1991a, b; Schmid et al., 2008). The basin evolved through a four-stage rifting process (Šujan et al., 2021) corresponding to: (1) lower Badenian (Langhian), (2) upper Badenian (lower Serravallian), (3) Sarmatian (upper Serravallian), and (4) lower Pannonian (Tortonian). Thermal subsidence prevailed from the mid–upper Pannonian onward, while basin inversion likely began in the Pliocene and continues today (Royden et al., 1983; Horváth, 1995; Balázs et al., 2016, 2021; Šujan et al., 2016, 2021). The Danube Basin trends NE–SW, is ~200 km long and ~100 km wide, and is bounded by the Eastern Alps (W), Central Western Carpathians (N), and the Transdanubian Range (SE) (Vass, 2002; Sztanó et al., 2016). The Hurbanovo-Diósjenő Fault Zone represents a major tectonic boundary within the southeastern sector (Klučiar et al., 2016).

Basement structure

The pre-Neogene basement of the Danube Basin consists predominantly of Paleozoic crystalline basement rocks of the Tatric and Veporic units with their late Paleozoic to Mesozoic sedimentary cover (Fusán et al., 1987; Droppa et al., 2024). In the northern sector, these are overlain by Fatric and Hronic Mesozoic nappe units (Biely et al., 1996; Hók et al., 2014). The northwestern margin locally preserves remnants of the Central Carpathian Paleogene Basin (Biela, 1978). South of the Hurbanovo-Diósjenő Fault Zone, the basement includes Paleozoic and Mesozoic sedimentary units of the Transcarpathian Central Range (Fusán et al., 1987) and locally Paleogene sediments (Tari et al., 1993; Sztanó & Tari, 1993). The structural framework reflects Late Cretaceous nappe stacking which was later reactivated during Miocene back-arc extension (Hók et al., 2014; Konečný et al., 2002).

Syn-rift evolution and sub-basin development

The Slovak part of the basin comprises several Miocene sub-basins, including the Blatné, Želiezovce, Rišňovce, Komjatice, and Gabčíkovo-Győr sub-basins (Vass, 2002; Šujan et al., 2021; Rybár et al., 2024). The cumulative Neogene sedimentary fill locally exceeds 8 km in the Gabčíkovo-Győr sub-basin, although this total includes deposits accumulated during syn-rift and post-rift stages (Killényi & Šefara, 1989; Hrušecký, 1999; Šujan et al., 2021; Rybár et al., 2024). By contrast, the approximately 3-km-thick fill of the Blatné sub-basin is largely represented by Badenian deposits associated with the first two syn-rift phases (Csibri et al., 2018; Šujan et al., 2021; Rybár et al., 2025).

Lower Badenian (Langhian) interval

Rifting initiated in the Blatné and Želiezovce sub-basins during the lower Badenian (Šarinová et al., 2018, 2021; Rybár & Kotulová, 2023; Rybár et al., 2025). This stage coincided with marine transgression of the Central Paratethys (e.g. Popov et al., 2004) and deposition of mudstones, sandstones, and volcanogenic sediments of the Špačince Formation (Biela, 1978; Vass, 2002; Rybár et al., 2016). Volcanic activity in the Danube Basin before approximately 14.1 Ma is documented by $^{40}Ar/^{39}Ar$ dating (Rybár et al., 2024). The Middle Miocene volcanic flare-up preceded and accompanied the Langhian/Serravallian sea-level fall (~13.8 Ma) and was dominated by high-K calc-alkaline magmatism (Karátson et al., 2000, 2007; Lexa et al., 2010; Chernyshev et al., 2013; Šarinová et al., 2021; Rybár et al., 2025; Lexa et al., 2025).

Upper Badenian (lower Serravallian) interval

Rifting continued during the upper Badenian, increasing accommodation space, particularly in the Blatné sub-basin (Rybár & Kotulová, 2023; Rybár et al., 2025). Sedimentation included mudstones and sandy density-flow deposits of the Báhoň and Pozba formations (Vass, 2002; Šujan et al., 2021).

Sarmatian (upper Serravallian) interval

Major basin expansion occurred during the Sarmatian, particularly in the northern and central sub-basins (Šujan et al., 2021; Rybár et al., 2024). Sedimentation shifted toward restricted marine, brackish, and freshwater environments, reflected in the Vráble and Ripňany formations (Fordinál & Elečko, 2000). Calc-alkaline volcanism persisted into the Sarmatian and was followed by smaller-volume alkaline magmatism (Harangi et al., 1995; Wijbrans et al., 2007; Harangi & Lenkey, 2007; Pécskay et al., 2006; Seghedi & Downes, 2011; Chernyshev et al., 2013; Sant et al., 2020; Nováková et al., 2020), reflecting progressive lithospheric thinning (Lexa et al., 2010).

Pannonian (Tortonian)

The lower Pannonian marks the final syn-rift phase and transition to thermal post-rift subsidence (Šujan et al., 2021). Deep-basin mudstones and gravity sediments of

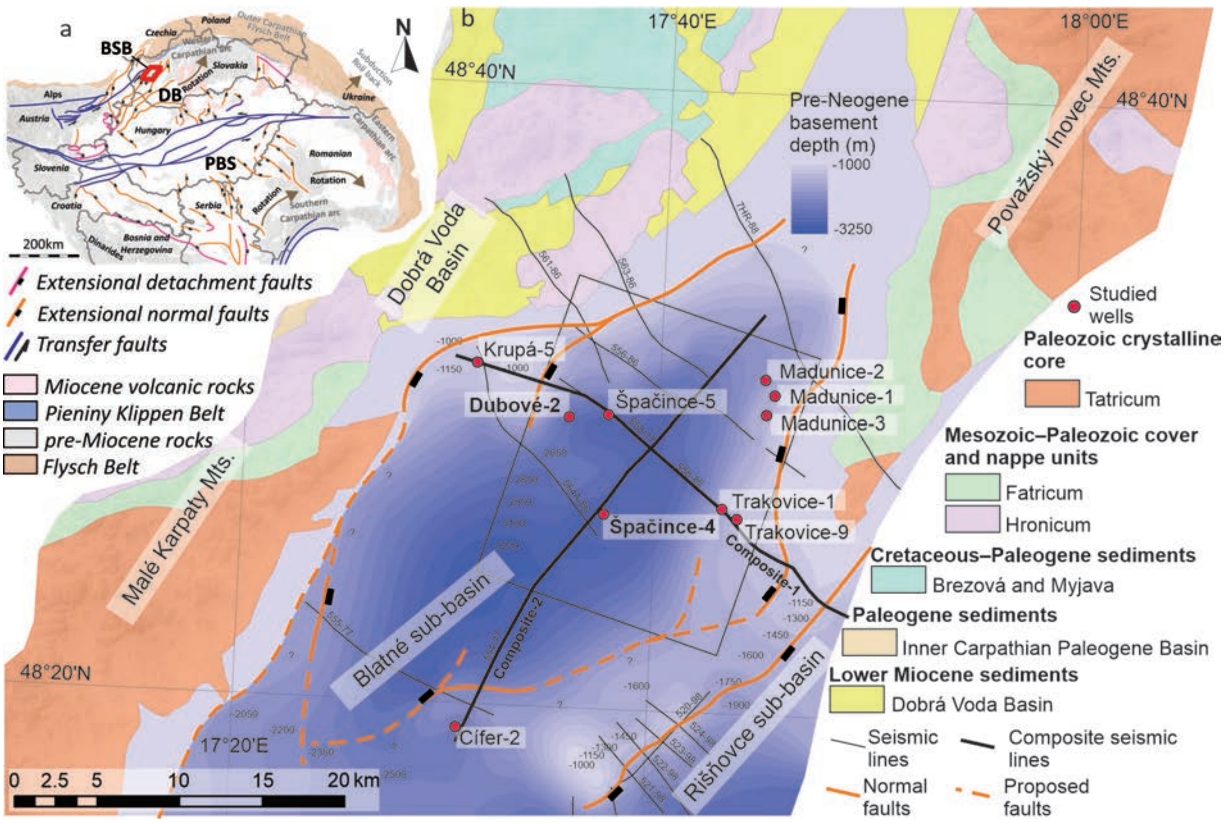

Fig. 1. (a) Location of the Blatné sub-basin (BSB) within the Danube Basin (DB) and Pannonian Basin System (PBS), modified from Fodor et al. (2021). (b) Locations of the studied and referenced wells and reflection-seismic profiles, modified from Šarinová et al. (2021).

the Ivanka Formation were followed by deltaic (Beladice Fm.) and fluvial-lacustrine deposits (Volkovce Fm.) (Vass, 2002; Sztanó et al., 2016).

Post-rift subsidence dominated during the upper Pannonian (upper Tortonian–Messinian) (Royden et al., 1983; Horváth, 1995), and basin inversion since ~6–5 Ma resulted in erosion at basin margins and subsequent deposition of Plio-Pleistocene sediments (Šujan et al., 2016, 2018).

Materials and Methods

Core material and framework

The well-core material from the Špačince-4 and Dubové-2 deep wells was obtained from the NAFTA, a. s., repository in Gbely (Slovakia). Well-core preparation, sedimentological description, micropalaeontological analyses, and palaeoecological interpretation were conducted at the Department of Geology and Paleontology, Comenius University in Bratislava. All samples and slides are archived in the departmental collection and at NAFTA, a. s. The study integrates sedimentological core analysis, well-log and seismic interpretation, and multiproxy micropalaeontological investigation to reconstruct depositional environments and refine the biostratigraphic framework of the Blatné sub-basin (Fig. 1).

Data sources and provenance

The micropalaeontological dataset comprises 29 foraminiferal, 41 calcareous-nannofossil and 16 palynological samples originally processed and analysed for the unpublished technical report of Hudáčková et al. (2018). That report also included preliminary lithological descriptions, SP/RT-log observations and palaeoenvironmental interpretations of the Špačince-4 and Dubové-2 wells. In the present study, the original dataset was reinterpreted using updated taxonomic, biostratigraphic and palaeoecological frameworks. Selected archived residues and slides were also re-examined where clarification or revision of individual identifications was required. New work includes substantially expanded core-facies description and imaging, handheld-XRF analysis of the Špačince-4 succession, and reflection-seismic interpretation. The new thin-section data and existing SP/RT logs were re-evaluated and integrated with these new datasets. Published numerical

Tab. 1
Summary of datasets used in this study

Dataset	Špačince-4	Dubové-2	Origin and use
Foraminifera	15 samples	14 samples	Hudáčková et al. (2018); reinterpreted and partly re-examined
Calcareous nannofossils	22 samples, 998–3,098 m	19 samples, 1,501–2,707 m	Hudáčková et al. (2018); reinterpreted and partly re-examined
Palynology	12 samples	4 samples	Hudáčková et al. (2018); qualitative reinterpretation
Sedimentological cores	28 spot cores; 52.2 m recovered, 1,190–3,348 m	23 spot cores; 89.9 m recovered, 1,501–2,751 m	Expanded core description and facies interpretation
Thin sections	6 samples	1 at a depth of 1,705 m	Existing petrographic data re-evaluated in this study
XRF	160 samples from 31 intervals, 697–3,347 m	None	New semiquantitative handheld-XRF dataset
SP and RT logs	Available	Available	Legacy data reinterpreted and correlated with core data
Seismic data	Four legacy 2D line segments combined into two composite profiles		New seismic-stratigraphic interpretation
Numerical ages	Published regional age constraints		Used for calibration only; no new radiometric dating

Note to Tab. 1. The wells were sampled by discontinuous spot coring; the stated depth ranges represent the distribution of examined cores and not continuously recovered intervals.
Detailed sample depths, core identifiers, analytical metadata and the distribution of the 16 palynological samples between the two wells are provided in Supplementary Tab. S1.

ages and results from neighbouring wells were used for regional correlation. No new radioisotopic dating was undertaken (Tab. 1).

Sedimentology and subsurface data interpretation

Sedimentological and petrographic analysis

Preliminary lithological descriptions were provided by Hudáčková et al. (2018). In this study, the cores were re-examined in substantially greater sedimentological detail, focusing on lithofacies, depositional processes and sediment provenance. The dataset comprised 28 discontinuous spot cores from Špačince-4 (C6–C32 and C34), representing 52.2 m of recovered material from intervals between 1,190 and 3,348 m, and 23 spot cores from Dubové-2 (C1–C23), representing 89.9 m between 1,501 and 2,751 m. Core samples were cut perpendicular to bedding, washed, stabilized with a dispersive adhesive where necessary, and then photographed, scanned and digitized. Lithofacies were defined from grain size, sorting, matrix or clast support, clast composition, bed contacts, grading, lamination, ripple structures, intraclasts, soft-sediment deformation, bioturbation and fossil content. Depositional processes were interpreted from combinations of these criteria, following Boggs (2006), Nichols (2009), Talling et al. (2012), Patruno et al. (2015), Rossi et al. (2017) and Pellegrini et al. (2020). Intervals lacking direct core control were interpreted from SP/RT-log motifs and seismic character and are therefore considered lower-confidence interpretations. The observed criteria, facies associations, depositional interpretations, chronostratigraphic assignments and confidence levels for both wells are summarized in Tabs. 4 and 5.

Petrographic analysis was based on seven thin sections: six from Špačince-4 – C34 at 3,347–3,348 m, C32 at 3,257–3,259 m, C30a at 3,158–3,159.3 m, C24 at 2,848–2,850 m, C18 at 2,405–2,408 m and C17 at 2,298–2,303 m – and one from Dubové-2 at ~1,705 m. The sections were examined qualitatively under transmitted and cross-polarized light to identify volcanic, carbonate, sedimentary and metamorphic components and assess changes in sediment provenance. Because no modal point counting was performed, the compositional results are treated as qualitative.

Well-log data and correlation

Spontaneous-potential (SP) and resistivity (RT) logs were examined for the Špačince-4 and Dubové-2 wells. These digitized legacy records were supplied by NAFTA, a. s.; no additional paper-to-digital conversion was performed. SP is expressed in millivolts and RT in Ω m. The working dataset did not specify the original vertical sampling or digitization interval, or any pre-processing, filtering or depth adjustments applied before delivery. Relevant technical metadata are retained in the legacy documentation and digital repository of NAFTA, a. s. Regional lithological correlation and log-motif interpretation followed Emery and Myers (1996) and Rider and Kennedy (2011). Funnel-shaped motifs indicate sustained upward coarsening, bell-shaped motifs upward fining, symmetrical motifs paired coarsening- and fining-upward trends, and serrated motifs irregular high-frequency fluctuations without a persistent trend. Motifs were identified from the relative shapes of the SP and RT curves and their departures from local baselines, rather than from universal numerical thresholds (Rider & Kennedy, 2011). Log responses were calibrated locally against the discontinuous core record by matching recovered intervals to the corresponding curves and comparing log motifs with observed grain-size trends, lithofacies and vertical facies arrangements. Because spot coring and core recovery were discontinuous, calibration could not be applied throughout either well; interpretations based solely on log character are therefore considered tentative and assigned lower confidence than those supported directly by core observations.

Seismic interpretation and well ties

Four legacy 2D seismic line segments were assembled into two composite profiles: Composite 1 combines lines 558_77, 558_86 and 558a_86, whereas Composite 2 comprises line 554_77. The data are archived in the digital repository of NAFTA, a. s., were used with the company's permission, and were imported, displayed and interpreted in Petrel. The accompanying spatial metadata specify the Pulkovo 1942 / Gauss-Krüger Zone 3N coordinate reference system (EPSG:28463). SEG-Y header inspection indicated a nominal trace spacing of approximately 25 m and a record length of about 6 s two-way travel time for all lines. Line 554_77 contains 1,246 traces with 3,000 samples per trace at a 2 ms sampling interval and is approximately 31.2 km long. Lines 558_77, 558_86 and 558a_86 contain 515, 194 and 176 traces, respectively, each with 1,500 samples per trace at a 4 ms interval; their approximate lengths are 12.9, 4.8 and 4.4 km. Seismic amplitudes were stored as 32-bit IEEE floating-point values. Because the original acquisition and processing parameters, including frequency content, were unavailable, vertical resolution was assessed qualitatively and no bed-scale interpretation was attempted. Interpretation followed sequence- and seismic-stratigraphic principles outlined by Mitchum and Vail (1977) and Fischer and Veeken (2015). Horizons were identified from laterally traceable reflections, changes in amplitude, continuity and configuration, and systematic reflection terminations. Faults were recognized from reflector offsets and terminations, abrupt changes in dip or continuity, and associated deformation and growth geometries. Onlap and downlap were identified from systematic updip and downdip reflection terminations, respectively. Growth strata were defined as wedge-shaped packages that thicken toward faults, locally display fanning reflectors and show upward changes in fault displacement (Mitchum & Vail, 1977; Fischer & Veeken, 2015). Composite 1 was constrained by lithological and well-log data from the Kr-5, Du-2, Sp-5, Tra-1 and Tra-9 wells, whereas Composite 2 was constrained by the Ci-2 and Šp-4 wells (Fig. 1). Available check-shot time-depth relationships were used to convert well-log and lithological markers from depth to two-way travel time before seismic correlation. The underlying check-shot and sonic data are retained by NAFTA, a. s., and may be made available on reasonable request, subject to the data owner's permission. Interpretive confidence is highest near well ties and along laterally continuous, clearly expressed reflections. It decreases with distance from well control, across joins between legacy line segments, and within intervals containing weak, discontinuous or structurally complex reflections. Stratigraphic assignments and depositional interpretations in these areas are therefore considered tentative.

X-ray fluorescence analysis

A total of 160 homogenized core samples from 31 discontinuous intervals in the Špačince-4 well, spanning 697.08–3,347.30 m, were analysed on 31 August and 1 September 2022 using a handheld BRUKER TITAN S1 600 X-ray fluorescence analyser with GeoMining calibration. The instrument reported 48 major- and trace-element variables and an analytical total in percent; values below the detection threshold were recorded as "< LOD". The analytical report does not specify numerical detection limits, measurement uncertainty, replicate quality-control analyses, matrix-matched reference-standard results, measurement duration or further details of sample preparation. The data are therefore treated as semiquantitative and used to assess relative downhole compositional variations rather than exact absolute concentrations. The complete dataset is provided in Appendix 3 and summarized in Supplementary Table S1.

Micropalaeontology

The micropalaeontological dataset comprises 15 quantitative foraminiferal samples and 22 calcareous-nannofossil samples from Špačince-4, and 14 quantitative foraminiferal samples and 19 calcareous-nannofossil samples from Dubové-2, together with 16 palynological samples: 12 from Špačince-4 and four from Dubové-2. These samples were originally analysed for Hudáčková et al. (2018). For the present study, the results were reinterpreted, and selected archived residues and slides were re-examined to clarify or revise individual taxonomic identifications, biozonal assignments and palaeoecological interpretations. Sample depths and analytical status are listed in Supplementary Tab. S1.

Foraminifera

Approximately 100 g of sediment per sample was treated with hydrogen peroxide and wet-sieved through 0.071 and 1 mm meshes. Residues were examined using an Olympus SZ75 stereomicroscope and a polarizing microscope, and selected specimens were imaged with a QUANTA FEG 250 SEM (Appendix 1). Where possible, residues were split to obtain approximately 300 identifiable specimens; when fewer were available, all recovered specimens were recorded and used cautiously, mainly for taxonomic and biostratigraphic interpretation. Taxonomy follows Loeblich and Tappan (1992), Cicha et al. (1998) and Holbourn et al. (2013). Palaeoecological interpretation follows Boltovskoy (1976), Boltovskoy and Wright (1976), Murray (2006), and Murray and Alve (2011); agglutinated morphogroups follow Murray et al. (2011), palaeodepth estimates follow Murray (2006), Hohenegger (2005), and taphonomic assessment follows Holcová (1997). Water-depth interpretations were treated as indicative and were applied only where assemblages were sufficiently preserved and plausibly in situ. Benthic assemblages were evaluated jointly with food supply and organic flux, oxygen availability, substrate and sedimentological context. Assemblages affected by dissolution, mould preservation, selective preservation, sorting or reworking were not treated as direct depth indicators. Interpretations were based on the proportional composition of ecological groups and morphogroups, visualized using POLPAL (Nalepka & Walanus, 2003), and supplemented by the chemical data in Appendix 3. Relative abundances of the palaeoecological groups were calculated as percentages of the total benthic-foraminiferal assemblage, whereas agglutinated morphogroup abundances were calculated as percentages of the total agglutinated-foraminiferal assemblage. Samples with fewer than 30 identifiable specimens were excluded from percentage-based palaeoecological and morphogroup analyses. Samples without foraminifera were classified as barren, whereas assemblages dominated by moulds, dissolved tests or mechanically damaged specimens were classified as poorly preserved. Photodocumentation was performed using an TESCAN SEM at the Department of Geology and Paleontology, Faculty of Sciences, Comenius University.

Calcareous nannofossils

Nannofossils were prepared using smear-slide and decantation techniques following Bown (1998). Slides were mounted using Norland 61 adhesive and examined under an Olympus BX50 polarized-light microscope at 1,250× magnification. Photodocumentation was performed using an Olympus Infinity 2 camera with QuickPHOTO CAMERA 2.3 and ScopeImage 9.0 software. No fixed-count protocol was applied. Slides were examined systematically for taxonomic composition, preservation, reworked taxa, biostratigraphic markers and zonal assignment. The resulting qualitative to semiquantitative sample-by-sample observations are provided in Appendix 4. Taxonomy follows Young (1998) and Young et al. (2022).

Palynology

Approximately 20 g of sediment per sample was processed using cold HF and HCl to remove silicates and carbonates. Heavy liquid separation ($ZnCl_2$, density 2 g/cm³) concentrated organic residues containing pollen, spores, and other palynomorphs. Slides mounted in glycerine were examined using a Zeiss Axioscope microscope (40× and 63×).

Chronostratigraphic framework

Correlation between the Central Paratethys regional stages and the Mediterranean scale follows Piller et al. (2007), Kováč et al. (2007), Hohenegger (2014) and Wade et al. (2011). Stratigraphically significant taxa were used to constrain depositional timing and relate sedimentation to tectonic phases and sea-level changes. No direct geochronological analyses were conducted on material from the Špačince-4 or Dubové-2 wells; all numerical ages used for correlation were derived from published studies of neighbouring wells and regional volcanic and sedimentary successions (e.g. Šarinová et al., 2021; Rybár et al., 2024).

The complete tables are provided with the manuscript as supplementary material. Tab. S1 lists the complete dataset inventory, including sample depths, core identifiers, analytical status and available methodological metadata. Appendices 1 and 2 provide species-by-sample foraminiferal data for Špačince-4 and Dubové-2, respectively. Appendix 3 contains the complete handheld-XRF dataset, including depths, reported variables, units and below-detection values, whereas Appendix 4 presents nannofossil sample identifiers, taxonomic inventories, preservation assessments, reworked taxa, biostratigraphic events and zonal assignments. Appendices 1–4 accompany the manuscript as supplementary material.

The principal methodological limitations are discontinuous core coverage, locally poor microfossil preservation, incomplete metadata for the legacy geophysical datasets and the semiquantitative nature of the handheld-XRF measurements. Interpretations based primarily on well logs, seismic geometry or regional correlation are therefore considered less certain than those supported directly by core and fossil evidence.

Results

Lithological description of the studied wells

Špačince-4 well

The deepest cored interval (3,356–3,320 m; Core/C34) consists of poorly sorted, matrix-supported carbonate conglomerate with angular clasts embedded in a black calcareous matrix (Fig. 2).

Core C33 at approximately 3,301–3,302 m was not available for direct examination, and borehole-log data are absent for this interval. Core C32 at 3,257–3,259 m contains a poorly sorted volcanic conglomerate composed predominantly of altered volcanic lithoclasts derived from intermediate volcanism, together with spherulitized vitroclasts. The non-volcanic components include granitoid, biotite paragneiss, shale, carbonate and chert fragments, and the groundmass is chloritized. Carbonized plant fragments are also present. Tectonically deformed mudstones and sandstones were reported from this depth by Gaža (1963). Both SP and RT logs display pronounced funnel-shaped trends (Fig. 2).

The interval 3,200–3,125 m (C31, 30) consists of a massive grey-green zeolitized crystal-vitric tuff, where glass shards were replaced by analcime. Two distinct excursions are visible on the SP log, and the RT log shows a low-amplitude bell-shaped trend.

The interval between 3,125 and 2,850 m (C28–C25) is dominated by dark grey heterolithic mudstone-siltstone with subordinate light grey siltstone to very fine sandstone beds. Bedding is mm–cm scale, with parallel to wavy lamination and sharp to irregular/wavy contacts. Mud-rich intervals are laminated to locally mottled/weak-moderately bioturbated. Silty to very fine sandy beds show local normal grading, massive to faintly laminated bases, parallel/ripple lamination, and thin mud drapes. Irregular, lobate, loaded, and contorted laminae indicate soft-sediment deformation and possible dewatering. The core is locally fractured. The SP log displays a serrated pattern with minor excursions, whereas the RT log shows symmetrical to bell-shaped excursions of higher amplitude (Fig. 2).

The interval between 2,848 and 2,850 m (C24) consists of a massive, granule-pebble conglomerate/breccia with poorly sorted angular to subrounded lithic clasts. Larger platy/tabular clasts, some internally laminated, likely represent ripped-up mudstone-siltstone intraclasts. Bedding, grading, tractional lamination, bioturbation, and clear imbrication are absent; fabric is chaotic to weakly organized (Fig. 2). The conglomerates differ significantly from the underlying volcanic sequence in terms of clast composition. The clast assemblage is dominated by sedimentary lithologies, including sandstones (some of Eocene–Oligocene age, as indicated by enclosed foraminifera), calpionellid and radiolarian biomicrites, and other carbonate rocks, accompanied by chert, granitoid, and quartz-mica schist clasts.

The interval 2,850–2,150 m (C23 to 16) consists of alternating laminated to wavy-laminated mudstone-siltstone, massive to normally graded sandstone/pebbly sandstone, and matrix-rich fine conglomerate. The composition of the conglomerates and sandstones indicates a renewed input from volcanic sources. Volcanic grains are associated with granitoid, mica-schist, carbonate, siltstone, and sandstone clasts. Marine fossils, including red-algae (lithothamnia) fragments, suggest redeposition from a shallow-marine environment. Upsection, the abundance of unstable grains decreases, whereas quartz becomes progressively more abundant. Conglomeratic and pebbly beds are poorly sorted and contain abundant angular to subrounded lithic clasts, including common platy mudstone-siltstone intraclasts/rafts up to ~10 cm. Contacts are sharp to locally erosive or irregular, with chaotic to weakly stratified fabric, local clast clustering, ripple lamination, and thin laminated intervals. Bioturbation is limited, and clear imbrication is absent (Fig. 2). Both SP and RT logs show serrated trends, with consistently high RT amplitudes.

The interval between 2,150 and 1,125 m (C15–C6) is dominated by brown, finely laminated mudstone-siltstone, with subordinate thin fine-sandstone and siltstone laminae. Lamination is mainly parallel to low-angle/wavy, with common mud drapes/stringers and bedding-parallel partings/fractures. Conglomeratic material, large intraclasts, clear grading, and strong bioturbation are absent to rare (Fig. 2). According to Gaža (1963) carbonized plant fragments and marine macrofaunal remains are present. The SP and RT logs remain serrated with low amplitudes throughout this interval.

Between 1,125–625 m (C5 to C1), no core was available for this study, although core material exists. This interval is characterized by higher-amplitude serrations on the SP log. Gaža (1963) reported the presence of carbonized plant fragments and marine macrofaunal remains.

The uppermost interval, 625–0 m, lacks core material and is defined by high-amplitude serrated RT trends and medium-amplitude serrated SP trends.

XRF description of the Špačince-4 well

To further constrain compositional changes within the succession, XRF analyses were performed on drill-core samples. The results demonstrate that the volcanic horizon at depths of 3,158 and 3,258 m is characterized by elevated relative values of Zr, U, Si, and K, whereas Ca concentrations are lower compared to the surrounding sediments. The highest relative Ca values correspond to the occurrence of carbonate conglomerates at depths of approximately 3,350 and 2,850 m. Additional Ca enrichment was recorded in core samples from depths of 3,010 and 3,050 m. The systematic decrease in S values above a depth of 905 m, approaching near-zero values, is also observed (Appendix 3).

Dubové-2 well

The interval 3,000–2,780 m (C31 to 24) consists of tectonically deformed shale, limestone, quartz arenite, sandstone, and conglomerate (Gaža, 1968). SP and RT logs display high-amplitude symmetrical to bell-shaped excursions.

Between 2,780 and 2,720 m (C23), grey massive, bioturbated sandstones occur. The SP log shows a symmetrical trend, while the RT log exhibits funnel and bell-shaped patterns. The sandstones are dominated by carbonate clasts, some of which are clearly epiclastic. Quartz, feldspar, mica, chert, siltstone, volcanic lithic fragments, glauconite and bioclasts are also present in a micritic matrix.

The interval between 2,720 and 2,535 m (C22–C16) consists of grey to black sandy mudstone and muddy siltstone, locally grading into very fine sandstone. Bedding is laminated to faintly wavy/ripple laminated, with local mud-rich streaks, elongate mudstone intraclasts, diffuse grading, and bioturbation. Minor soft-sediment deformation is present (Fig. 3). SP and RT logs are mainly serrated, with minor high-amplitude excursions.

The interval between 2,535 and 2,060 m (C15–C6) consists of dark grey to brown mudstone, sandy mudstone and muddy siltstone that are massive to faintly laminated and locally bioturbated. Thin-shelled bivalves and other micro- to macrofauna are present. Coarse-grained beds and clear traction structures are absent to rare; the core is locally fractured (Fig. 3). SP and RT logs remain serrated.

A pronounced high-amplitude symmetrical trend is visible on both logs between 2,060–1,975 m.

The interval 1,975–470 m (C5 to 1) consists of brown mudstone to muddy siltstone/fine sandstone, massive to finely/wavy laminated and locally bioturbated. Synsedimentary folding, bedding-parallel partings, and minor fractures occur locally. A thin section from the fine-grained conglomerate in core C3 at approximately 1,705 m was examined for provenance. Its composition is dominated by carbonate, quartzite, arenite, phyllite, chert, and quartz

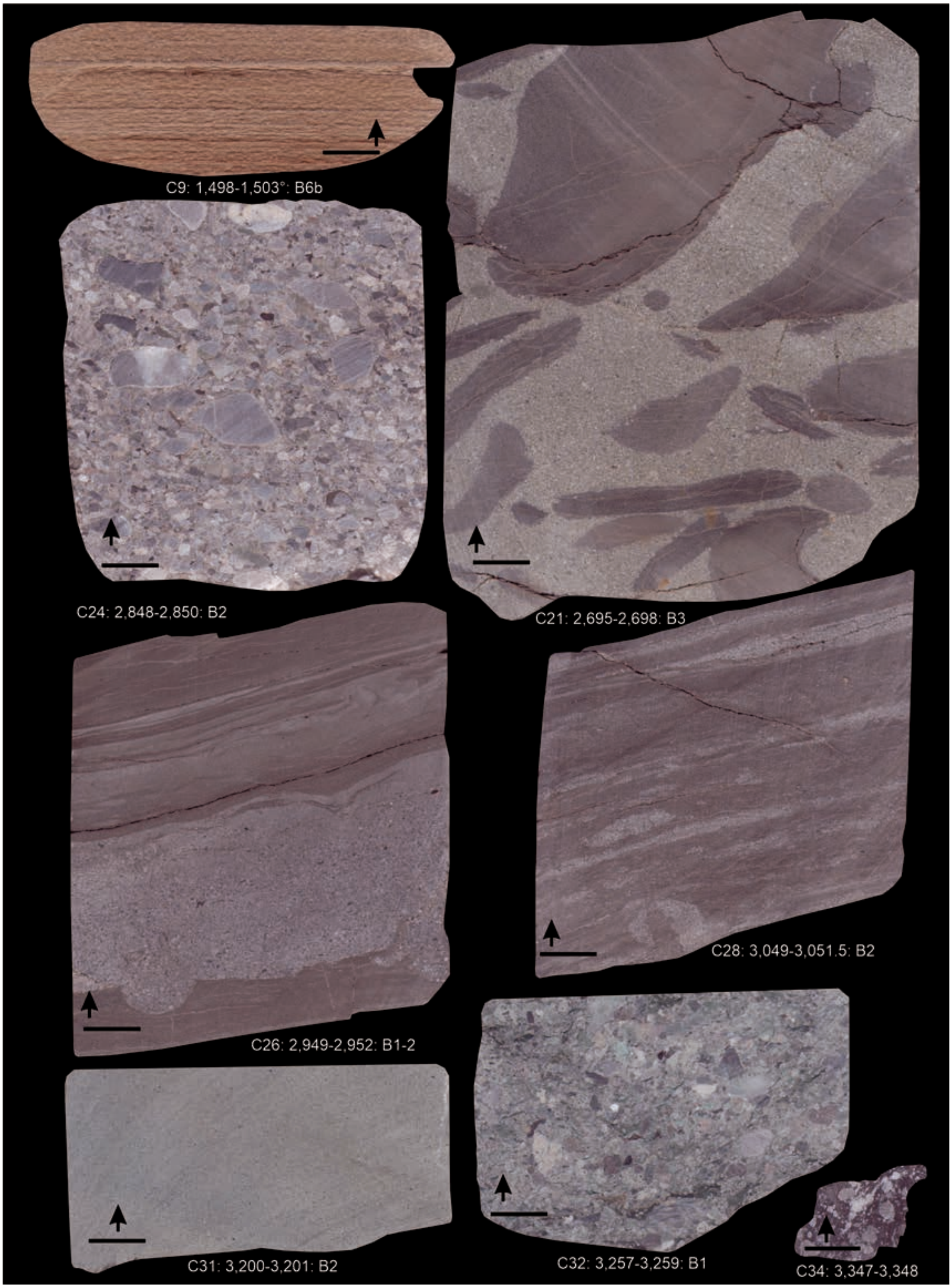

Fig. 2. Representative core slabs from the Špačince-4 well. Labels give core number, depth and box. The illustrated facies include basal paraconglomerate (C34), volcanic conglomerate (C32), zeolitized tuff (C31), heterolithic mudstone-siltstone and fine sandstone (C28 and C26), matrix-rich conglomerate and pebbly sandstone (C24 and C21), and laminated mudstone-siltstone (C9). Arrows indicate younging direction; 1 cm scale bars are shown in individual images.

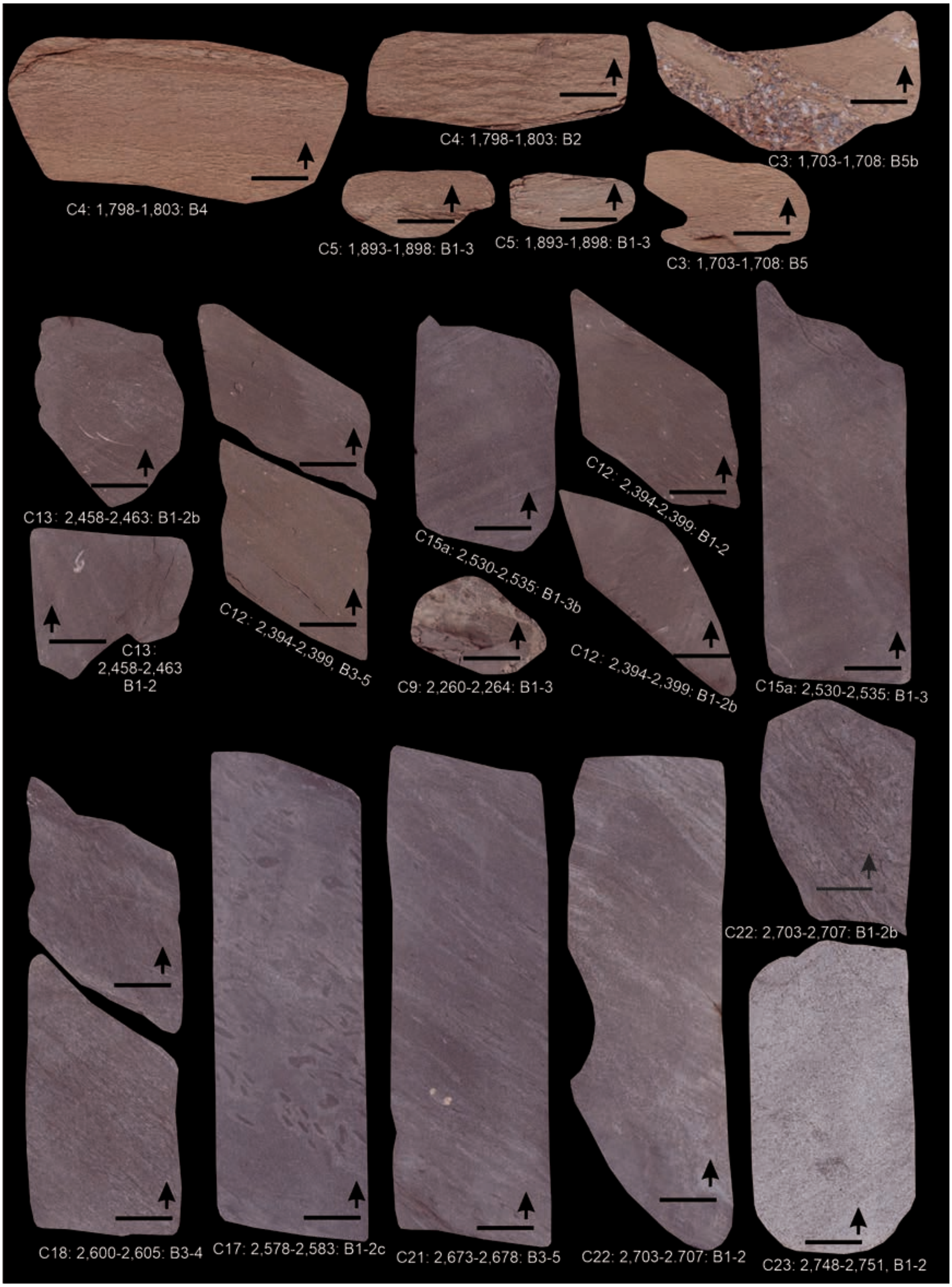

Fig. 3. Representative core slabs from the Dubové-2 well. Labels give core number, depth and box. The illustrated facies include bioturbated sandstone (C23), laminated sandy mudstone–muddy siltstone and fine sandstone (C22–C12), shell-rich reworked event beds (C9 and C3), and laminated muddy siltstone–fine sandstone (C5–C3). Arrows indicate younging direction; 1 cm scale bars are shown in individual images.

grains, whereas volcanic grains are rare. The conglomerate also contains bioclasts, including shell fragments, foraminifera, red algae, as well as the above-mentioned muddy intraclasts. Rare shell-rich paraconglomerate/bioclastic beds contain fragmented macrofossils and likely represent reworked event layers (Fig. 3). SP and RT logs display low-amplitude serrated trends.

Above 470 m, core material is absent. SP and RT logs display high-amplitude serrated to symmetrical excursions.

Between 80–0 m, excursions become more pronounced.

Biostratigraphy

The micropalaeontological results presented below are based on the dataset originally generated by Hudáčková et al. (2018), subsequently reinterpreted for the present study and supplemented by partial re-examination of selected archived residues and slides. The principal biostratigraphic events, zonal assignments, regional stages, formation correlations and confidence levels are summarized in Tabs. 2 and 3; complete sample-level data are provided in Appendices 1, 2 and 4 and Supplementary Tab. S1.

Špačince-4 well (Šp-4)

Biostratigraphically informative samples and events are summarized below and in Tab. 2; complete taxonomic, accessory-residue and sample-level data are provided in Appendices 1 and 4 and Supplementary Tab. S1.

Foraminiferal assemblages are generally poorly preserved, particularly in the deepest intervals of the well. In cores 29 and 28 (3,098–3,049 m), foraminifera are retained in open nomenclature, because only moulds were preserved, whereas the original shell material was dissolved or mechanically damaged by compaction. Agglutinated genera, mainly *Reophax, Bathysiphon, Haplophragmoide*s and *Saccammina*, dominate the assemblages, likely due to early diagenetic processes. Planktonic foraminifera are absent in core 28; therefore, the biostratigraphic interpretation is based on the benthic species *Saccammina grzybowskii*, whose first occurrence in the Badenian was reported by Cicha et al. (1998). Calcareous nannofossils from the same interval are represented by low-diversity and poorly preserved assemblages containing rare zonal markers *Sphenolithus heteromorphus* and *Helicosphaera walbersdorfensis*, indicating the ?NN4–NN5 nannofossil zones. Rare diatoms and silicoflagellates occur locally; their complete sample distribution is provided in Appendix 1.

Planktonic foraminifera from core 27 (3,002–3,004.5 m) are poorly preserved and commonly occur only as moulds. The first occurrence of the stratigraphically important species *Orbulina suturalis* (Fig. 4, item 1) was identified in core 26 at 2,949–2,952 m. The occurrence of *Sphenolithus heteromorphus* and *Helicosphaera waltrans* in cores 21 and 17, at 2,695–2,698 m and 2,298–2,303 m, respectively, indicates the NN5 Zone and a Langhian age.

The important biostratigraphic event was recognized in core 12 (1,798–1,804 m), where the acme of *Globorotalia bykovae* together with a bloom of small planktonic foraminifera indicates an Upper Badenian age following Gonera (2013). This interpretation is further supported by the benthic foraminiferal assemblage characterized by the occurrence of *Bolivina dilatata maxima* and the dominance of the genera *Bulimina* and *Bolivina*, in agreement with Cicha et al. (1998) and Kováčová & Hudáčková (2009). Nannofossil assemblages throughout most of the Šp-4 well are generally poorly preserved and of low diversity, apart from core 9 (1,503–1,498 m). In this interval, increased diversity was recorded, including *Coronocyclus nitescens*, *Orthorhabdus rioi* and *Sphenolithus abies*, together with frequent occurrence of *Reticulofenestra pseudoumbilicus* > 7 μm. According to Bartol (2009), this event represents an alternative marker for the NN5/NN6 zonal boundary. The core 9 (1,498–1,503 m) was likewise assigned to the upper Badenian.

Dubové-2 well (Du-2)

Biostratigraphically informative samples and events are summarized below and in Tab. 3; complete taxonomic, accessory-residue and sample-level data are provided in Appendices 2 and 4 and Supplementary Tab. S1.

The lowermost studied samples from core 22 (2,707–2,703 m) yielded abundant planktonic specimens of *Ciperoella ciperoensis*, suggesting a Karpatian to Lower Badenian age according to Cicha et al. (1998). In cores 18–16 (2,605–2,555 m), foraminiferal tests are generally poorly preserved, predominantly occurring as molds; therefore, many taxa remain indeterminable and are left in open nomenclature. Low-diversity and low-abundance calcareous nannofossil assemblages were documented in the interval 2,707–2,535 m. Rare and poorly preserved specimens of the stratigraphically important species ?*Helicosphaera ampliaperta* were identified in the interval 2,707–2,703 m, indicating the NN4 Zone. Due to the absence of planktonic foraminifera in cores 18–17 (2,605–2,555 m), the biostratigraphic interpretation of this interval remains uncertain.

The most abundant and diverse foraminiferal assemblage was identified in core 15a (2,535–2,530 m). The assemblage contains a small proportion of planktonic taxa dominated by indeterminate *Globigerina* species and rare *Ciperoella ciperoensis*, which does not allow more precise stratigraphic assignment. Within the benthic assemblage, the occurrence of *Uvigerina macrocarinata* and *Lenticulina echinata* represents an important stratigraphic marker supporting assignment to the lower Badenian, corresponding to the CPN7 Zone (Cicha et al., 1975). The occur-

Tab. 2
Biostratigraphic summary of the Špačince-4 well

Depth/core	Analysed sample	Foraminiferal markers	Nannofossil markers	CPN zone	NN zone	Regional stage	Formation	Confidence
3,098–3,049 m; C29–C28	29/1–2/20; 29/1–2/80; 28/2/10; 28/2/80	No reliable zonal marker; poorly preserved agglutinated and benthic assemblages	Rare *Sphenolithus heteromorphus* and *Helicosphaera walbersdorfensis*; some specimens questionable	Not assigned	?NN4–NN5	lower Badenian, Langhian; tentative	Špačince Fm.	**L–M:**
2,949–2,952 m; C26	26/1/60	*Orbulina suturalis*, *Saccammina grzybowskii*, *Dentoglobigerina altispira*	*Helicosphaera walbersdorfensis*, *H. carteri*, *Reticulofenestra pseudoumbilicus* > 7 µm	Not assigned	Not formally assigned	lower Badenian, Langhian	Špačince Fm.	**M–H:**
2,695–2,698 m; C21	21/1/90	Barren of diagnostic foraminifera	*S. heteromorphus* and *Helicosphaera waltrans*	Not assigned	NN5	lower Badenian, Langhian	Špačince Fm.	**H for NN zone:**
2,298–2,303 m; C17	17/2/X	Reworked *Cassigerinella chipolensis*; no reliable in-situ foraminiferal marker	*S. heteromorphus*; *H. waltrans* not confirmed	Not assigned	NN5	lower Badenian, Langhian	Špačince Fm.	**M:**
1,798–1,804 m; C12	12/1–2/X	Acme of *Globorotalia bykovae*; *Orbulina universa*; *Pappina neudorfensis*; *Bolivina dilatata*	*Coccolithus pelagicus* and ?*Calcidiscus pataecus*; no diagnostic zonal marker	Not formally assigned	Not assigned	upper Badenian, lower Serravallian	Báhoň/ Pozba formations	**M–H:**
1,498–1,503 m; C9	9/1/X; 9/5/X	*Turborotalita quinqueloba*, *Globigerina praebulloides*, *Bolivina dilatata brevis*	*S. heteromorphus*, *R. pseudoumbilicus* > 7 µm, *Coronocyclus nitescens*, *Orthorhabdus rioi*, *Sphenolithus abies*	Not assigned	NN6/?NN5; NN5/NN6 boundary interval	Upper Badenian, lower Serravallian	Báhoň/ Pozba formations	**M–H:**

Formation assignments are regional lithostratigraphic correlations and are not determined directly from the fossil assemblages. **H** – high confidence: concordant evidence from adequately preserved foraminiferal and nannofossil assemblages; **M** – moderate confidence: supported by one fossil group, rare markers or partly affected preservation; **L** – low/tentative confidence: questionable identification, poor preservation, reworking or dependence on regional correlation. “Not assigned” means that the available assemblage does not justify a formal zonal designation.

Fig. 4. SEM images of selected foraminifera from the Špačince-4 and Dubové-2 wells. 1 – *Orbulina suturalis* – Šp-4/26/1/60; 2 – *Globigerina regularis* – Du-2/14/1–2–3/x; 3 – *Globorotalia* sp. – Du-2/14/1–2–3/x; 4–5 – *Globorotalia bykovae* – Šp-4/12/1–2/x; 6 – *Cassigerinella chipolensis* – Šp-4/16/4/x; 7 – *Trilobatus quadrilobatus* – Du-2/14/1–2–3/x; 8 – *Globigerina* cf. *bulloides* – Du-2/14/1–2–3/x; 9 – *Globoturborotalita druryi* – Du-2/3/3/50; 10 – *Globigerinella obesa* – Du-2/16/1–2/x; 11 – *Ciperoella ciperoensis* – Du-2/22/1–2/x; 12 – *Trilobatus quadrilobatus* – Du-2/14/1–2–3/x; 13 – *Globigerina* cf. *bulloides* – Du-2/14/1–2–3/x; 14 – *Paraglo-borotalia nana* – Šp-4/12/1–2/x; 15 – *Globotruncana* sp. – Šp-4/16/5/x; 16 – *Spirosigmoilina tenuis* – Du-2/18/3–4/x; 17 – *Bolivina hebes* – Du-2/16/1–2/x; 18 – *Bolivina* cf. *hebes* – Du-2/22/1–2/x; 19 – *Bolivina dilatata* – Du-2/16/1–2/x; 20 – *Bulimina striata* – Šp-4/12/1–2/x; 21 – *Uvigerina macrocarinata* – Du-2/22/1–2/x; 22 – *Uvigerina venusta* – Du-2/14/1–2–3/x; 23 – *Uvigerina bononiensis* subsp. *primiformis* – Du-2/18/3–4/x; 24 – *Uvigerina semiornata* – Du-2/14/1–2–3/x; 25 – *Trifarina angulosa* – Du-2/14/1–2–3/x; 26 – *Bulimina elongata* – Šp-4/11a/2/x; 27 – *Stilostomella* sp. indet. – Du-2/22/1–2/x; 28 – *Ammonia parkinsoniana* – Šp-4/16/4/x; 29 – *Cibicidoides ungerianus* – Du-2/14/1–2–3/x; 30 – *Valvulineria complanata* – Du-2/14/1–2–3/x; 31 – *Hanzawaia boueana* – Du-2/14/1–2–3/x; 32 – *Ceratocancris hauerii* – Šp-4/26/1/60; 33 – *Hansenisca soldanii* – Du-2/14/1–2–3/x; 34 – *Sahulia conica* – Du-2/14/1–2–3/x; 35 – *Gaudryina megagranosa* – Du-2/22/1–2/x; 36 – *Quinqueloculina* sp. indet. – Du-2/18/3–4/x; 37 – *Bathysiphon taurinensis* – Šp-4/11a/2/x; 38 – *Ammobaculites agglutinans* – Du-2/14/1–2–3/x; 39 – *Rhizammina algaeformis* – Du-2/14/1–2–3/x; 40 – *Lagenammina atlantica* – Du-2/14/1–2–3/x; 41 – *Uvigerina* aff. *bononiensis* subsp. primiformis – Du-2/14/1–2–3/x.

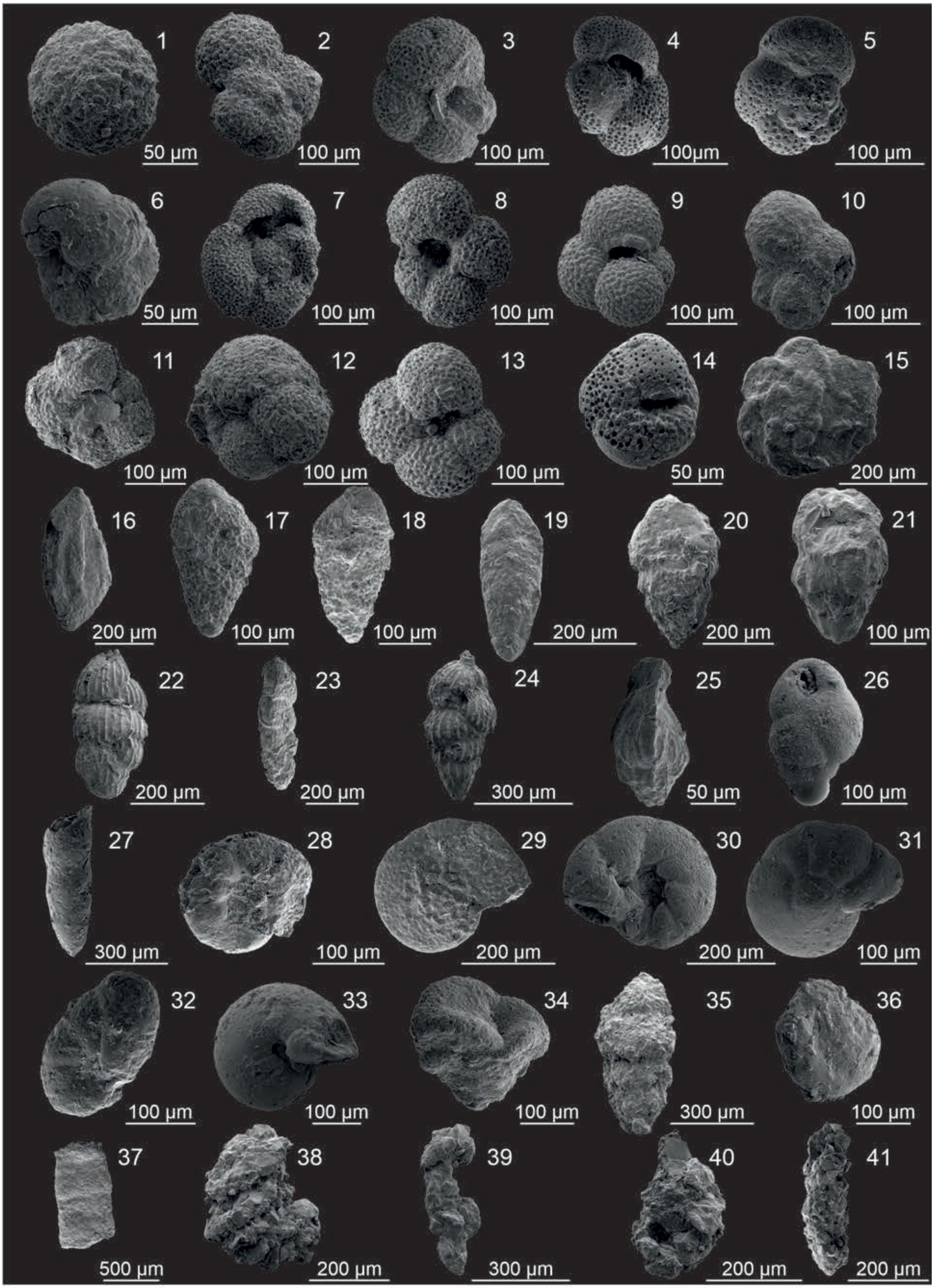
1
50 µm
2
100 µm
3
100 µm
4
100µm
5
100 µm
6
50 µm
7
100 µm
8
100 µm
9
100 µm
10
100 µm
11
100 µm
12
100 µm
13
100 µm
14
50 µm
15
200 µm
16
200 µm
17
100 µm
18
100 µm
19
200 µm
20
200 µm
21
100 µm
22
200 µm
23
200 µm
24
300 µm
25
50 µm
26
100 µm
27
300 µm
28
100 µm
29
200 µm
30
200 µm
31
100 µm
32
100 µm
33
100 µm
34
100 µm
35
300 µm
36
100 µm
37
500 µm
38
200 µm
39
300 µm
40
200 µm
41
200 µm

Tab. 3
Biostratigraphic summary of the Dubové-2 well

Depth/core	Analysed sample	Foraminiferal markers	Nannofossil markers	CPN zone	NN zone	Regional stage	Formation	Confidence	References
2,703–2,707 m; C22	22/1–2/XX	Reported *Ciperoella ciperoensis*; *Lenticulina* cf. *echinata*; *Bolivina dilatata*; *Bulimina striata*	?*Helicosphaera ampliaperta*	Not assigned	?NN4	Karpatian–lower Badenian; lower Badenian favoured regionally	Špačince Fm.	L–M:	*L. echinata* FO: Lagenidae Zone Grill (1943), CPN Cicha et al. (1975)
2,605–2,555 m; C18–C16	18/3–4/XX; 17/1–2/XX; 16/1–2/X	*Saccammina grzybowskii* in C18–C17; *Bolivina dilatata maxima* in C17; C16 poorly preserved	Mainly long-ranging *Coccolithus pelagicus*; *Reticulofenestra haqii* and associated taxa	CPN7 in C18–C17	Not assigned	lower Badenian, Langhian	Špačince Fm.	M:	*Saccammina grzybowskii* FO: Cicha et al. (1998)
2,530–2,535 m; C15a	15A/1–2–3/X	*Uvigerina macrocarinata*; *Lenticulina calcar*; rare *L. echinata*; reported *Ciperoella ciperoensis*	*Sphenolithus heteromorphus*; *Helicosphaera walbersdorfensis*; *Orthorhabdus serratus*	CPN7	NN5	lower Badenian, Langhian	Špačince Fm.	M–H:	*Uvigerina macrocarinata* FO: Cicha et al. (1975, 1998)
2,502–2,507 m; C14	14/1–2–3/X	*Pappina neudorfensis*; *Uvigerina bellicostata*; *Turborotalita quinqueloba*	*Helicosphaera walbersdorfensis*; *H. carteri*; *Reticulofenestra pseudoumbilicus*	CPN8	NN5	lower Badenian, Langhian; upper Badenian for Forams	Špačince Fm.	M–H:	*Pappina neudorfensis*, *Uvigerina bellicostata* – Bulimina/ Bolivina Zone, Upper Badenian (Steininger & Rögl, 1984; Haunold, 1995; Płonka, 1917)
1,703–1,708 m; C3	3/3/50; 3/5/50	Acme of *Globorotalia bykovae*‡; *Globoturborotalita druryi*; Bulimina-Bolivina acmes	*R. pseudoumbilicus* > 7 µm; *Coronocyclus nitescens* (circular)	CPN8	NN6	upper Badenian, lower Serravallian	Báhoň formations	M–H:	*Globoturborotalita druryi* – (NN6 Rybár et al., 2015; FO – 13,82 Ma Bojar et al., 2018)

Formation assignments are regional lithostratigraphic correlations and are not determined directly from the fossil assemblages. H – high confidence: concordant evidence from adequately preserved foraminiferal and nannofossil assemblages; M – moderate confidence: supported by one fossil group, rare markers or partly affected preservation; L – low/tentative confidence: questionable identification, poor preservation, reworking or dependence on regional correlation. "Not assigned" means that the available assemblage does not justify a formal zonal designation.

Fig. 5. Selected calcareous-nannofossil taxa and associated microfossils from the Špačince-4 and Dubové-2 wells. A – *Reticulofenestra minuta*, Šp-4, core 9; B – *Reticulofenestra haqii*, Du-2, core 9; C–D – *Reticulofenestra pseudoumbilicus*, Šp-4, core 9; E – *Coccolithus pelagicus*, Šp-4, core 21; F – *Cyclicargolithus floridanus*, Šp-4, core 9; G – *Coronocyclus nitescens*, Šp-4, core 9; H – *Braarudosphaera bigelowii*, Du-2, core 12; I – *Helicosphaera carteri*, Šp-4, core 9; J – *Helicosphaera waltrans*, Šp-4, core 21; K – *Helicosphaera walbersdorfensis*, Šp-4, core 9; L – *Sphenolithus heteromorphus*, Šp-4, core 17; M – *Orthorhabdus serratus*, Du-2, core 15; N – *Orthorhabdus rioi*, Du-2, core 17; O – *Umbilicosphaera rotula*, Šp-4, core 26; P – *Discoaster deflandrei*, Šp-4, core 29; Q – *Zygrhablithus bijugatus*, Šp-4, core 9; R – *Coccolithus eopelagicus*, Du-2, core 15; S – *Discoaster barbadiensis*, Du-2, core 10; T – *Tribrachiatus* orthostylus, Du-2, core 10; U – *Isthmolithus recurvus*, Šp-4, core 9; V – *Arkhangelskiella cymbiformis*, Du-2, core 17; W – *Eiffellithus turriseiffelii*, Du-2, core 22; X – *Eiffellithus eximius*, Du-2, core 15. Scale bars are 5 µm.

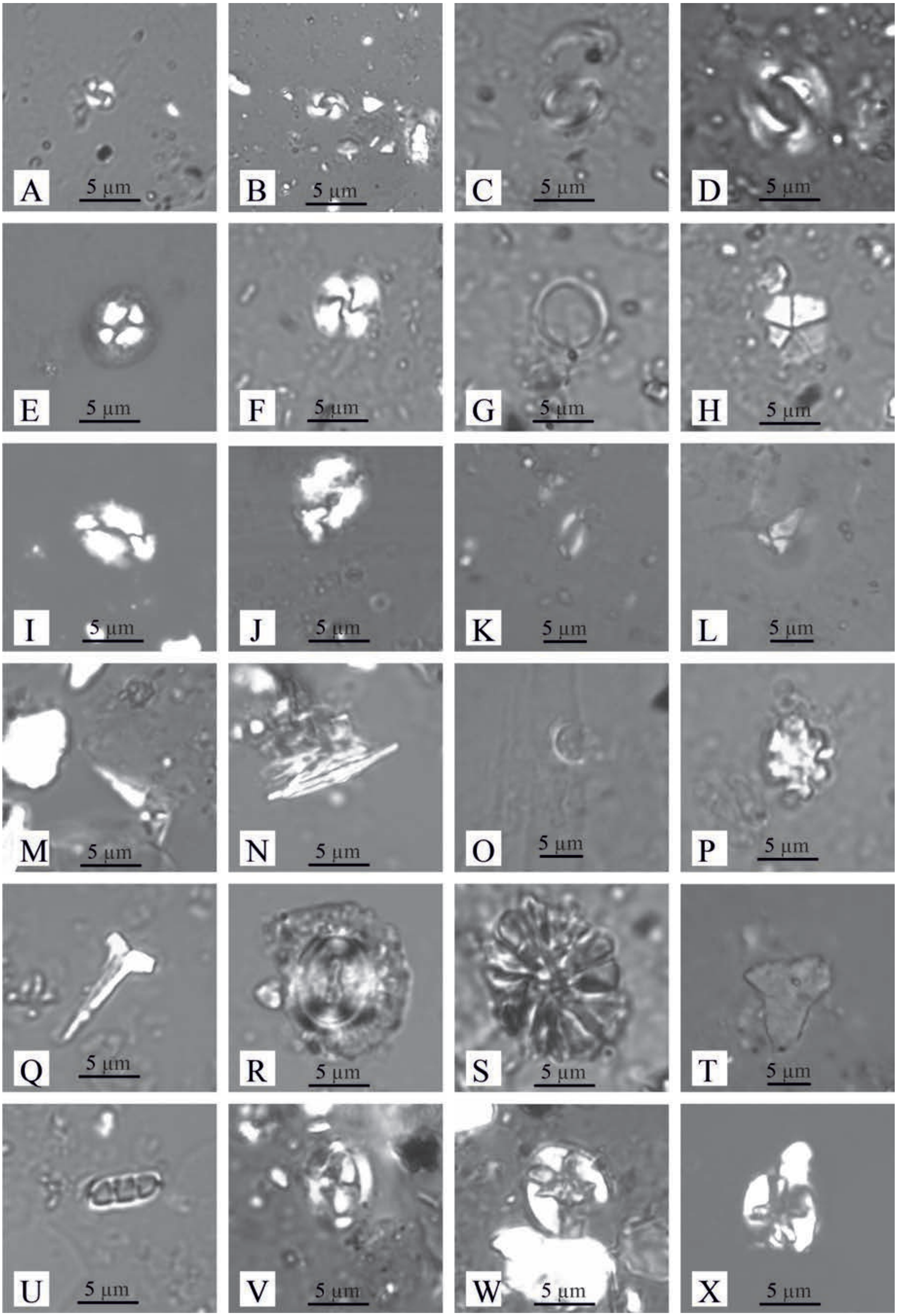
A 5 µm
B 5 µm
C 5 µm
D 5 µm
E 5 µm
F 5 µm
G 5 µm
H 5 µm
I 5 µm
J 5 µm
K 5 µm
L 5 µm
M 5 µm
N 5 µm
O 5 µm
P 5 µm
Q 5 µm
R 5 µm
S 5 µm
T 5 µm
U 5 µm
V 5 µm
W 5 µm
X 5 µm

rence of the zonal marker *Sphenolithus heteromorphus* in the interval 2,535–2,530 m indicates a Langhian age for the studied sediments. Another important stratigraphic event was identified in core 14 (2,507–2,502 m), where the occurrence of *Pappina neudorfensis* and *Uvigerina bellicostata*, together with a bloom of small *Turborotalita quinqueloba,* indicates an upper Badenian age, consistent with interpretations by Cicha et al. (1998) and Gonera (2013).

Assemblages from cores 5–1, particularly core 3 at 1,703–1,708 m, contain abundant *Globorotalia bykovae* and *Globoturborotalita druryi*, supporting the CPN8 Zone and an upper Badenian assignment (Cicha et al., 1998). The associated nannofossil assemblage, including *Reticulofenestra pseudoumbilicus > 7* µm and *Coronocyclus nitescens*, indicates the NN5/NN6 boundary interval. Comparable assemblages have previously been correlated with a broader late Badenian–Sarmatian interval, but the combined evidence used here favours an upper Badenian, lower Serravallian age. This interpretation is consistent with the results of Kováčová et al. (2009) and Rybár et al. (2015), who associated these assemblages with the NN6 Zone and a late Badenian–Sarmatian (Serravallian) age. Furthermore, the same interval yields a characteristic assemblage of the *Bulimina/Bolivina* Zone described by Grill (1941).

Pollen

Špačince-4 and Dubové-2 wells

All studied samples contain approximately 90 % phytoclasts, including plant tissues, dispersed gymnosperm cuticles and unidentified plant-derived particles, together with highly corroded pollen grains, mainly Pinaceae. Sporomorph preservation is very poor. Most phytoclasts show moderate to high maturity and some may be reworked; angular particles in at least half of the assemblage suggest short, rapid transport.

Paleoecology of Foraminifera

Špačince-4 well

Agglutinated taxa dominate the interval between 3,056 and 2,901.5 m. Considering that benthic foraminiferal assemblages may be significantly affected by taphonomic processes such as dissolution and dilution, while agglutinated assemblages are generally more resistant and remain better preserved, the relative abundances of agglutinated morphogroups were evaluated for palaeoecological interpretation following Murray et al. (2011). Morphogroup distributions in the intervals 3,056–2,901.5 m, 2,801.5–2,406 m and 1,897–1,700 m are compatible with upper-bathyal to outer-shelf ecological affinities only where the assemblages are reasonably preserved and plausibly in situ. The occurrence of shallow-water epiphytic taxa, together with evidence of dissolution, selective preservation and possible gravity-flow redeposition, reduces confidence in direct palaeodepth estimates. The C1-dominated assemblage at 1,498.5 m and the increasing abundance of epiphytic taxa at 1,082.5–799 m are consistent with shallowing, although changes in substrate, food supply and oxygenation may also have influenced the assemblages.

Calcareous assemblages between 2,598 and 2,406 m and between 1,412 and 1,082.5 m contain taxa tolerant of elevated organic flux and reduced oxygen availability. The change from high-productivity taxa at 2,598 m, through a mixed assemblage at 2,588 m, to low-oxygen-tolerant taxa at 2,406 m is consistent with increasing organic loading and/or decreasing oxygen availability, but does not independently demonstrate bottom-water dysoxia. These assemblages are therefore used to infer relative changes in organic supply and bottom- or pore-water oxygenation rather than direct water depth or a quantified redox state. Samples containing only agglutinated forms or clear evidence of reworking, including those at 2,405, 2297 and 698 m, are not used for confident palaeodepth or redox reconstruction.

Dubové-2 well

Foraminiferal tests are generally poorly preserved, indicating partial dissolution and alteration of the original assemblages. More resistant agglutinated taxa dominate the intervals between 2,531 and 2,212 m and occur again at 1,704 m (Fig. 7).

Morphogroup proportions based on Murray et al. (2011) show a predominance of morphogroup C1 in the lower and upper parts of the well. The assemblage at 2,601–2,577 m is compatible with a middle-bathyal ecological affinity only if it is reasonably in situ; poor preservation, dissolution and sorting reduce the confidence of this interpretation. The associated hyaline taxa and low proportion of epiphytic oligotrophic forms are consistent with enhanced organic flux and reduced oxygen availability at the sediment–water interface and/or within pore waters, but do not independently demonstrate the presence of an Oxygen Minimum Zone (OMZ). The B3- and C1-dominated assemblages at 2,556–2,531 m are compatible with a broad outer-shelf affinity. The sample at 1,791 m is not used as a direct depth indicator because sorting probably modified the original assemblage. The upward increase in shallow-water and epiphytic components is consistent with progressive shallowing, although changes in substrate, nutrient supply and oxygenation cannot be excluded as contributing controls (Fig. 7).

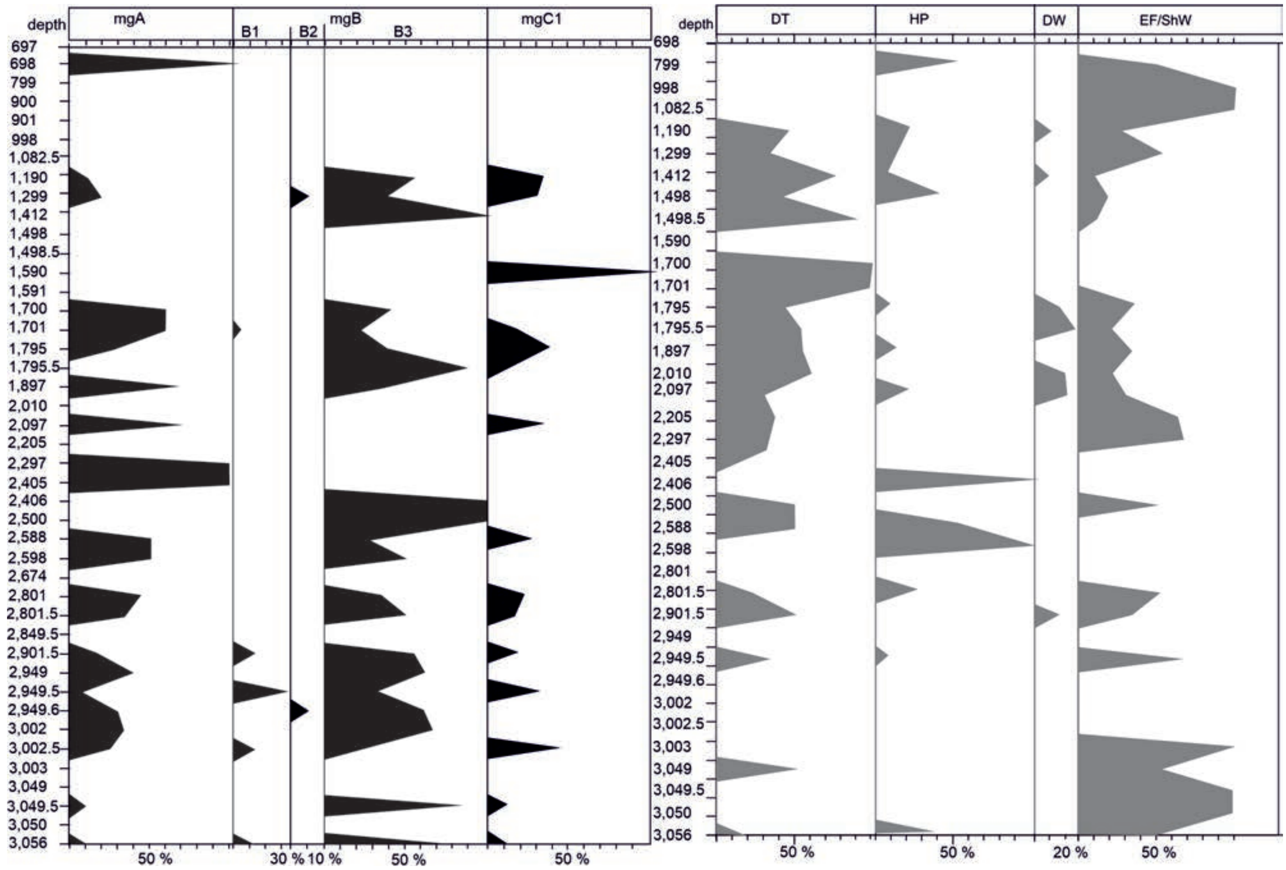

Fig. 6. Relative abundances of palaeoecologically significant benthic-foraminiferal groups in the Špačince-4 well. (Left side) Morphogroups of agglutinated foraminifera adapted from Murray et al. (2011). (Right side) palaeoecological groups of benthic foraminifera based on Murray (2006) and other authors. Abbreviations: HP – high productivity; DT – dysoxia-tolerant taxa; DW – deep-water taxa; EF/ShW – epifaunal/shallow-water taxa.

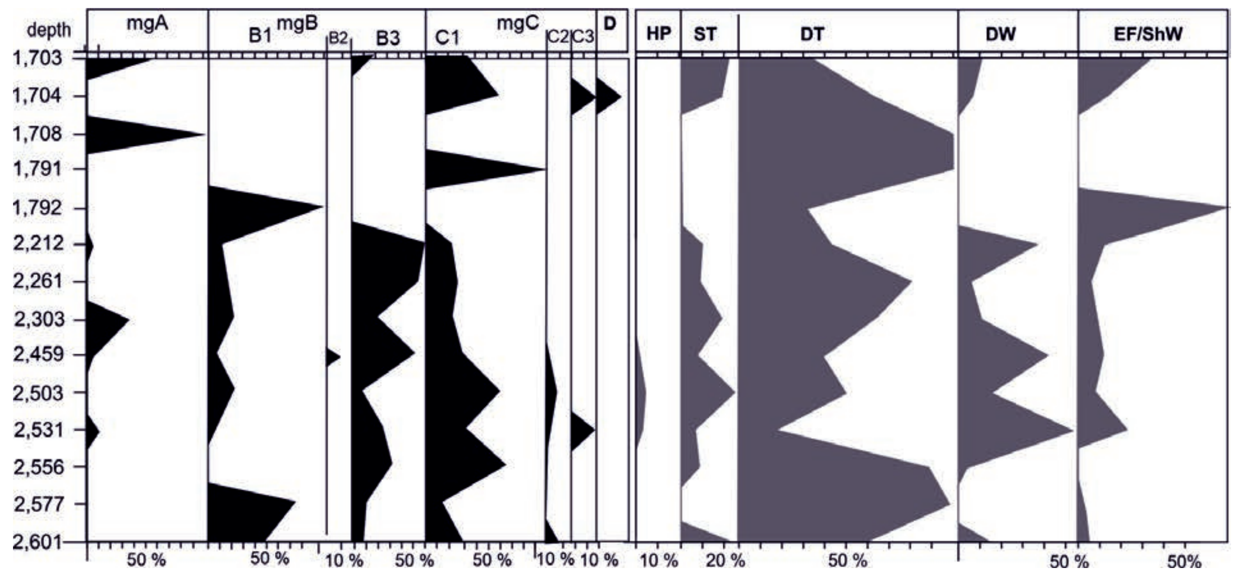

Fig. 7. Relative abundances of palaeoecologically significant groups of benthic foraminifera in samples from the Dubové-2 well. (Left) Morphogroups of agglutinated foraminifera adapted from Murray et al. (2011). (Right) Palaeoecological groups of benthic foraminifera based on Murray (2006) and other authors. Abbreviations: HP – high productivity; DT – dysoxia-tolerant taxa; DW – deep-water taxa; EF/ShW – epifaunal/shallow-water taxa.

Discussion

Well-scale depositional and chronostratigraphic interpretation

The interpretations below distinguish among evidence documented directly in core or thin section, age and environmental interpretations supported by fossil evidence, interpretations supported mainly by SP/RT logs or seismic geometry, and correlations inferred from the regional stratigraphic framework. Interpretations lacking direct core or fossil control are explicitly identified as tentative. The diagnostic observations and facies-association criteria are summarized in Tables 4 and 5; the following text focuses on their depositional and chronostratigraphic significance.

Špačince-4 well

Basal coarse-clastic interval, 3,356–3,259 m; C34–C33. The criteria summarized in Tab. 4 support high-energy, short-distance sediment transport within a proximal fan-delta or subaqueous debris-flow apron during early depocentre development, consistent with Blair (1999). The early lower Badenian age is regionally inferred.

Volcaniclastic interval, 3,259–3,125 m; C32–C30. The criteria summarized in Tab. 4 support volcaniclastic gravity-flow deposition in a fan-delta to subaqueous mass-flow system, consistent with Smith (1986). The massive zeolitized tuff may represent a subaqueous eruption-fed density current or secondary volcanoclastic deposit following the volcaniclastic model of Di Capua and Groppelli (2016) and Di Capua et al. (2023). Together, the interval indicates active volcanism, rapid sediment supply and early syn-rift subsidence. Its early lower Badenian age is regionally inferred.

Lower gravity-flow slope interval, 3,125–2,850 m; C29–C25. The criteria summarized in Tab. 4 indicate deposition from low-density turbidity currents and related fine-grained sediment-gravity flows in a slope to basin-floor setting, following the process framework of Talling et al. (2012). The abundance of agglutinated foraminifera and morphogroup ratios between ~3,003 and 2,849 m are compatible with upper- to middle-bathyal affinities only where the assemblages are plausibly in situ; taphonomic overprinting makes these palaeodepth estimates indicative rather than absolute. The FO of *Orbulina suturalis* and nannofossils including *Sphenolithus heteromorphus* and *Helicosphaera walbersdorfensis* constrain this interval to the lower Badenian (Langhian). The absence of reworked volcanic material within this interval suggests the waning and progressive burial of the volcanic centre. The presence of clasts derived from Eocene sandstones indicates predominantly sediment transport from the west, in contrast to the underlying and overlying volcanically dominated successions. High pyrite content in the heavy fraction, elevated relative S and detectable Mo, together with benthic taxa tolerant of low oxygen availability, are consistent with decreasing of oxygen in bottom waters during deposition of this interval.

Submarine channel-turbidite system, 2,850–2,150 m; C24–C16. The criteria summarized in Tab. 4 support episodic high-density sediment-gravity flows within a submarine channel system, alternating with lower-density turbidites and suspension settling, following the process criteria of Talling et al. (2012). The reappearance of a volcanic source within this interval may be explained in two ways: either by tectonically driven uplift and exhumation of the original volcanic center, and/or by renewed volcanic activity. Radioisotopic ages from volcanic material in the Kráľová-1 and Madunice-3 wells show that volcanic activity in this area began before 14.1 Ma and persisted until 13.83 Ma (Šarinová et al., 2021; Rybár et al., 2024). Consequently, the persistence of volcanic activity appears to represent the more plausible interpretation. The upward decrease in unstable clasts accompanied by an increasing proportion of quartz suggests progressive reworking of the material. Nannofossil assemblages with *S. heteromorphus* and *H. waltrans* support an NN5 lower Badenian (Langhian) age or younger.

Outer shelf-slope distal gravity-flow interval, 2,150–1,125 m; C15–C6. The criteria summarized in Tab. 4 support suspension-dominated outer-shelf to slope deposition with episodic distal gravity-flow or weak traction-current input, consistent with Talling et al. (2012). The occurrence of *Globorotalia bykovae* acme, small planktonic foraminiferal blooms, and *Bulimina-Bolivina*-dominated assemblages indicates an upper Badenian (lower Serravallian) age and is consistent with enhanced organic flux and locally reduced bottom- or pore-water oxygen availability, rather than providing a direct measure of water depth or redox state.

Shelf to marginal-marine interval, 1,125–625 m; C5–C1. No core from this interval was examined in the present study. Carbonized plant fragments and marine macrofauna reported by Gaža (1963), together with high-amplitude serrated SP and RT motifs, are consistent with progressive shallowing toward shelf to marginal-marine conditions. The interpretation remains tentative. The interval is regionally assigned to the upper Badenian, although a transition into the Sarmatian cannot be excluded. The systematic decrease in S values above a depth of approximately 905 m, approaching near-zero values, is consistent with a trend toward lower salinity. However, given the limitations of the dataset, this observation cannot be regarded as direct evidence of decreasing water salinity, although it may support the interpretation of a transition to a marginal-marine depositional setting.

Upper log-defined interval, 625–0 m. No core material or direct fossil control is available. High-amplitude serrated RT and medium-amplitude serrated SP patterns indicate variable clastic input. Shallow- to marginal-marine, deltaic and younger lacustrine–fluvial environments are inferred from the log character, seismic architecture and regional stratigraphic framework. The Sarmatian–Pannonian age assignment is therefore regionally inferred and tentative.

Dubové-2 well

Pre-Cenozoic basement interval, 3,000–2,780 m; C31–C24. Legacy lithological and log evidence summarized in Tab. 5 supports interpretation of this interval as Permian-Cretaceous pre-Cenozoic basement, with possible Hronic and/or Fatric nappe affinity based on Biela (1978) and Droppa et al. (2024). The high-amplitude symmetrical

Tab. 4
Facies associations of the. For explanations, see Tab. 2.

Depth/core	Analysed sample	Foraminiferal markers	Nannofossil markers	CPN zone	NN zone	Regional stage	Formation	Confidence	References
3,098–3,049 m; C29–C28	29/1–2/20; 29/1–2/80; 28/2/10; 28/2/80	No reliable zonal marker; poorly preserved agglutinated and benthic assemblages	Rare *Sphenolithus heteromorphus* and *Helicosphaera walbersdorfensis*; some specimens questionable	Not assigned	?NN5	lower Badenian, Langhian; tentative	Špačince Fm.	L–M:	
2,949–2,952 m; C26	26/1/60	*Orbulina suturalis*; *Saccammina grzybowskii*; *Dentoglobigerina altispira*	*Helicosphaera walbersdorfensis*; *H. carteri*; *Reticulofenestra pseudoumbilicus*	CPN7-8	?NN5	lower Badenian, Langhian	Špačince Fm.	M–H:	*Saccammina grzybowskii* FO: Cicha et al. (1998)
2,695–2,698 m; C21	21/1/90	Barren of diagnostic foraminifera	*Sphenolithus heteromorphus* and *Helicosphaera waltrans*	Not assigned	NN5	lower Badenian, Langhian / upper Badenian, lower Serravallian	Špačince/ Báhoň Fm.	H for NN zone	
2,298–2,303 m; C17	17/2/X	Reworked *Cassigerinella chipolensis*; no reliable in-situ foraminiferal marker	*Sphenolithus heteromorphus*;	Not assigned	NN5	lower Badenian, Langhian / upper Badenian, lower Serravallian	Špačince/ Báhoň Fm.	M:	
1,798–1,804 m; C12	12/1–2/X	Acme of *Globorotalia bykovae*; *Orbulina universa*; *Pappina neudorfensis*; *Bolivina dilatata*	*Coccolithus pelagicus* and ?*Calcidiscus pataecus*; no diagnostic zonal marker	CPN8, Bulimina/ Bolivina	Not assigned	upper Badenian, lower Serravallian	Báhoň Fm.	H for forams	*Globorotalia bykovae*; *Orbulina universa* – CPN8 (Gonera, 2013)
1,498–1,503 m; C9	9/1/X; 9/5/X	*Turborotalita quinqueloba*; *Globigerinella obesa*; *Bolivina dilatata brevis*	*Sphenolithus abies*; *R. pseudoumbilicus* > 7 µm; *Coronocyclus nitescens*; *Orthorhabdus rioi*;	Not assigned	NN6	upper Badenian, lower Serravallian	Báhoň Fm.	M–H	

Confidence and evidence codes: H – high confidence – directly observed in core and supported by fossil or independent evidence; M – moderate confidence – core-supported but age or environment depends partly on logs, seismic or regional correlation; L – low/tentative – no direct core or fossil control. C – core observation; P – petrography; F – fossil evidence; L – well logs; S – seismic evidence; R – regional correlation. Confidence may differ between process and age assignments.

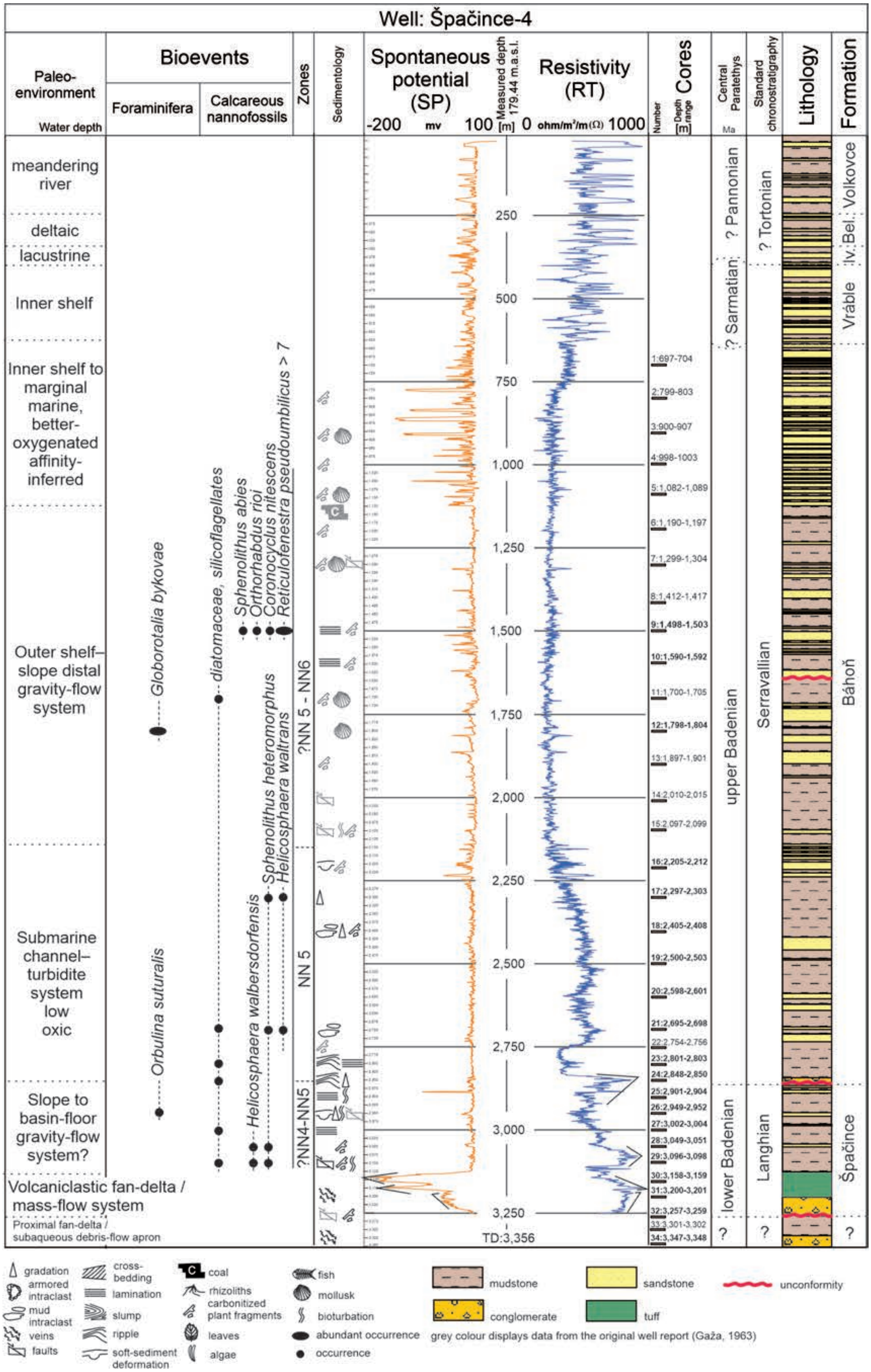
Well: Špačince-4
Paleo-environment
Water depth
Bioevents
Foraminifera
Calcareous nannofossils
Zones
Sedimentology
Spontaneous potential (SP)
-200 mv 100
Measured depth 179.44 m.a.s.l. [m]
Resistivity (RT)
0 ohm/m²/m(Ω) 1000
Number
Depth range [m]
Cores
Central Paratethys
Standard chronostratigraphy
Ma
Lithology
Formation
meandering river
deltaic
lacustrine
Inner shelf
Inner shelf to marginal marine, better-oxygenated affinity-inferred
Outer shelf–slope distal gravity-flow system
Submarine channel–turbidite system low oxic
Slope to basin-floor gravity-flow system?
Volcaniclastic fan-delta / mass-flow system
Proximal fan-delta / subaqueous debris-flow apron
Globorotalia bykovae
Orbulina suturalis
diatomaceae, silicoflagellates
Sphenolithus abies
Orthorhabdus rioi
Coronocyclus nitescens
Reticulofenestra pseudoumbilicus > 7
Sphenolithus heteromorphus
Helicosphaera waltrans
Helicosphaera walbersdorfensis
?NN 5 - NN6
NN 5
?NN4-NN5
250
500
750
1,000
1,250
1,500
1,750
2,000
2,250
2,500
2,750
3,000
3,250
TD:3,356
1:697-704
2:799-803
3:900-907
4:998-1003
5:1,082-1,089
6:1,190-1,197
7:1,299-1,304
8:1,412-1,417
9:1,498-1,503
10:1,590-1,592
11:1,700-1,705
12:1,798-1,804
13:1,897-1,901
14:2,010-2,015
15:2,097-2,099
16:2,205-2,212
17:2,297-2,303
18:2,405-2,408
19:2,500-2,503
20:2,598-2,601
21:2,695-2,698
22:2,754-2,756
23:2,801-2,803
24:2,848-2,850
25:2,901-2,904
26:2,949-2,952
27:3,002-3,004
28:3,049-3,051
29:3,096-3,098
30:3,158-3,159
31:3,200-3,201
32:3,257-3,259
33:3,301-3,302
34:3,347-3,348
? Pannonian
? Sarmatian
upper Badenian
lower Badenian
?
? Tortonian
Serravallian
Langhian
?
Volkovce
Iv.
Bel.
Vráble
Báhoň
Špačince
?
gradation
armored intraclast
mud intraclast
veins
faults
cross-bedding
lamination
slump
ripple
soft-sediment deformation
coal
rhizoliths
carbonitized plant fragments
leaves
algae
fish
mollusk
bioturbation
abundant occurrence
occurrence
mudstone
conglomerate
sandstone
tuff
unconformity
grey colour displays data from the original well report (Gaža, 1963)

Fig. 8. Integrated stratigraphic log of the Špačince-4 well showing palaeoenvironmental interpretation, fossil bioevents, and NN zones, sedimentary structures, SP and RT logs, core positions, lithology and formation assignments. Sarmatian and Pannonian assignments in intervals without direct fossil control are based on well-log, seismic and regional stratigraphic correlation and are considered tentative. Palaeodepth and redox interpretations derived from benthic assemblages are indicative and are subject to ecological, taphonomic and post-depositional controls.

to bell-shaped SP/RT responses are consistent with strong lithification and lithological contrasts following Rider and Kennedy (2011). A major hiatus separates the basement from the overlying Neogene succession.

Bioturbated sandstone interval, 2,780–2,720 m; C23. The criteria summarized in Tab. 5 support energetic shallow-marine shelf deposition involving tractional reworking and bioturbation, consistent with Howard and Reineck (1981). The symmetrical SP and funnel- to bell-shaped RT motifs indicate a discrete sand-rich body following Rider and Kennedy (2011). The precise shelf position remains uncertain, and gravity-influenced sand deposition cannot be excluded. The lower Badenian age is regionally inferred.

Sandy mudstone-muddy siltstone interval, 2,720–2,535 m; C22–C16. The criteria summarized in Tab. 5 support mixed suspension and distal gravity-flow deposition in a lower-energy outer-shelf to slope setting, following Talling et al. (2012). *Ciperoella ciperoensis* and rare ?*Helicosphaera ampliaperta* suggest a Karpatian to lower Badenian age, while the FO of *Saccammina grzybowskii* supports a Badenian (Langhian–lower Serravallian) assignment. The fossil evidence permits a Karpatian-Badenian assignment, whereas seismic and regional correlation favour a lower Badenian (Langhian) age.

Outer shelf-slope mudstone interval, 2,535–2,060 m; C15–C6. The criteria summarized in Tab. 5 support suspension-dominated outer-shelf to slope deposition, consistent with the fine-grained marine depositional framework of Macquaker et al. (2010). Agglutinated foraminiferal morphogroups from 2,503–2,212 m suggest bathyal-equivalent conditions if in situ, but sorting and dissolution may have modified the original assemblages. Benthic assemblages containing *Uvigerina macrocarinata*, *Lenticulina echinata*, *Pappina neudorfensis*, and *Uvigerina bellicostata*, together with *Sphenolithus heteromorphus*, constrain the interval mainly to Badenian (Langhian–lower Serravallian). Increased *Bulimina-Bolivina-Uvigerina* components are consistent with enhanced organic flux and locally reduced oxygen availability, but are not treated as direct depth indicators. The fossil evidence constrains the interval broadly to the Badenian, whereas seismic correlation favours a lower Badenian (Langhian) age.

Log-defined coarse-influx interval, 2,060–1,975 m. No core material is available from this interval. A pronounced high-amplitude symmetrical response is observed on both the SP and RT logs and is interpreted as a relatively sand-rich or coarse-clastic pulse. Possible explanations include a channelized sand body, a gravity-flow pulse or a sequence-stratigraphic surface associated with local tectonic or sediment-supply reorganization. Regional correlation suggests that the interval may correspond to the Langhian-Serravallian sea-level fall documented by Šarinová et al. (2021), but this event and age correlation remains tentative because it lacks direct core and fossil control.

Upper laminated mudstone and bioclastic interval, 1,975–470 m; C5–C1. The criteria summarized in Tab. 5 support low-energy marine suspension deposition interrupted by episodic reworked event beds, consistent with the event-bed framework of Kidwell et al. (1986). Fragmented macrofossils in shell-rich beds suggest storm, gravity-flow, or local mass-flow reworking. *Globorotalia bykovae*, *Globoturborotalita druryi*, and nannofossils near the NN5/NN6 boundary indicate an upper Badenian (lower Serravallian) age. The upward increase in shallow-water epiphytic forms suggests gradual shallowing in the upper part of the well.

Upper log-defined post-rift interval, < 470 m.

No core material or direct fossil control is available. High-amplitude serrated to symmetrical SP/RT responses indicate variable clastic input (Rider & Kennedy, 2011). Shallow-marine, marginal-marine, deltaic and younger lacustrine-fluvial environments are regionally inferred by comparison with the seismic architecture and published Danube Basin stratigraphy context (e.g., Šujan et al., 2016). The late syn-rift to post-rift interpretation and the Sarmatian-Pannonian age assignment are therefore tentative.

Seismic interpretation and well integration

The interpreted seismic profiles (lines 558_77, 558_86, 558a_86-Composite_1, and 554_77-Composite_2) image the structural framework and stratigraphic architecture of the Blatné sub-basin and adjacent areas (Figs. 10, 11). The profiles show a strongly asymmetric half-graben bounded by major listric normal faults that flatten downward and sole into the Paleozoic basement (Figs. 10, 11). This fault zone controlled Middle Miocene accommodation space and the thickness distribution of syn-rift deposits. The Paleozoic basement, together with overlying Late Paleozoic to Mesozoic cover and nappe units of the Inner Western Carpathians (Hók et al., 2014), forms a rugged

Tab. 5
Facies associations of the Dubové-2 well

Depth/core	Lithology	Structures	Fossils	SP/RT motif	Process/ environment; diagnostic criteria	Age	Confidence
3,000–2,780 m; C31–C24	Deformed shale, limestone, quartz arenite, sandstone and conglomerate	Tectonic deformation; primary structures poorly documented	No diagnostic fossil	High-amplitude symmetrical-bell SP/RT	Pre-Cenozoic basement; strong lithification, deformation and marked log contrasts	Permian–Cretaceous; possible Hronic/Fatric affinity	**M** Legacy C, L
2,780–2,720 m; C23	Massive-mottled bioturbated sandstone with carbonate clasts, quartz, feldspar, mica, chert, volcanics and glauconite	Massive, mottled and bioturbated	Bioclasts; glauconite	Symmetrical SP; funnel-bell RT	Energetic shallow-marine shelf; discrete sand body, bioturbation and probable tractional reworking. Exact shelf position uncertain	lower Badenian; regionally inferred	**M** C, L, R
2,720–2,535 m; C22–C16	Sandy mudstone-muddy siltstone; local very fine sandstone	Faint lamination, ripple/wavy fabric, diffuse grading, mud streaks, bioturbation	*G. ciperoensis, S. grzybowskii, rare H. ampliaperta*	Mainly serrated; minor high-amplitude excursions	Mixed suspension and distal gravity-flow deposition; fine grain size, diffuse grading and ripples; outer shelf-slope	lower Badenian favoured	**M–H** C, F, L, S
2,535–2,060 m; C15–C6	Mudstone, sandy mudstone and muddy siltstone	Massive-faintly laminated; bioturbated; coarse beds rare	Bivalves and micro-/ macrofauna; agglutinated forams; *S. heteromorphus*	Serrated SP/RT	Suspension-dominated outer shelf-slope; mud-dominated facies and scarcity of tractional beds	Badenian; lower Badenian favoured by seismic correlation	**M–H** C, F, S
2,060–1,975 m; uncored	Unknown	Not observed	No fossil control	High-amplitude symmetrical SP/RT	Log-defined coarse/ sand-rich influx; possible channel body, gravity-flow pulse or sequence surface	Tentative intra-Badenian event correlation	**L** L, R
1,975–470 m; C5–C1	Laminated mudstone-siltstone/fine sandstone; rare shell-rich beds	Parallel-wavy lamination; bioturbation; folding and partings	Fragmented macrofossils; *G. bykovae*, *G. druryi*; NN5/NN6 nannofossils	Low-amplitude serrated SP/RT	Low-energy suspension with reworked event beds; discrete shell-rich layers and fragmented fossils indicate storm/ gravity-flow reworking; upward shallowing	upper Badenian	**H** C, F, L
< 470 m; uncored	No core	Not observed	No direct fossil control	High-amplitude serrated-symmetrical SP/RT	Shallow-/marginal-marine, deltaic and younger lacustrine-fluvial deposition; inferred from logs, seismic and regional stratigraphy	Sarmatian–Pannonian; regionally inferred	**L** L, S, R

Confidence and evidence codes: H – high confidence – directly observed in core and supported by fossil or independent evidence; M – moderate confidence – coresupported but age or environment depends partly on logs, seismic or regional correlation; L – low/tentative – no direct core or fossil control. C – core observation; P – petrography; F – fossil evidence; L – well logs; S, seismic evidence; R – regional correlation. Confidence may differ between process and age assignments.

Fig. 9. Integrated stratigraphic log of the Dubové-2 well showing palaeoenvironmental interpretation, fossil bioevents, CPN and NN zones, sedimentary structures, SP and RT logs, core positions, lithology and formation assignments. Sarmatian and Pannonian assignments in intervals without direct fossil control are based on well-log, seismic and regional stratigraphic correlation and are considered tentative. Palaeodepth and redox interpretations derived from benthic assemblages are indicative and are subject to ecological, taphonomic and post-depositional controls.

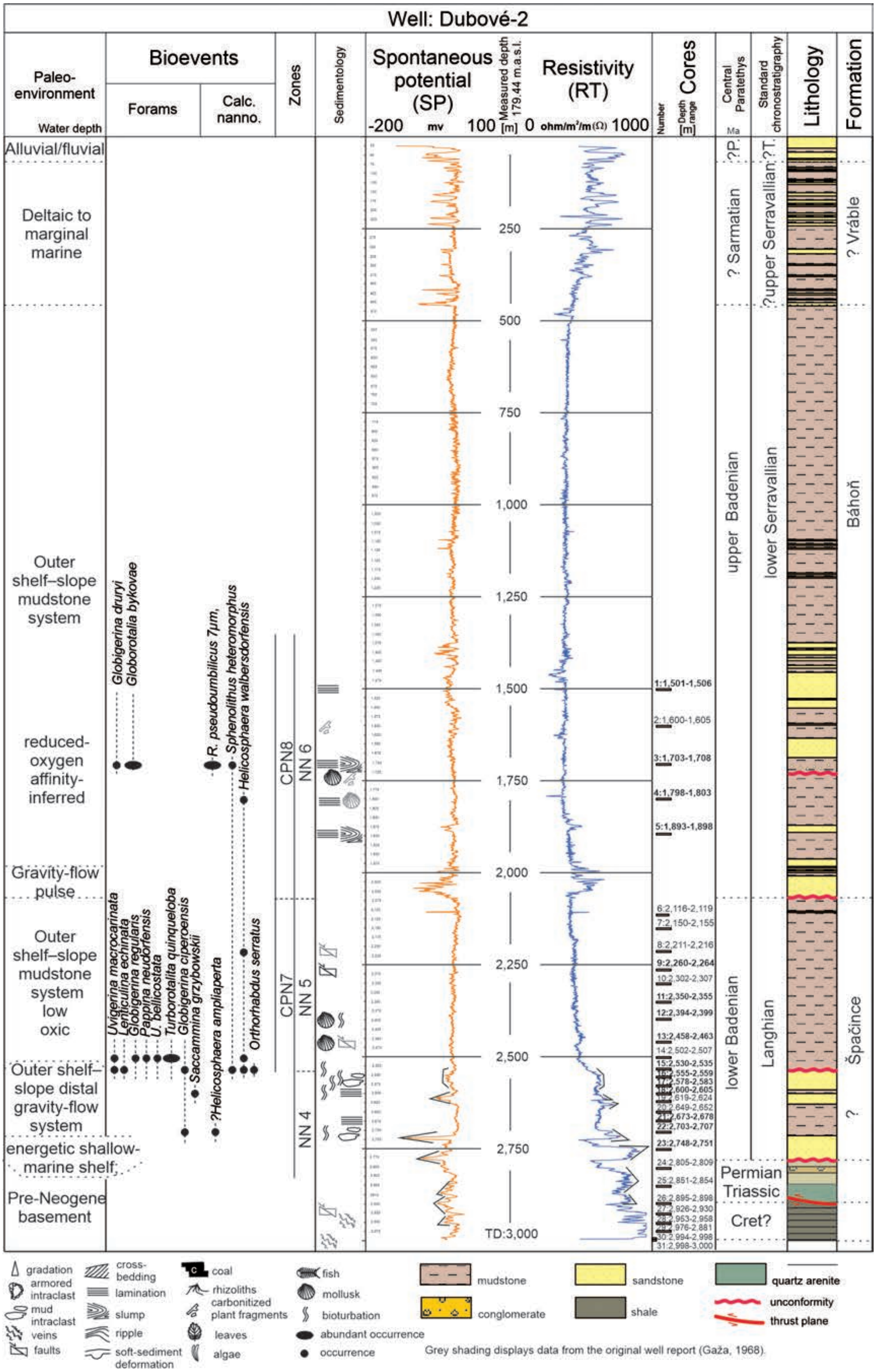
Well: Dubové-2
Paleo-environment
Water depth
Bioevents
Forams
Calc. nanno.
Zones
Sedimentology
Spontaneous potential (SP)
-200 mv 100
Measured depth 179.44 m.a.s.l.
[m]
Resistivity (RT)
0 ohm/m²/m(Ω) 1000
Number
Depth range [m]
Cores
Central Paratethys
Standard chronostratigraphy
Ma
Lithology
Formation
Alluvial/fluvial
Deltaic to marginal marine
Outer shelf–slope mudstone system
reduced-oxygen affinity-inferred
Gravity-flow pulse
Outer shelf–slope mudstone system low oxic
Outer shelf–slope distal gravity-flow system
energetic shallow-marine shelf
Pre-Neogene basement
Globigerina druryi
Globorotalia bykovae
R. pseudoumbilicus 7µm,
Sphenolithus heteromorphus
Helicosphaera walbersdorfensis
Uvigerina macrocarinata
Lenticulina echinata
Globigerina regularis
Pappina neudorfensis
U. bellicostata
Turborotalita quinqueloba
Globigerina ciperoensis
Saccammina grzybowskii
?Helicosphaera ampliaperta
Orthorhabdus serratus
CPN8
NN 6
CPN7
NN 5
NN 4
250
500
750
1,000
1,250
1,500
1,750
2,000
2,250
2,500
2,750
TD:3,000
1:1,501-1,506
2:1,600-1,605
3:1,703-1,708
4:1,798-1,803
5:1,893-1,898
6:2,116-2,119
7:2,150-2,155
8:2,211-2,216
9:2,260-2,264
10:2,302-2,307
11:2,350-2,355
12:2,394-2,399
13:2,458-2,463
14:2,502-2,507
15:2,530-2,535
23:2,748-2,751
24:2,805-2,809
25:2,851-2,854
26:2,895-2,898
31:2,998-3,000
?P.
? Sarmatian
upper Badenian
lower Badenian
?T.
?upper Serravallian
lower Serravallian
Langhian
Permian
Triassic
Cret?
? Vráble
Báhoň
Špačince
?
gradation
armored intraclast
mud intraclast
veins
faults
cross-bedding
lamination
slump
ripple
soft-sediment deformation
coal
rhizoliths
carbonitized plant fragments
leaves
algae
fish
mollusk
bioturbation
abundant occurrence
occurrence
mudstone
conglomerate
sandstone
shale
quartz arenite
unconformity
thrust plane
Grey shading displays data from the original well report (Gaža, 1968).

surface that deepens toward the basin centre (Figs. 10, 11). Thin and discontinuous Paleogene to Lower Miocene deposits are locally preserved on faulted structural highs in the northwestern part of the area, probably related to the Inner Carpathian Paleogene Basin and the Dobrá Voda Basin (Fig. 1). Above this surface, a thick Badenian syn-rift succession fills the half-graben. These deposits thicken toward the main fault zones and show inclined to divergent reflector geometries typical of growth strata (Gawthorpe et al., 1997; Figs. 10, 11). Their internal seismic facies are commonly chaotic to high-amplitude, locally corresponding to gravity-flow-dominated facies documented in the Špačince-4 and Dubové-2 wells (Figs. 8, 9). The lower Badenian (Langhian; Špačince Fm.; Vass, 2002) forms a laterally continuous seismic unit that thickens into the main depocentre and locally toward the eastern and southern basin margins, where large alluvial-fan to fan-delta bodies are preserved (Figs. 10, 11). Reflectors onlap intrabasinal highs and downlap toward the basin axis, consistent with active syn-rift deepening (Gawthorpe & Leeder, 2000). The overlying upper Badenian interval (lower Serravallian; Báhoň Fm.; Vass, 2002) is thicker and shows smoother reflector geometries, with downlap onto underlying units. This geometry indicates continued syn-rift subsidence (Gawthorpe & Leeder, 2000), but with higher sediment accumulation rates in line with models presented in Rybár et al. (2025). Above the Badenian growth packages, the seismic profiles show a regionally extensive, gently dipping package with limited thickness variation and common onlap onto the underlying syn-rift succession (Nøttvedt et al., 1995). This is overlain by comparatively subhorizontal reflectors that pond in the basin centre and thin across structural highs. Fault offsets also decrease upward. These seismic geometries indicate progressive basin infilling and waning fault activity. Based on correlation with the regional lithostratigraphic framework (e.g., Šujan et al., 2016), the onlapping package is inferred to represent the Sarmatian Vráble Formation (Vass, 2002), whereas the upper subhorizontal package is inferred to represent the Pannonian succession. The post-rift (Contreras et al., 1997) interpretation of the upper package is supported by its seismic geometry (Figs. 10, 11), but the detailed Sarmatian and Pannonian age assignments remain tentative because direct biostratigraphic control is absent.

Syn-rift sedimentation, marine deepening, and post-rift infilling of the Blatné sub-basin

The integrated well-log, core, micropalaeontological, and seismic data provide an opportunity to evaluate how the Blatné sub-basin (Fig. 1) evolved during the Badenian–Pannonian interval. The key question is how the variations between the Špačince-4 and Dubové-2 successions (Figs. 8, 9) reflect the timing of basin opening, changes in depositional environments, and the transition from syn-rift subsidence to post-rift infilling. We interpret these differences as the result of contrasting structural and depositional positions within an asymmetric Badenian half-graben, later modified by Sarmatian–Pannonian shallowing and progressive basin filling (Figs. 10, 11).

The principal advance of this study is the placement of the contrasting Špačince-4 and Dubové-2 successions within an asymmetric, fault-controlled half-graben and the reconstruction of their syn-rift to post-rift evolution. The basin-scale synthesis integrates core facies, biostratigraphy, palaeoecology, SP/RT logs and seismic architecture. Core and fossil evidence provide the strongest constraints, whereas interpretations based mainly on well logs, seismic geometry or uncored intervals are treated as lower confidence.

The contrasting successions in the Špačince-4 and Dubové-2 wells are interpreted as the result of different positions within the same evolving half-graben system. Špačince-4 contains a thicker syn-rift succession with basal coarse-clastic deposits, volcaniclastic material, and abundant gravity-flow facies (Figs. 2, 8), whereas Dubové-2 reaches pre-Neogene basement and contains a thinner Neogene succession beginning with sand-rich marine deposits (Figs. 3, 9). This interpretation is supported by the seismic architecture, which shows an asymmetric half-graben bounded by normal faults, syn-rift thickening toward fault zones, and growth-strata geometries (Figs. 10, 11). Špačince-4 was therefore probably located closer to an active depocentre and/or sediment-entry system, while Dubové-2 occupied a more marginal position, possibly near a structural high or fault block (Fig. 10). However, the observed contrast may also partly reflect local erosion, variable fault-block subsidence, or incomplete core and log control.

Lower Badenian deposition was strongly influenced by syn-rift subsidence and fault-controlled accommodation (Figs. 10, 11). In Špačince-4, basal paraconglomerates, volcanic conglomerate, zeolitized tuff, matrix-rich conglomerates, mudstone-siltstone intraclasts, chaotic fabrics, and locally erosive contacts (Fig. 2) indicate rapid sediment supply from unstable basin margins (Fig. 10). These core observations are consistent with the seismic evidence for growth strata and thickening toward normal faults (Fig. 10). Together, the data support deposition during active accommodation creation, short sediment-transport pathways, local volcanic input, and repeated gravity-flow activity along the margins of the developing depocentre. Nevertheless, the coverage of the volcanic sequence by non-volcanic sediments, followed by the renewed dominance of volcanic-derived material in the sedimentary record, suggests a temporary cessation of volcanic activity accompanied by burial of the volcanic centre. The sub-

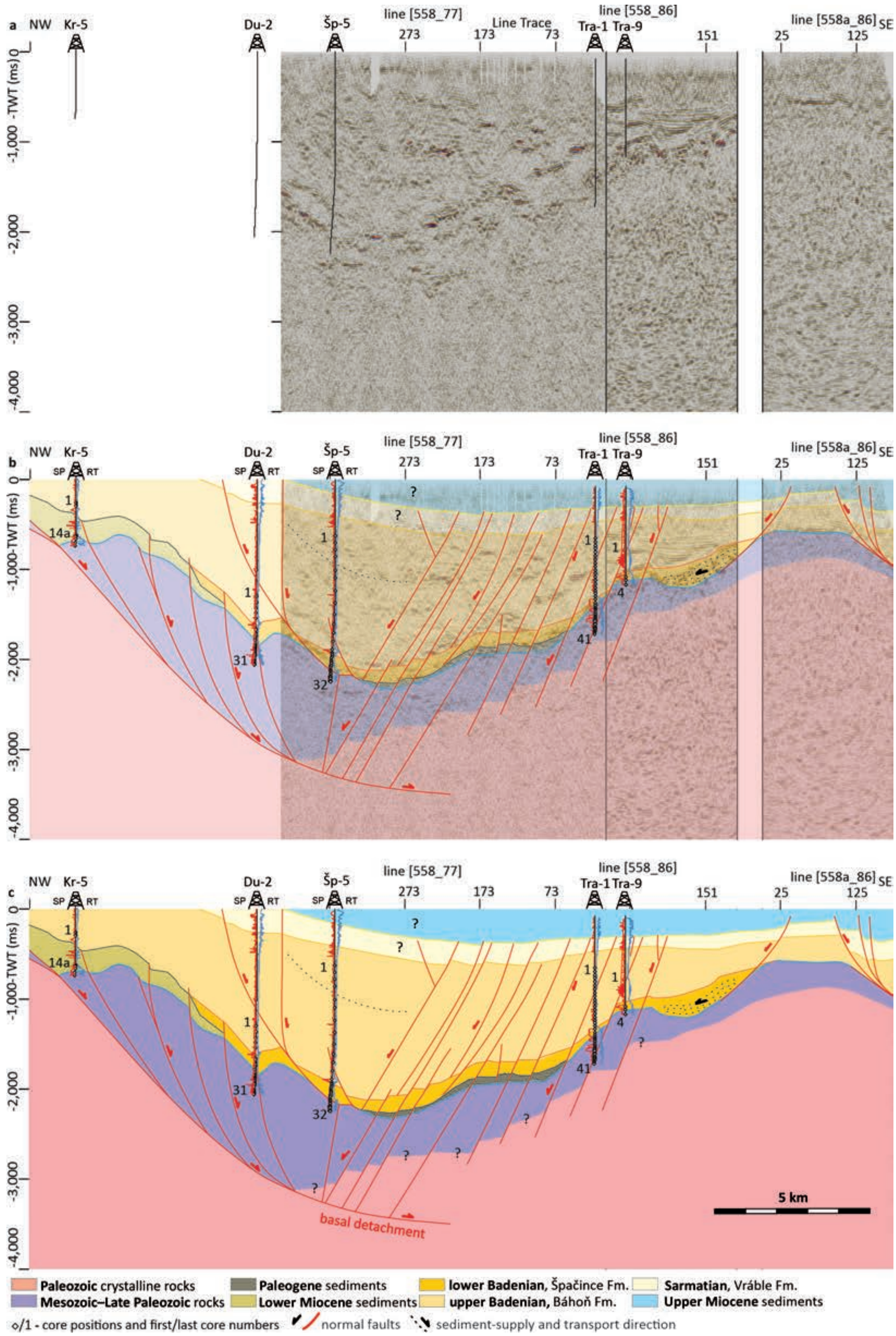

Fig. 10. Composite seismic profile 1 across the Blatné sub-basin. (a) Uninterpreted seismic data. (b) Seismic data with interpreted horizons, faults and well ties. (c) Geological interpretation. The Kr-5, Du-2, Šp-5, Tra-1 and Tra-9 wells provide lithological and well-log control. The vertical axis shows two-way travel time in milliseconds; horizontal distance and trace positions are indicated. Stratigraphic colours, faults, core positions and sediment-transport directions are explained in the legend. Sarmatian and Pannonian assignments in intervals without direct fossil control are based on seismic, well-log and regional stratigraphic correlation and are considered tentative.

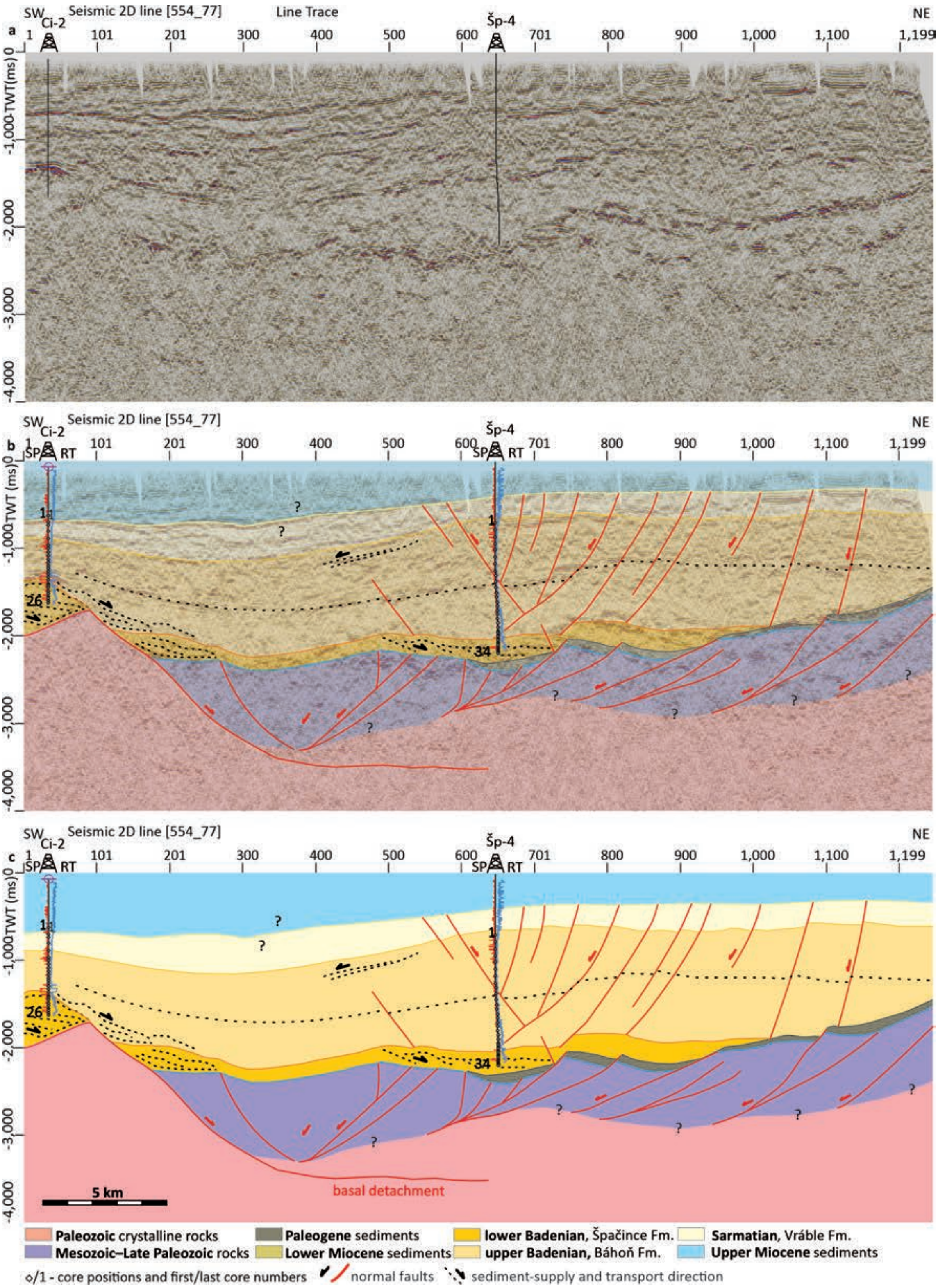

Fig. 11. Composite seismic profile 2, based on line 554_77, across the Blatné sub-basin. (a) Uninterpreted seismic data. (b) Seismic data with interpreted horizons, faults and well ties. (c) Geological interpretation. The Ci-2 and Šp-4 wells provide lithological and well-log control. The vertical axis is two-way travel time in milliseconds; the horizontal scale is displayed. Stratigraphic colours, faults and sediment-transport directions are explained in the legend. Sarmatian and Pannonian assignments without direct fossil control are tentative.

sequent reappearance of volcanic material is most plausibly linked to the renewal of volcanic activity. Although less likely, renewed exposure of the volcanic source due to tectonic uplift or a fall in sea level cannot be entirely excluded.

During the upper Badenian, marine environments developed unevenly across the sub-basin. Fine-grained mudstone-siltstone intervals, low-density turbidites, distal gravity-flow deposits, and suspension-dominated facies indicate outer shelf to shelf-slope deposition in both wells (Figs. 2, 3, 8, 9). Agglutinated foraminiferal morphogroups are compatible with bathyal-equivalent conditions in several intervals, particularly where they are interpreted as in situ (Figs. 4–7). However, poor preservation, dissolution, sorting, reworking, and the presence of damaged tests and moulds show that the original assemblages were locally modified. *Bulimina-Bolivina-Uvigerina*-rich assemblages indicate enhanced organic flux and locally reduced oxygenation rather than water depth alone, because benthic foraminiferal distributions are controlled mainly by food supply, organic flux, and oxygen availability (Jorissen et al., 1995; Van der Zwaan et al., 1999; Hayward et al., 2002). The occurrence of dysoxia-tolerant taxa, together with laminated fine-grained sediments, weak to variable bioturbation, phytoclasts, and terrestrial organic input, suggests enhanced organic flux to the sea floor. Reduced oxygenation may therefore reflect enhanced organic-matter production and export, limited ventilation caused by stratification or restricted circulation, and reduced oxygen exposure during rapid sediment accumulation and burial (Demaison & Moore, 1980; Hartnett et al., 1998; den Dulk et al., 2000; Rabalais et al., 2010). The XRF evidence is used only as supporting information. Elevated relative S and detectable Mo may be associated with reducing conditions, but they may also reflect early-diagenetic pyrite formation, organic-matter preservation, sediment mineralogy and provenance, or salinity effects (Tribovillard et al., 2006). Without independent mineralogical, organic-carbon or Fe-speciation data, bottom-water and pore-water redox conditions cannot be distinguished confidently.

The high-amplitude SP and RT interval in Dubové-2 between 2060 and 1975 m (Fig. 9) may represent a short-lived increase in sandier or coarser clastic input (Rider & Kennedy, 2011). It is tentatively correlated with the coarse gravity-flow interval in Špačince-4 at 2,848–2,850 m (Fig. 8) and may correspond to a sediment-supply pulse or sequence-stratigraphic surface (Coe et al., 2003) near the Langhian/Serravallian, intra-Badenian boundary, similar to the event described from the Madunice well series area by Šarinová et al. (2021) dated to ~13.8Ma. However, this interpretation remains tentative because the Dubové-2 interval is not core-confirmed (Fig. 9). Alternative explanations include local channelized deposition (Posamentier & Kolla, 2003), fault-controlled sediment routing within the evolving half-graben system (Gawthorpe & Leeder, 2000), or a lithological/log response that cannot be confidently interpreted as a basin-wide sequence-stratigraphic surface without additional regional correlation and stratal-geometry evidence (Catuneanu et al., 2009).

The well-based interpretation is consistent with the regional model of the Blatné sub-basin, where lower Badenian basin opening during Rift 1 was followed by continued upper Badenian syn-rift subsidence during Rift 2. The Sarmatian interval remains tectonically ambiguous. The upper subhorizontal seismic succession of Pannonian age is interpreted as post-rift, although its detailed correlation is only inferred by regional data (Šujan et al., 2016, 2021; Rybár et al., 2025). The lower Badenian coarse-clastic, volcaniclastic, and gravity-flow deposits in Špačince-4 (Figs. 2, 8) support the interpretation of an actively subsiding Blatné depocentre during the early syn-rift stage and are compatible with regional evidence for Middle Miocene volcanic activity around the Langhian/Serravallian transition (Šarinová et al., 2021; Rybár et al., 2024, 2025). The upper Badenian mudstone–siltstone and gravity-flow intervals can be correlated with the marine Špačince and Báhoň/Pozba formations, whereas the overlying shallowing trend and log-defined upper intervals are consistent with the transition toward the Vráble Formation and later Ivanka-Beladice-Volkovce depositional systems sensu Vass (2002) and Šujan et al. (2016, 2021). Compared with the Madunice well series on the eastern basin margin (Šarinová et al., 2021), the Špačince-4 and Dubové-2 data indicate that facies distribution was strongly controlled by local depocentre architecture, fault-block position, and sediment-entry pathways (Figs. 10, 11).

The volcaniclastic component may include reworked older or nearby deposits rather than exclusively primary eruptive input (Schneider et al., 2001), although contemporaneous volcanism is documented in neighbouring wells (Šarinová et al., 2021; Rybár et al., 2024). The resulting short transport pathways and localized sediment entry are consistent with fault-controlled sediment routing in extensional basins (Gawthorpe & Leeder, 2000).

Several limitations should be considered when evaluating this interpretation. Core coverage is incomplete, particularly in the upper parts of both wells (Figs. 2, 3, 8, 9), where depositional environments are inferred mainly from SP/RT log motifs, seismic architecture (Figs. 8–11), and regional stratigraphic correlation (Šujan et al., 2016, 2021; Šarinová et al., 2021; Rybár et al., 2024, 2025) rather than direct lithological evidence. Foraminiferal preservation is poor in several intervals, and agglutinated assemblages may have been affected by dissolution, sorting, and reworking; therefore, palaeodepth estimates based on these assemblages should be treated as indicative rather than absolute (Figs. 4–7). The Sarmatian and especially Pannonian interpretations are partly inferred from seismic and log-defined patterns calibrated by the regional lithostratigraphic framework. Similarly, the proposed correlation between the Dubové-2 high-amplitude interval at 2,060–1,975 m and the Špačince-4 coarse gravity-flow interval at 2,848–2,850 m remains tentative because the Dubové-2 interval lacks core confirmation (Figs. 8, 9).

The integrated data support a five-stage conceptual depositional model for the Badenian-Pannonian evolution of the Blatné sub-basin. (1) During the early lower Badenian, fault-controlled accommodation created a rapidly subsiding depocentre supplied by proximal coarse-clastic, debris-flow and fan-delta systems. This interval was also associated with volcanic activity, which ceased in this area at approximately 13.8 Ma (Šarinová et al., 2021). (2) Continued lower- to upper-Badenian subsidence was accompanied by marine transgression and deepening, leading to outer-shelf-slope to basin-floor deposition dominated by turbidites, debris flows and suspension settling, with locally bathyal-equivalent benthic assemblages where preservation permits and the assemblages are plausibly in situ. (3) During the late upper Badenian, high sediment supply and enhanced organic and nutrient flux accompanied fine-grained marine sedimentation and evidence consistent with locally reduced bottom- or pore-water oxygen availability. (4) A regionally inferred Sarmatian interval records progressive shallowing, increasing terrestrial influence and a transition towards restricted to marginal-marine environments. (5) The upper subhorizontal seismic package is tentatively correlated with the Pannonian and interpreted as a post-rift infill system characterized by aggradation and deltaic, lacustrine and fluvial sedimentation (Figs. 10, 11).

The present results refine, rather than replace, the established regional tectonic model of the Danube Basin. The integrated data show that lower Badenian basin opening was expressed differently within individual fault blocks: Špačince-4 records initial coarse-clastic and volcaniclastic deposition followed by marine deepening, whereas Dubové-2 records a thinner marine succession directly overlying pre-Neogene basement. Seismic growth strata and faultward thickening indicate that Špačince-4 occupied a position closer to the active depocentre, while Dubové-2 was situated closer to a structural high or marginal fault block. Nevertheless, the correlation of the uncored 2,060–1,975 m interval in Dubové-2 with the intra-Badenian coarse-clastic event, as well as the detailed age assignment of the Sarmatian–Pannonian upper intervals, remains tentative.

Conclusions

The integrated data support a conceptual depositional model for the Badenian-Pannonian evolution of the Blatné sub-basin:

(1) Calcareous nannofossils and foraminifera constrain the studied Neogene succession mainly to the lower–upper Badenian (Langhian–lower Serravallian). Nannofossil assemblages document NN4–NN6 zones, and planktonic foraminifera locally indicate CPN7–CPN8 zones. Important stratigraphic markers include *Orbulina suturalis, Globorotalia bykovae* acme, *?Helicosphaera ampliaperta, Sphenolithus heteromorphus, Sphenolithus abies* and large *Reticulofenestra pseudoumbilicus > 7 µm.* Sarmatian-Pannonian deposits are inferred mainly from upper log-defined and seismic intervals.

(2) Continued lower to upper Badenian subsidence was accompanied by marine transgression and deepening, leading to outer-shelf-slope to basin-floor deposition dominated by turbidites, debris flows and suspension settling, with locally bathyal-equivalent benthic assemblages where preservation permits and the assemblages are plausibly in situ.

(3) During the late upper Badenian, fine-grained marine sedimentation coincided with high sediment input, increased organic-matter and nutrient fluxes, and evidence of locally reduced oxygen availability in bottom waters or pore waters.

(4) Where sufficiently preserved and plausibly in situ, agglutinated-foraminiferal morphogroups are compatible with bathyal-equivalent conditions in several Badenian intervals. These palaeodepth estimates remain indicative because of dissolution, selective preservation, sorting, reworking and poor test preservation. *Bulimina-Bolivina-Uvigerina*-rich assemblages are consistent with enhanced organic flux and locally reduced bottom- or pore-water oxygen availability rather than water depth alone.

(5) Seismic profiles show that Badenian deposition occurred within an asymmetric half-graben controlled by listric normal faults soling into a low-angle detachment. Lower–upper Badenian (Langhian–lower Serravallian) strata thicken toward major faults and display growth-strata geometries, indicating active syn-rift subsidence. The onlap of an upper seismic package, regionally inferred to be Sarmatian (upper Serravallian), together with the upward decrease in fault offset, indicates waning tectonic activity, although it remains uncertain whether this package represents the final syn-rift stage or a transitional phase. The overlying subhorizontal reflectors are tentatively correlated with the Pannonian (Tortonian) succession and interpreted as evidence of major fault cessation and post-rift aggradation.

(6) The Špačince-4 and Dubové-2 successions represent different structural and depositional positions within the Blatné sub-basin. Špačince-4 was located closer to an active depocentre and sediment-entry system, whereas Dubové-2 occupied a more marginal position near a structural high or a fault block. This explains the contrast between the thick coarse-clastic/volcaniclastic gravity-flow succession in Špačince-4 and the thinner marine succession above basement in Dubové-2.

(7) Overall, the integrated data record a transition from Badenian fault-controlled syn-rift sedimentation to regionally inferred Sarmatian shallowing and tentatively correlated Pannonian post-rift deltaic-lacustrine-fluvial infilling.

Acknowledgements

We thank NAFTA, a. s., for access to its core repository and permission to sample. This work was supported by the APVV agency under contracts APVV-22-0523, APVV-23-0227 and APVV-20-0079, and by VEGA project 2/0106/23. The study was also funded by the EU NextGenerationEU through the Recovery and Resilience Plan for Slovakia under project 09I03-03-V04-00127. We also thank Schlumberger Ltd. for providing a Petrel software licence and Prof. M. Kováč for insightful comments. We are grateful to the editor and reviewer O. Pelech and to the anonymous reviewer.

References

Balázs, A., Matenco, L., Magyar, I., Horváth, F. & Cloetingh, S., 2016: The link between tectonics and sedimentation in back-arc basins: New genetic constraints from the analysis of the Pannonian Basin. *Tectonics*, 35, 6, 1526–1559. https://doi.org/10.1002/2015TC004109.

Balázs, A., Matenco, L., Granjeon, D., Alms, K., François, T. & Sztanó, O., 2021: Towards stratigraphic-thermo-mechanical numerical modelling: Integrated analysis of asymmetric extensional basins. *Global and Planetary Change*, 196, 103386. https://doi.org/10.1016/j.gloplacha.2020.103386.

Bartol, M., 2009: Middle Miocene calcareous nannoplankton of NE Slovenia (Western Central Paratethys). *Paleontološki institut Ivana Rakovca ZRC SAZU*, 1–136.

Biela, A., 1978: Hlboké vrty v zakrytých oblastiach Vnútorných Západných Karpát [Deep boreholes in the Western Carpathian basins.] *Regionálna geológia Západných Karpát*, 10, 1–224 (in Slovak).

Biely, A. (ed.), Bezák, V., Elečko, M., Kaličiak, M., Konečný, V., Lexa, J., Mello, J., Nemčok, J., Potfaj, M., Rakús, M., Vass, D., Vozár, J. & Vozárová, A., 1996: Explanation to the Geological Map of Slovakia 1 : 500 000. *Bratislava, Dionýz Štúr Publishers*, 76 pp. https://www.geology.sk/wp-content/uploads/documents/foto/geol_mapy_rep_500k1M/1995_Geologicka_mapa_SR_Biely_500000/pdf/Vysv_1-500_000_Explanation-to-geological-map-of-Slovakia_Biely.pdf.

Blair, T. C., 1999: Sedimentology of the debris-flow-dominated Warm Spring Canyon alluvial fan, Death Valley, California. *Sedimentology*, 46, 5, 941–965. https://doi.org/10.1046/j.1365-3091.1999.00260.x.

Boggs, S. Jr., 2006: Principles of sedimentology and stratigraphy, 4th edition. *Pearson Prentice Hall, Upper Saddle River*, 662 pp.

Bojar, A.-V., Barbu, V., Wojtowicz, A., Bojar, H.-P., Hałas, S. & Duliu, O. G., 2018: Miocene Slănic Tuff, Eastern Carpathians, Romania, in the context of the Badenian Salinity Crisis. *Geosciences*, 8, 2, 73. https://doi.org/10.3390/geosciences8020073.

Boltovskoy, E., 1976: Distribution of recent foraminifera of the South American region. In: Hedley, R. H. & Adams, C. G. (eds.): Foraminifera, Volume 2. *London, Academic Press*, 171–236.

Boltovskoy, E. & Wright, R., 1976: Recent Foraminifera. *W. Junk, The Hague*, 515 pp.

Bown, P. R. (ed.), 1998: Calcareous nannofossil biostratigraphy. *London, Chapman & Hall*, 315 pp.

Catuneanu, O., Abreu, V., Bhattacharya, J. P., Blum, M. D., Dalrymple, R. W., Eriksson, P. G., Fielding, C. R., Fisher, W. L., Galloway, W. E., Gibling, M. R., Giles, K. A., Holbrook, J. M., Jordan, R., Kendall, C. G. St. C., Macurda, B., Martinsen, O. J., Miall, A. D., Neal, J. E., Nummedal, D., Pomar, L., Posamentier, H. W., Pratt, B. R., Sarg, J. F., Shanley, K. W., Steel, R. J., Strasser, A., Tucker, M. E. & Winker, C., 2009: Towards the standardization of sequence stratigraphy. *Earth-Science Reviews*, 92, 1–2, 1–33. https://doi.org/10.1016/j.earscirev.2008.10.003.

Chernyshev, I. V., Konečný, V., Lexa, J., Kovalenker, V. A., Jeleň, S., Lebedev, V. A. & Goltsman, Y. V., 2013: K-Ar and Rb-Sr geochronology and evolution of the Štiavnica Stratovolcano, Central Slovakia. *Geologica Carpathica*, 64, 4, 327–360. https://doi.org/10.2478/geoca-2013-0023.

Cicha, I., Čtyroká, J., Jiříček, R. & Zapletalová, I., 1975: Principal biozones of the Late Tertiary in Eastern Alps and West Carpathians. In: Cicha, I. (ed.): Biozonal division of the Upper Tertiary basins of the Eastern Alps and West Carpathians. *Bratislava, IUGS Proceedings of the VI Congress*, 19–34.

Cicha, I., Rögl, F., Rupp, Ch. & Čtyroká, J., 1998: Oligocene-Miocene foraminifera of the Central Paratethys. *Abhandlungen der Senckenbergischen Naturforschenden Gesellschaft*, 549, 1–325.

Coe, A. L., Bosence, D. W. J., Church, K. D., Flint, S. S., Howell, J. A. & Wilson, R. C. L., 2003: The sedimentary record of sea-level change. *Cambridge, Cambridge University Press*, 288 pp.

Contreras, J., Scholz, C. H. & King, G. C. P., 1997: A model of rift basin evolution constrained by first-order stratigraphic observations. *Journal of Geophysical Research: Solid Earth*, 102, B4, 7673–7690. https://doi.org/10.1029/96JB03832.

Demaison, G. J. & Moore, G. T., 1980: Anoxic environments and oil source bed genesis. *Organic Geochemistry*, 2, 1, 9–31. https://doi.org/10.1016/0146-6380(80)90017-0.

Droppa, D. M., Hók, J., Rybár, S., Vojtko, R., Pelech, O., Kronome, B., Bielik, M., Šujan, M. & Šipka, F., 2024: Tectonic map of the pre-Cenozoic basement of the northern Danube Basin. *Geologica Carpathica*, 75, 6, 375–386. https://doi.org/10.31577/GeolCarp.2024.24.

den Dulk, M., Reichart, G. J., van Heyst, S., Zachariasse, W. J. & van der Zwaan, G. J., 2000: Benthic foraminifera as proxies of organic matter flux and bottom water oxygenation? A case history from the northern Arabian Sea. *Palaeogeography, Palaeoclimatology, Palaeoecology*, 161, 3–4, 337–359. https://doi.org/10.1016/S0031-0182(00)00074-2.

Di Capua, A. & Groppelli, G., 2016: Emplacement of pyroclastic density currents (PDCs) in a deep-sea environment: The Val d'Aveto Formation case, Northern Apennines, Italy. *Journal of Volcanology and Geothermal Research*, 328, 1–8. https://doi.org/10.1016/j.jvolgeores.2016.08.003.

Di Capua, A., De Rosa, R., Kereszturi, G., Le Pera, E., Rosi, M. & Watt, S. F. L., 2023: Volcanically-derived deposits and sequences: a unified terminological scheme for application in modern and ancient environments. *Geological Society, London, Special Publications*, 520, 11–27. https://doi.org/10.1144/SP520-2021-201.

Emery, D. & Myers, K. J., 1996: Sequence stratigraphy. *Oxford, Blackwell Science,* 297 pp. https://doi.org/10.1002/9781444313710.

Fischer, K. C. & Veeken, P., 2015: Seismic and sequence stratigraphy. *Montan Universität,* 112 pp.

Fodor, L., Balázs, A., Csillag, G., Dunkl, I., Héja, G., Jelen, B., Kelemen, P., Kövér, S., Németh, A., Nyíri, D., Selmeczi, I., Trajanova, M., Vrabec, M. & Vrabec, M., 2021: Crustal exhumation and depocenter migration from the Alpine orogenic margin towards the Pannonian extensional back-arc basin controlled by inheritance. *Global and Planetary Change*, 201, 103475. https://doi.org/10.1016/j.gloplacha.2021.103475.

Fordinál, K. & Elečko, M., 2000: Ripnianske súvrstvie – sladkovodné sedimenty sarmatu a spodného panónu rišňovskej priehlbiny. *Mineralia Slovaca*, 32, 1, 55–60.

Fusán, O., Biely, A., Ibrmajer, J., Plančár, J. & Rozložník, L., 1987: Basement of the Tertiary of the Inner Western Carpathians. *Bratislava, Geological Institute of Dionýz Štúr* (in Slovak).

Csibri, T., Rybár, S., Šarinová, K., Jamrich, M., Sliva, Ľ. & Kováč, M., 2018: Miocene fan delta conglomerates in the north-western part of the Danube Basin: provenance, paleoenvironment, paleotransport and depositional mechanisms. *Geologica Carpathica*, 69, 5, 467–482. https://doi.org/10.1515/geoca-2018-0027.

Gaža, B., 1963: Záverečná geologická správa o pionierskom vrte Špačince-4. Manuscript. Plavecký Štvrtok, Archive of Nafta.

Gaža, B., 1968: Záverečná geologická správa o pionierskom vrte Dubové-2. Manuscript. Plavecký Štvrtok, Archive of Nafta.

Gawthorpe, R. L., Sharp, I., Underhill, J. R. & Gupta, S., 1997: Linked sequence stratigraphic and structural evolution of propagating normal faults. *Geology*, 25, 9, 795–798. https://doi.org/10.1130/0091-7613(1997)025%3C0795:LSSASE%3E2.3.CO;2.

Gawthorpe, R. L. & Leeder, M. R., 2000: Tectono-sedimentary evolution of active extensional basins. *Basin Research*, 12, 3–4, 195–218. https://doi.org/10.1111/j.1365-2117.2000.00121.x.

Gonera, M., 2013: Globorotaliid intervals of the sub-evaporite Badenian, Middle Miocene, in the Upper Silesia Basin, Central Paratethys, Poland. *Geological Quarterly*, 57, 4, 757–768. https://doi.org/10.7306/gq.1125.

Grill, R., 1941: Stratigraphische Untersuchungen mit Hilfe von Mikrofaunen im Wiener Becken und den benachbarten Molasse-anteilen. *Öl und Kohle*, 37, 31, 595–602.

Harangi, S., Vaselli, O., Tonarini, S., Szabó, C., Harangi, R. & Coradossi, N., 1995: Petrogenesis of Neogene extension-related alkaline volcanic rocks of the Little Hungarian Plain Volcanic Field (Western Hungary). *Acta Vulcanologica,* 7, 2, 173–187.

Harangi, S. & Lenkey, L., 2007: Genesis of the Neogene to Quaternary volcanism in the Carpathian-Pannonian region: Role of subduction, extension, and mantle plume. In: Beccaluva, L., Bianchini, G. & Wilson, M. (eds.): Cenozoic volcanism in the Mediterranean area. *Geological Society of America Special Paper*, 418, 67–92. https://doi.org/10.1130/2007.2418(04).

Harangi, S., Seghedi, I. & Lukács, R., 2025: The Neogene-Quaternary volcanism of the Carpathian-Pannonian region: from initial plate tectonic models to quantitative petrogenetic explanations. In: Tari, G. C., Kitchka, A., Krézsek, C., Lučić, D., Markič, M., Radivojević, D., Sachsenhofer, R. F. & Šujan, M. (eds.): The Miocene Extensional Pannonian Superbasin, Volume 1: Regional Geology. *Geological Society, London, Special Publications*, 554 pp. https://doi.org/10.1144/SP554-2024-84.

Hartnett, H. E., Keil, R. G., Hedges, J. I. & Devol, A. H., 1998: Influence of oxygen exposure time on organic carbon preservation in continental margin sediments. *Nature,* 391, 572–575. https://doi.org/10.1038/35351.

Hayward, B. W., Neil, H., Carter, R., Grenfell, H. R. & Hayward, J. J., 2002: Factors influencing the distribution patterns of Recent deep-sea benthic foraminifera, east of New Zealand, Southwest Pacific Ocean. *Marine Micropaleontology*, 46, 1–2, 139–176. https://doi.org/10.1016/S0377-8398(02)00047-6.

Hohenegger, J., 2005: Estimation of environmental paleogradient values based on presence/absence data: A case study using benthic foraminifera for paleodepth estimation. *Palaeogeography, Palaeoclimatology, Palaeoecology,* 217, 115–130.

Hohenegger, J., Ćorić, S. & Wagreich, M., 2014: Timing of the Middle Miocene Badenian Stage of the Central Paratethys. *Geologica Carpathica*, 65, 1, 55–66. https://doi.org/10.2478/geoca-2014-0004.

Hók, J., Šujan, M. & Šipka, F., 2014: Tectonic division of the Western Carpathians: An overview and a new approach. *Acta Geologica Slovaca*, 6, 2, 135–143.

Hók, J., Kováč, M., Pelech, O., Pešková, I., Vojtko, R. & Králiková, S., 2016: The Alpine tectonic evolution of the Danube Basin and its northern periphery, southwestern Slovakia. *Geologica Carpathica*, 67, 5, 495–505. https://doi.org/10.1515/geoca-2016-0031.

Holcová, K., 1997: Can detailed sampling and taphonomical analysis of foraminiferal assemblages offer new data for paleoecological interpretations? *Revue de Micropaléontologie*, 40, 4, 313–329. https://doi.org/10.1016/S0035-1598(97)90664-4.

Holbourn, A., Kuhnt, W., Clemens, S., Prell, W. & Andersen, N., 2013: Middle to late Miocene stepwise climate cooling: Evidence from a high-resolution deep water isotope curve spanning 8 million years. *Paleoceanography*, 28, 1–12.

Horváth, F., 1995: Phases of compression during the evolution of the Pannonian Basin and its bearing on hydrocarbon exploration. *Marine and Petroleum Geology*, 12, 8, 837–844. https://doi.org/10.1016/0264-8172(95)98851-U.

Horváth, F., Bada, G., Szafián, P., Tari, G., Ádám, A. & Cloetingh, S., 2006: Formation and deformation of the Pannonian Basin: Constraints from observational data. In: Gee, D. G. & Stephenson, R. A. (eds.): European lithosphere dynamics. *Geological Society, London, Memoirs*, 32, 191–206.

Horváth, F., Musitz, B., Balázs, A., Végh, A., Uhrin, A., Nádor, A., Koroknai, B., Pap, N., Tóth, T. & Wórum, G., 2015: Evolution of the Pannonian Basin and its geothermal resources. *Geothermics*, 53, 328–352.

Howard, J. D. & Reineck, H.-E., 1981: Depositional facies of high-energy beach-to-offshore sequence: Comparison with low-energy sequence. *AAPG Bulletin*, 65, 5, 807–830. https://doi.org/10.1306/2F919B0C-16CE-11D7-8645000102C1865D.

Hrušecký, I., 1999: Central part of the Danube Basin in Slovakia: Geophysical and geological model in regard to hydrocarbon prospection. *Exploration Geophysics, Remote Sensing and Environment*, 6, 1, 2–55.

Hudáčková, N. H., Kováč, M., Ruman, A., Halásová, E., Jamrich, M., Kováčová, M., Rybár, S., Šujan, M. & Šarinová, K., 2018: Biostratigraphy and paleoenvironmental interpretation of the Špačince-4 and Dubové-2 wells. Unpublished technical report, Order No. 45045664, prepared for NAFTA a.s. GEMINI. *Bratislava, Association of the Faculty of Natural Sciences, Comenius University in Bratislava and PRICOM*, 35 pp.

Haunold, T. G., 1995: Zur Taxonomie, Systematik und stratigraphischen Bedeutung uvigerinider Foraminiferen im Neogen des Wiener Beckens und benachbarter Gebiete – 40 Jahre nach Papp & Turnowsky (1953). *Jahrbuch der Geologischen Bundesanstalt*, 138, 1, 67–87.

Jorissen, F. J., de Stigter, H. C. & Widmark, J. G. V., 1995: A conceptual model explaining benthic foraminiferal microhabitats. *Marine Micropaleontology*, 26, 1–4, 3–15. https://doi.org/10.1016/0377-8398(95)00047-X.

Karátson, D., Márton, E., Harangi, S., Józsa, S., Balogh, K., Pécskay, Z., Kovácsvölgyi, S., Szakmány, Gy. & Dulai, A., 2000: Volcanic evolution and stratigraphy of the Miocene Börzsöny Mountains, Hungary: An integrated study. *Geologica Carpathica*, 51, 5, 325–343.

Karátson, D., Oláh, I., Pécskay, Z., Márton, E., Harangi, S., Dulai, A., Zelenka, T. & Kósik, S., 2007: Miocene volcanism in the Visegrád Mountains, Hungary: An integrated approach to regional volcanic stratigraphy. *Geologica Carpathica*, 58, 6, 541–563.

Kidwell, S. M., Fürsich, F. T. & Aigner, T., 1986: Conceptual framework for the analysis and classification of fossil concentrations. *Palaios*, 1, 3, 228–238. https://doi.org/10.2307/3514687.

Killényi, E. & Šefara, J. (eds.), 1989: Pre-Tertiary basement contour map of the Carpathian Basin beneath Austria, Czechoslovakia and Hungary, 1:500,000. *Budapest, Eötvös Loránd Geophysical Institute of Hungary*.

Klučiar, T., Kováč, M., Vojtko, R., Rybár, S., Šujan, M. & Králiková, S., 2016: The Hurbanovo-Diósjenő Fault: A crustal-scale weakness zone at the boundary between the Central Western Carpathians and Northern Pannonian Domain. *Acta Geologica Slovaca*, 8, 1, 59–70.

Konečný, V., Kováč, M., Lexa, J. & Šefara, J., 2002: Neogene evolution of the Carpatho-Pannonian region: An interplay of subduction and back-arc diapiric uprise in the mantle. *EGS Stephan Mueller Special Publication Series*, 1, 105–123.

Kováč, M., Andreyeva-Grigorovich, A., Bajraktarević, Z., Brzobohatý, R., Filipescu, S., Fodor, L., Harzhauser, M., Nagymarosy, A., Oszczypko, N., Pavelić, D., Rögl, F., Saftić, B., Sliva, Ľ. & Studencka, B., 2007: Badenian evolution of the Central Paratethys Sea: Paleogeography, climate and eustatic sea-level changes. *Geologica Carpathica*, 58, 6, 579–606.

Kováč, M., Synak, R., Fordinál, K., Joniak, P., Tóth, C., Vojtko, R., Nagy, A., Baráth, I., Maglay, J. & Minár, J., 2011: Late Miocene and Pliocene history of the Danube Basin: inferred from development of depositional systems and timing of sedimentary facies changes. *Geologica Carpathica*, 62, 6, 519–534.

Kováčová, P. & Hudáčková, N., 2009: Late Badenian foraminifers from the Vienna Basin (Central Paratethys): stable isotope study and paleoecological implications. *Geologica Carpathica*, 60, 1, 59–70. https://doi.org/10.2478/v10096-009-0006-3.

Lexa, J., Seghedi, I., Szakács, A., Németh, K., Konečný, V., Pécskay, Z., Fülöp, A. & Kovacs, M., 2010: Neogene-Quaternary volcanic forms in the Carpathian-Pannonian region: A review. *Central European Journal of Geosciences*, 2, 3, 207–270. https://doi.org/10.2478/v10085-010-0024-5.

Lexa, J., Yi, K., Broska, I., Ciesielska, Z., Koděra, P., Kohút, M., Mathur, R., Prcúch, J., Szczerba, M., Uhlík, P. & Vojtko, R., 2025: Evolution of the Štiavnica Stratovolcano revisited: SHRIMP U-Th-Pb zircon dating of subvolcanic intrusions, caldera fill and B. Hodruša precious/base metal deposit (including Re/Os and K/Ar data). *Geologica Carpathica*, 76, 1–24. https://doi.org/10.31577/GeolCarp.2025.05.

Loeblich, A. R. & Tappan, H., 1992: Present status of foraminiferal classification. In: Takayanagi, Y. & Saito, T. (eds.): Studies in Benthic Foraminifera. *Tokai University Press*, 93–102.

Macquaker, J. H. S., Bentley, S. J. & Bohacs, K. M., 2010: Wave-enhanced sediment-gravity flows and mud dispersal across continental shelves: Reappraising sediment transport processes operating in ancient mudstone successions. *Geology*, 38, 10, 947–950. https://doi.org/10.1130/G31093.1.

Matenco, L. & Radivojević, D., 2012: On the formation and evolution of the Pannonian Basin: Constraints derived from the structure of the junction area between the Carpathians and Dinarides. *Tectonics*, 31, 6, TC6007. https://doi.org/10.1029/2012TC003206.

Mitchum, R. M. Jr. & Vail, P. R., 1977: Seismic stratigraphy and global changes of sea level. Part 6: Stratigraphic interpretation of seismic reflection patterns in depositional sequences. In: Payton, C. E. (ed.): Seismic Stratigraphy – Applications to Hydrocarbon Exploration. *AAPG Memoir*, 26, 135–144.

Murray, J. W., 2006: Ecology and applications of benthic foraminifera. *Cambridge, Cambridge University Press*, 426 pp. https://doi.org/10.1017/CBO9780511535529.

Murray, J. W. & Alve, E., 2011: The distribution of agglutinated foraminifera in NW European seas: Baseline data for the interpretation of fossil assemblages. *Palaeontologia Electronica,* 14, 2.

Murray, J. W., Alve, E. & Jones, B. W., 2011: A new look at modern agglutinated benthic foraminiferal morphogroups: Their value in palaeoecological interpretation. *Palaeogeography, Palaeoclimatology, Palaeoecology*, 309, 229–241. https://doi.org/10.1016/j.palaeo.2011.06.006.

Nalepka, D. & Walanus, A., 2003: Data processing in pollen analysis. *Acta Palaeobotanica*, 43, 1, 125–134.

Nichols, G., 2009: Sedimentology and stratigraphy. *Chichester, Wiley-Blackwell*, 432 pp.

Nováková, P., Rybár, S., Šarinová, K., Nagy, A., Hudáčková, N., Jamrich, M., Teodoridis, V., Kováčová, M., Šujan, M., Vlček, T. & Kováč, M., 2020: The late Badenian--Sarmatian, Serravallian, environmental transition calibrated by sequence stratigraphy, eastern Danube Basin, Central Paratethys. *Geologica Carpathica,* 71, 4, 291–313. https://doi.org/10.31577/GeolCarp.71.4.1.

Nøttvedt, A., Gabrielsen, R. H. & Steel, R. J., 1995: Tectonostratigraphy and sedimentary architecture of rift basins, with reference to the northern North Sea. *Marine and Petroleum Geology*, 12, 8, 881–901. https://doi.org/10.1016/0264-8172(95)98853-W.

Patruno, S., Hampson, G. J. & Jackson, C. A.-L., 2015: Quantitative characterisation of deltaic and subaqueous clinoforms. *Earth-Science Reviews*, 142, 79–119. https://doi.org/10.1016/j.earscirev.2015.01.004.

Pécskay, Z., Lexa, J., Szakács, A., Seghedi, I., Balogh, K., Konečný, V., Zelenka, T., Kovacs, M., Póka, T., Fülöp, A., Márton, E., Panaiotu, C. & Cvetković, V., 2006: Geochronology of Neogene magmatism in the Carpathian arc and intra-Carpathian area. *Geologica Carpathica*, 57, 6, 511–530.

Pellegrini, C., Patruno, S., Helland-Hansen, W., Steel, R. J. & Trincardi, F., 2020: Clinoforms and clinothems: Fundamental elements of basin infill. *Basin Research,* 32, 2, 187–205. https://doi.org/10.1111/bre.12446.

Piller, W. E., Harzhauser, M. & Mandic, O., 2007: Miocene Central Paratethys stratigraphy: Current status and future directions. *Stratigraphy*, 4, 151–168.

Płonka, K., 2017: Palaeontological analysis of Middle Miocene siltstones at Wiślica, Carpathian Foredeep, Poland. *Geologos,* 23, 29–43. https://doi.org/10.1515/logos-2017-0003.

Popov, S. V., Rögl, F., Rozanov, A. Y., Steininger, F. F., Shcherba, I. G. & Kováč, M. (eds.) 2004: Lithological--paleogeographic maps of Paratethys. 10 maps, Late Eocene to Pliocene. *Courier Forschungsinstitut Senckenberg*, 250, 1–46.

Posamentier, H. W. & Kolla, V., 2003: Seismic geomorphology and stratigraphy of depositional elements in deep-water settings. *Journal of Sedimentary Research*, 73, 3, 367–388. https://doi.org/10.1306/111302730367.

Rabalais, N. N., Díaz, R. J., Levin, L. A., Turner, R. E., Gilbert, D. & Zhang, J., 2010: Dynamics and distribution of natural and human-caused hypoxia. *Biogeosciences,* 7, 585–619. https://doi.org/10.5194/bg-7-585-2010.

Ratschbacher, L., Merle, O., Davy, P. & Cobbold, P., 1991a: Lateral extrusion in the Eastern Alps, Part 1: Boundary conditions and experiments scaled for gravity. *Tectonics*, 10, 2, 245–256. https://doi.org/10.1029/90TC02622.

Ratschbacher, L., Frisch, W., Linzer, H.-G. & Merle, O., 1991b: Lateral extrusion in the Eastern Alps, Part 2: Structural analysis. *Tectonics*, 10, 2, 257–271. https://doi.org/10.1029/90TC02623.

Rider, M. & Kennedy, M., 2011: The geological interpretation of well logs, 3rd edition. *Rider-French Consulting Limited*, 432 pp.

Rossi, V. M., Perillo, M. M., Steel, R. J. & Olariu, C., 2017: Quantifying mixed-process variability in shallow-marine depositional systems: What are sedimentary structures really telling us? *Journal of Sedimentary Research*, 87, 10, 1060–1074. https://doi.org/10.2110/jsr.2017.49.

Royden, L. H., Horváth, F. & Burchfiel, B. C., 1982: Transform faulting, extension, and subduction in the Carpathian--Pannonian region. *Geological Society of America Bulletin,* 93, 8, 717–725.

Royden, L. H., Horváth, F. & Rumpler, J. 1983: Evolution of the Pannonian Basin system: 1. Tectonics. *Tectonics,* 2, 1, 63–90. https://doi.org/10.1029/TC002i001p00063.

Rybár, S., Halásová, E., Hudáčková, N., Kováč, M., Kováčová, M., Šarinová, K. & Šujan, M., 2015: Biostratigraphy, sedimentology and paleoenvironments of the northern Danube Basin: Ratkovce-1 well case study. *Geologica Carpathica*, 66, 1, 51–67.

Rybár, S., Kováč, M., Šarinová, K., Halásová, E., Hudáčková, N., Šujan, M., Kováčová, M., Ruman, A. & Klučiar, T., 2016: Neogene changes in paleogeography, paleoenvironment and the provenance of sediment in the northern Danube Basin. *Bulletin of Geosciences*, 91, 2, 367–398.

Rybár, S. & Kotulová, J., 2023: Petroleum play types and source rocks in the Pannonian Basin, insight from the Slovak part of the Danube Basin. *Marine and Petroleum Geology,* 149, 106092. https://doi.org/10.1016/j.marpetgeo.2022.106092.

Rybár, S., Šarinová, K., Jourdan, F., Mayers, C. & Sliva, Ľ., 2024: Middle Miocene volcanic flare-up preceding and synchronous with the Langhian/Serravallian sea-level decline in the North Pannonian Basin: Insights from $^{40}Ar/^{39}Ar$ dating, geo-seismic analysis and 3D visualization of the subterranean Kráľová stratovolcano. *Basin Research*, 36, e12844. https://doi.org/10.1111/bre.12844.

Rybár, S., Nováková, P., Šarinová, K., Kotulová, J., Jourdan, F. & Mayers, C., 2025: Tectono-sedimentary evolution of the North Danube Basin: Insights from $^{40}Ar/^{39}Ar$ geochronology and basin modeling within the Pannonian back-arc system. *International Journal of Earth Sciences*, 114, 907–932. https://doi.org/10.1007/s00531-025-02524-z.

Sant, K., Kuiper, K. F., Rybár, S., Grunert, P., Harzhauser, M., Mandic, O., Jamrich, M., Šarinová, K., Hudáčková, N. & Krijgsman, W., 2020: $^{40}Ar/^{39}Ar$ geochronology using high sensitivity mass spectrometry: Examples from middle Miocene horizons of the Central Paratethys. *Geologica Carpathica*, 71, 2, 166–182. https://doi.org/10.31577/GeolCarp.71.2.5.

Schmid, S. M., Bernoulli, D., Fügenschuh, B., Matenco, L., Schefer, S., Schuster, R., Tischler, M. & Ustaszewski, K., 2008: The Alpine-Carpathian-Dinaridic orogenic system: Correlation and evolution of tectonic units. *Swiss Journal of Geosciences*, 101, 1, 139–183. https://doi.org/10.1007/s00015-008-1247-3.

Schneider, J.-L., Le Ruyet, A., Chanier, F., Buret, C., Ferrière, J., Proust, J.-N. & Rosseel, J.-B., 2001: Primary or secondary distal volcaniclastic turbidites: How to make the distinction? An example from the Miocene of New Zealand, Mahia Peninsula, North Island. *Sedimentary Geology*, 145, 1–2, 1–22. https://doi.org/10.1016/S0037-0738(01)00108-7.

Seghedi, I. & Downes, H., 2011: Geochemistry and tectonic development of Cenozoic magmatism in the Carpathian--Pannonian region. *Gondwana Research*, 20, 4, 655–672. https://doi.org/10.1016/j.gr.2011.06.009.

Smith, G. A., 1986: Coarse-grained nonmarine volcaniclastic sediment: Terminology and depositional process. *Geological Society of America Bulletin*, 97, 1, 1–10. https://doi.org/10.1130/0016-7606(1986)97<1:CNVSTA>2.0.CO;2.

Steininger, F. F. & Rögl, F., 1984: Paleogeography and palinspastic reconstruction of the Neogene of the Mediterranean and Paratethys. *Geological Society, London, Special Publications*, 17, 659–668.

Šarinová, K., Rybár, S., Halásová, E., Hudáčková, N., Jamrich, M., Kováčová, M. & Šujan, M., 2018: Integrated biostratigraphical, sedimentological and provenance analyses with implications for lithostratigraphic ranking: The Miocene Komjatice Depression of the Danube Basin. *Geologica Carpathica*, 69, 4, 382–409. https://doi.org/10.1515/geoca-2018-0023,

Šarinová, K., Hudáčková, N., Rybár, S., Jamrich, M., Jourdan, F., Frew, A., Mayers, C., Ruman, A., Subová, V. & Sliva, Ľ., 2021: $^{40}Ar/^{39}Ar$ dating and palaeoenvironments at the boundary of the early–late Badenian, Langhian–Serravallian, in the northwest margin of the Pannonian Basin System. *Facies*, 67, 29. https://doi.org/10.1007/s10347-021-00637-w.

Šujan, M., Braucher, R., Kováč, M., Bourlès, D., Rybár, S., Guillou, V. & Hudáčková, N., 2016: Application of the authigenic $^{10}Be/^{9}Be$ dating method to Late Miocene--Pliocene sequences in the northern Danube Basin, Pannonian Basin System: Confirmation of heterochronous evolution of sedimentary environments. *Global and Planetary Change*, 137, 35–53.

Šujan, M., Braucher, R., Rybár, S., Maglay, J., Nagy, A., Fordinál, K., Šarinová, K., Sýkora, M., Józsa, Š., ASTER Team & Kováč, M., 2018: Revealing the late Pliocene to Middle Pleistocene alluvial archive in the confluence of the Western Carpathian and Eastern Alpine rivers: $^{26}Al/^{10}Be$ burial dating from the Danube Basin (Slovakia). *Sedimentary Geology*, 377, 131–146. https://doi.org/10.1016/j.sedgeo.2018.10.001.

Šujan, M., Rybár, S., Kováč, M., Bielik, M., Majcin, D., Minár, J., Plašienka, D., Nováková, P. & Kotulová, J., 2021: The polyphase rifting and inversion of the Danube Basin revised. *Global and Planetary Change*, 196, 103375. https://doi.org/10.1016/j.gloplacha.2020.103375.

Šujan, M., Šarinová, K., Hók, J., Vlček, T., Ruman, A., Jamrich, M., Kováčová, M., Droppa, D. M., Fordinál, K., Nagy, A., Moravcová, M., Sztanó, O. & Kováč, M., 2026: Miocene to Quaternary evolution of the northern Danube Basin: a review of geodynamics, depositional systems and stratigraphy. *Geological Society, London, Special Publications*, 554, SP554-2024-66. https://doi.org/10.1144/SP554-2024-66.

Sztanó, O. & Tari, G., 1993: Early Miocene basin evolution in northern Hungary: Tectonics and eustasy. *Tectonophysics*, 226, 1–4, 485–502.

Sztanó, O., Kováč, M., Magyar, I., Šujan, M., Fodor, L., Uhrin, A., Rybár, S., Csillag, G. & Tőkés, L., 2016: Late Miocene sedimentary record of the Danube/Kisalföld Basin: Interregional correlation of depositional systems, stratigraphy and structural evolution. *Geologica Carpathica*, 67, 6, 525–542. https://doi.org/10.1515/geoca-2016-0033.

Talling, P. J., Masson, D. G., Sumner, E. J. & Malgesini, G., 2012: Subaqueous sediment density flows: Depositional processes and deposit types. *Sedimentology*, 59, 7, 1937–2003. https://doi.org/10.1111/j.1365-3091.2012.01353.x.

Tari, G., Horváth, F. & Rumpler, J., 1992: Styles of extension in the Pannonian Basin. *Tectonophysics*, 208, 1–3, 203–219. https://doi.org/10.1016/0040-1951(92)90345-7.

Tari, G., Báldi, T. & Báldi-Béke, M., 1993: Paleogene retroarc flexural basin beneath the Neogene Pannonian Basin: A geodynamic model. *Tectonophysics*, 226, 3–4, 433–456. https://doi.org/10.1016/0040-1951(93)90133-5.

Tari, G., Bada, G., Beidinger, A., Csizmeg, J., Danišik, M., Gjerazi, I., Grasemann, B., Kováč, M., Plašienka, D., Šujan, M. & Szafián, P., 2021: The connection between the Alps and the Carpathians beneath the Pannonian Basin: Selective reactivation of Alpine nappe contacts during Miocene extension. *Global and Planetary Change*, 197, 103401. https://doi.org/10.1016/j.gloplacha.2020.103401.

Tribovillard, N., Algeo, T. J., Lyons, T. W. & Riboulleau, A., 2006: Trace metals as paleoredox and paleoproductivity proxies: An update. *Chemical Geology*, 232, 1–2, 12–32. https://doi.org/10.1016/j.chemgeo.2006.02.012.

Vass, D., 2002: Litostratigrafia Západných Karpát: neogén a budínsky paleogén [Lithostratigraphy of the Western Carpathians: Neogene and Budín Paleogene sediments]. *Bratislava, Štátny geologický ústav Dionýza Štúra*, 202 pp.

Van der Zwaan, G. J., Duijnstee, I. A. P., den Dulk, M., Ernst, S. R., Jannink, N. T. & Kouwenhoven, T. J., 1999: Benthic foraminifers: Proxies or problems? A review of paleoecological concepts. *Earth-Science Reviews*, 46, 1–4, 213–236. https://doi.org/10.1016/S0012-8252(99)00011-2.

Wade, B. S., Pearson, P. N., Berggren, W. A. & Pälike, H., 2011: Review and revision of Cenozoic tropical planktonic foraminiferal biostratigraphy and calibration to the geomagnetic polarity and astronomical time scale. *Earth-Science Reviews*, 104, 1–3, 111–142. https://doi.org/10.1016/j.earscirev.2010.09.003.

Wijbrans, J., Németh, K., Martin, U. & Balogh, K., 2007: $^{40}Ar/^{39}Ar$ geochronology of Neogene phreatomagmatic volcanism in the western Pannonian Basin, Hungary. *Journal of Volcanology and Geothermal Research*, 164, 4, 193–204. https://doi.org/10.1016/j.jvolgeores.2007.05.009.

Young, J. R., 1998: Neogene. In: Bown, P. R. (ed.): Calcareous Nannofossil Biostratigraphy. *British Micropalaeontological Society Publications Series, Chapman & Hall*, 225–265.

Young, J. R., Bown, P. R. & Lees, J. A., 2022: Nannotax3 website. *International Nannoplankton Association*. Accessed 20 July 2026. https://www.mikrotax.org/Nannotax3.

Vývoj blatnianskej priehlbiny počas bádenu až panónu (lang – tortón) v severozápadnej časti Dunajskej panvy (centrálna Paratetýda): integrované biostratigrafické, faciálne a seizmické údaje z vrtov Špačince-4 a Dubové-2

Miocénny vývoj severozápadnej časti centrálnej Paratetýdy ovplyvňovala zaoblúková extenzia spojená s vývojom alpsko-karpatského orogénu a laterálnym únikom megajednotky ALCAPA (Royden et al., 1983; Tari et al., 1992; Schmid et al., 2008). V tomto geodynamickom prostredí vznikol panónsky panvový systém ako sústava synriftových depocentier charakterizovaných rýchlou subsidenciou, vysokou rýchlosťou sedimentácie a vulkanickou aktivitou. Dunajská panva predstavuje jedno z hlavných depocentier tohto systému. Jej severozápadná časť vrátane blatnianskej priehlbiny zachováva hrubú miocénnu sedimentárnu sukcesiu, ktorá dokumentuje prechod od synriftovej extenzie k postriftovej termálnej subsidencii. Regionálny model extenzného vývoja Dunajskej panvy vrátane viacfázového riftingu a následnej postriftovej subsidencie je v súčasnosti dobre zdokumentovaný (Hók et al., 2016; Šujan et al., 2021, 2026). Menej objasnený však zostáva jeho lokálny prejav v jednotlivých tektonických blokoch blatnianskej priehlbiny. Otázky sa týkajú najmä prechodu od proximálnej hruboklastickej a vulkanoklastickej sedimentácie k jednoznačne morským podmienkam, ako aj laterálnej korelácie a priestorovej architektúry bádenských gravitačných sedimentov medzi skúmanými vrtmi a priľahlými časťami priehlbiny. Táto štúdia prináša integrované vyhodnotenie hlbokých vrtov Špačince-4 a Dubové-2. Nadväzuje na predchádzajúcu biostratigrafickú správu (Hudáčková et al., 2018), ktorú významne rozširuje o podrobný sedimentologický a seizmostratigrafický výskum a o koreláciu s publikovanými údajmi absolútneho datovania. Analýza zahŕňa biostratigrafiu vápnitého nanoplanktónu a planktonických a bentických foraminifer, palynologické údaje, sedimentologický opis vrtných jadier a interpretáciu karotážnych záznamov a seizmických profilov. Cieľom štúdie je: 1. spresniť biostratigrafické členenie miocénnej sukcesie pomocou viacerých skupín mikrofosílií, 2. rekonštruovať sedimentárne prostredie a faciálnu architektúru, 3. posúdiť, či rozdiely medzi sukcesiami vo vrtoch Špačince-4 a Dubové-2 odrážajú ich odlišnú pozíciu v rámci tektonicky kontrolovaného halfgrabenu blatnianskej priehlbiny.

Biostratigrafické údaje zaraďujú prevažnú časť skúmanej neogénnej sukcesie do spodného až vrchného bádenu, teda do langu až spodného seravalu. Asociácie vápnitého nanoplanktónu dokumentujú zóny NN4 – NN6 a planktonické foraminifery miestami zóny CPN7 – CPN8. Sarmatské a panónske sedimenty boli identifikované predovšetkým na základe karotážnych záznamov, seizmickej geometrie a regionálnych korelácií. Vrt Špačince-4 zachytáva hrubú bádenskú synriftovú sukcesiu. Bazálne parakonglomeráty, vulkanické konglomeráty a zeolitizované tufy prechádzajú smerom nahor do pieskovcov, konglomerátov a laminovaných ílovcov a prachovcov. Tieto sedimenty dokumentujú proximálny prínos hruboklastického materiálu, vulkanoklastickú sedimentáciu, úlomkotoky, turbiditné prúdy a distálnu sedimentáciu zo suspenzie. Vrt Dubové-2 dosahuje predneogénne podložie a obsahuje tenšiu neogénnu sukcesiu, tvorenú najmä bioturbovanými pieskovcami, piesčitými ílovcami, prachovcami a jemnozrnnými sedimentmi vonkajšieho šelfu až svahu, ktoré sú miestami prerušované gravitačnými alebo preplavenými bioklastickými polohami. Geoseizmické profily zobrazujú blatniansku priehlbinu ako asymetrický halfgraben ohraničený listrickými poklesovými zlomami, ktoré sa smerom do hĺbky napájajú na nízkouhlovú plochu odlepenia (*detachment*). Bádenské sedimenty hrubnú smerom k hlavným zlomom a vytvárajú typickú geometriu syntektonických rastových vrstiev. Mladšie, sarmatské sedimenty na tieto telesá nasadajú a dokumentujú postupné zoslabovanie tektonickej aktivity. Subhorizontálne panónske reflexy zodpovedajú postriftovému vypĺňaniu panvy deltovými, jazernými a fluviálnymi sedimentmi. Rozdiely medzi skúmanými vrtmi sú výsledkom ich odlišnej pozície v rámci toho istého polpriekopového systému. Vrt Špačince-4 sa nachádza bližšie k aktívnemu depocentru a k hlavným prívodným trasám sedimentov, zatiaľ čo vrt Dubové-2 leží v okrajovej polohe v blízkosti štruktúrnej elevácie alebo vyzdvihnutého zlomového bloku. Integrované výsledky tak spresňujú lokálnu chronostratigrafickú a tektonicko-sedimentárnu architektúru blatnianskej priehlbiny bez toho, aby menili zavedený regionálny model zaoblúkového extenzného vývoja Dunajskej panvy.

Doručené / Received: 1. 6. 2026
Prijaté na publikovanie / Accepted: 15. 7. 2026

Electronic supplementary material available online: https://www.geology.sk/mineralia/

Supplementary	Table S1. Summary of datasets used in this study
Appendix 1.	Foraminifera from the Špačince-4 well
Appendix 2.	Foraminifera from the Dubové-2 well
Appendix 3.	Complete Špačince-4 handheld-XRF dataset
Appendix 4a.	Nannofossil sample data from the Špačince-4 well
Appendix 4b.	Nannofossil sample data from the Dubové-2 well

Mineralia Slovaca, Web ISSN 1338-3523, ISSN 0369-2086, https://doi.org/10.56623/ms.2026.58.1.2
58, 1 (2026), 37 – 50,

Picritic rocks (meimechites) from Poniky: mineralogy and petrology (Western Carpathians)

†JÁN SPIŠIAK[1], JURAJ BUTEK[1,*], VIERA ŠIMONOVÁ[1], RICHARD KOPÁČIK[1], ANGELIKA OBERTOVÁ[1] and SERGIY KURYLO[2]

[1] Department of Geography and Geology, Faculty of Natural Sciences, Matej Bel University, Tajovského 40, 974 01 Banská Bystrica, Slovak Republic,

[2] Earth Science Institute, Slovak Academy of Sciences, Ďumbierska 1, 974 11, Banská Bystrica, Slovak Republic

* Corresponding author, juraj.butek@umb.sk

Abstract: New data on picritic rocks from the Poniky area are presented in this contribution. In addition to the major mafic minerals (clinopyroxene, kaersutite, phlogopite), spinels, Sr-rich apatite (up to 6.4 wt% SrO), and sodalite are also described. Sodalite is documented for the first time in the Central Western Carpathians, and together with the mineralogical and whole-rock compositions, it confirms the alkaline character of these rocks. Petrological data, including REE, show that they are equivalent to the Cretaceous volcanic rocks occurring in the Fatric Unit as well as to picritic rocks of the teschenite-picrite association occurring in the External Western Carpathians. The high MgO content (>18 wt%) allows these rocks to be classified as meimechites.

Key words: picrite, mineralogy, whole-rock geochemistry, Cretaceous, Western Carpathians

Introduction

Picrite is a hypoabyssal rock, often porphyritic, with a high content of mafic minerals and an elevated MgO content compared to basalts (>12 wt%; Le Bas, 2000). Its occurrences are rare in the Western Carpathians. Picrites occur in the External Western Carpathians as part of the Cretaceous teschenite-picrite association within the Silesian Unit (Brunarska & Anczkiewicz, 2019; Buriánek et al., 2013; Hovorka, 1976; Hovorka & Spišiak, 1988; Kudělásková, 1987; Mahmood, 1973; Šmíd, 1962; Szopa et al., 2014). In the Central Western Carpathians, only limited occurrences of picrite were reported from boreholes in Mesozoic sedimentary sequences near Banská Bystrica (Hovorka & Slavkay, 1966; Hovorka & Spišiak, 1988; Slavkay, 1979). These picritic rocks are Cretaceous in age and are genetically associated with alkaline volcanism. A solitary occurrence of a metamorphosed picrite was also documented in the Gelnica Group of the Gemeric Unit (Ivan, 1991).

A substantial amount of information on the picrite occurrence near Banská Bystrica was published by Spišiak & Hovorka (2000) and in the monograph Mesozoic Volcanism of the Western Carpathians (in Slovak; Hovorka & Spišiak, 1988). Despite this, we present new and interesting mineralogical and petrological data on an older picritic sample from a borehole near Poniky.

Geological setting

Picritic rocks from the vicinity of Banská Bystrica were documented in both boreholes Po-1 and St-2 in the Poniky area (Fig. 1A; Spišiak & Hovorka, 2000; Slavkay et al., 1968). The analysed sample came from the Po-1 borehole, located approximately 250 m west of the northern edge of Poniky (48.715751 °N, 19.287881 °E; Fig. 1B). The rocks occur at a depth of 460 m. The host rocks are significantly brecciated Middle Triassic dolomites. These dolomites were originally affiliated with the Hronic Unit (Hovorka & Slavkay, 1966).

The geological structure of the broader Poniky area is characterized by the tectonic superposition of three units: the Fatric Unit, the Hronic Unit, and the Silicic Unit. The Fatric Unit comprises Middle Triassic to Cretaceous deposits. Shallow-water organodetritic carbonates are typical of the Triassic. The Jurassic-Lower Cretaceous succession continues with shallow-water crinoidal and nodular limestones, which are gradually replaced by deeper-water clayey limestones, mudstones, and shales (Slavkay, 1971). The Hronic Unit is structurally higher. The succession begins with Middle Triassic dark-grey limestones. These are overlain by strongly weathered dolomites, which represent the host rock of the aforementioned biotitic picrites. According to Hovorka and Slavkay (1966), these represent submarine lava flows emplaced into the Triassic sedimentary environment. The succession continues with Upper Triassic carbonates. The uppermost unit is the Silicic Unit. Its lower part comprises Lower Triassic variegated arkosic sandstones, shales, mudstones, and clayey limestones with abundant Campilian fauna (Slavkay, 1971). These complexes also include extensive Permian volcanic rocks (Ondrejka et al., 2022). At the base, violet-brown paleoandesites occur, separated from alkaline rhyolites and their pyroclastics by clayey limestones (Slavkay, 1971). Shallow-water carbonate complexes rich in organic debris are again typical of the Middle and Upper Triassic age.

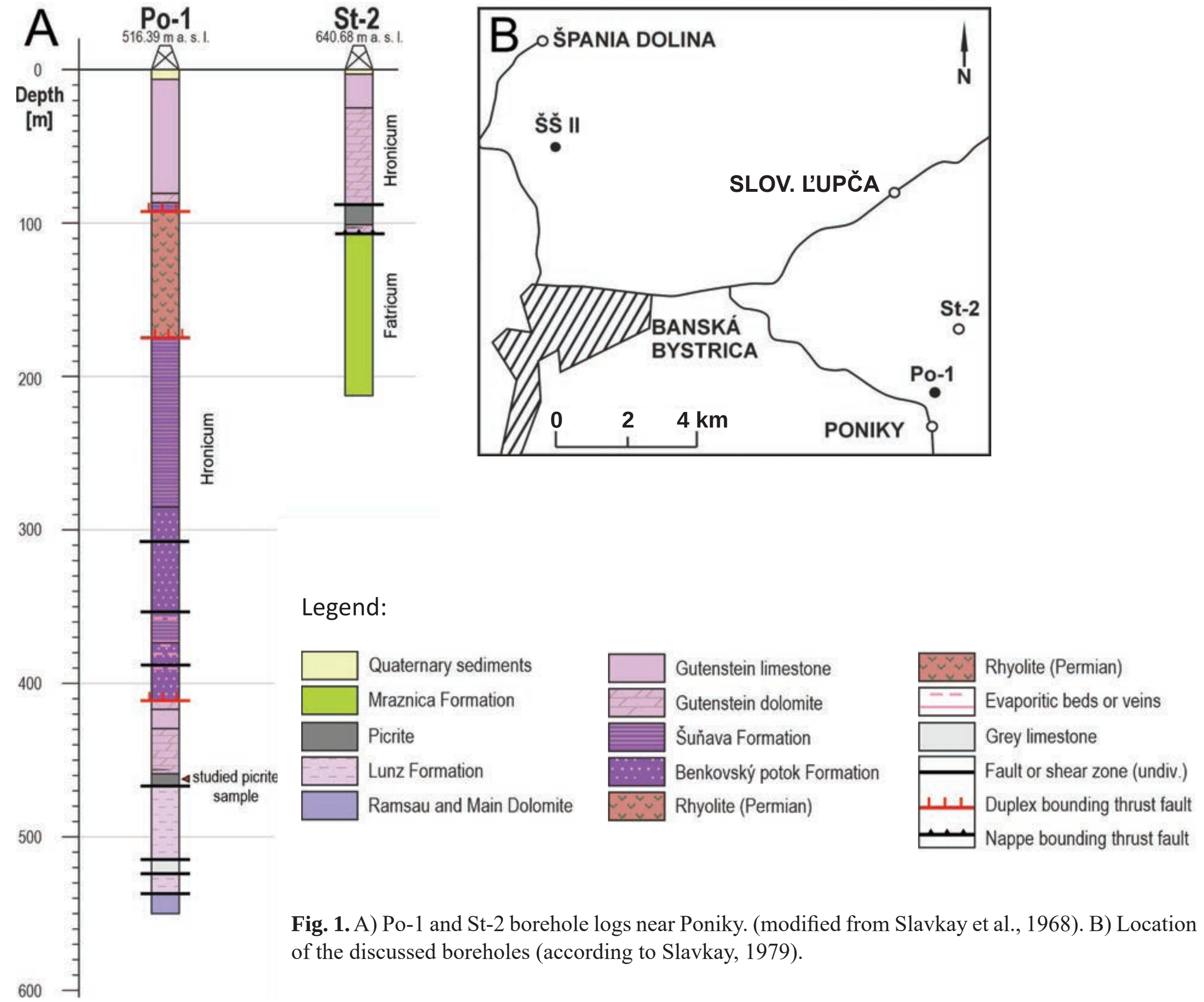

Fig. 1. A) Po-1 and St-2 borehole logs near Poniky. (modified from Slavkay et al., 1968). B) Location of the discussed boreholes (according to Slavkay, 1979).

Methods

Silicate minerals and apatite were analysed using a JEOL JXA-8530F electron microprobe at the Earth Sciences Institute of the Slovak Academy of Sciences in Banská Bystrica under the following conditions: accelerating voltage 15 kV, probe current 20 nA, beam diameter 3–8 μm, counting time 10 s on the peak and 5 s on the background. Raw counts were converted to oxide wt% using a ZAF matrix correction. The EPMA was calibrated using natural and synthetic minerals. Whole-rock analysis was performed at the Bureau Veritas Analytical Laboratories (Vancouver, Canada). Total abundances of major-element oxides were determined by inductively coupled plasma emission spectrometry (ICP-ES) following lithium metaborate-tetraborate fusion and dilute nitric acid treatment.

Results

Petrography and mineralogy

Analysed picritic rocks exhibit a porphyritic texture with olivine and clinopyroxene phenocrysts. Olivine (approximately 35 %) predominates over pyroxene. Other major minerals include biotite, amphibole, spinel, and sodalite.

Olivine is extensively serpentinised, forming typical mesh textures. Because only textural relics are preserved, olivine analyses are unavailable.

Two types of clinopyroxene occur in the rocks. The first type (Cpx I) occurs as small, inclusion-free phenocrysts (Fig. 2A). In contrast, the second type (Cpx II) forms large phenocrysts (2 – 5 mm) that poikilitically enclose other minerals, mainly sodalite, carbonate, chlorite and pyrite (Fig. 2B). Clinopyroxenes are weakly zoned; rims have slightly higher TiO_2 content. The chemical compositions of both clinopyroxenes are similar (Tab. 1). According to the IMA classification (Morimoto, 1988; Fig. 3), they are classified as diopside.

Amphibole coexists with clinopyroxene (Cpx I, Fig. 2A). It has elevated TiO_2 (up to 4.5 wt%) and Na_2O (up to 3.4 wt%; Tab. 2). According to the amphibole classification by Hawthorne et al. (2012), the analysed amphibole, with Ti reaching 0.5 apfu, falls at the boundary between pargasite and kaersutite. It is compositionally similar to amphiboles from Cretaceous alkaline rocks in the Fatric unit (Višňové, Krpeľany, Salatín, etc.) (Hovorka & Spišiak, 1988; Spišiak & Hovorka, 1997).

Biotite occurs as tabular phenocrysts together with clinopyroxene (Cpx I) and amphibole (Fig. 2A, 5B). It is dark brown to reddish brown, strongly pleochroic, and partially altered. It has high MgO (up to 16.69 wt%) and Na_2O (up to 1.5 wt%) contents, with an average TiO_2 content of 2.3 wt% that locally reaches up to 4 wt% (Tab. 3). Based on the mica classification by Tischendorf et al. (2007), it is classified as phlogopite (Fig. 4).

Sodalite occurs as discrete grains or as inclusions in diopside (Fig. 5). The composition of both types of sodalite is similar (Tab. 4) and matches that of sodalite in alkaline basic rocks (Deer et al., 2013). Sodalite is a common mineral in alkaline rocks and thus serves as an index mineral for the geochemical classification of the studied picritic rocks.

Spinel forms irregular grains that coexist with clinopyroxene and biotite (Fig. 6). It has high Al_2O_3 and elevated MgO, Cr_2O_3, and FeO contents (Tab. 5). Spinel is strongly altered at the rims; marginal parts show higher MnO, SiO_2, and TiO_2 contents and lower Cr_2O_3, MgO, and Al_2O_3 contents. According to the nomenclature and classification by Bosi et al. (2019), with Mg as the dominant bivalent cation and Al as the trivalent cation, it is classified as spinel *sensu stricto*. The chemical composition reflects that of a peridotitic spinel, consistent with the genetic classification of Deer et al. (2013) and with spinels from MORB and peridotites, as classified by Kamenetsky et al. (2001). Spinels from other occurrences of Cretaceous alkaline rocks in the Western Carpathians show a similar chemical composition (Mikuš et al., 2006).

Apatite forms subhedral to euhedral grains (Fig. 7). Given its chemical composition, apatite plots at the boundary between hydroxyapatite and fluorapatite (Fig. 8) and shows elevated LREE contents (Tab. 6). Apatite also exhibits distinct chemical zonation, primarily driven by variations in SrO content. SrO-rich rims reach up to 6 wt% SrO, whereas the cores are relatively SrO-poor (around 0.5 wt%). The increase in SrO is compensated by a corresponding decrease in CaO. Apatite from Cretaceous basic volcanics in the Western Carpathians is also characterized by elevated REE contents (Kynický et al., 2009; Szopa et al., 2014).

Pyrite is abundant in the form of veins (Fig. 6). Chlorite, serpentine-group minerals and calcite are common minor mineral phases.

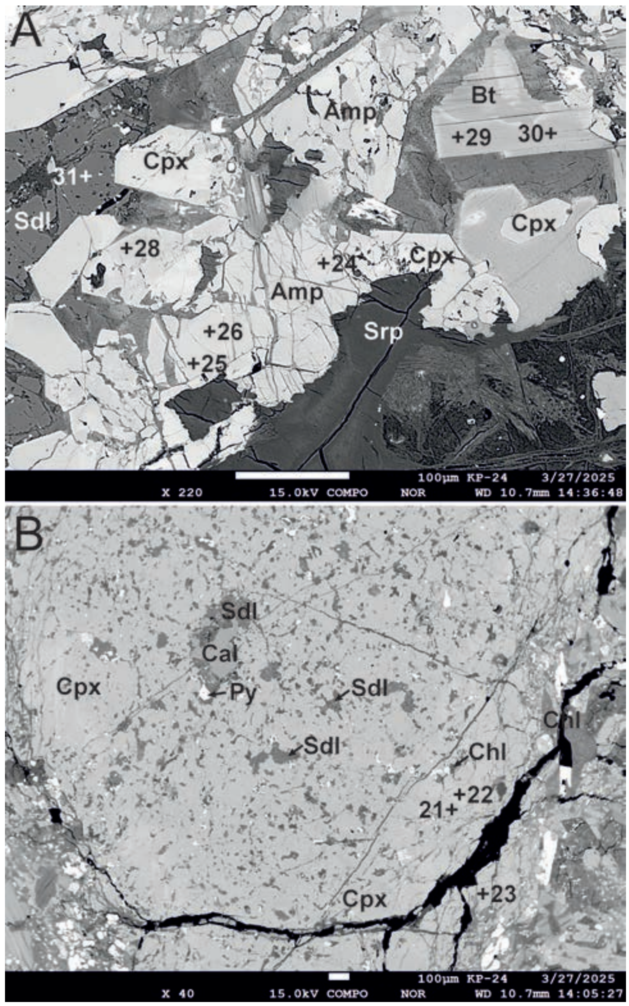

Fig. 2. Backscattered electron images of clinopyroxenes. A) Cpx phenocrysts without inclusions (Cpx I) coexisting with amphibole, phlogopite, and sodalite; B) a poikilitic clinopyroxene phenocryst (Cpx II) with inclusions of sodalite, pyrite, and calcite. Cpx – clinopyroxene, Amp – amphibole, Bt – biotite, Sdl – sodalite, Srp – serpentine, Chl – chlorite, Py – pyrite, Cal – calcite. Numbers in the figures correspond to the number of analyses in Tables 1, 2, and 3.

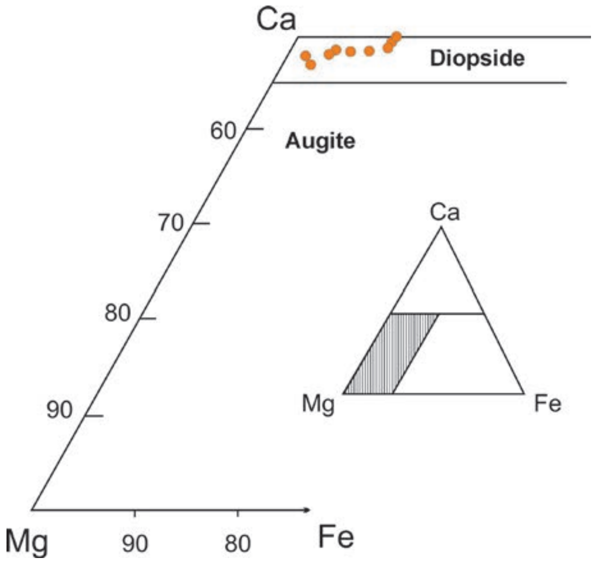

Fig. 3. Classification diagram of clinopyroxenes (after Morimoto, 1988).

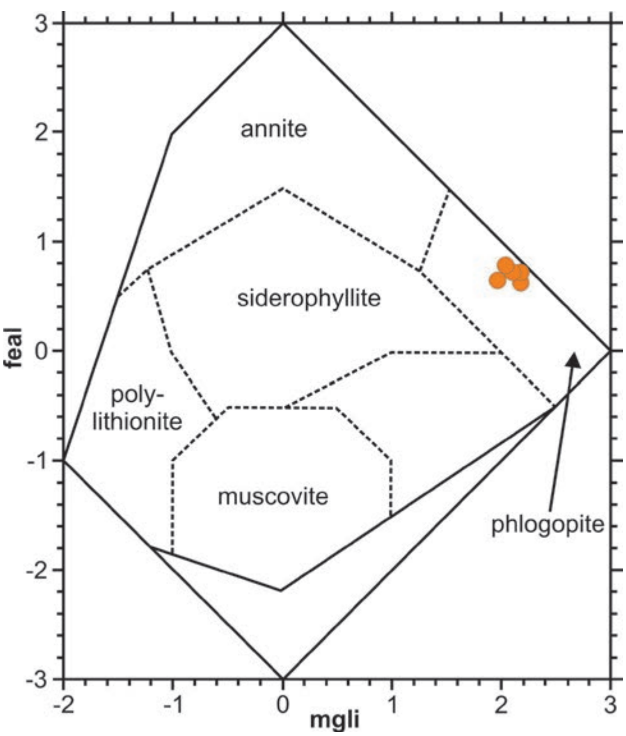

Fig. 4. Classification diagram of micas (after Tischendorf et al., 2007).

Whole rock geochemistry

The whole-rock chemical compositions of picritic rocks from the studied area are shown in Tab. 7. The whole-rock Mg# [molar Mg/(Mg + Fe)] ranges from 0.75 to 0.82. Based on the IUGS classification of high-MgO and low-SiO_2 rocks (Le Bas, 2000), the samples are classified as meimechites (Fig. 9). TiO_2 contents above 1 wt% and the absence of spinifex structures (Kerr & Arndt, 2001) exclude the name komatiite. This is the first description of meimechite in the Central Western Carpathians.

We use the ternary diagram TiO_2 vs MnO x 10 vs P_2O_5 x 10 (Mullen, 1983) for geotectonic classification (Fig. 10). The diagram shows that analyses of the studied rocks plot within the Ocean Island Alkaline Basalts field, consistent with their assumed geotectonic setting. Furthermore, the chondrite-normalized REE pattern shows significant enrichment in light REEs, a steeply descending curve, and no Eu anomaly (Fig. 11A). The chondrite-normalized spider diagram shows strong enrichment in incompatible elements and no visible Nb anomaly (Fig. 11B). It also displays positive Nd and Y anomalies.

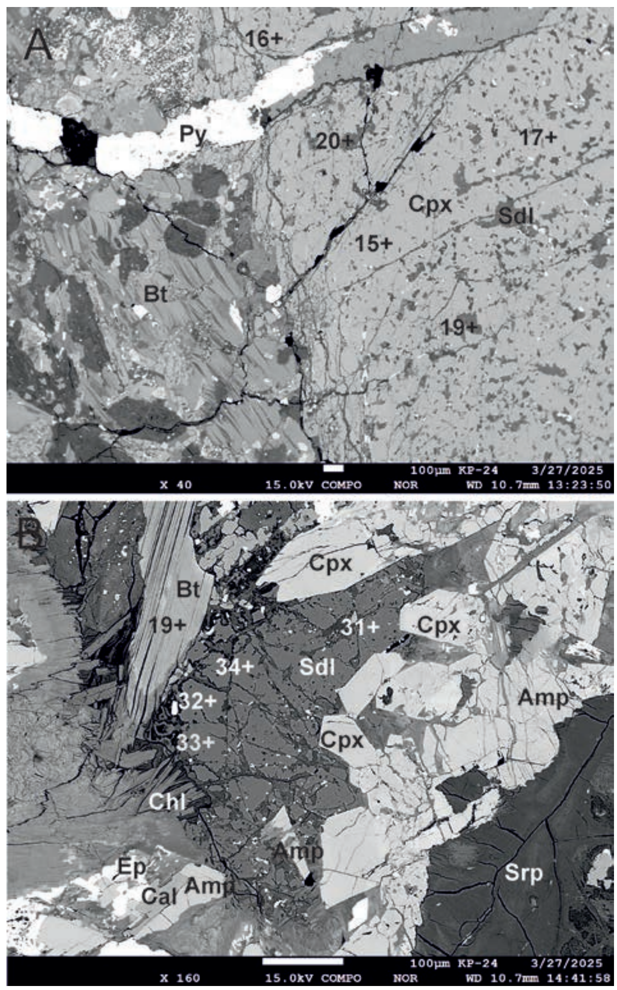

Fig. 5. Backscattered electron images of sodalite. A) Cpx phenocrysts with inclusions of sodalite, pyrite and calcite; B) a large single grain of sodalite. Cpx – clinopyroxene, Amp – amphibole, Bt – biotite, Sdl – sodalite, Srp – serpentine, Chl – chlorite, Py – pyrite, Cal – calcite, Ep – epidote. Numbers in the figures correspond to the number of analyses in Tables 1, 3 and 4.

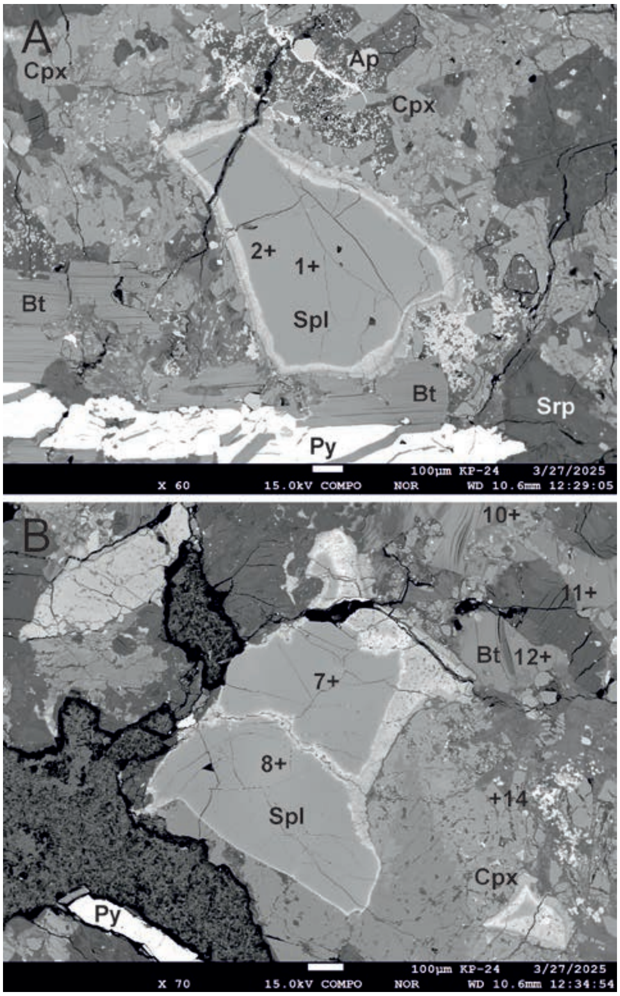

Fig. 6. Backscattered electron images of spinel. Cpx – clinopyroxene, Amp – amphibole. Numbers in the figures correspond to the number of analyses in Table 5.

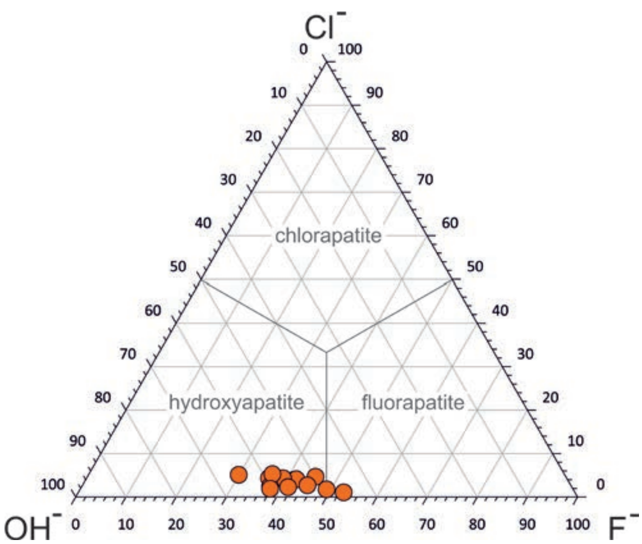

Fig. 8. Classification diagram of apatites from the studied picrites.

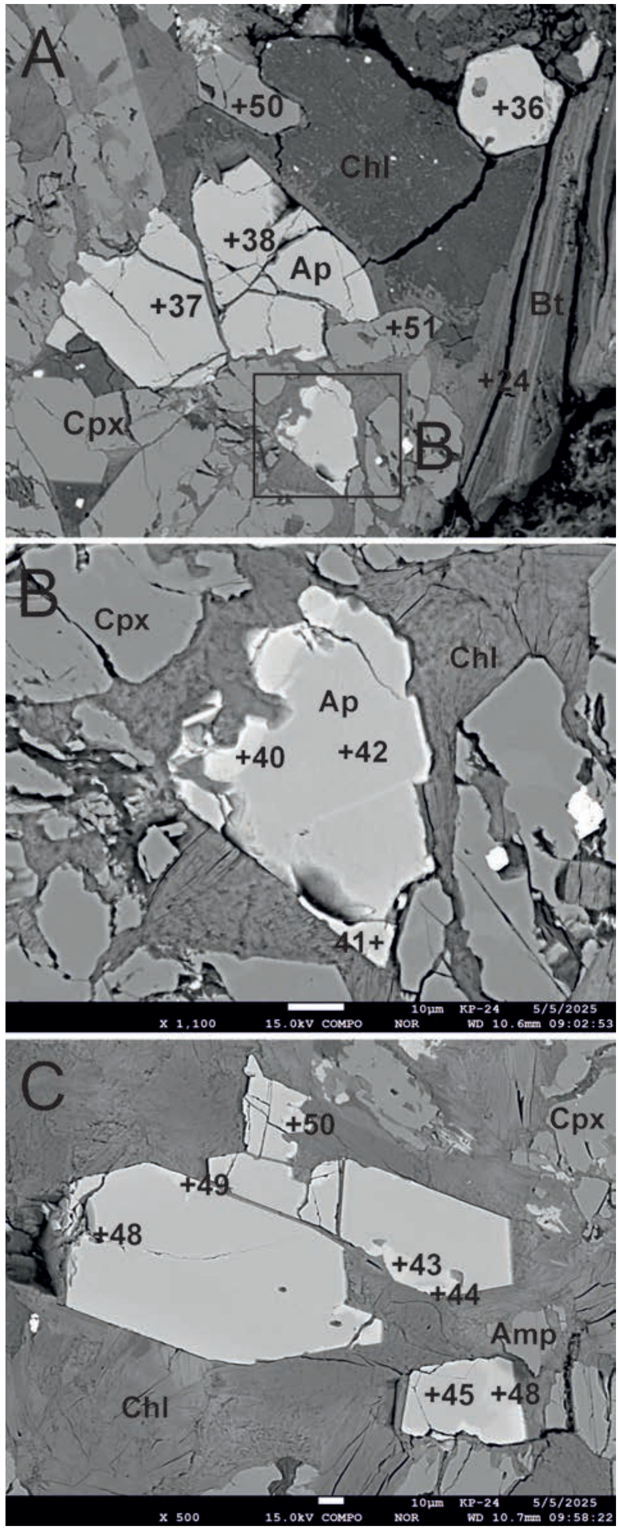

Fig. 7. Backscattered electron images of apatite. Spl – spinel, Cpx – clinopyroxene, Ap – apatite, Bt – biotite, Srp – serpentine, Py – pyrite. Numbers in the figure correspond to the number of analyses in Table 6.

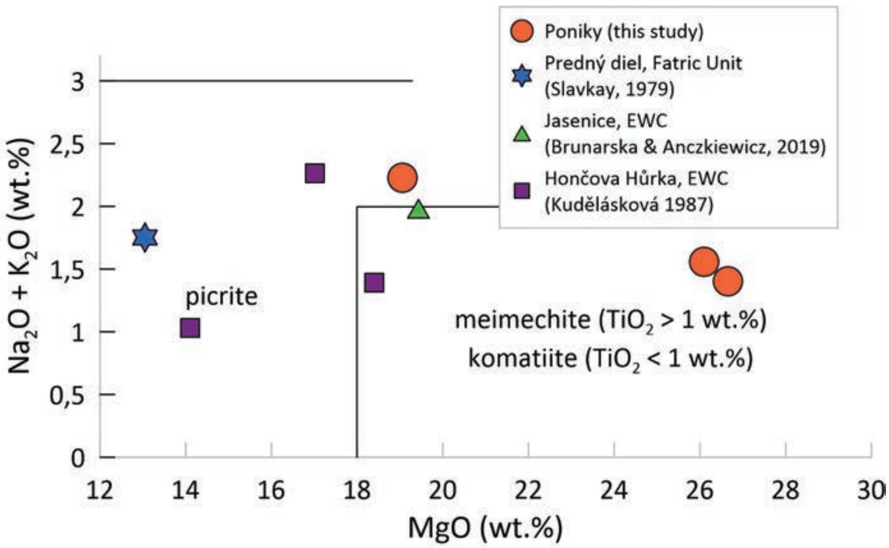

Fig. 9. IUGS classification of high MgO picritic rocks (Le Bas, 2000). A sample from Predný diel (Fatric Unit) and picritic samples from the teschenite association are shown for comparison.

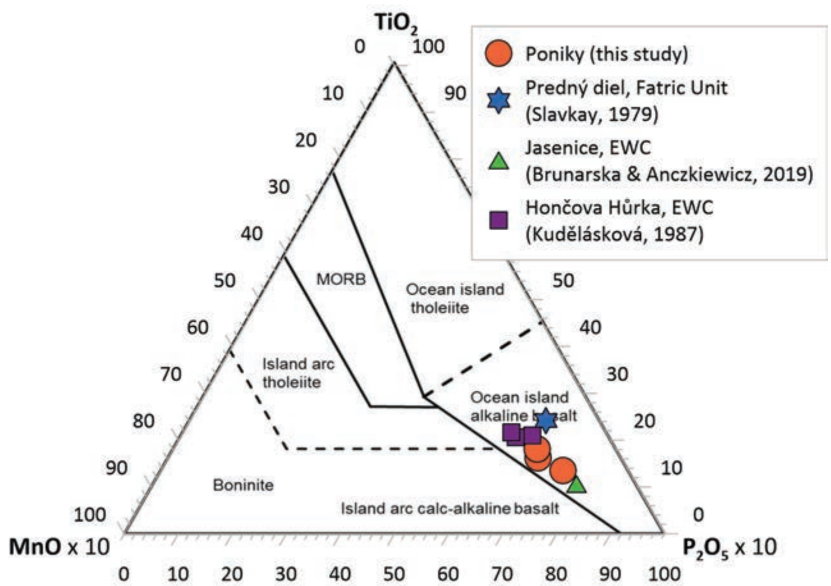

Fig. 10. Ternary discrimination diagram of TiO_2 vs MnO x 10 vs P_2O_5 x 10 (after Mullen, 1983). A sample from Predný diel (Fatric Unit) and picritic samples from the teschenite association are shown for comparison.

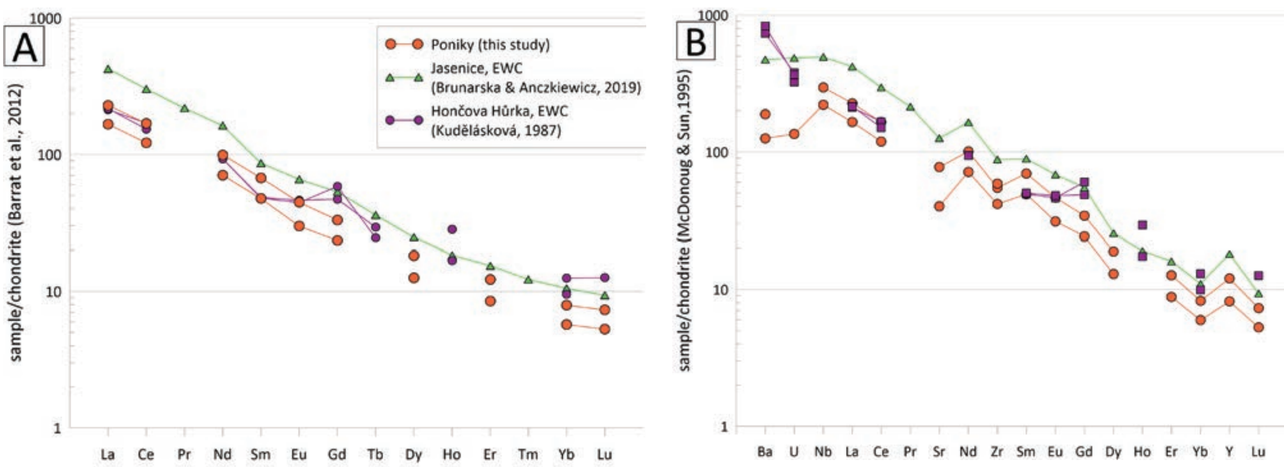

Fig. 11. A) Chondrite-normalized REE diagram (normalized to chondrite using Barrat et al., 2012); B) chondrite-normalized multielement diagram (McDonough & Sun, 1995).

Tab. 1

Selected EPM analyses of clinopyroxene. Fe^{3+} calculated by charge balance. Numbers correspond to those in Fig. 2.

Number anal.	14	15	16	17	21	23	28	51	52
Comment	Cpx II	Cpx II	Cpx II	Cpx II	Cpx II	Cpx II	Cpx I	Cpx I	Cpx I
SiO_2	47.73	49.87	49.54	48.99	47.10	46.77	49.23	48.92	48.72
TiO_2	1.21	0.92	0.66	1.09	1.46	1.74	1.34	2.28	1.86
Al_2O_3	5.97	4.28	5.43	5.01	6.29	6.85	4.70	5.52	5.49
Cr_2O_3	0.02	0.00	0.00	0.03	0.10	0.01	0.01	0.00	0.00
FeO^+	5.46	6.69	8.32	7.52	6.26	5.68	5.89	6.87	7.47
MnO	0.03	0.09	0.14	0.05	0.21	0.04	0.10	0.00	0.00
MgO	13.56	14.08	12.85	13.27	13.55	13.18	14.04	13.37	13.51
CaO	23.83	23.24	21.71	22.82	23.62	23.33	23.50	22.16	22.03
Na_2O	0.45	0.46	0.96	0.76	0.34	0.43	0.49	0.71	0.55
K_2O	0.00	0.01	0.01	0.00	0.01	0.00	0.02	0.16	0.16
TOTAL	98.27	99.63	99.61	99.54	98.92	98.02	99.32	99.99	99.79
Formula based on 6 oxygens									
Si	1.79	1.85	1.84	1.82	1.76	1.76	1.83	1.81	1.81
Ti	0.03	0.03	0.02	0.03	0.04	0.05	0.04	0.06	0.05
Al	0.26	0.19	0.24	0.22	0.28	0.30	0.21	0.24	0.24
Fe^{3+}	0.13	0.10	0.12	0.14	0.15	0.11	0.11	0.07	0.09
Fe^{2+}	0.04	0.10	0.14	0.10	0.04	0.06	0.08	0.14	0.14
Mn	0.00	0.00	0.00	0.00	0.01	0.00	0.00	0.00	0.00
Mg	0.76	0.78	0.71	0.73	0.75	0.74	0.78	0.74	0.75
Ca	0.96	0.92	0.86	0.91	0.94	0.94	0.93	0.88	0.88
Na	0.03	0.03	0.07	0.05	0.02	0.03	0.04	0.05	0.04
K	0.00	0.00	0.00	0.00	0.00	0.00	0.00	0.01	0.01
Wo	54.48	51.14	50.36	52.23	54.22	53.91	52.25	50.01	49.61
En	43.15	43.12	41.47	42.25	43.27	42.37	43.44	41.98	42.33
Fs	2.37	5.75	8.16	5.52	2.51	3.72	4.30	8.00	8.06

Tab. 2

Selected EPM analyses of amphibole. Structural formula recalculated according to Locock (2014). Numbers correspond to those shown in Figs. 2A and 2B.

Number anal.	24	25	26
SiO_2	40.58	41.00	40.49
TiO_2	4.47	4.54	4.17
Al_2O_3	12.37	11.83	12.49
FeO^+	10.62	10.99	10.66
MnO	0.16	0.22	0.26
MgO	13.78	13.74	13.64
CaO	11.61	11.75	11.63
Na_2O	3.20	3.36	3.09
K_2O	1.00	0.95	0.98
Cl	0.02	0.02	0.02
F	0.00	0.00	0.04
Total	97.80	98.41	97.46
Formula besed on 22 oxygens			
Si	6.00	6.04	6.01
Al^{IV}	2.00	1.96	1.99
Ti	0.50	0.50	0.47
Al^{VI}	0.16	0.10	0.19
Fe^{3+}	0.00	0.00	0.05
Mn^{2+}	0.00	0.03	0.01
Fe^{2+}	1.31	1.35	1.28
Mg	3.04	3.02	3.02
Mn^{2+}	0.02	0.00	0.03
Ca	1.84	1.86	1.85
Na	0.13	0.14	0.12
Na	0.79	0.82	0.77
K	0.19	0.18	0.19

Tab. 3

Selected EPM analyses of biotite. Numbers correspond to those shown in Fig. 2.

Number anal.	11	12	29	30	35
SiO	38.17	38.69	38.80	38.92	37.75
TiO_2	2.41	2.22	2.13	2.12	4.01
Al_2O_3	15.56	15.61	15.43	15.63	16.56
FeO^+	10.51	10.25	10.50	11.00	10.25
MnO	0.03	0.07	0.09	0.08	0.14
MgO	19.09	19.69	19.34	19.23	18.54
CaO	0.02	0.03	0.01	0.04	0.11
Na_2O	1.47	1.50	1.54	1.45	1.37
K_2O	8.81	8.62	8.86	8.93	8.67
Total	96.07	96.68	96.70	97.41	97.39
Formula based on 11 oxygens (all ferous iron)					
Si^{IV}	2.77	2.78	2.79	2.78	2.70
Al^{IV}	1.23	1.22	1.21	1.22	1.31
Al^{VI}	0.11	0.11	0.10	0.10	0.08
Ti	0.131	0.12	0.12	0.11	0.215
Fe^{3+}	0.00	0.00	0.00	0.00	0.00
Fe^{2+}	0.64	0.62	0.63	0.66	0.61
Mn	0.00	0.00	0.01	0.01	0.01
Mg	2.06	2.11	2.07	2.05	1.97
Ca	0.00	0.00	0.00	0.00	0.01
Na	0.21	0.21	0.22	0.20	0.19
K	0.82	0.79	0.81	0.82	0.79

Tab. 4

Selected EPM analyses of sodalite. Numbers correspond to those shown in Fig. 5.

Number anal.	18	19	20	31	32	33	34
SiO_2	36.99	37.33	36.79	37.27	36.28	36.73	36.41
TiO_2	0.00	0.00	0.00	0.00	0.00	0.00	0.00
Al_2O_3	31.52	32.20	31.98	31.87	31.31	31.38	31.46
FeO	0.15	0.19	0.05	0.40	0.13	0.08	0.07
MnO	0.00	0.04	0.00	0.00	0.00	0.00	0.06
MgO	0.02	0.05	0.00	0.01	0.00	0.00	0.00
CaO	0.06	0.06	0.07	0.10	0.01	0.02	0.01
Na_2O	24.63	24.53	24.77	24.59	25.04	24.70	24.87
K_2O	0.00	0.05	0.01	0.04	0.00	0.00	0.01
F	0.02	0.00	0.00	0.00	0.00	0.00	0.00
Cl	7.11	7.12	7.11	6.86	7.28	7.31	7.35
Total	100.50	101.57	100.78	101.14	100.05	100.23	100.24
Normalized on 12 T-cations							
Si	5.99	5.95	5.93	5.98	5.95	5.98	5.95
Al	6.01	6.05	6.07	6.02	6.05	6.02	6.05
Fe	0.02	0.03	0.01	0.05	0.02	0.01	0.01
Mn	0.00	0.01	0.00	0.00	0.00	0.00	0.01
Mg	0.01	0.01	0.00	0.00	0.00	0.00	0.00
Ca	0.01	0.01	0.01	0.02	0.00	0.00	0.00
Na	7.73	7.58	7.74	7.65	7.96	7.80	7.87
K	0.00	0.01	0.00	0.01	0.00	0.00	0.00
F	0.01	0.00	0.00	0.00	0.00	0.00	0.00
Cl	1.95	1.92	1.94	1.86	2.02	2.02	2.03

Tab. 5

Selected EPM analyses of spinel. Normalized to 3 cations and 4 oxygens; where not analytically determined, Fe^{3+} is calculated based on charge balance. Numbers correspond to those shown in Fig. 6.

Number anal.	1	2	7	8	09	010	011
SiO_2	0.01	0.02	0.01	0.00	0.09	0.00	0.00
TiO_2	0.16	0.10	0.07	0.02	0.00	0.14	0.00
Al_2O_3	52.57	52.48	53.11	50.54	52.52	50.06	52.09
Cr_2O_3	12.99	13.06	13.00	14.74	13.36	16.76	14.35
Fe_2O_3	NA	NA	NA	NA	3.37	3.25	4.10
FeO	13.00	12.76	12.86	13.31	11.20	11.51	10.80
MnO	0.12	0.14	0.11	0.14	0.00	0.00	0.00
MgO	18.11	18.41	18.44	18.06	18.99	18.74	19.37
NiO	0.32	0.29	0.25	0.26	NA	NA	NA
ZnO	0.22	0.20	0.25	0.30	NA	NA	NA
Total	97.50	97.46	98.10	97.36	99.54	100.46	100.71
Normalized on 3 cations and 4 oxygens							
Si	0.00	0.00	0.00	0.00	0.00	0.00	0.00
Ti	0.00	0.00	0.00	0.00	0.00	0.00	0.00
Al	1.68	1.67	1.68	1.63	1.65	1.58	1.62
Cr	0.28	0.28	0.28	0.32	0.28	0.35	0.30
Fe^{3+}	0.04	0.04	0.04	0.05	0.07	0.07	0.08
Fe^{2+}	0.26	0.25	0.25	0.25	0.25	0.26	0.24
Mn	0.00	0.00	0.00	0.00	0.00	0.00	0.00
Mg	0.73	0.74	0.74	0.74	0.75	0.75	0.76
Ni	0.01	0.01	0.01	0.01			
Zn	0.00	0.00	0.00	0.00			

Tab. 6

Selected EPM analyses of apatite. Numbers correspond to those shown in Fig. 5

Number anal.	36	37	38	40	41	42	43	45	46	47	48	49	50
Na_2O	0.02	0.03	0.00	0.21	0.08	0.04	0.18	0.11	0.05	0.24	0.18	0.21	0.17
MgO	0.14	0.13	0.12	0.06	0.19	0.16	0.07	0.24	0.09	0.12	0.05	0.12	0.08
CaO	53.76	54.43	54.00	49.69	54.24	54.20	50.16	53.88	53.03	47.90	48.37	49.61	50.59
SrO	0.75	0.56	0.73	5.78	0.58	0.49	4.55	0.41	1.37	6.18	6.40	5.18	4.13
MnO	0.00	0.03	0.02	0.01	0.02	0.00	0.00	0.00	0.06	0.00	0.00	0.03	0.01
FeO	0.22	0.12	0.12	0.17	0.25	0.14	0.23	0.52	0.27	0.28	0.17	0.30	0.31
Al_2O_3	0.02	0.00	0.01	0.00	0.00	0.01	0.00	0.00	0.01	0.02	0.00	0.02	0.02
Y_2O_3	0.06	0.05	0.07	0.01	0.08	0.11	0.03	0.05	0.01	0.09	0.04	0.00	0.00
La_2O_3	0.44	0.06	0.22	0.47	0.47	0.00	0.23	0.19	0.00	0.75	0.51	0.46	0.00
Ce_2O_3	0.52	0.33	0.45	0.87	0.45	0.29	0.77	0.25	0.42	0.93	0.82	0.83	0.67
Pr_2O_3	0.00	0.11	0.14	0.00	0.21	0.61	0.00	0.00	0.21	0.16	0.14	0.42	0.01
Nd_2O_3	0.20	0.15	0.10	0.13	0.34	0.29	0.00	0.16	0.03	0.18	0.00	0.18	0.00
SiO_2	0.89	0.65	0.59	0.32	0.94	0.93	0.33	1.38	0.45	0.45	0.34	0.42	0.28
P_2O_5	40.53	41.00	41.68	40.06	41.26	41.23	41.26	40.43	41.00	39.79	40.01	40.21	40.34
SO_3	0.02	0.14	0.03	0.00	0.14	0.21	0.03	0.39	0.01	0.04	0.00	0.00	0.01
F^-	1.66	1.52	1.54	1.88	1.45	1.34	1.35	1.34	1.08	1.58	1.73	1.47	1.34
Cl^-	0.32	0.27	0.28	0.07	0.30	0.30	0.17	0.36	0.35	0.18	0.12	0.15	0.13
Σ wt%	99.53	99.56	100.10	99.74	101.01	100.34	99.36	99.71	98.43	98.88	98.88	99.62	98.07
H_2O*	1.73	1.90	1.88	1.56	1.96	2.07	2.06	2.03	2.26	1.77	1.66	1.92	2.07
Σ wt%*	101.27	101.47	101.98	101.30	102.98	102.41	101.42	101.74	100.69	100.65	100.54	101.54	100.14
Empirical formula (calculated on 13 oxygens)													
Na	0.003	0.005	0.000	0.037	0.014	0.007	0.031	0.018	0.009	0.042	0.032	0.037	0.029
Mg	0.017	0.017	0.016	0.008	0.025	0.021	0.009	0.031	0.012	0.016	0.007	0.016	0.011
Ca	4.995	5.034	4.964	4.728	4.963	4.976	4.724	4.965	4.975	4.609	4.644	4.719	4.831
Sr	0.038	0.028	0.036	0.298	0.029	0.024	0.232	0.020	0.070	0.322	0.333	0.267	0.214
Mn	0.000	0.002	0.001	0.001	0.002	0.000	0.000	0.000	0.004	0.000	0.000	0.002	0.000
Fe	0.016	0.008	0.009	0.013	0.018	0.010	0.017	0.037	0.020	0.021	0.013	0.022	0.023
Al	0.002	0.000	0.001	0.000	0.000	0.001	0.000	0.000	0.001	0.002	0.000	0.002	0.002
Y	0.003	0.002	0.003	0.001	0.004	0.005	0.001	0.002	0.000	0.004	0.002	0.000	0.000
La	0.014	0.002	0.007	0.015	0.015	0.000	0.007	0.006	0.000	0.025	0.017	0.015	0.000
Ce	0.017	0.010	0.014	0.028	0.014	0.009	0.025	0.008	0.013	0.031	0.027	0.027	0.022
Pr	0.000	0.003	0.004	0.000	0.007	0.019	0.000	0.000	0.007	0.005	0.004	0.014	0.000
Nd	0.006	0.005	0.003	0.004	0.010	0.009	0.000	0.005	0.001	0.006	0.000	0.006	0.000
Si	0.077	0.056	0.051	0.028	0.080	0.079	0.029	0.118	0.040	0.040	0.031	0.037	0.025
P	2.975	2.996	3.027	3.012	2.983	2.991	3.070	2.943	3.040	3.025	3.035	3.022	3.044
S	0.001	0.009	0.002	0.000	0.009	0.013	0.002	0.025	0.001	0.003	0.000	0.000	0.001
F	0.454	0.415	0.419	0.529	0.392	0.363	0.375	0.366	0.299	0.448	0.491	0.412	0.378
Cl	0.047	0.039	0.041	0.011	0.043	0.044	0.025	0.053	0.051	0.027	0.018	0.023	0.019
OH	0.499	0.546	0.540	0.461	0.565	0.593	0.600	0.582	0.649	0.525	0.491	0.565	0.603

* H_2O content is calculated on the number of OH in empirical formula

Tab. 7

Whole-rock chemical composition of picritic rocks from the Poniky boreholes. KP-24, KP-27 (Hovorka & Slavkay, 1966), MV-81 – new analysis. For sample MV-81, only total iron as Fe_2O_3 was determined.

	KP-24	KP-27	MV-81
SiO_2	34.06	38.12	37.3
TiO_2	1.34	2.02	1.74
Al_2O_3	5.72	7.57	6.24
Fe_2O_3	6.75	6.52	9.65
FeO	3.93	4.04	
MnO	0.12	0.19	0.14
MgO	22.26	16.94	22.83
CaO	9.05	10.65	5.92
Na_2O	0.41	0.96	0.26
K_2O	0.92	1.02	0.94
P_2O_5	0.74	0.85	0.65
LOD	3.07	1.86	
LOI	10.87	8.15	13.5
Total	99.24	98.89	99.17
La	53.85		39.17
Ce	101.21		72.94
Nd	46.02		32.63
Sm	10.3		7.27
Eu	2.61		1.75
Gd	6.82		4.83
Dy	4.64		3.19
Er	2.03		1.41
Yb	1.33		0.96
Lu	0.18		0.13
Y	18.85		12.83
Ba	455		303
Co	110	117	114
Cu	48	27	39
Nb	71		53
Ni	873	1,040	1,232
Sc	18	21	15
Sr	562		291
V	173		138
Zn	135	117	124
Zr	209	224	159
B	21.4	24.5	
Cr	680	710	
Ga	14	10	
U			1
Th			8

Discussion

Petrogenesis

The chemical signature of mantle-crust interaction in subduction zones is characterized by a negative Nb-Ta anomaly (Pearce, 2008). Our sample does not display such an anomaly (Fig. 11B); we thus suggest that the studied melt is a product of intraplate magmatic activity and was not modified by subduction processes. The absence of an Eu anomaly suggests limited plagioclase fractionation and supports a relatively primitive, mantle-derived magma source. This interpretation is also supported by the high whole-rock Mg# (> 0.75). However, some degree of mantle metasomatism cannot be ruled out. First, Sr-rich rims on apatites, which were probably formed during late magmatism by residual melts enriched in Sr, volatiles, LREE, and LILE, as suggested by Zhang et al. (2011). Secondly, Ti-rich amphibole (kaersutite) is not commonly found in primary melts (Martin, 2007). The presence of these phases thus suggests that the magma that formed the picritic rocks near Poniky was derived from a metasomatized mantle source (Pilet et al., 2008; O'Reilly & Griffin, 2000).

Alkaline affinity

All presented results, including mineral composition, mineral chemistry and whole-rock chemistry, are consistent with the interpretation that the studied meimechites formed as part of an alkaline volcanic series. This interpretation is clearly supported by the newly documented occurrence of sodalite, a characteristic phase of alkaline rocks (Deer et al., 2013). Moreover, the strong enrichment in LILE, the high LREE content relative to HREE, and the elevated P_2O_5 content (> 0.65 wt%) are consistent with an alkaline affinity. The analysed samples are equivalent to oceanic-island alkaline basalts (Fig. 10). Most importantly, by comparing these data with picrite occurrences from the External Western Carpathians, we infer a genetic similarity between these rocks and the teschenite-picrite association. (Figs. 10, 11A, B) (Brunarska & Anczkiewicz, 2019; Kudělásková, 1987).

Regional comparison and tectonic implications

Hovorka & Slavkay (1966) considered the relationship between the Poniky picrites and the dolomites to be a normal stratigraphic relationship, i.e., synsedimentary volcanism. However, the relationship between the overlying and underlying complexes could not be clearly demonstrated due to the low drill core yield (Spišiak & Hovorka, 2000). Because the host dolomites were affiliated with the Hronic Unit, this was the only documented occurrence of such volcanic rocks in the Hronic Unit. However, similar alkaline volcanic rocks (although significantly altered) were documented near Banská Bystrica at Predný diel in carbonate rocks of the Fatric Unit (borehole ŠŠ II, Fig. 1; Slavkay, 1979), and, in fact, they are widespread in the Fatric Unit (Hovorka & Spišiak, 1988; Spišiak & Hovorka, 1997). This raised the question of whether similar rocks could occur in two different tectonic units with allochthonous provenance. From a lithostratigraphic perspective, based on current knowledge, there is no problem with classifying the studied Mesozoic sequence as part of the Hronicum (Fig. 1a). However, correlation with other picrite occurrences near Banská Bystrica also suggests an alternative interpretation: that the host dolomites belong to the Fatric Unit and that the studied meimechite occurrence is one of many manifestations of Cretaceous alkaline volcanic activity documented in the Fatric Unit (Spišiak & Hovorka, 2000). Taking all available evidence into account, the most plausible interpretation is that the Fatric and Hronic tectonic units were already in close proximity during the volcanic activity discussed herein.

Ivan (1991) documented an occurrence of a metamorphosed picritic rock near Medzev in the Gemeric Unit. However, this occurrence differs significantly in chemical composition from the picritic rock presented from Poniky. It has markedly lower TiO_2 (0.48 wt%), P_2O_5 (0.14 wt%), and alkali element concentrations (0.01 wt% Na_2O, 0.01 wt% K_2O), as well as lower REE concentrations, which exclude the possibility that it is a part of the same alkaline suite. In fact, it is interpreted as a differentiated basic (MOR) magma associated with basalts of the Gelnica Group (Ivan, 1991). Therefore, the picritic rock from Medzev is genetically and geochronologically unrelated to the studied rocks from Poniky.

Conclusion

- The mineral composition of picritic rocks from the Poniky area is consistent with picrites associated with alkaline rocks. This classification is supported not only by the presence of sodalite but also by whole-rock chemical composition.
- The analysed picritic rocks are equivalent to Cretaceous alkaline basalts/basanites occurring in the Fatric Unit of the Western Carpathians. Consequently, they are also similar in composition to picrites from the ‘teschenite association’ in the External Western Carpathians.
- Whole-rock chemical composition classifies the analysed picritic rocks as meimechites. This is the first documentation of a meimechite in the Central Western Carpathians.

Acknowledgments:

This paper is dedicated to the memory of Prof. Ján Spišiak, who passed away in April 2026. We are grateful to the chief editor, Ondrej Pelech, and the two reviewers, Irena Brunarská and Martin Ondrejka, for their insightful comments and recommendations, which significantly improved this manuscript. This work was funded by the Slovak Research and Development Agency under contract APVV-22-0092 and by the Matej Bel University Grants Agency (UGA-02-PDS-2024 and UGA-PD-05-2024).

References

Bosi, F., Biagioni, C. & Pasero, M., 2019: Nomenclature and classification of the spinel supergroup. *European Journal of Mineralogy*, 31, 1, 183–192. https://doi.org/10.1127/ejm/2019/0031-2788.

Brunarska, I. & Anczkiewicz, R., 2019: Geochronology and Sr-Nd-Hf isotope constraints on the petrogenesis of teschenites from the type-locality in the Outer Western Carpathians. *Geologica Carpathica*, 70, 3, 222–240. https://doi.org/ 10.2478/geoca-2019-0013.

Buriánek, D., Kropáč, K. & Dolníček, Z., 2013: Ultrabazické horniny těšínitové asociace v západní části Slezské jednotky. *Geologické výzkumy na Moravě a ve Slezsku*, 20, 1–2, 79–84.

Deer, W. A., Howie, R. A. & Zussman, J., 2013: An introduction to the rock-forming minerals. Mineral Society of Great Britain and Ireland. *Stevenage, Berforts Information Press*, 510 pp.

Hawthorne, F. C., Oberti, R., Harlow, G. E., Maresch, W. V., Martin, R. F., Schumacher, J. C. & Welch, M. D., 2012: Nomenclature of the amphibole supergroup. *American Mineralogist*, 97, 11–12, 2031–2048. https://doi.org/10.2138/am.2012.4276.

Hovorka, D., 1976: Predterciérne formácie bazitov Západných Karpát. *Mineralia Slovaca*, 2 8, 113–132.

Hovorka, D. & Slavkay, M., 1966: Pikrit od Poník. *Geologické práce, Správy*, 39, 41–51.

Hovorka, D. & Spišiak, J., 1988: Vulkanizmus mezozoika Západných Karpát. *Bratislava, Veda*, 272 pp.

Ivan, P., 1991: Metamorfovaný pikrit zo Strážneho vrchu pri Medzeve (gelnická skupina, paleozoikum gemerika). *Mineralia Slovaca*, 23, 155–159.

Kamenetsky, V. S., Crawford, A. J. & Meffre, S., 2001: Factors Controlling Chemistry of Magmatic Spinel: an Empirical Study of Associated Olivine, Cr-spinel and Melt Inclusions from Primitive Rocks. *Journal of Petrology*, 42, 4, 655–671. https://doi.org/10.1093/petrology/42.4.655.

Kerr, A. C. & Arndt, N. T., 2001: A Note on the IUGS Reclassification of the High-Mg and Picritic Volcanic Rocks. *Journal of Petrology*, 42, 11, 2169–2171. https://doi.org/10.1093/petrology/42.11.2169.

Kudělásková, J., 1987: Petrology and Geochemistry of Selected Rock Types of Teschenite Association, Outer Western Carpathians. *Geologický zborník – Geologica Carpathica*, 38, 5, 545–573.

Kynický, J., Xu, C., Bajer, A., Samec, P. & Kynická, A., 2009: Nové výzkumy v horninách těšínitové asociace: fluorapatit se zvýšenými obsahy Sr a REE. *Geologické výzkumy na Moravě a ve Slezsku*, 66–69.

Le Bas, M. J., 2000: IUGS Reclassification of the High-Mg and Picritic Volcanic Rocks. *Journal of Petrology,* 41, 10, 1467–1470. https://doi.org/10.1093/petrology/41.10.1467.

Locock, A. J., 2014: An Excel spreadsheet to classify chemical analyses of amphiboles following the IMA 2012 recommendations. *Computers & Geosciences*, 62, 1–11. https://doi.org/10.1016/j.cageo.2013.09.011.

Mahmood, A., 1973: Petrology of the teschenitic rock series from the type area of Cieszyn (Teschen) in the Polish Carpathians. *Annales Societatis Geologorum Poloniae*, 43, 2, 153–216.

Martin, R. F., 2007: Amphiboles in the Igneous Environment. *Reviews in Mineralogy and Geochemistry*, 67, 1, 323–358. https://doi.org/10.2138/rmg.2007.67.9.

McDonough, W. F. & Sun, S. S., 1995: The composition of the Earth. Chemical Geology, 120, 3–4, 223–253. https://doi.org/10.1016/0009-2541(94)00140-4.

Mikuš, T., Spišiak, J., Sýkora, M. & Demko, M., 2006: Chemical composition of spinels from Mesozoic alkali basalts of the Western Carpathians: implications for sources of detrital spinels in flysch sediments. *Geologica Carpathica*, 57, 6, 447–460.

Morimoto, N., 1988: Nomenclature of pyroxenes. *Bulletin de Minéralogie*, 111, 5, 535–550.

Mullen, E. D., 1983: $MnO/TiO_2/P_2O_5$: a minor element discriminant for basaltic rocks of oceanic environments and its implications for petrogenesis. *Earth and Planetary Science Letters*, 62, 1, 53–62. https://doi.org/10.1016/0012-821X(83)90070-5.

Ondrejka, M., Vojtko, R., Putiš, M., Chew, D. M., Olšavský, M., Uher, P., Nemec, O., Drakou, F., Molnárová, A. & Spišiak, J., 2022: Permian A-type rhyolites of the Drienok Nappe, Inner Western Carpathians, Slovakia: Tectonic setting from in-situ zircon U-Pb LA-ICP-MS dating. *Geologica Carpathica*, 73, 2, 123–136. https://doi.org/10.31577/GeolCarp.73.2.2.

O'Reilly, S. Y. & Griffin, W. L., 2000: Apatite in the mantle: implications for metasomatic processes and high heat production in Phanerozoic mantle. *Lithos*, 53, 3–4, 217–232. https://doi.org/10.1016/S0024-4937(00)00026-8.

Pearce, J. A., 2008: Geochemical fingerprinting of oceanic basalts with applications to ophiolite classification and the search for Archean oceanic crust. *Lithos*, 100, 1–4, 14–48. https://doi.org/10.1016/j.lithos.2007.06.016.

Pilet, S., Baker, M.B. & Stolper, E.M., 2008: Metasomatized Lithosphere and the Origin of Alkaline Lavas. *Science,* 320, 5878, 916–919. https://doi.org/10.1126/science.115656

Slavkay, M., 1971: Ložiská polymetalických rúd pri Ponikách. *Mineralia Slovaca*, 11, 3, 181–213.

Slavkay, M., 1979: Ďalšie výskyty ultrabázických efuzív v chočskom a krížňanskom príkrove pri Banskej Bystrici. *Mineralia Slovaca*, 11, 3, 239–245.

Slavkay, M., Tomko, I., Lukaj, M. & Barkáč, Z., 1968: Poniky – Pb rudy, záverečná správa z etapy vyhľadávacieho prieskumu a výpočet zásob so stavom k 30. XI. 1968. *Manuscript. Bratislava, Archive of St. Geol. Inst. of D. Štúr* (arch. no. 22903), 274 pp.

Šmíd, B., 1962: Přehled geologie a petrografie hornin těšínitové asociace na severním úpatí Beskyd. *Geologické práce, Zošit,* 63, 53–60.

Spišiak, J. & Hovorka, D., 1997: Petrology of the Western Carpathians Cretaceous Primitive Alkaline Volcanics. *Geologica Carpathica*, 48, 2, 113–121.

Spišiak, J. & Hovorka, D., 2000: Picrite Rocks in the Vicinity of Banská Bystrica (Krížna unit, Western Carpathians). *Slovak Geological Magazine*, 6, 4, 419–429.

Szopa, K., Włodyka, R. & Chew, D., 2014: LA-ICP-MS U-Pb apatite dating of Lower Cretaceous rocks from teschenite-picrite association in the Silesian Unit (southern Poland). *Geologica Carpathica*, 65, 4, 273–284. https://doi.org/10.2478/geoca-2014-0018.

Tischendorf, G., Förster, H.-J., Gottesmann, B. & Rieder, M., 2007: True and brittle micas: composition and solid-solution series. *Mineralogical Magazine*, 71, 3, 285–320. https://doi.org/10.1180/minmag.2007.071.3.285.

Zhang, W., Shao, J., Wang, R., Xu, X., Che, X. & Yang, Y., 2011: Sr-rich apatite from the Dangzishan leucitite-ijolite xenoliths (Heilongjiang Province): Mineralogy and mantle-fluid metasomatism. *Chinese Science Bulletin*, 56, 1, 53–63. https://doi.org/10.1007/s11434-010-4228-7.

Pikritické horniny (mejmečity) z Poník: mineralógia a petrológia (Západné Karpaty)

Pikrit je definovaný ako hypoabysálna, často porfýrická hornina s vysokým obsahom mafických minerálov a so zvýšeným obsahom MgO v porovnaní s bazaltmi (> 12 hm. %; Le Bas, 2000). Výskyty pikritov sú v Západných Karpatoch zriedkavé. Vo Vonkajších Západných Karpatoch sa vyskytujú ako súčasť kriedovej těšínitovo-pikritovej asociácie v sliezskej jednotke (Brunarska & Anczkiewicz, 2019; Buriánek et al., 2013; Hovorka, 1976; Hovorka & Spišiak, 1988; Kudělásková, 1987; Mahmood, 1973; Šmíd, 1962; Szopa et al., 2014). Vo Vnútorných Západných Karpatoch boli obmedzené výskyty pikritov opísané len z vrtov v mezozoických sedimentárnych sekvenciách v okolí Banskej Bystrice (Hovorka & Slavkay, 1966; Hovorka & Spišiak, 1988; Slavkay, 1979). Tieto pikritické horniny majú kriedový vek a geneticky súviseli s alkalickým vulkanizmom. Ojedinelý výskyt metamorfovaného pikritu bol zdokumentovaný aj v gelnickej skupine gemerika (Ivan, 1991).

Podstatné množstvo informácií o výskyte pikritov v okolí Banskej Bystrice bolo publikované už v monografii *Mezozoický vulkanizmus Západných Karpát* (Hovorka & Spišiak, 1988). Napriek tomu v tejto práci prezentujeme nové zaujímavé mineralogické a petrologické údaje o staršej vzorke pikritu z vrtu pri Ponikách. Okrem hlavných mafických minerálov (klinopyroxén, kaersutit, flogopit) sú opísané aj spinely, apatit bohatý na Sr (až do 6,4 hm. % SrO) a sodalit. Sodalit je vo Vnútorných Západných Karpatoch zdokumentovaný po prvýkrát a spolu s minerálnym a celohorninovým chemickým zložením hornín potvrdzuje ich alkalický charakter. Petrologické údaje vrátane REE ukazujú, že tieto horniny sú ekvivalentné kriedovým vulkanickým horninám vyskytujúcim sa vo fatriku, ako aj pikritickým horninám těšínitovo-pikritovej asociácie vo Vonkajších Západných Karpatoch. Vysoký obsah MgO (> 18 hm. %) umožňuje klasifikovať tieto horniny ako mejmečity.

Doručené / Received: 27. 3. 2026
Prijaté na publikovanie / Accepted: 15. 7. 2026

Mineralia Slovaca, Web ISSN 1338-3523, ISSN 0369-2086, https://doi.org/10.56623/ms.2026.58.1.3
58, 1 (2026), 51 – 66,

Pre-Cenozoic basement of the northeastern part of the Internal Western Carpathians from the perspective of the geological structure of the Tatry and Branisko mountains

JOZEF HÓK[1,*], ONDREJ PELECH[2], MÁRIO OLŠAVSKÝ[3], MARTIN ŠUJAN[4], IVANA PEŠKOVÁ[1], DAVID MILOŠ DROPPA[1], FRANTIŠEK ŠIPKA[3] and MIROSLAV BIELIK[5]

[1] Department of Geology and Paleontology, Faculty of Natural Sciences, Comenius University Bratislava, Mlynská dolina, Ilkovičova 6, 842 15 Bratislava, Slovak Republic
[2] State Geological Institute of Dionýz Štúr, Mlynská dolina 1, 817 04 Bratislava, Slovak Republic
[3] State Geological Institute of Dionýz Štúr, Zelená 5, 974 04 Banská Bystrica
[4] EQUIS, spol. s r. o., Račianska 57, 831 02 Bratislava, Slovak Republic
[5] Department of Applied and Environmental Geophysics, Faculty of Natural Sciences, Comenius University Bratislava, Mlynská dolina, Ilkovičova 6, 842 15 Bratislava, Slovak Republic
* Corresponding author: jozef.hok@uniba.sk

Abstract: The area between the Tatry and Branisko mountain ranges in northeastern Slovakia represents the most extensive territory covered by Paleogene sediments within the Internal Western Carpathians. In order to compile a tectonic map of the pre-Cenozoic basement, the locations at which the basement was present on the surface were analysed in detail to determine their tectonic affiliation. The Havran structure, previously classified as Fatricum, has been reclassified as Veporicum in the eastern part of the Tatry Mts. The rock complexes in the Branisko Mts. that were previously classified as part of the Tatric tectonic unit are now considered an integral part of the Veporicum. The pre-Cenozoic basement of the studied area comprises the Fatricum, Veporicum and Hronicum. The Mesozoic sediments of Fatric tectonic unit occur south of the surface outcrops of Oravic sediments. South of this, the pre-Cenozoic basement contains the Veporicum and Hronicum tectonic units.

Key words: tectonics, Tatricum, Veporicum, Fatricum, Hronicum

Introduction

Cenozoic sediments and volcanic rocks cover more than half of the territory of Slovakia. Together with locally preserved Upper Cretaceous rocks, they represent post-nappe sedimentary sequences within the Internal Western Carpathians (*sensu* Hók et al., 2019). Knowledge of the geological structure of the areas buried beneath the Cenozoic basins is essential not only for understanding the geometry and relationships of the Alpine tectonic units in their basement, but also for applied purposes, such as the exploration of geothermal water and energy.

The study area is situated in the northeastern part of the Internal Western Carpathians (IWECA) and represents the largest coherent region covered by Paleogene sediments (Fig. 1). The geological structure of the study area is depicted on several regional geological maps at a scale of 1:50,000 (Bajaník et al., 1984; Biely et al., 1992; Gross et al., 1999; Mello et al., 2000; Nemčok, 1990; Nemčok et al., 1994; Polák et al., 1996) or on the Geological Map of Slovak Republic (2013). The tectonic setting of the pre-Cenozoic basement was published by Fusán et al. (1987).

The surface geological structure is significantly dominated by Paleogene sediments of the Sub-Tatra Group (*sensu* Gross et al., 1984; Gross, 2008). Pre-Cenozoic rock complexes consist mainly of Mesozoic and locally Upper Paleozoic sedimentary cover of the Tatricum, Veporicum (Northern Veporicum) or Gemericum and allochthonous Fatric, Hronic, and Silicic cover nappes. Pre-Mesozoic crystalline basement complexes are represented by Paleozoic plutonic and metamorphic rocks of the Tatric, Veporic, and Gemeric thick-skinned tectonic units (Hók et al., 2019). Based on a detailed and critical analysis of the surface geological structure in the Tatry and Branisko Mts., supplemented borehole data and geophysical interpretations, this paper re-evaluates existing knowledge on the geological structure of the pre-Cenozoic basement, and provides new innovative view which differs from the previous interpretation (e.g., Fusán et al., 1987) mainly in terms of the tectonic categorization of the Tatric and Veporic rock complexes.

They also include information on structural geology concerning paleostress fields and significant faults.

The method employed involved mutual extrapolation and interpolation of surface data, borehole results, geophysical data and structural data. The principle of constructing a pre-Cenozoic basement map by extrapolation involves projecting surface data no more than halfway to different geological object (tectonic unit). In contrast, interpolation involves connecting identical surface geological objects or assuming their continuous extension into the basement be-

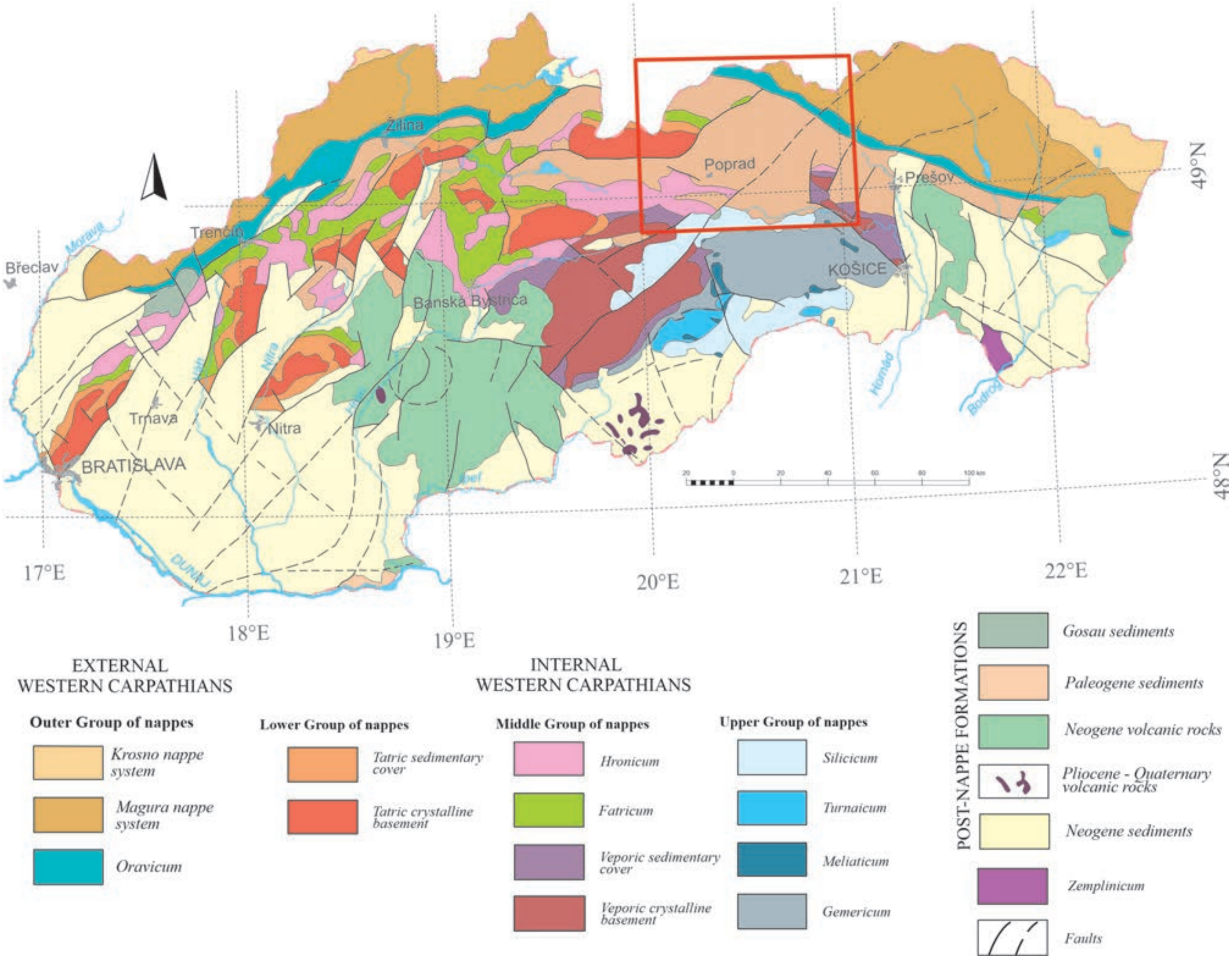

Fig. 1. Simplified tectonic map of Slovakia (Hók et al., 2019). The red rectangle represents the study area.

Methodology

The map of the pre-Cenozoic bedrock is based on a comprehensive review of published works and archived reports. The collected data have been categorized and expertly analysed. The input data primarily consists of the results of geological surveys (i.e. geological maps), boreholes (i.e. lithology and stratigraphy) and geophysical surveys (i.e. gravimetric, electric and seismic methods).

neath Cenozoic sediments or volcanic rocks. Continuous extension from the surface may be modified if limiting data from boreholes, geophysical surveys or structural data are available in the given area. Knowledge of the geological structure, especially the lithostratigraphic composition of individual tectonic units and their superposition, plays an important role here. Information obtained from boreholes represents the most important source, which largely complements or expands upon the previous one. A borehole ultimately provides only point data. Therefore, the results obtained are always extrapolated or interpolated between individual boreholes or between a borehole and surface data.

When collecting data on the characteristics of pre-Cenozoic bedrock, especially from boreholes, the original description of the rock complexes encountered is important, as its quality can and often does vary. In this case, an expert decision must be made, either based on a direct inspection of the drill cores or based on a correlation with the geological conditions of the nearest surface or with other nearby boreholes, and finally based on a comparison with the latest generally accepted tectonic conditions.

The information obtained from the geophysical data was primarily derived from gravimetry (see Fig. 2), as these data are of supraregional significance and the results are consistently available across Slovakia (Kilényi & Šefara, 1989; Pašteka et al., 2017; Zahorec et al., 2021). To a lesser extent, results from seismic, magnetotelluric and electrical sounding, or electrical resistivity tomography have been used. These are mostly limited to individual areas and their correct interpretation often depends on correct correlation with surface or borehole data.

Structural and tectonic data are integral to correctly interpreting tectonic conditions in areas covered by Cenozoic sediments. Understanding these conditions and their proper extrapolation is of primary importance. The fundamental aspects of the Variscan orogeny must be considered, as well as the strict distinction of the structural character of Paleo-Alpine tectonic deformation (Jurassic–Cretaceous) from the consequences of Neo-Alpine tectonic processes (Cenozoic), and their mutual interaction, within the Alpine tectonic stage.

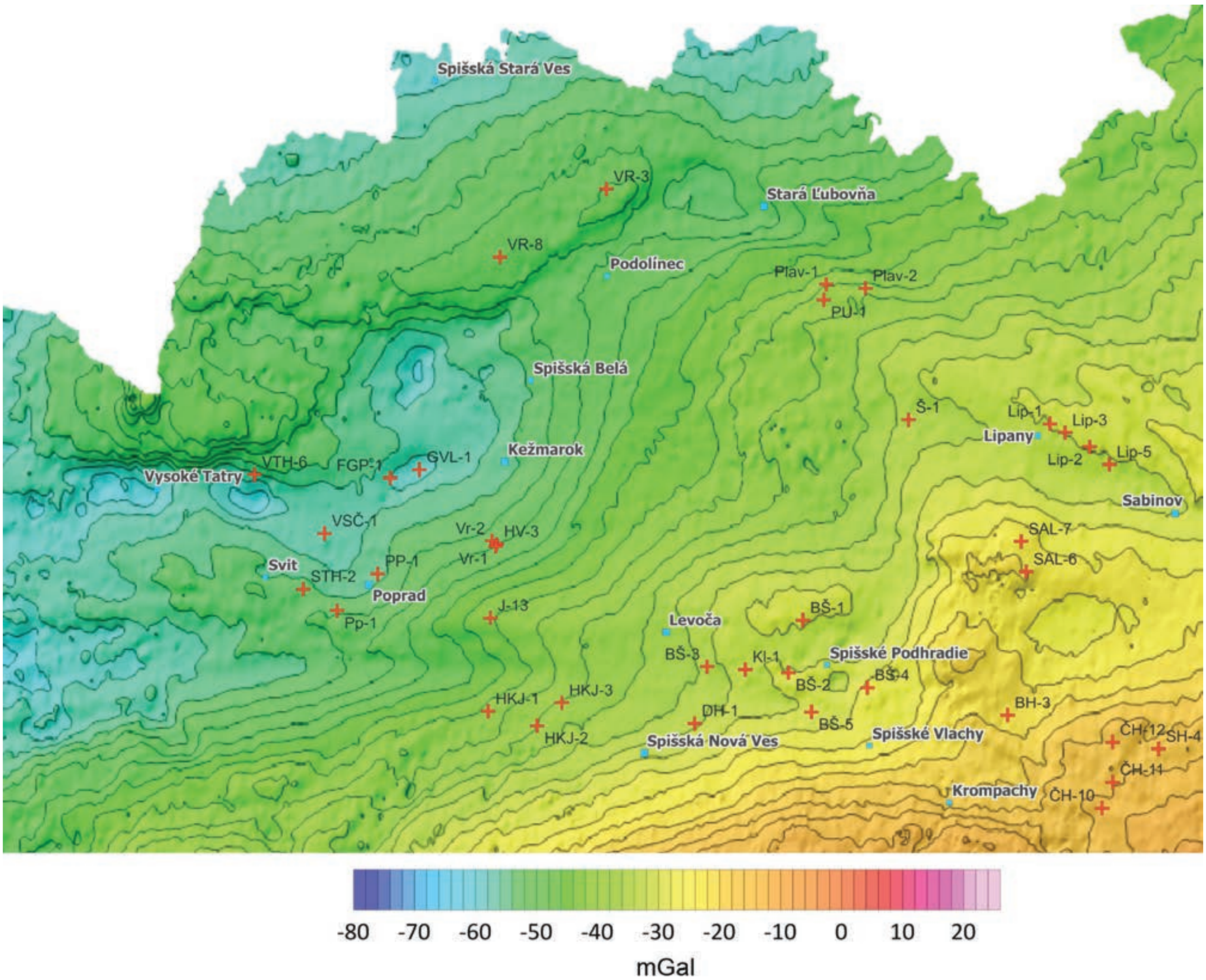

Fig. 2. Map of complete Bouguer anomalies in the study area showing the locations of boreholes that reached the pre-Cenozoic basement (Pašteka et al., 2017; Zahorec et al., 2021).

Surface occurrences of the pre-Cenozoic basement

Pre-Cenozoic basement in the area of interest (Fig. 3) is exposed at the surface in the Tatry Mts., the Vikartovský chrbát Ridge, Slovenský raj, Galmus, Spišsko-gemerské rudohorie Mts., Branisko, and Čierna Hora Mts., as well as in the Pieniny Klippen Belt. The Mesozoic formations of the Pieniny Klippen Belt have no significant impact on the structure of the pre-Cenozoic basement in the IWECA region.

The Tatry Mountains

The geological structure of the Tatry Mts. is depicted on the geological map and in the accompanying explanatory notes (Nemčok et al., 1993, 1994). In many aspects, the map is based on earlier publications by Uhlig (1900), Lugeon (1903), and especially Andrusov (1950). Notably, the geological map of the Vysoké Tatry area between the Bielovodská dolina and Javorová dolina Valleys has not been re-examined in detail since Andrusov's work in 1950. According to Nemčok et al. (1993, 1994), the Vysoké Tatry and Belianske Tatry regions comprise the Tatric and Fatric tectonic units. The crystalline basement rocks are represented by several types of granitoid and metamorphic rocks, which are generally considered to be part of the Tatricum. However, Andrusov (1950) states: *"... the origin of the crystalline cores of the recumbent folds of the Široká massif must be placed far to the south of their present location."*

The tectonic setting of the Vysoké Tatry (VT) and Belianske Tatry (BT) mountains differs markedly to the west, roughly along the north-south line connecting the Bielovodská dolina Valley, the Roztoky Valley and the Kôprová dolina Valley (the Kôprová dolina Valley Fault, as defined (the Kôprová dolina Valley fault, as defined by Bezák et al., 2004). The tectonic affiliation of parts of the Tatric and Fatric rock complexes is disputed. The Kôprová dolina Valley (also known as the Kôprová Fault Zone; Nemčok et al., 1993) runs through the Tatra Mountains, separating the elevated western part from the depressed eastern part.

To the west of the Kôprová dolina Valley Fault (KVF), the Mesozoic sedimentary rocks of the Tatricum are divided into an autochthonous part, represented by the Tomanová sequence, and cover-unit duplexes, namely Czerwone Wierchy, Giewont and Goryczkowa (Nemčok et al., 1993; Ostrowski et al., 2026). Granitoids are also present here, alongside cover Mesozoic sedimentary sequences in several duplexes (Bac-Moszaszwili et al., 1984). From a lithofacial and lithostratigraphic perspective, the Tatric cover has been divided and grouped into a number of different sequences (Kotański, 1961). However, defining the Tatricum in this area does not pose any significant problems. To the east of the KVF, duplexes of the cover sediments are absent, with only sediments of the cover units present in the Široká area (2,210 m a.s.l.). There, a rudimentary cover of crystalline basement rocks, in the form of the Lúžna Formation (Lower Triassic), is preserved. The Fatricum is present in two superimposed structures, the Havran and the Bujačí nappes (Nemčok et al., 1993, 1994).

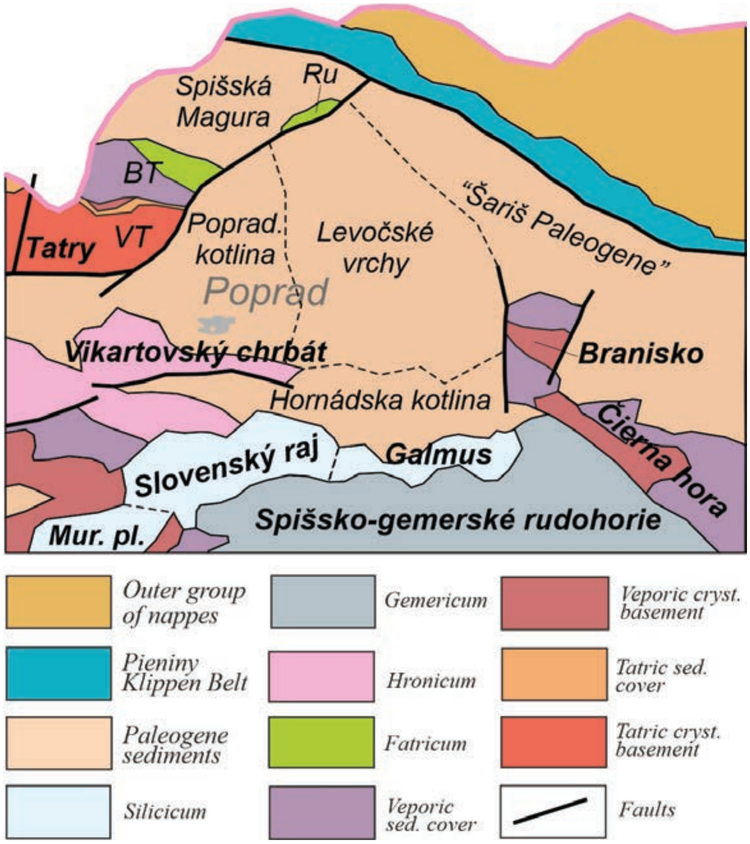

Fig. 3. Simplified tectonic map and regional geological division (Vass et al., 1988) of the study area. VT – Vysoké Tatry subunit, BT – Belianske Tatry subunit, Ru – ružbašský ostrov.

Fig. 4. A section from the geological map of the Tatry Mountains (Nemčok et al., 1994) with explanations and markings of the presumed Veporicum structures. The inverted stratigraphic sequence of a recumbent fold, whose core consists of crystalline rock and which today represents the Veporic outlier, is illustrated in Fig. 5.

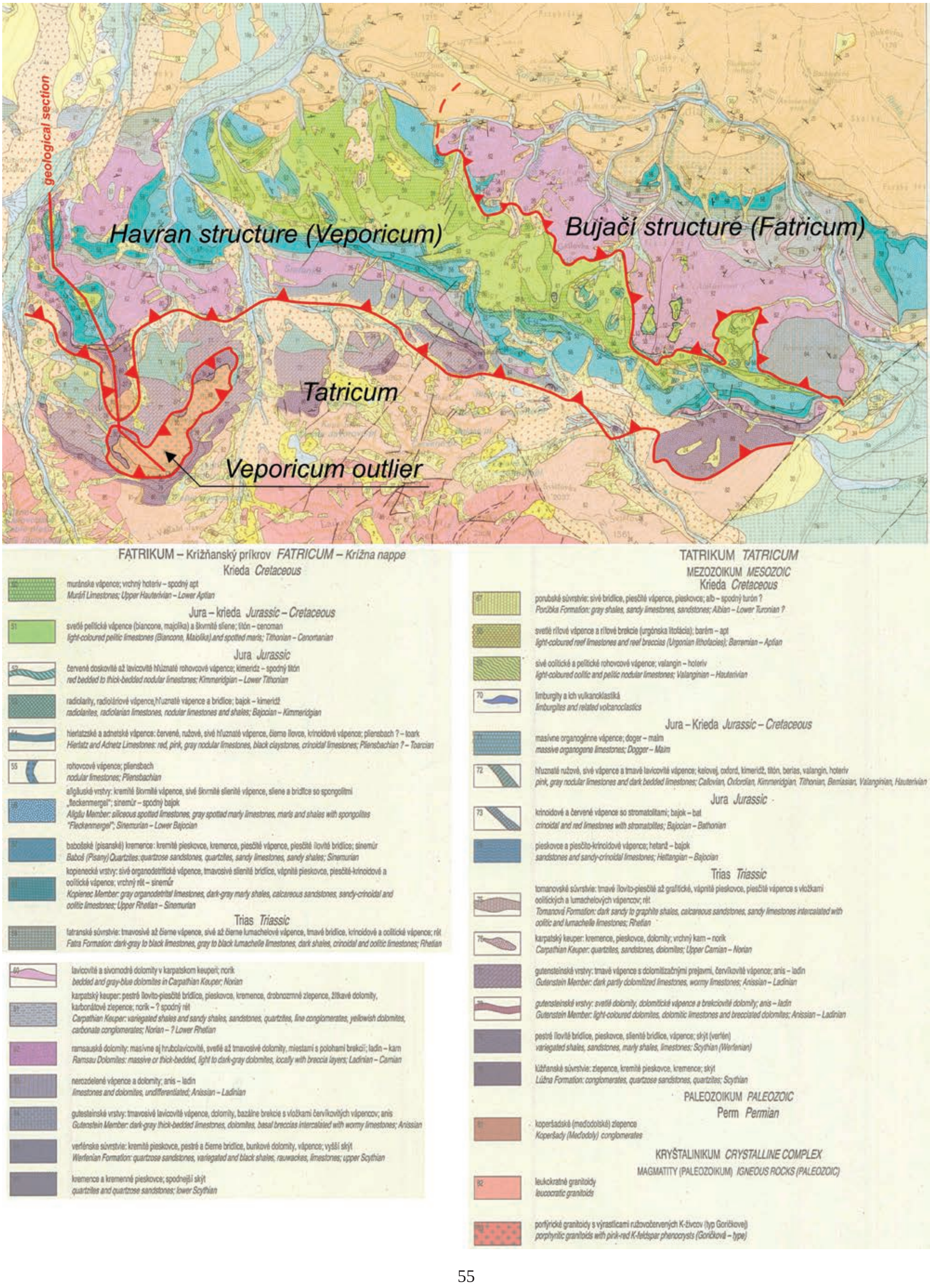
geological section
Havran structure (Veporicum)
Bujačí structure (Fatricum)
Tatricum
Veporicum outlier
FATRIKUM – Krížňanský príkrov FATRICUM – Krížna nappe
Krieda Cretaceous
muránske vápence; vrchný hoteriv – spodný apt
Muráň Limestones; Upper Hauterivian – Lower Aptian
Jura – krieda Jurassic – Cretaceous
svetlé pelitické vápence (biancone, majolika) a škvrnité sliene; titón – cenoman
light-coloured pelitic limestones (Biancone, Maiolika) and spotted marls; Tithonian – Cenomanian
Jura Jurassic
červené doskovité až lavicovité hľuznaté rohovcové vápence; kimeridž – spodný titón
red bedded to thick-bedded nodular limestones; Kimmeridgian – Lower Tithonian
radiolarity, radioláriové vápence, hľuznaté vápence a bridlice; bajok – kimeridž
radiolarites, radiolarian limestones, nodular limestones and shales; Bajocian – Kimmeridgian
hierlatzské a adnetské vápence: červené, ružové, sivé hľuznaté vápence, čierne ílovce, krinoidové vápence; pliensbach ? – toark
Hierlatz and Adnetz Limestones: red, pink, gray nodular limestones, black claystones, crinoidal limestones; Pliensbachian ? – Toarcian
55
rohovcové vápence; pliensbach
nodular limestones; Pliensbachian
allgäuské vrstvy: kremité škvrnité vápence, sivé škvrnité slienité vápence, sliene a bridlice so spongolitmi „fleckenmergel"; sinemúr – spodný bajok
Allgäu Member: siliceous spotted limestones, gray spotted marly limestones, marls and shales with spongolites "Fleckenmergel"; Sinemurian – Lower Bajocian
babošské (pisanské) kremence: kremité pieskovce, kremence, piesčité vápence, piesčité ílovité bridlice; sinemúr
Baboš (Pisany) Quartzites: quartzose sandstones, quartzites, sandy limestones, sandy shales; Sinemurian
kopienecké vrstvy: sivé organodetritické vápence, tmavosivé slienité bridlice, vápnité pieskovce, piesčito-krinoidové a oolitické vápence; vrchný rét – sinemúr
Kopienec Member: gray organodetrital limestones, dark-gray marly shales, calcareous sandstones, sandy-crinoidal and oolitic limestones; Upper Rhetian – Sinemurian
Trias Triassic
fatranské súvrstvie: tmavosivé až čierne vápence, sivé až čierne lumachelové vápence, tmavé bridlice, krinoidové a oolitické vápence; rét
Fatra Formation: dark-gray to black limestones, gray to black lumachelle limestones, dark shales, crinoidal and oolitic limestones; Rhetian
60
lavicovité a sivomodré dolomity v karpatskom keuperi; norik
bedded and gray-blue dolomites in Carpathian Keuper; Norian
karpatský keuper: pestré ílovito-piesčité bridlice, pieskovce, kremence, drobnozrnné zlepence, žltkavé dolomity, karbonátové zlepence; norik – ? spodný rét
Carpathian Keuper: variegated shales and sandy shales, sandstones, quartzites, fine conglomerates, yellowish dolomites, carbonate conglomerates; Norian – ? Lower Rhetian
ramsauské dolomity: masívne aj hrubolavicovité, svetlé až tmavosivé dolomity, miestami s polohami brekcií; ladin – karn
Ramsau Dolomites: massive or thick-bedded, light to dark-gray dolomites, locally with breccia layers; Ladinian – Carnian
nerozdelené vápence a dolomity; anis – ladin
limestones and dolomites, undifferentiated; Anissian – Ladinian
gutesteinské vrstvy: tmavosivé lavicovité vápence, dolomity, bazálne brekcie s vložkami červíkovitých vápencov; anis
Gutenstein Member: dark-gray thick-bedded limestones, dolomites, basal breccias intercalated with wormy limestones; Anissian
verfénske súvrstvie: kremité pieskovce, pestré a čierne bridlice, bunkové dolomity, vápence; vyšší skýt
Werfenian Formation: quartzose sandstones, variegated and black shales, rauwackes, limestones; upper Scythian
kremence a kremenné pieskovce; spodnejší skýt
quartzites and quartzose sandstones; lower Scythian
TATRIKUM TATRICUM
MEZOZOIKUM MESOZOIC
Krieda Cretaceous
67
porubské súvrstvie: sivé bridlice, piesčité vápence, pieskovce; alb – spodný turón ?
Porúbka Formation: gray shales, sandy limestones, sandstones; Albian – Lower Turonian ?
svetlé rífové vápence a rífové brekcie (urgónska litofácia); barém – apt
light-coloured reef limestones and reef breccias (Urgonian lithofacies); Barremian – Aptian
sivé oolitické a pelitické rohovcové vápence; valangin – hoteriv
light-coloured oolitic and pelitic nodular limestones; Valanginian – Hauterivian
70
limburgity a ich vulkanoklastiká
limburgites and related volcanoclastics
Jura – Krieda Jurassic – Cretaceous
masívne organogénne vápence; doger – malm
massive organogene limestones; Dogger – Malm
72
hľuznaté ružové, sivé vápence a tmavé lavicovité vápence; kelovej, oxford, kimeridž, titón, berias, valangin, hoteriv
pink, gray nodular limestones and dark bedded limestones; Callovian, Oxfordian, Kimmeridgian, Tithonian, Berriasian, Valanginian, Hauterivian
Jura Jurassic
73
krinoidové a červené vápence so stromatolitami; bajok – bat
crinoidal and red limestones with stromatolites; Bajocian – Bathonian
pieskovce a piesčito-krinoidové vápence; hetanž – bajok
sandstones and sandy-crinoidal limestones; Hettangian – Bajocian
Trias Triassic
tomanovské súvrstvie: tmavé ílovito-piesčité až grafitické, vápnité pieskovce, piesčité vápence s vložkami oolitických a lumachelových vápencov; rét
Tomanová Formation: dark sandy to graphite shales, calcareous sandstones, sandy limestones intercalated with oolitic and lumachelle limestones; Rhetian
karpatský keuper: kremence, pieskovce, dolomity; vrchný karn – norik
Carpathian Keuper: quartzites, sandstones, dolomites; Upper Carnian – Norian
gutensteinské vrstvy: tmavé vápence s dolomitizačnými prejavmi, červíkovité vápence; anis – ladin
Gutenstein Member: dark partly dolomitized limestones, wormy limestones; Anissian – Ladinian
gutensteinské vrstvy: svetlé dolomity, dolomitické vápence a brekciovité dolomity; anis – ladin
Gutenstein Member: light-coloured dolomites, dolomitic limestones and brecciated dolomites; Anissian – Ladinian
pestré ílovité bridlice, pieskovce, slienité bridlice, vápence; skýt (verfén)
variegated shales, sandstones, marly shales, limestones; Scythian (Werfenian)
lúžňanské súvrstvie: zlepence, kremité pieskovce, kremence; skýt
Lúžna Formation: conglomerates, quartzose sandstones, quartzites; Scythian
PALEOZOIKUM PALEOZOIC
Perm Permian
koperšadské (meďodolské) zlepence
Koperšady (Meďodoly) conglomerates
KRYŠTALINIKUM CRYSTALLINE COMPLEX
MAGMATITY (PALEOZOIKUM) IGNEOUS ROCKS (PALEOZOIC)
82
leukokratné granitoidy
leucocratic granitoids
porfýrické granitoidy s výrastlicami ružovočervených K-živcov (typ Goričkovej)
porphyritic granitoids with pink-red K-feldspar phenocrysts (Goričková – type)

At the mouth of the Kežmarská Biela voda Valley, above the Lúžna Formation, the Gutenstein Limestones (Middle Triassic) appear in their normal stratigraphic position. However, the Gutenstein Limestones are tectonically separated from the Lúžna Formation sediments by a nappe contact (Nemčok et al., 1994). This contact can be traced westward to the area east of Veľké Biele pleso and to the west of the Napájadlový potok Valley (near the Kežmarská chata hut), where the Gutenstein Limestones are again separated from the Lúžna Formation by a nappe contact. The same situation occurs far as the upper part of of the Meďodolský potok Valley, where a fold structure is present. In its synform parts, the Gutenstein limestones or the shales of the Lúžna Formation are found in their normal stratigraphic position, above the Lower Triassic and Permian sediments (Meďodoly conglomerates), with fragments of the Goryczkowa-type granite in their footwall (Gorek, 1954). The Gutenstein Limestones bordering the north-eastern edge of the aforementioned fold structure occupy a normal position as the upper fold limb and passes upwards into higher members of the lithostratigraphic sequence. Despite these apparently normal stratigraphic relationships is tectonically assigned to the Fatricum on the geological map (Nemčok et al., 1994).

To the west, the Gutenstein Limestones lie above massive organodetritic limestones (Middle to Upper Jurassic), and both formations belong to the Tatricum tectonic unit. On the left bank of the Javorová dolina Valley, on the northeastern slopes of Svišťovka (2,070 m a.s.l.), crinoidal and red limestones with stromatolites (Bajocian–Bathonian) and Carpathian Keuper Formation are found overlying leucocratic granitoids. The entire rock complex, apparently in an inverted stratigraphic position, is assigned to the Tatric tectonic unit (Nemčok et al., 1994). In the hanging wall of the Tatric cover sequence, a crystalline basement thrust slice is present, represented by porphyritic granites (Goryczkowa-type, e.g. Kohút et al., 2019) and sediments of the Lúžna Formation (Fig. 5). The aforementioned rock complex is tectonically separated from the Tatric crystalline basement. In Zadná kopa (1,674 m a.s.l.) and Holica (1,628 m a.s.l.), the same granites, together with the Lúžna Formation and Mesozoic sediments ranging in age from the Middle Triassic to Cenomanian form a continuous lithostratigraphic sequence that connects seamlessly to the Havran nappe. The presence of a crystalline basement as an integral part of the Havran structure above the Tatric sedimentary cover indicates its tectonic affinity with the Veporicum.

It is reasonable to consider the Havran structure to be part of the Veporicum, in a similarly to the Nízke Tatry Mountains (Biely et al., 1992), the Staré Hory Mountains (Polák et al., 2003) and the Tribeč Mountains (Ivanička et al., 1988), as well as in the context of the Šariš-1 borehole results (Š-1, Koráb et al., 1986).

Meanwhile, the Fatricum sensu stricto could be represented by the Bujačí nappe/structure (cf. Nemčok et al., 1994; Geological Map of Slovak Republic, 2013).

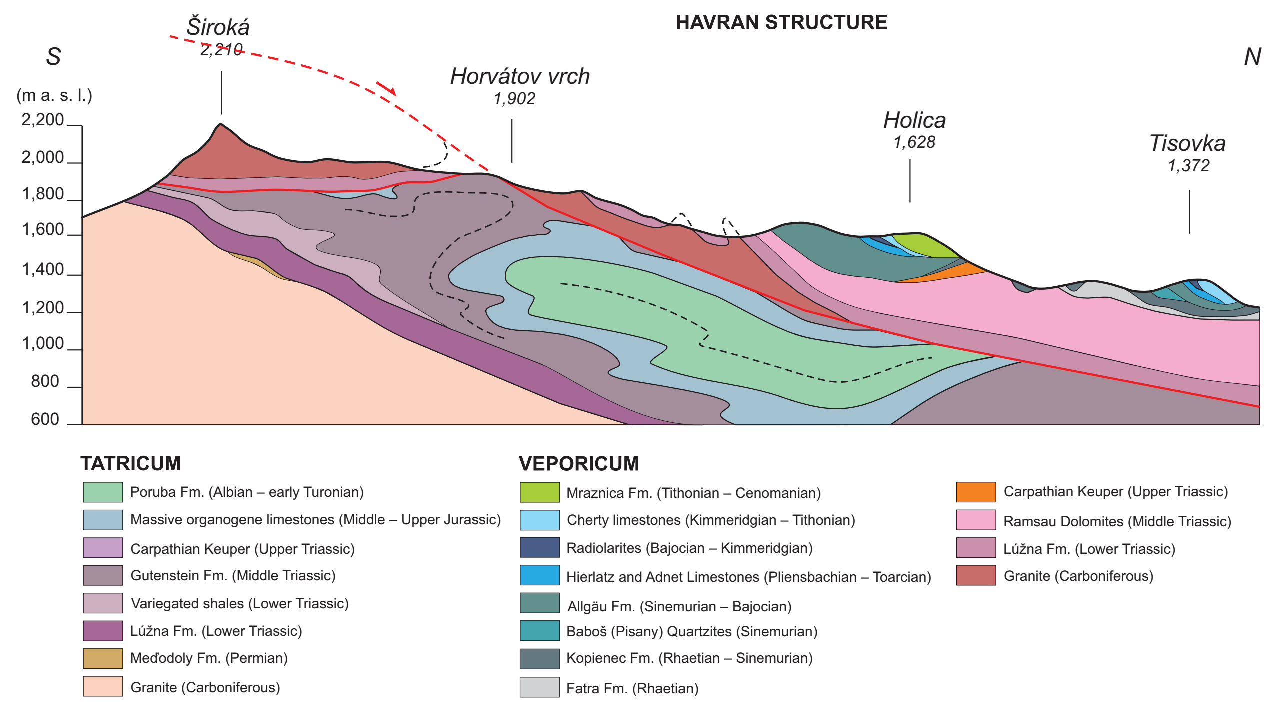

Fig. 5. Geological section between Široká (2,210 m a.s.l.) and Tisovka (1,372 m a.s.l.) documenting the allochthonous position of the Veporic tectonic unit (Havran structure) on the Tatricum (for the location of the section, see Fig. 3).

The Bujačí structure may also represent a continuous, folded structure of the Havran nappe, with Middle Triassic dolomites forming its core. In that case, it would require a southward displacement of the dolomites and the associated lithostratigraphic units in the upper limb of the fold. There is no evidence of south-vergent displacements in the Tatra Mts. Furthermore, the high rheological resistance of dolomites to folding suggests that their presence in the core of a recumbent fold is less likely. It is simpler and more energetically plausible to assume that this is a separate duplex structure. However, this assumption requires further research. On the southeastern edge, the pre-Cenozoic rock sequences of the Tatry Mountains are separated from the Paleogene sedimentary sequences by the Ružbachy Fault (RuF). The RuF was tectonically active throughout the Cenozoic (Jacko, 2000).

Vikartovský chrbát Ridge

The Vikartovský chrbát Ridge is largely composed of the Hronic tectonic unit. The rock complexes of the Lower Paleozoic Ipoltica Group form the prevailing portion of the area (Vozárová & Vozár, 1979). Mesozoic rocks of the Hronicum are present in the stratigraphic range from the Lower Triassic to the Lower Jurassic. Lithofacially, imbricated Hronic sedimentary rocks of both the Čierny Váh and Biely Váh facial type are present here (Havrila, 2011). The rocks formations are monoclinally inclined to the north (c.f. Biely et al., 1992; Geological Map of Slovak Republic, 2013) and the basement of the Hronicum consists of rocks of the Northern Veporicum.

Slovenský raj Mountains

In the Slovenský raj region, the geological structure is characterised by the Stratená Group of the Silicic tectonic unit (Mello et al., 2000). The stratigraphic range extends from the Lower to the Middle Triassic, with the Wetterstein Limestones making up most of the surface (see Mello et al., 2000; Geological Map of Slovak Republic, 2013).

Galmus Mountains

The Galmus area in the study region borders the northern edge of the Gemeric belt (Vass et al., 1988). Its rock composition consists of Middle Triassic carbonates of the Silicicum, Paleozoic rocks of the northern Gemeric cover sequences, and Paleozoic sedimentary sequences and volcanic rocks of the Rakovec Group of the Gemericum (Mello et al., 2000; Polák et al., 1996; Bajaník et al., 1984; Geological Map of Slovak Republic, 2013).

Branisko Mountains

The Branisko Mts. (Fig. 6) is a horst structure, with the Poľanovce Fault (PF) to the west and the Šindliar Fault (ŠF) to the east. Both faults are normal faults, with a displacement of more than 500 metres on the fault surface. The ŠF has shown evidence of recent instrumental movement (Stercz et al., 2025).

Along the southern edge of the Branisko Mts., there are sequences of Paleozoic crystalline basement rocks (granites, migmatites and gneisses), which are part of the Miklušovce Complex within the Veporicum (Polák et al., 1996). Further north, the crystalline basement rocks belong to the Patria Complex (amphibolites, migmatites and granites), and are alternatively classified as part of the Tatricum or the Veporicum. Paleozoic sedimentary rocks (arkoses, breccias and conglomerates) have likewise been assigned to both the Veporicum and the Tatricum (the Brusno and Korytné formations).

Other Carboniferous and Permian sedimentary and volcanic rocks form part of the Ipoltica Group and are classified as belonging to the Hronicum. Mesozoic sedimentary sequences are tectonically classified as either Veporicum or Tatricum, although an alternative interpretation is sometimes presented (Polák et al., 1996). In contrast, the Middle to Upper Triassic dolomites and the rare occurrences of the Gutenstein Limestone along the northern margin of the Branisko Mountains have consistently been assigned to the Hronicum (Polák et al., 1996; Geological Map of Slovak Republic, 2013). The overview of the geological structure indicates that the tectonic affiliation of some rock complexes remains uncertain, with alternative assignments to either the Tatricum or the Veporicum. Moreover, these interpretations do not fully correspond to the generally accepted tectonic superposition of the Alpine tectonic units. The tectonic attribution of the rock complexes assigned to the Hronicum is likewise opened to question.

The rock complexes in the Branisko Mountains are generally dipping northwards (Polák et al., 1996). In this configuration, the Miklušovce Complex (classified as Veporicum) would dip beneath the Patria Complex (classified as either Tatricum or Veporicum). This would imply that the Tatricum is in tectonic superposition above the Veporicum. In this configuration, neither the Paleozoic-Mesozoic sedimentary rocks nor the rocks of the Patria Complex can be considered part of the Tatricum.

A similar situation occurs west of the village of Šindliar, where the Hronic sedimentary rocks (Gutenstein limestone) occur in a tectonic position above the Tatric and Veporic sedimentary complexes (Lúžna Formation). The occurrence of the Hronicum directly above the Tatricum, in the absence of the Veporicum and/or Fatricum, would constitute an exceptional tectonic configuration within the IWECA region. Therefore, both the Miklušovce and Patria complexes, together with their Paleozoic and Mesozoic sedimentary cover, more likely belong to the Veporicum. However, a more detailed analysis of the geological map raises fundamental questions regarding the tectonic affiliation of several Mesozoic rock formations assigned to the Hronicum. In the northern part of the Branisko Mountains, there is a significant volume of Triassic dolomites generally interpreted as the Middle Triassic Hronic dolomites. However, their description on the geological map is inconsistent. In the western part of the area, they are identified as the Ramsau Dolomite (Upper Anisian–Ladinian), whereas in the eastern part, they are described simply as grey massive dolomites (Middle–Upper Triassic). Regarding the grey massive dolomites of the Middle–Upper Triassic, which occur northwest of the Šindliar village above the Gutenstein Limestone (Anisian), the Lúžna Formation (Lower Triassic) and the Patria Crystalline Complex, there is reasonable doubt about their tectonic affiliation with the Hronicum. Their lithostratigraphy suggests a single uninterrupted sequence belonging to the Veporicum. The presence of a thrust contact between the Gutenstein Limestone and the grey dolomites, which normally form part of a continuous lithostratigraphic succession, appears highly improbable. This interpretation is further challenged by the situation along the southwestern margin of the Branisko Mts., east of the village of Dúbrava, where an analogous stratigraphic succession is exposed without a nappe boundary between the dolomites and the Gutenstein Limestones.

Additional support is provided by the SAL-7 borehole, located approximately 5 km northeast of the village of Šindliar in the valley of the Renčišovský potok creek (Haluška et al., 1995; Geological Map of Slovak Republic, 2013). The borehole penetrated the Carpathian Keuper Formation beneath the Paleogene sedimentary sequences, at depth interval between 362 and 742 m (Polák et al., 1992). The presence of the Carpathian Keuper Formation definitively excludes the occurrence of the Hronicum in the wider surroundings of the SAL-7 borehole. Therefore, if the grey dolomites dip northwards, they would have been found below the sediments of the Carpathian Keuper Formation in the SAL-7 borehole. If we consider their tectonic affiliation with the Hronicum, however, such a position is almost impossible. However, if the dolomites are part of the Veporicum, the Carpathian Keuper rocks represent a nor-

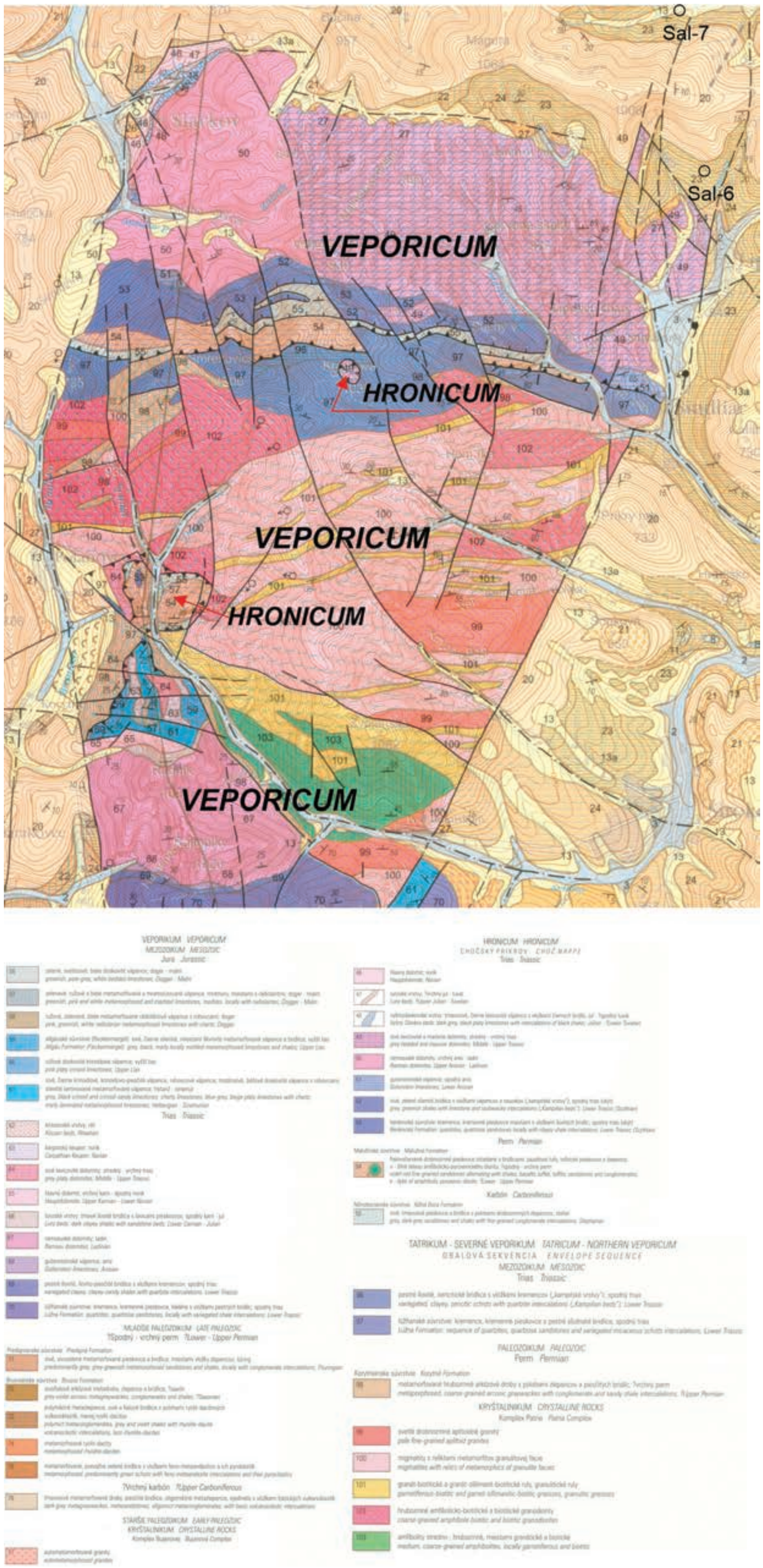

Fig. 6. A section from the geological map of Branisko and Čierna hora (Polák et al., 1996) with explanations and marking of the presumed Veporic structures.

mal continuation of the stratigraphic sequence and can be correlated with the Veporicum (Fig. 6).

Based on the analysis of the geological map and field observations, it can be assumed that north and northeast of the Branisko Mts., a tectonic unit of the Veporicum (Northern Veporicum) occurs beneath the Paleogene sedimentary sequence. Data from boreholes also support this assumption, as explained below.

Interpretation of the tectonic affiliation of pre-Cenozoic basement rocks

The Šariš-1 (Š-1) borehole (Figs. 7, 8), located approximately 10 km north of the village of Vyšný Slavkov, plays a crucial role in compiling a tectonic map of the pre-Cenozoic basement north and northeast of Branisko Mts.

The Š-1 borehole penetrated a Mesozoic stratigraphic sequence ranging from the Lower Triassic (Induan) to the Lower Cretaceous (Albian). The Lower Triassic sedimentary sequences overlie directly the crystalline basement composed of granitic rocks in the upper part and gneiss in the lowermost part of the borehole. The Mesozoic rocks were originally tectonically classified as part of the Fatricum, and the crystalline complex was considered part of the Tatricum (Koráb et al., 1986). However, upon critical review of this configuration, there is no convincing evidence to place a nappe boundary between the crystalline basement rocks and the Mesozoic sedimentary sequences, which form the autochthonous Mesozoic cover of the crystalline basement complex. Therefore, the entire pre-Cenozoic section of the borehole, including the crystalline basement complex, can be correlated with the Northern Veporicum. It should also be noted that the Mesozoic sedimentary sequences of Northern Veporicum and Fatricum are largely identical in terms of lithostratigraphy. Their tectonic affiliation is often determined by the presence of crystalline basement rocks at the base of the complex or by the arrangement of clearly defined tectonic units with their characteristic features, particularly their typical lithostratigraphic members on a broader regional scale.

Mesozoic rocks of the Veporic cover sequence also occur on the northeastern margin of the Čierna hora Mts. and have been documented in borehole SH-1, Bzenov (Cibuľka et al., 1993), SH-4, Kvačany (Cibuľka et al., 1993), BH-3, Víťaz (Frankovič et al., 1974) and boreholes ČH-10, 11, 12 of the Čierna hora series (Frankovič et al., 1981). Middle Triassic dolomites were observed beneath the Paleogene sediments, representing a continuation of the surface

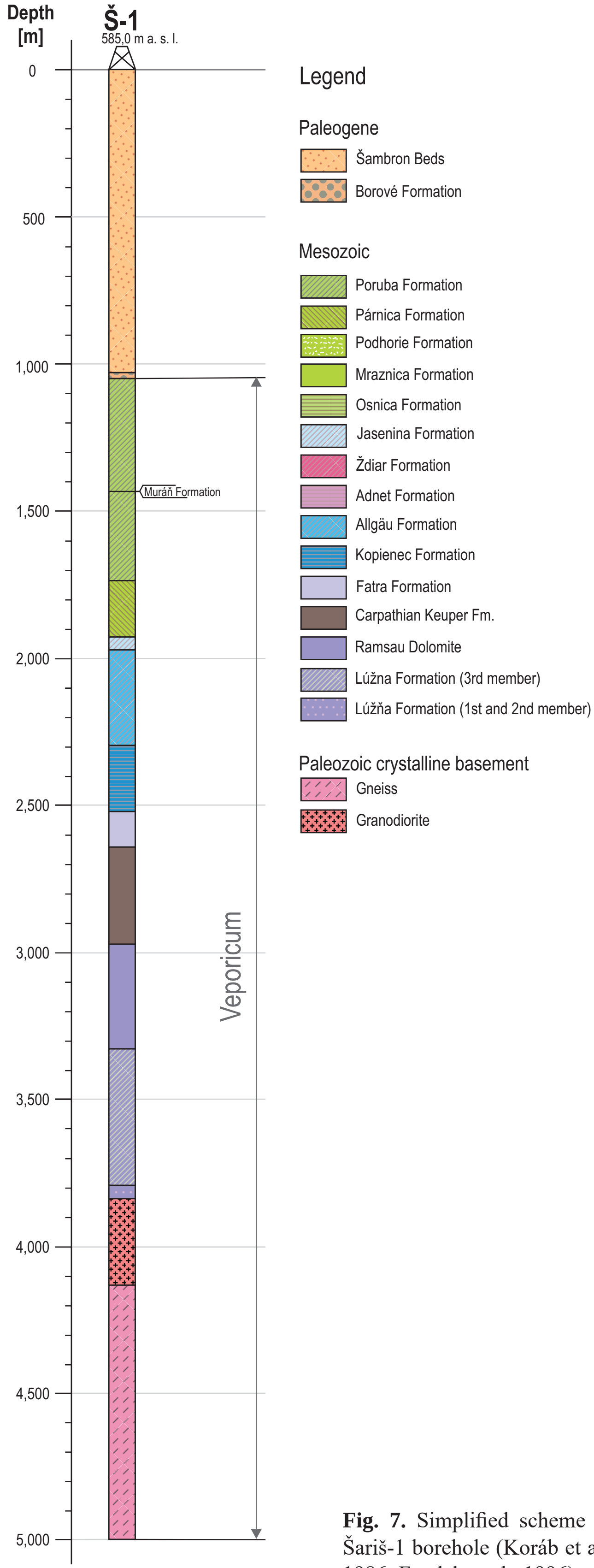

Fig. 7. Simplified scheme of Šariš-1 borehole (Koráb et al., 1986; Fendek et al., 1996).

occurrences of Veporic sedimentary cover exposed on the surface. Similar results were also obtained from the P-1 (Prešov-1) borehole (Mořkovský & Filková, 1978).

The boreholes of the Lipany series (L-1, L-2, L-3, and L-5) penetrated Lower Jurassic rocks, Norian Carpathian Keuper Formation, and Middle Triassic dolomite beneath the Paleogene sedimentary sequences (Leško et al., 1982; Rudinec, 1992). In the tectonic map of the pre-Cenozoic basement (Fusán et al., 1987), these rock complexes are assigned to the Fatricum together with the rocks in borehole Š-1. At the same time, the area between Branisko Mts. in the west and Čierna hora Mts., in the south, is classified within the Tatricum (Fusán et al., 1987).

As already mentioned in the case of pre-Cenozoic rocks in borehole Š-1, the presence of the Tatricum is unacceptable, like the situation in Branisko Mts. and, to some extent, in the northeastern Tatry Mts. (Fig. 8). In this case, the Mesozoic sedimentary sequences in the borehole profiles of the Lipany and Plavnica series have been correctly assigned to the Fatricum (Kullmanová & Rudinec, 1988). Although their stratigraphic range is reduced, they contain Carpathian Keuper Formation in a continuous lithostratigraphic sequence and are clearly tectonically separated from their crystalline basement (cf. Leško et al., 1979; Leško et al., 1982). The interpretation that the boreholes penetrate the Hronicum (Gross et al.,

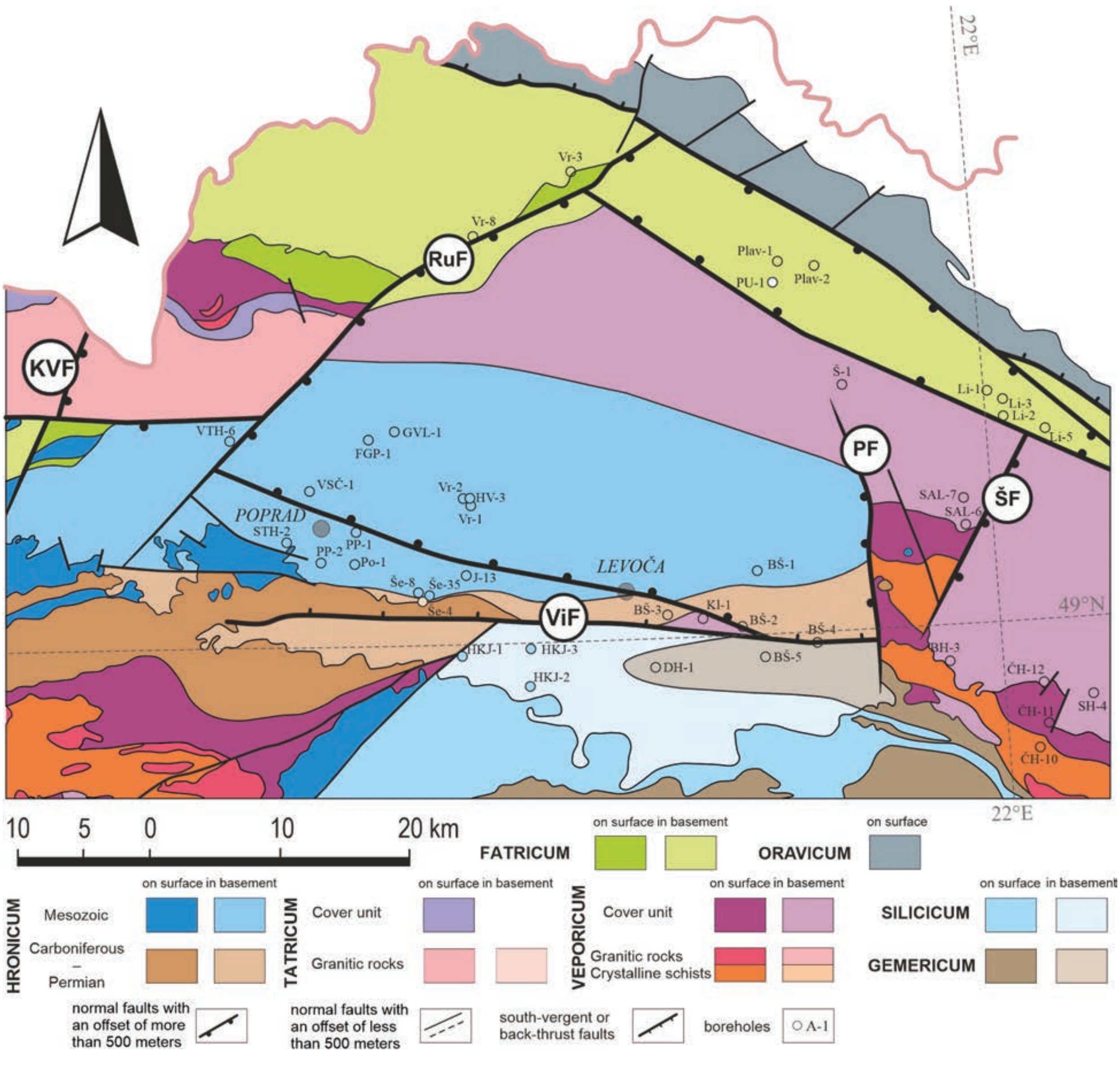

Fig. 8. Tectonic map of the pre-Cenozoic basement. KVF – Kôprová dolina Valley Fault; RuF – Ružbachy Fault; ViF – Vikartovce Fault; PF – Poľanovce Fault; ŠF – Šindliar Fault.

1999) cannot be accepted for several reasons. Similar sedimentary rock complexes occur on the surface in the Humenské vrchy Mts., southeast of the studied area, where they are likewise assigned to the Fatricum (Žec et al., 1997).

At the northern margin of the Gemeric region (Galmus and Slovenský raj, Fig. 2), south-vergent reverse faults (back-thrusts) were documented in borehole BŠ-4 (Haluška, 1993; Vozárová, 1995). The borehole is in the vicinity of the eastern continuation of the Vikartovce Fault (ViF), the tectonic transport is interpreted to have been directed southwards (Marko et al., 2022), although its current tectonic activity should be regarded as normal fault (Vojtko et al., 2011). The pre-Cenozoic basement in the central part of the studied area contains Mesozoic formations of the Hronicum. These formations were documented in boreholes in the Vrbov area (HV-3, Vr-1, Vr-2), Veľká Lomnica (GVL-1), Stará Lesná (FGP-1), Veľký Slavkov (VSČ-1) (Fendek et al., 1996; Pereszlényi in Daniel et al., 1998; Halás et al., 2008).

Discussion

Classifying the rock complexes in the pre-Cenozoic basement is closely linked to the arrangement of the formations exposed at the surface. When interpretating the pre-Cenozoic basement in the area of the Sub-Tatra Group in north-eastern Slovakia, two problematic areas were identified. In the eastern part of the Tatry Mts. (west of the Kôprová dolina fault, Fig. 4), the original classification of the crystalline basement thrust sheets, together with their Mesozoic cover, in the area between the Javorinka Valley and the Bielovodská dolina Valley as part of the Tatricum is largely arbitrary (Nemčok et al., 1994). The Mesozoic sedimentary sequence is divided here without justification. The outliers of the crystalline complex, together with the Lúžňa Formation, at the Široká (2,210 m a.s.l.) and Horvátov vrch (1,902 m a.s.l.) are depicted correctly. However, in the case of the third, structurally highest thrust sheet between Horvátov vrch Hill and the elevation point 1,674 m a.s.l., the sedimentary sequence normally continues with Middle Triassic carbonates, which may form a normal sedimentary sequence with an overlying Jurassic and Cretaceous formation originally considered to be the Fatric Havran partial nappe. A similar situation is also found further east on the southern slope of the Hlúpy hill (2,061 m a.s.l.). In this work, we consider repeated sequences composed of granite and Mesozoic sedimentary cover overlying the rocks of the Tatric tectonic unit to be part of the Veporicum.

Such an alternative interpretation may be considered unconventional or speculative and raises a nomenclatural problem regarding tectonic classification. Mesozoic rock complexes representing the hangingwall of the Tatricum are traditionally classified as Fatricum (Andrusov & Samuel, 1983), in the past also referred to as the Krížna nappe (Maheľ, 1986) or the Lower Sub-Tatra nappe (Andrusov, 1936).

The Tatricum in the Nízke Tatry and the Tribeč Mts., (Biely et al., 1992; Ivanička et al., 1998) occurs beneath a crystalline complex that is considered to represent Veporicum. Overlying this crystalline basement complex is a second crystalline basement unit, which includes subautochthonous Mesozoic sedimentary sequences ranging from the Lower Triassic to the Lower Cretaceous. A crystalline basement complexes beneath the Mesozoic cover are also present in the Starohorské vrchy Mts. (Polák et al., 2003), Žiar Mts. (Kováčik et al., 2015), and in the Tatry Mts. (Nemčok et al., 1993). Although, their tectonic origin is undoubtedly Veporic, problem arises with the correct tectonic affiliation.

The Fatricum is therefore considered to be a heterogeneous cover nappe consisting of the Vysoká and Zliechov facies. These facies are composed of Mesozoic lithostratigraphic units that have been tectonically detached from their original Variscan crystalline basement. They have also been displaced over a distance several orders of magnitude greater than their vertical thickness. In the eastern part of the Tatry Mts., the Veporic tectonic unit (Havran structure) can be interpreted. The Bujačí structure, which was previously considered a partial nappe of the Fatricum, can now be interpreted as part of the Fatricum cover nappe itself.

The rock complexes in the Branisko Mts. belong to the Veporicum. Crystalline basement rocks, as well as Paleozoic and Mesozoic sediments from the Branisko and Čierna hora regions, undoubtedly extend southeastwards into the pre-Cenozoic basement of the East Slovak Basin.

Conclusions

The area in the north-eastern part of the Internal Western Carpathians is largely covered by Paleogene sedimentary sequences of the Sub-Tatra Group (Figs. 1, 3 and 8). Based on a re-evaluation of surface geology, borehole data, geophysical evidence and structural relationships, the pre-Cenozoic basement of the study area is interpreted as comprising the Fatricum, Veporicum and Hronicum (see Fig. 8). Alternative interpretations are based on a critical review of published geological maps. They represent a different view of the crystalline basement and its cover in the Šariš-1 borehole (Fig. 7), as well as the structure of the crystalline basement duplexes in the eastern Tatry Mts. and Branisko Mts.

Acknowledgements

The work was financially supported by the Slovak Research and Development Agency under contract No.

APVV-21-0281, APVV-SK-UA-25-0003, APVV-24-0445 and the Slovak Grant Agency under project Vega 1/0021/25, 1-0107-23, 2-0002-23 and the project of the Ministry of the Environment of the Slovak Republic No. 03 24 Update of the digital geological map and geological study of the problematic areas of SR – Deep borehole database of Slovak Republic. The authors thank Balázs Kronome and an anonymous reviewer for their constructive comments. The editorial work was done by handing editor Klement Fordinál.

References

Andrusov, D., 1936: Subtatranské příkrovy Západních Karpat. *Praha, Sbor. pro výzkum Slovenska a Podkarpatské Rusi při Slovanském ústavu*, 49 s.

Andrusov, D., 1950: Tektonická stavba masívu Širokej (Vysoké Tatry). *Geologický sborník Slovenskej akadémie vied*, 1, 19 – 31.

Andrusov, D. & Samuel, O. (eds.), 1983: Stratigrafický slovník Západných Karpát 1, A – K. *Bratislava, Geologický ústav Dionýza Štura*.

Bac-Moszaszwili, M., Jaroszewski, W. & Passendorfer, E., 1984: On the tectonics of Czerwone Wierchy and Giewont area in the Tatra Mts., Poland. *Annales Societatis Geologorum Poloniae*, 52, 67 – 88.

Bajaník, Š. (ed.), Ivanička, J., Mello, J., Reichwalder, P., Pristaš, J., Snopko, L., Vozár, J. & Vozárová, A., 1984: Geologická mapa Slovenského rudohoria – východná časť 1 : 50 000. *Bratislava, Geologický ústav Dionýza Štúra*.

Bezák, V., Broska, I., Ivanička, J., Reichwalder, P., Vozár, J., Polák, M., Havrila, M., Mello, J., Biely, A., Plašienka, D., Potfaj, M., Konečný, V., Lexa, J., Kaličiak, M., Žec, B., Vass, D., Elečko, M., Janočko, J., Pereszlényi, M., Marko, F., Maglay, J. & Pristaš, J., 2004: Tektonická mapa Slovenskej republiky (1 : 500 000). *Bratislava, Ministerstvo životného prostredia Slovenskej republiky – Štátny geologický ústav Dionýza Štúra*.

Biely, A. (ed.), Beňuška, P., Bezák, V., Bujnovský, A., Halouzka, R., Ivanička, J., Kohút, M., Klinec, A., Lukáčik, E., Maglay, J., Miko, O., Pulec, M., Putiš, M. & Vozár, J., 1992: Geologická mapa Nízkych Tatier 1 : 50 000. *Bratislava, Geologický ústav Dionýza Štúra.*

Biely, A., Bezák, V., Elečko, M., Gross, P., Kaličiak, M., Konečný, V., Lexa, J., Mello, J., Nemčok, J., Potfaj, M., Rakús, M., Vass, D., Vozár, J. & Vozárová, A., 1996: Vysvetlivky ku geologickej mape Slovenska 1 : 500 000. *Bratislava, GS SR, Vydavateľstvo Dionýza Štúra*, 77 pp.

Cibuľka, Ľ., Bajo, I., Šťastný, V. & Szabová, A., 1993: Paleogén povodia Svinky – hydrogeologický prieskum. *Manuscript. Bratislava, Archive of St. Geol. Inst. of D. Štúr* (arch. no. AP 80 484).

Daniel, J., Fendek, M., Novotný, L., Šefara, J., Grand, T., Lučivjanský, L., Máťuš, J., Vika, K., Michalko, J., Král, M. & Peruňský, I., 1998: Popradská kotlina – záverečná správa. *Manuscript. Bratislava, Archive of St. Geol. Inst. of D. Štúr* (arch. no. 82 663).

Fendek, M., Remšík, A., Polák, M., Král, M., Boorová, D., Siráňová, Z., Gross, P., Karoli, S., Michalko, J., Zlinská, A. & Snopková, P., 1996: Záverečná správa za geotermálny vrt FGP-1 Stará Lesná v Popradskej kotline. *Manuscript. Bratislava, Archive of St. Geol. Inst. of D. Štúr* (arch. no. 80 620), 99 pp.

Frankovič, J., Tkáčik, P., Gazda, S., Szabová, A. & Vráblová, M., 1974: Branisko – vyhľadávací hydrogeologický prieskum. *Manuscript. Bratislava, Archive of St. Geol. Inst. of D. Štúr* (arch. no. 41 344).

Frankovič, J., Szabová, A. & Vráblová, M., 1981: Čierna hora – hydrogeológia. *Manuscript. Bratislava, Archive of St. Geol. Inst. of D. Štúr* (arch. no. 55 481).

Fusán, O., Biely, A., Ibrmajer, J., Plančár, J. & Rozložník, L., 1987: Podložie terciéru Vnútorných Západných Karpát. *Bratislava, Geologický ústav Dionýza Štúra*, 123 pp.

Geological Map of the Slovak Republic at scale 1:50 000 [online], 2013: *Bratislava, Štátny geologický ústav Dionýza Štúra*. Available online: https://app.geology.sk/gm50/.

Gross, P., Biely, A., Marschalko, R., Franko, O., Klablenová, K., Samuel, O. & Gazda, S., 1966: Vyhodnotenie štruktúrneho vrtu Klčov-1 (Kl-1). *Manuscript. Bratislava, Archive of St. Geol. Inst. of D. Štúr*.

Gross, P., Köhler, E. & Samuel, O., 1984: Nové litostratigrafické členenie vnútrokarpatského paleogénu. *Geologické práce, Správy*, 81, 103 – 117.

Gross, P. (ed.), Buček, S., Ďurkovič, T., Filo, I., Karoli, S., Maglay, J., Nagy, A., Halouzka, R., Spišák, Z., Žec, B., Vozár, J., Borza, V., Lukáčik, E., Mello, J., Polák, M. & Janočko, J., 1999a: Geologická mapa Popradskej kotliny, Hornádskej kotliny, Levočských vrchov, Spišsko-šarišského medzihoria, Bachurne a Šarišskej vrchoviny 1 : 50 000. *Bratislava, MŽP SR – GS SR.*

Gross, P. (ed.), Buček, S., Ďurkovič, T., Filo, I., Halouzka, R., Karoli, S., Maglay, J., Nagy, A., Spišák, Z., Žec, B., Vozár, J., Borza, V., Lukáčik, E., Mello, J., Janočko, J., Polák, M., Siráňová, Z., Samuel, O., Snopková, P., Raková, J., Zlinská, A. & Vozárová, A., 1999b: Vysvetlivky ku geologickej mape Popradskej kotliny, Hornádskej kotliny, Levočských vrchov a Spišsko-šarišského medzihoria, Bachurne a Šarišskej vrchoviny 1 : 50 000. *Bratislava, GS SR, Vydavateľstvo Dionýza Štúra*, 239 pp.

Gross, P., 2008: Litostratigrafia Západných Karpát: Paleogén – podtatranská skupina. *Bratislava, Štátny geologický ústav Dionýza Štúra*, 77 pp.

Halás, O., Bondarenková, Z., Drozd, V., Brichta, R. & Dzúrik, J., 2008: Geotermálny vrt VSČ-1 Veľký Slavkov. Final report. *Manuscript. Bratislava, Archive of St. Geol. Inst. of D. Štúr* (arch. no. 88 164), 70 pp.

Haluška, M., 1993: Baldovce – ochranné pásma. *Manuscript. Bratislava, Archive of St. Geol. Inst. of D. Štúr* (arch. no. 80 562).

Haluška, M., Petrivaldský, P. & Cibuľka, Ľ., 1995: Lipovce – Salvator – ochranné pásma, vyhľadávací HGP. *Manuscript. Bratislava, Archive of St. Geol. Inst. of D. Štúr* (arch. no. 82 183), 171 pp.

Havrila, M., 2011: Hronikum: paleogeografia a stratigrafia (vrchný pelsón – tuval), štrukturalizácia a stavba. *Geologické práce, Správy*, 117, 7 – 103.

Hók, J., Pelech, O., Teťák, F., Németh, Z. & Nagy, A., 2019: Outline of the geology of Slovakia (W. Carpathians). *Mineralia Slovaca*, 51, 1, 31 – 60.

Ivanička, J. (ed.), Polák, M., Hók, J., Határ, J., Greguš, J., Vozár, J., Nagy, A., Fordinál, K., Pristaš, J., Konečný, V. & Šimon, L., 1998: Geologická mapa Tribeča 1 : 50 000. *Bratislava, MŽP SR – GS SR.*

Jacko, S., 2000: Kinematic evolution of the Subtatric – Ružbachy Fault System in the Spišská Magura region (Slovakia). *Journal of the Czech Geological Society*, 45, 3 – 4, 234.

Kilényi, E. & Šefara, J., 1989: Pre-Tertiary basement contour map of the Carpathian basin beneath Austria, Czechoslovakia and Hungary, 1 : 500 000. *Budapest, Eötvös Loránd Geophysical Institute of Hungary*.

Kohút, M., Madarás, J. & Siman, P., 2019: 100 rokov granitu typu Goryczkowa v Tatrách – mýtus a realita. *Mineralia Slovaca*, 41, 4, *Geovestník*, 550 – 551.

Koráb, T., Ďurkovič, T., Kullmanová, A., Martinský, L., Miko, O., Határ, J., Krištín, J., Kantor, J., Gašpariková, V., Snopková, P., Harča, J., Franců, J., Zembjak, O., Michalíček, M., Procházková, V., Rudinec, R., Řeřicha, M., Smetana, J., Jandová, B., Píchová, E., Plička, M., Filková, V., Hradil, F. & Wunder, D., 1986: Záverečné naftovo-geologické zhodnotenie oblasti na základe vrtu Šariš-1. *Manuscript. Bratislava, Archive of St. Geol. Inst. of D. Štúr*.

Kováčik, M., Kohút, M., Sentpetery, M., Olšavský, M., Havrila, M., Filo, I., Maglay, J., Nagy, A., Laurinc, D., Šimon, L. & Baráth, I., 2015: Geologická mapa Žiaru 1 : 50 000. *Bratislava, MŽP SR, Štátny geologický ústav Dionýza Štúra*.

Kotański, Z., 1961: Tectogénese et réconstruction de la paléógéographie de la zone hauttarrique dans les Tatras. *Acta geologica polonica*, 11, 187 – 474.

Kullmanová, A. & Rudinec, R., 1988: Paleogénne súvrstvie a jeho mezozoické podložie v Spišsko-šarišskom medzihorí (vrt Plavnica-1). *Mineralia Slovaca*, 20, 5, 455 – 461.

Leško, B., Nemčok, J., Ďurkovič, T., Gašpariková, V., Kullmanová, A., Vaňová, M., Snopková, P., Harča, V., Franko, O. & Rudinec, R., 1979: Oporný vrt Lipany-1, záverečné geologické a naftovo-geologické vyhodnotenie. *Manuscript. Bratislava, Archive of St. Geol. Inst. of D. Štúr* (arch. no. 45 332), 15 pp.

Leško, B., Ďurkovič, T., Franko, O., Gašpariková, V., Harča, V., Nemčok, J., Kullmanová, A., Jandová, V., Krištek, J., Vaňová, M., Štěrba, L., Rudinec, R., Smetana, J., Šupina, Z., Wunder, D., Kuděra, L. & Fáber, P., 1982: Oporný vrt Lipany-1 (4 000 m). *Regionálna geológia Západných Karpát*, 18, 5 – 78.

Lugeon, M., 1903: Les nappes de recouvrement de la Tatra et l'origine des klippes des Carpathes. *Bull. Lab. Géol. Géogr. pbys. min. pal. Univ. Lausanne*, 4.

Maheľ, M., 1986: Geologická stavba československých Karpát – Paleoalpínske jednotky. *Bratislava, Veda*, 503 pp.

Marko, F., Mojzeš, A., Gajdoš, V., Rozimant, K., Dyda, M., Bezák, V., Daniel, S., Smetanová, I., Brixová, B., Zvara, I. & Andrássy, E., 2022: Multi-method field detection of map-scale faults and their parameters: Case study from the Vikartovce fault (Western Carpathians). *Geologica Carpathica*, 73, 5, 391 – 410. https://doi.org/10.31577/GeolCarp.73.5.1.

Mello, J., Filo, I., Havrila, M., Ivanička, J., Madarás, J., Németh, Z., Polák, M., Pristaš, J., Vozár, J., Koša, E. & Jacko, S. jr., 2000: Geologická mapa Slovenského raja, Galmusu a Hornádskej kotliny 1 : 50 000. *Bratislava, Ministerstvo životného prostredia, Štátny geologický ústav Dionýza Štúra*.

Mořkovský, M. & Filková, V., 1978: Nové poznatky o geologii prešovské časti Košické kotliny. *Geologické práce, Správy*, 70, 183 – 195.

Mořkovský, M., 1981: Hlubinný styk centrálně karpatského paleogénu s bradlovým pásmem v Šarišské vrchovině podle výsledků reflexně seismických měření. *Geologické práce, Správy*, 75, 63 – 76.

Nemčok, J. (ed.), Bezák, V., Janák, M., Kahan, Š., Ryka, W., Kohút, M., Lehotský, I., Wieczorek, J., Zelman, J., Mello, J., Halouzka, R., Rackowski, W. & Reichwalder, P., 1993: Vysvetlivky ku geologickej mape Tatier 1 : 50 000. *Bratislava, Geologický ústav Dionýza Štúra*, 135 pp.

Nemčok, J. (ed.), Bezák, V., Biely, A., Gorek, A., Gross, P., Halouzka, R., Janák, M., Kahan, Š., Kotański, Z., Lefeld, J., Mello, J., Reichwalder, P., Rackowski, W., Roniewicz, P., Ryka, W., Wieczorek, J. & Zelman, J., 1994: Geologická mapa Tatier 1 : 50 000. *Bratislava, MŽP SR – Geologický ústav Dionýza Štúra, MOSZNL, PIG.*

Ostrowski, S., Rybak-Ostrowska, B., Iwańczuk, J., Lasocki, M., Wilkołazki, P. & Uroda, J., 2026: Near-surface seismic imaging for deciphering the internal structure of crystalline thrust sheets: insights from the Goryczkowa Subunit, Tatra Mountains, Poland. *Journal of Structural Geology*. https://doi.org/10.1016/j.jsg.2026.105691.

Pašteka, R., Záhorec, P., Kušnirák, D., Bošanský, M., Papčo, J., Marušiak, I., Mikuška, J. & Bielik, M., 2017: High resolution Slovak Bouguer gravity anomaly map and its enhanced derivative transformations: new possibilities for interpretation of anomalous gravity fields. *Contributions to Geophysics and Geodesy*, 47, 2, 81 – 94.

Plašienka, D., Soták, J. & Prokešová, R., 1998: Structural profiles across the Šambron-Kamenica Periklippen Zone of the Central Carpathian Paleogene Basin in NE Slovakia. *Mineralia Slovaca*, 30, 173 – 184.

Polák, M., 1987: Mezozoikum severnej časti Braniska. *Geologické práce, Správy*, 87, 7 – 18.

Polák, M., Gross, P., Samuel, O., Snopková, P. & Vozárová, A., 1992: Litologické a petrografické vyhodnotenie vzoriek z hydrogeologických vrtov SAL 1 – 7 a BŠ 1 – 5. *Manuscript. Bratislava, Archive of State Geol. Inst. of D. Štúr* (arch. no. AP 91 48).

Polák, M. (ed.), Jacko, S., Vozár, J., Vozárová, A., Gross, P., Harčár, J., Sasvári, T., Zacharov, M., Baláž, B., Karoli, S., Nagy, A., Buček, S., Maglay, J., Spišák, Z., Žec, B., Filo, I. & Janočko, J., 1996: Geologická mapa Braniska a Čiernej hory 1 : 50 000. *Bratislava, MŽP SR – GS SR*.

Polák, M. (ed.), Filo, I., Havrila, M., Bezák, V., Kohút, M., Kováč, P., Vozár, J., Mello, J., Maglay, J., Elečko, M., Olšavský, M., Pristaš, J., Siman, P., Buček, S., Hók, J., Rakús, M., Lexa, J. & Šimon, L., 2003: Geologická mapa

Starohorských vrchov, Čierťaže a severnej časti Zvolenskej kotliny 1 : 50 000. *Bratislava, MŽP SR – Štátny geologický ústav Dionýza Štúra.*

Rudinec, R., 1992: Ropné a plynové akumulácie pri Lipanoch na východnom Slovensku, ich osobitosti a problémy. *Mineralia Slovaca*, 24, 5 – 6, 357 – 366.

Stercz, M., Grega, D., Petro, Ľ., Hók, J., Németh, Z., Bednarik, M., & Stemberk, J., 2025: 3D long-term monitoring of recent tectonic activity in the Branisko Tunnel (Eastern Slovakia). *Geologica Carpathica*, 76, 1, 55 – 67. https://doi.org/10.31577/GeolCarp.2025.04.

Uhlig, V., 1900: Geologie des Tatragebirges II. Tektonik des Tatragebirges Theil. *Wien, K.-K. Hof- und Staatsdruckerei,* 88 pp.

Vass, D., Began, A., Gross, P., Kahan, Š., Krystek, I., Köhler, E., Lexa, J., Nemčok, J., Růžička, M. & Vaškovský, I., 1988: Regionálne geologické členenie Západných Karpát a severných výbežkov Panónskej panvy na území ČSSR. Mapa 1 : 500 000. *Bratislava, Geologický ústav Dionýza Štúra*.

Vojtko, R., Marko, F., Preusser, F., Madarás, J. & Kováčová, M., 2011: Late Quaternary fault activity in the Western Carpathians: evidence from the Vikartovce Fault (Slovakia). *Geologica Carpathica*, 62, 6, 563 – 574. https://doi.org/10.2478/v10096-011-0040-9.

Vozárová, A., 1995: Spätné násuny na severnom okraji gemerika. *Geologické práce, Správy*, 100, 119 – 123.

Vozárová, A. & Vozár, J., 1979: Nižnobocianske a malužinské súvrstvie – nové litostratigrafické jednotky v mladšom paleozoiku hronika. *Mineralia Slovaca*, 11, 5, 477 – 478.

Zahorec, P., Papčo, J., Pašteka, R., Bielik, M., Bonvalot, S., Braitenberg, C., Ebbing, J., Gabriel, G., Gosar, A., Grand, A., Götze, H. J., Hetényi, G., Holzrichter, N., Kissling, E., Marti, U., Meurers, B., Mrlina, J., Nogová, E., Pastorutti, A., Scarponi, M., Sebera, J., Seoane, L., Skiba, P., Szűcs, E. & Varga, M., 2021: The first pan-Alpine surface-gravity database, a modern compilation that crosses frontiers. Earth System Science Data. *Earth Syst. Sci. Data*, 13, 2 165 – 2 209. https://doi.org/10.5194/essd-13-2165-2021.

Žec, B. (ed.), Kaličiak, M., Konečný, V., Lexa, J., Jacko, S. jr., Karoli, S., Baňacký, V., Potfaj, M., Rakús, M., Petro, Ľ. & Spišák, Z., 1997: Geologická mapa Vihorlatských a Humenských vrchov 1 : 50 000. *Bratislava, MŽP SR – GS SR*.

Predkenozoické podložie severovýchodnej časti interných Západných Karpát z perspektívy geologickej stavby Tatier a Braniska

Oblasť medzi Tatrami a pohorím Branisko, ktorú zo severovýchodu ohraničujú povrchové výskyty oravika a na juhu vikartovský chrbát, Slovenský raj a pohorie Galmus, predstavuje plošne najrozsiahlejšiu oblasť s výskytom sedimentov podtatranskej skupiny (*sensu* Gross et al., 1984; Gross, 2008) v interných Západných Karpatoch (obr. 1 a 3). Tektonické pomery predkenozoického podložia zhodnotili Fusán et al. (1987).

Na základe podrobnej analýzy povrchových geologických štruktúr v pohoriach Tatry a Branisko, ktorá je doplnená údajmi z vrtov a geofyzikálnymi interpretáciami, sú v práci prehodnotené existujúce poznatky o geologickej stavbe povrchových štruktúr v Tatrách a Branisku, ako aj predkenozoického podložia. Sú hodnotené hlavne z hľadiska tektonickej kategorizácie tatrických a veporických horninových komplexov.

Východná časť Tatier (Vysoké Tatry a Belianske Tatry) je zobrazená na geologickej mape Tatier v mierke 1 : 50 000 (Nemčok et al., 1994). Na geologickej stavbe sa podieľajú tektonické jednotky tatrika a fatrika. Fatrikum sa člení na príkrov Havrana a príkrov Bujačieho (Nemčok et al., 1993). V tektonickom nadloží sedimentov tatrika spočívajú v alochtónnej pozícii granity s autochtónnymi sedimentmi mezozoika, ktoré tvoria s granitmi kontinuálny litostratigrafický sled príkrovu Havrana (obr. 4 a 5). Celý spomenutý horninový komplex je možné považovať za súčasť tektonickej jednotky veporika (severného veporika, *cf.* Hók et al., 2019). Príkrov Bujačieho predstavuje alochtónny horninový súbor sedimentov mezozoika patriaci k tektonickej jednotke fatrika.

Geologická stavba pohoria Branisko je zobrazená na geologickej mape Braniska a Čiernej hory v mierke 1 : 50 000 (Polák et al., 1996). Tektonická príslušnosť horninových komplexov kryštalinika bola opísaná dvojznačne (tatrikum/veporikum), s čím súvisí aj tektonické zaradenie sedimentov mezozoika. Na základe priestorového usporiadania povrchových výskytov horninových komplexov a údajov z vrtov je možné presvedčivo preukázať, že na geologickej stavbe pohorí Branisko a Čierna hora sa podieľajú tektonické jednotky veporika (severného veporika) a hronika (obr. 6).

V rámci konštrukcie mapy predkenozoického podložia (obr. 8) boli kritickej revízii podrobené aj názory na tektonické zaradenie hornín zastihnutých vo vrte Šariš-1 (Koráb et al., 1986). Vrt Šariš-1 (Š-1) prenikol v predkenozoickom podloží (od hĺbky 1 050 m) cez kompletný vrstvový sled mezozoika v stratigrafickom rozsahu spodná krieda (alb) až spodný trias (obr. 7). Sedimenty spodného triasu ležia priamo na kryštaliniku tvorenom metamorfovanými granitmi, pod ktorými sú kryštalické bridlice (ruly). Litostratigrafický sled mezozoických sedimentov bol pôvodne tektonicky zaradený do fatrika. Kryštalinikum sa považovalo za súčasť tatrika (Koráb et al., 1986), a to aj napriek tomu, že neexistuje relevantný dôvod klásť príkrovový kontakt medzi horniny kryštalinika a sedimenty spodného triasu, ktoré spoločne s vyššími litostratigrafickými členmi tvoria autochtónny mezozoický obal kryštalinika. V danom prípade je však správne mezozoické sedimenty vo vrtoch série Lipany a Plavnica zaradiť do tektonickej jednotky fatrika (Kullmanová & Rudinec, 1988; Plašienka et al., 1998), aj keď ich stratigrafický rozsah je redukovaný, ale je jednoznačne tektonicky odlúčený od svojho kryštalinického podložia (*cf.* Leško et al., 1979). Nemôže byť akceptovaný predpoklad, že v uvedených vrtoch je prítomná tektonická jednotka hronika, ako to uvádzajú Gross et al. (1999). Z interpretovaných seizmických rezov realizovaných v oblasti vrtu Plavnica-1 (Mořkovský, 1981) je zrejmé, že kontakt mezozoických komplexov fatrika so sedimentmi bradlového pásma je sprostredkovaný výrazným poklesovým zlomom generálneho smeru SZ – JV, ukloneného smerom na JZ (obr. 8).

Pri severnom okraji gemerika (Galmus a Slovenský raj, obr. 3) boli vo vrtoch série Baldovce (Haluška, 1993) dokumentované juhovergentné presuny vo vrte BŠ-4 (Vozárová, 1995). Sú v bezprostrednej blízkosti východného pokračovania vikartovského zlomu považovaného za juhovergentný prešmyk v jeho západnej časti (Marko et al., 2022), aj keď jeho najmladšiu tektonickú aktivitu treba považovať za poklesovú (Vojtko et al., 2011). Na juhovergentný prešmyk poukazujú aj výsledky vrtu Kl-1 (Klčov-1, Gross et al., 1966), kde boli s veľkou mierou pravdepodobnosti zastihnuté súvrstvia veporika (strednotriasové dolomity, spodnotriasové kremence, permské bridlice a arkózy). V danom priestorovom usporiadaní a pri dokumentovaných juhovergentných vrásach v sedimentoch mezozoika Braniska (Polák, 1987), ako aj vo vrte BŠ-4 (Vozárová, 1995), sa alternatíva spätného, juhovergentného násunu javí ako najprijateľnejšia.

Centrálna časť územia (oblasť spišsko-šarišského paleogénu, sensu Vass et al., 1988) bola interpretovaná (obr. 8) hlavne na základe vrtov v oblasti Vrbova (HV-3, Vr-1, Vr-2), Veľkej Lomnice (GVL-1), Starej Lesnej (FGP-1) a Veľkého Slavkova (VSČ-1) a na základe interpretovaných seizmických rezov (Pereszlényi in Daniel et al., 1998).

Možno konštatovať, že predkenozoické podložie v severovýchodnej časti interných Západných Karpát tvoria tektonické jednotky veporika, fatrika a hronika (obr. 8). Nová interpretácia je ovplyvnená odlišným pohľadom na kryštalinické horniny a ich autochtónny mezozoický obal (Šariš-1, obr. 7), ako aj reinterpretáciou tektonického zaradenia horninových súborov vo východnej časti Tatier a v pohorí Branisko (obr. 4 a 6).

Doručené / Received: 30. 4. 2026
Prijaté na publikovanie / Accepted: 14. 8. 2026

Mineralia Slovaca, Web ISSN 1338-3523, ISSN 0369-2086, https://doi.org/10.56623/ms.2026.58.1.4
58, 1 (2026), 67 – 86,

Biostratigraphic framework of the Konkian-Sarmatian boundary based on microfossils from the well #20 Kerch Peninsula (Crimea)

YULIIA VERNYHOROVA[1,2], MICHAL JAMRICH[3], RADOVAN KYŠKA-PIPÍK[4] and NATÁLIA HUDÁČKOVÁ[3,*]

[1] Institute of Geological Sciences, National Academy of Sciences of Ukraine, O. Honchar str., 55b, Kyiv 01054, Ukraine

[2] Department of Invertebrate Fauna and Systematics, I.I. Schmalhausen Institute of Zoology of NAS of Ukraine, B. Khmelnitsky str. 15, Kyiv 01054, Ukraine

[3] Department of Geology and Paleontology, Faculty of Natural Sciences, Comenius University Bratislava, Mlynská dolina, Ilkovičova 6, 842 15, Bratislava, Slovak Republic

[4] Earth Science Institute, Slovak Academy of Sciences, Ďumbierska 1, 974 01, Banská Bystrica, Slovak Republic

* Corresponding author: natalia.hudackova@uniba.sk

Abstract: The Konkian-Sarmatian transition represents a major interval of biotic turnover and paleoenvironmental change in the Eastern Paratethys. This study investigates the upper Konkian and Lower Sarmatian deposits penetrated by well #20 on the western Kerch Peninsula (Crimea) using integrated analyses of benthic foraminifera, calcareous nannoplankton, mollusks, ostracods and rare planktic foraminifera. Three successive benthic foraminiferal assemblages were distinguished. The lower Konkian interval is characterized by assemblages containing *Spiroloculina konkensis*, *Quinqueloculina minakovae* group, and *Elphidium kudakoense*, together with the mollusks *Limacina konkensis* and *L. andrussovi*. The upper Konkian interval is dominated by *Elphidium horridum* and associated with *Obsoletiformes lithopodolicus ruthenicus* and *Musculus sarmaticus*. Early Sarmatian interval is marked by the appearance and common occurrence of *Varidentella reussi*, *Articularia articulinoides*, *Articulina sarmatica*, and *Elphidium reginum*. The transitional phase, termed the Konkian-Sarmatian Conversion Time (KSCT), represents a process of gradual basin reorganization. It is characterized by an abrupt decline in stenohaline elements occurring concurrently with the emergence of transitional mollusc and benthic foraminiferal species that appear in the late Konkian and span into the early phase of the Early Sarmatian. Calcareous nannoplankton assemblages containing *Orthorhabdus rugosus*, *Cyclicargolithus floridanus*, and common *Reticulofenestra pseudoumbilicus*, together with the absence of *Sphenolithus heteromorphus*, support assignment of the Konkian deposits to the NN6 Zone. The Early Sarmatian interval is characterized by abundant *Braarudosphaera bigelowii*, *B. bigelowii* ssp. *parvula*, and *Holodiscolithus macroporus*. The integrated microfossil and mollusc record documents a distinct turnover in biotic assemblages across the Konkian-Sarmatian transition and enables reliable correlation of the studied succession with regional Eastern Paratethyan stratigraphic schemes. The results contribute to a better understanding of the timing and character of biotic changes preceding and accompanying the establishment of Sarmatian environments.

Key words: Paratethys, Biostratigraphy, Serravallian, Foraminifera, Calcareous nannoplankton, Ostracods

Introduction

The Paratethys Sea (Laskarev, 1924) was a vast basin during the Neogene whose dynamic paleogeography, including intermittent connections between the Central and Eastern domains, strongly influenced regional paleoceanography and biotic evolution (Rögl, 1998; Popov et al., 2004; Harzhauser & Piller, 2007; Holcová, 2008; Kováč et al., 2017). A key event occurred at ~12.65 Ma ago, when temporary reconnection led to the replacement of the Badenian and Konkian seas by the Sarmatian Sea (e.g., Barbot de Marny, 1862, 1866, 1867; Suess, 1866; Andrusov, 1899; Paramonova & Belokrys, 1972; Nevesskaya et al., 1986; Palcu et al., 2017; Raffi et al., 2020). This transition is associated with major faunal and ecological changes, including the Badenian-Sarmatian Extinction Event in the Central Paratethys (Harzhauser & Piller, 2004, 2007; Holcová, 2008; Ter Borgh et al., 2014) and comparable turnover at the Konkian-Sarmatian boundary in the Eastern Paratethys (Muratov & Nevesskaya, 1986; Nevesskaya et al., 1986).

However, evidence from multiple Eastern Paratethys regions indicates that significant biotic changes began earlier, during the late Konkian (Bogdanovich, 1965; Maissuradze, 1971; Nevesskaya et al., 1986; Maissuradze et al., 2014; Vernyhorova, 2014, 2018).

The Konkian and Sarmatian regional stages of the Eastern Paratethys were formally defined by Nevesskaya et al. (1975). While the Konkian lacks a consistent regional subdivision and is represented by local biofacies (Vernyhorova, 2015, 2018), the Sarmatian is subdivided into Lower, Middle, and Upper substages with regionally defined horizons (Nevesskaya et al., 1984; Muratov & Nevesskaya, 1986). Magnetostratigraphic data constrain the Konkian to ~13.40–12.65 Ma and the Sarmatian s.l. to ~12.65–7.60 Ma (Palcu et al., 2017; Raffi et al., 2020; Lazarev et al., 2025).

Despite extensive research, the synchrony of biotic and ecological changes across different groups remains unresolved. This study addresses this issue by integrating benthic and planktic assemblages from the Konkian and Lower Sarmatian (Kuzhorian Horizon) based on clay-rich sequences from a well #20 in the western Kerch Peninsula (Figs. 1–2).

Geology of the studied area

The study area is in the western Kerch Peninsula, which during the Neogene formed part of the tectonically active Kerch-Taman folded zone between the Crimea and Caucasus mountains, characterized by folding and mud volcanism (e.g. Andrusov, 1893; Arkhangelsky et al., 1930; Shnyukov et al., 2006) (Fig. 1). Konkian and Sarmatian (s.l.) deposits are distributed across the peninsula (e.g. Andrusov, 1893; Osipov, 1927; Arkhangelsky et al., 1930; Archangelsky, 1940; Barg & Stepaniak, 2003; Vernigorova et al., 2012; Vernyhorova, 2014).

The studied sequence starts with Petrovske Fm. of the Konkian age and is composed of relatively uniform clay sediments with minor portion of sand, siltstone, marl, and shell detritus, reaching thicknesses of 36–155 m (e.g. Arkhangelsky et al., 1930; Archangelsky, 1940; Vernigorova et al., 2012; Vernyhorova, 2014). These deposits are overlain by Lower Sarmatian strata without clear hiatus (Vernigorova et al., 2012; Vernyhorova, 2014).

Lower Sarmatian deposits belong to the Krasnoperekopsk Fm. consisting predominantly of dark grey to black clays, massive or laminated, with thickness of 31–230 m (e.g. Andrusov, 1893; Arkhangelsky et al., 1930; Kolesnikov, 1935; Archangelsky, 1940; Barg & Stepaniak,

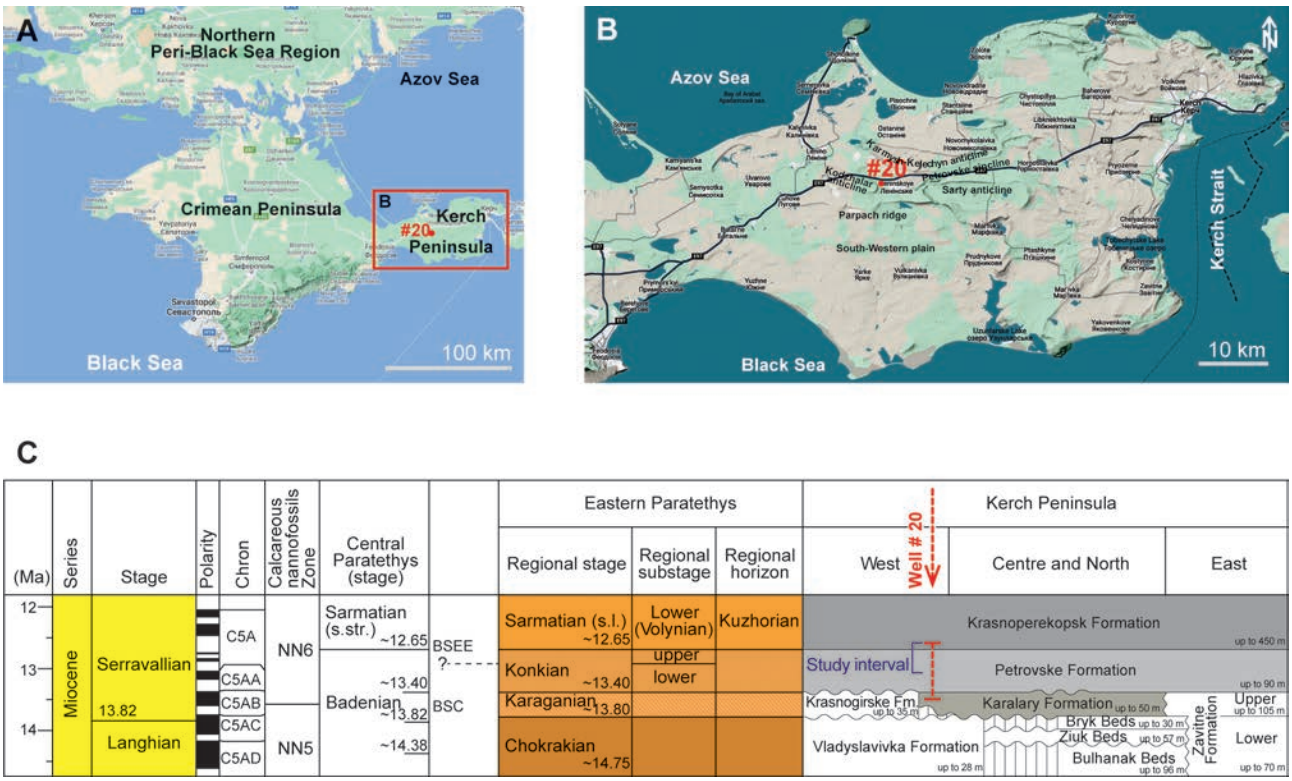

Fig. 1. Location map of the studied well #20 and explanation notes A – Crimean Peninsula and Kerch Peninsula B – Kerch Peninsula detailed map with well location. C – Miocene Chronostratigraphic framework of the Central Paratethys, Eastern Paratethys and Kerch Peninsula and position of the well, lithostratigraphy of the studied region (according to Arkhangelsky et al., 1930; Archangelsky, 1940; Vernigorova et al., 2012; Vernyhorova, 2014).

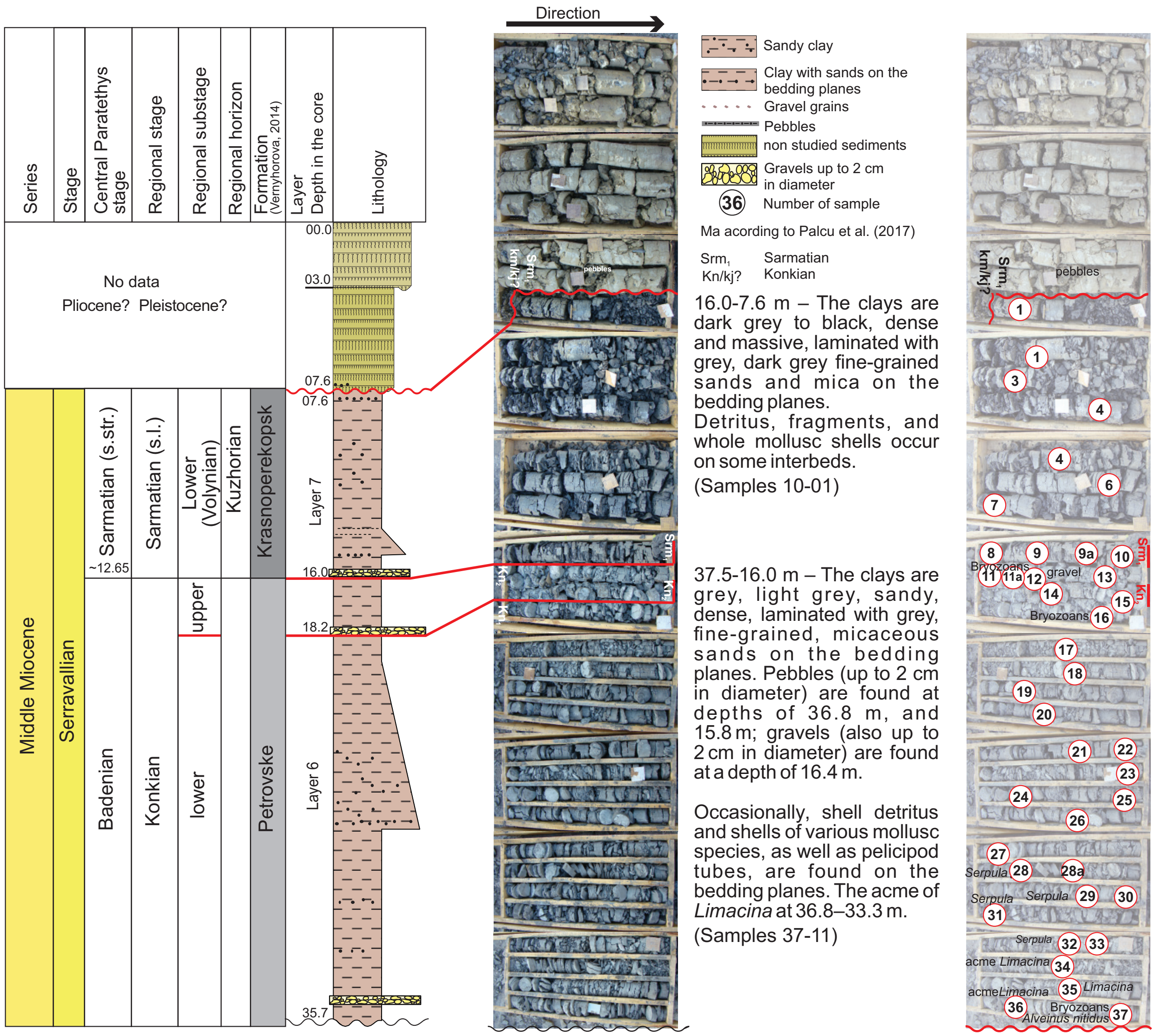

Fig. 2. Miocene Chrono/lithostratigraphic framework with horizons and formations of the discussed section with detailed well description.

2003; Vernigorova et al., 2012; Vernyhorova, 2014). This unit includes the Kuzhorian and Zbruchian horizons and part of the Middle Sarmatian and is overlain by younger Sarmatian deposits (Vernigorova et al., 2012; Vernyhorova, 2014).

Methods

Foraminifera, Ostracoda and Mollusca were obtained from 400 g of each well #20 sample, dried and washed through a 63 μm sieve, and all planktic and benthic specimens were picked separately. Identification and imaging were carried out using a Zeiss Stemi 750 stereomicroscope, a polarizing microscope (Comenius University in Bratislava), and a JEOL JSM-6390LV SEM (ESI, SAS). Taxonomic identification of benthic foraminifera followed Bogdanovich (1952), Krasheninnikov (1959), Didkovskiy (1961), Maissuradze (1971), Maissuradze & Koiava (2011), with generic revisions after Łuczkowska (1972, 1974) and Hayward et al. (2025). Planktic foraminifera were determined according to Cicha et al. (1998), Smart & Thomas (2007), Aze et al. (2011), Spezzaferri et al. (2015), and Wade et al. (2018). Poor preservation required some taxa to remain in open nomenclature (see Supplement 1).

Molluscs (mainly bivalves) were studied as a complementary group to determine the Konkian-Sarmatian stratigraphy. Molluscs were identified directly during sampling of the sections, as well as under a Zeiss Stemi 750 stereomicroscope (Comenius University in Bratislava). Traditional conchological methods were employed to identify species (Ilyina, 1993; Nevesskaya et al., 1993).

Calcareous nannofossils were observed in all 37 samples (Supplement S2). Calcareous nannofossils smear

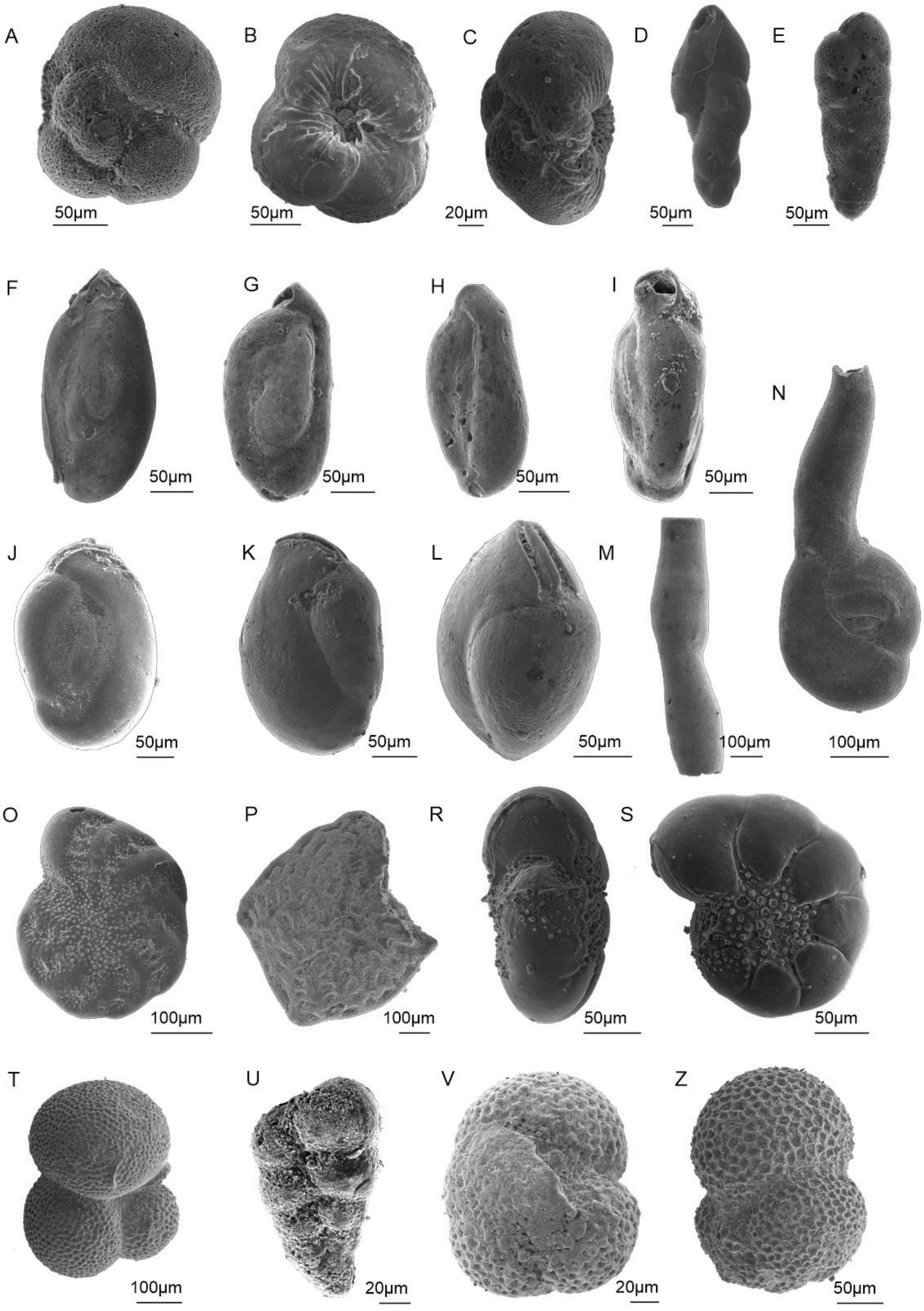

Fig. 3. The most important Foraminifera identified from the Kerch well #20.

A–B–C – *Glabratella kartvelicus* (Krasheninnikov) (sample 34); D – *Fursenkoina schreibersiana* Cžjžek (sample 34); E – *Bolivina sarmatica* Didkovskiy (sample 35); F–G–H–I – *Varidentella* ex gr. *latelacunata* (Venglinsky) (sample 34); J–K–L – *Affinetrina ucrainica* (Serova in Bogdanovich) (sample 32); M – *Articularia articulinoides* (Gerke & Issaeva) (uniserial part) (sample 9a); N – *A. articulinoides* (Gerke & Issaeva) (sample 9); O – *Elphidium horridum* Bogdanowicz (sample 11a); P – *Elphidium reginum* (d'Orbigny) (sample 2); R–S – *Elphidium granosum* (d'Orbigny); T – *Subbotina eocaena* (Guembel 1868) (sample 35); U – *Streptochilus subglobigerum* Resig, 1989 (sample 3); V – *Catapsydrax unicavus* Bolli, Loeblich & Tappan, 1957 (sample 8); Z – *Trilobatus trilobus* (Reuss, 1850) (sample 9a). Index species: (Konkian A – L); (Early Sarmatian M, N); (late Konkian – Early Sarmatian O); (Early Sarmatian P); (Konkian–Sarmatian R, S); (Planktic T – V, Z).

slides were prepared using the standard method of Bown and Young in Bown (1998) and were counted in 300 fields of view, using an Olympus BX 50, an objective with 100× magnification, and oil immersion. We used an Olympus Infinity 2 camera with QuickPHOTO CAMERA 2.3 software for photographic record. Systematic identification and taxonomy follow Young (1998) and Young et al. (2017). Standard NN zones are after Martini (1971).

Results

Foraminifera and Mollusca

A total of 97 species of benthic foraminifera belonging to 43 genera were identified in the studied interval (Supplement 1, Fig. 3). The assemblages are characterized by a marked difference between dominant and associated taxa. Dominant species constitute 10.00–95.34 % of the total assemblage in individual samples, corresponding to 7–961 tests per sample (Supplement 1, Fig. 4), whereas associated species account for 0.28–8.41 % and are generally represented by only a few specimens. The lower part of the studied section (samples 37–16; 35.7–18.8 m) is characterized by the occurrence of *Spiroloculina konkensis*, *Quinqueloculina minakovae minakovae*, *Q. minakovae ukrainica*, *Q. konkensis*, *Nodobaculariella* ex gr. *konkensis*, *Bolivina dilatata*, *Sigmoidella caucasica*, *Cassidulina* sp. 1, *Discorbis squamulus*, and *Elphidium kudakoense*. Mollusc assemblages in this interval include *Limacina konkensis* and *L. andrussovi*. In the middle part of the section (samples 15–11; 18.1–16.1 m), the foraminiferal assemblages are dominated by *Elphidium horridum*. The associated mollusc fauna comprises *Obsoletiformes*

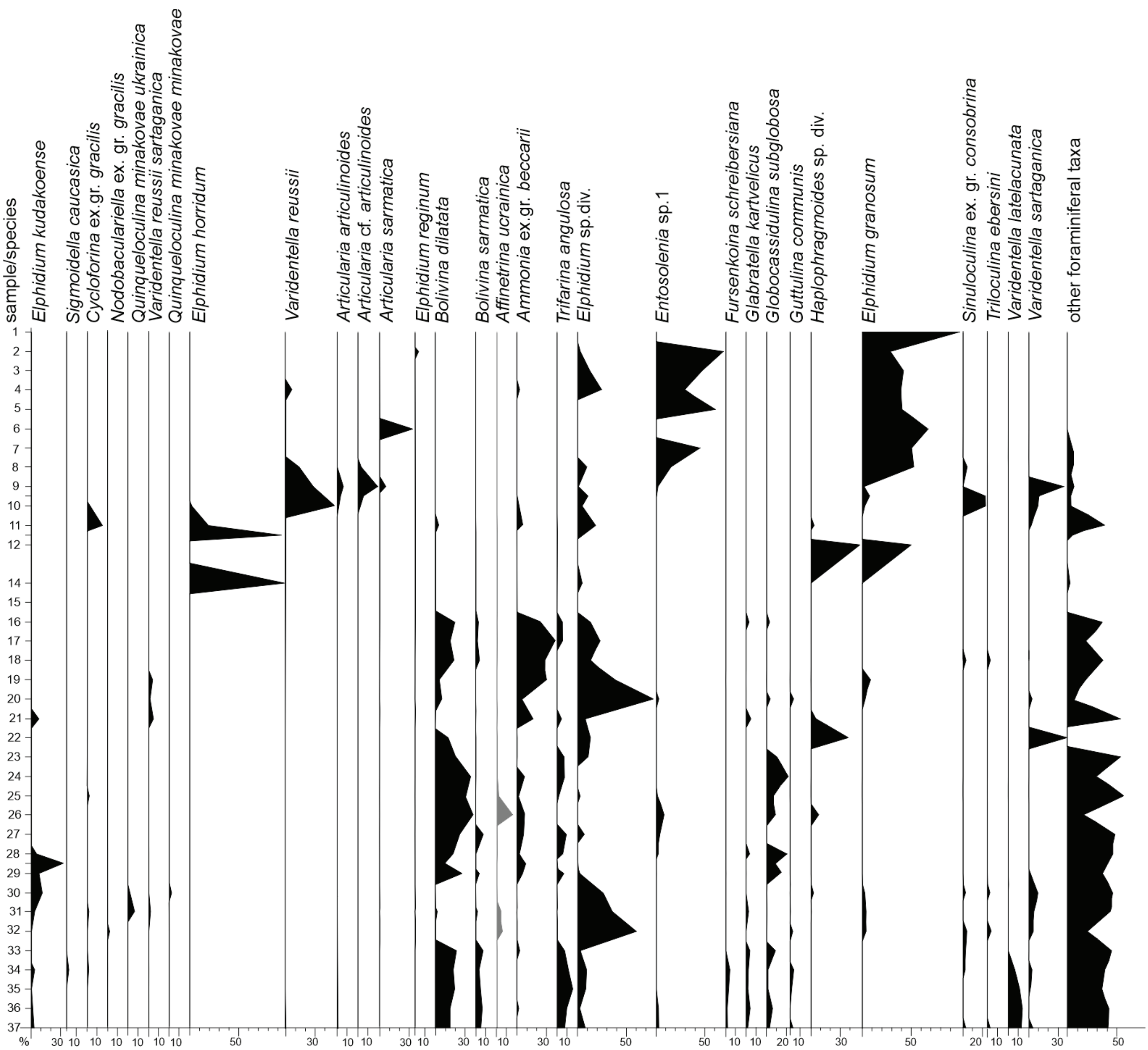

Fig. 4. Portion of stratigraphically important foraminifera in the samples studied from well #20 in the Kerch Peninsula.

lithopodolicus ruthenicus and *Musculus sarmaticus*. The upper part of the section (samples 10–01; 15.9–07.7 m) is characterized by the occurrence of *Varidentella reussi*, *Articularia articulinoides*, *Articulina sarmatica*, and *Elphidium reginum*. The mollusc assemblages continue to be represented by *Obsoletiformes lithopodolicus ruthenicus* and *Musculus sarmaticus*. This interval also contains abundant calcareous nannofossils, including *Holodiscolithus macroporus*, *Braarudosphaera bigelowii*, and *Braarudosphaera bigelowii* ssp. *parvula*.

Planktic foraminifera were identified in 11 samples; however, they were rare and poorly preserved. A total of 29 specimens representing 11 species were recorded (see Supplement 1). The majority of the assemblage is composed of reworked taxa exhibiting a broad stratigraphic range, spanning from the Eocene (e.g., *Pseudohastigerina* cf. *wilcoxensis*), through the Oligocene (*Subbotina gortanii*, *S. eocaena*), to the Miocene (*Catapsydrax unicavus*, *Paragloborotalia siakensis*, *Trilobatus trilobus*).

Ostracoda

Ostracod valves and complete carapaces constitute more than half of the collected specimens. The valves are translucent to opaque and display white, brown, and black coloration. Many specimens are infilled with authigenic minerals, probably pyrite and/or carbonate. Although the ornamentation is generally preserved, the observation of some taxonomically important features, particularly marginal pore canals, the inner lamella and muscle scars, are hindered by mineral infilling. This is especially problematic for the identification of leptocytherid taxa. The ornamentation is excellently preserved, but occasionally smoothed due to transport (sample 9). Both adults and juveniles are present, but due to the very low number of individuals in the samples, it is not possible to use the juvenile/adult ratio to consider post-mortem transport and autochthonism. However, the overall abundance of ostracods is low in most samples. Sixteen ostracod taxa were recognized, but none could be identified to the species level. *Cytheridea* sp. resembles *Cytheridea acuminata* Bosquet, 1852 in general outline but differs in its fine ornamentation. The remaining taxa are retained in open nomenclature. The assemblage comprises representatives of the genera *Aurila, Euxinocythere, Leptocythere, Callistocythere, Loxoconcha*, *Loxocauda*, *Cytheridea*, *Cytherura*, *Sclerochilus*, and *Xestoleberis*.

Calcareous nannoplankton

A total of 43 calcareous nannoplankton taxa were identified in the studied deposits. Preservation and abundance are generally moderate (Supplement 3). The highest abundances were recorded in samples 14, 19, 16, 13, 29, 35, 33, 37, and 32. The assemblages are dominated by reticulofenestrids in samples 4, 14, 19, 16, 13, and 29, where they comprise up to 97.9 % of the total assemblage. The highest abundances were recorded in samples 14 and 19, with *Reticulofenestra pseudoumbilicus* accounting for 50.5 % and *Reticulofenestra haqii* for 46.0% of the assemblage (Figs. 6, 7; Supplement 3). In contrast,

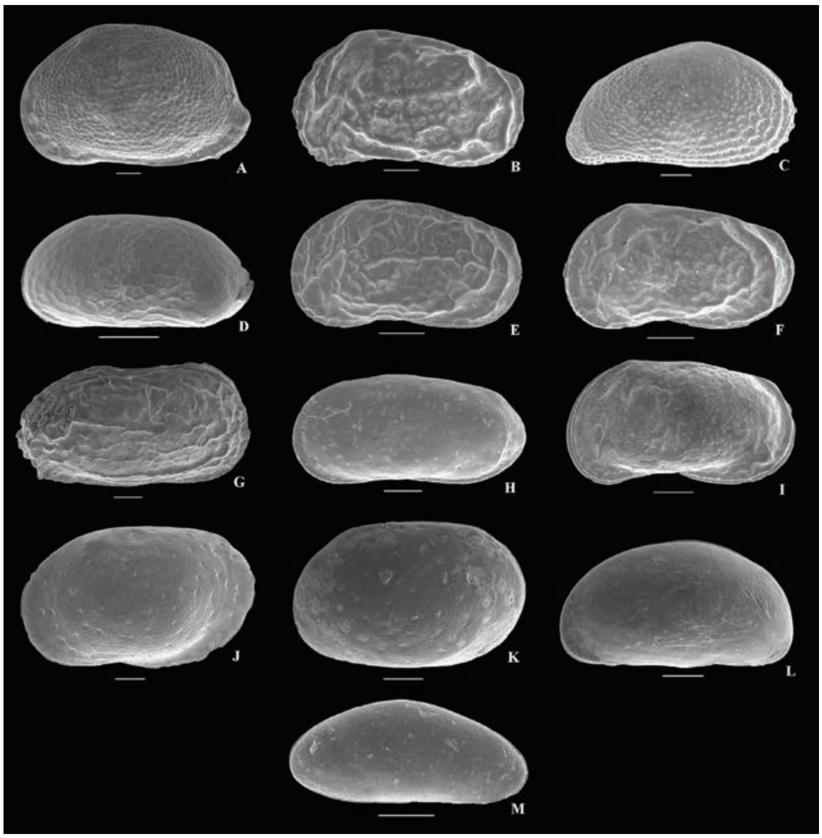

Fig. 5. Ostracoda from the samples of the well #20 Kerch.

A – *Aurila* sp., LV, sample 15; B – *Callistocythere* sp. 3, LV, sample 5; C – *Cytheridea* sp. aff. *Cytheridea acuminata* Bosquet, 1852, RV, sample 32; D – *Cytherura* sp., LV, sample 34; E – *Euxinocythere* sp. form A, LV, sample SV20 30; F – *Euxinocythere* sp. form B, LV, sample 9; G – *Hiltermannicythere* sp., RV, sample 32; H – *Leptocythere* sp. 1, LV, sample 32; I – *Leptocythere* sp. 2, LV, sample 9; J – *Loxoconcha* sp. 1, LV, sample 30; K – *Loxoconcha* sp. 2, LV, sample 31; L – *Xestoleberis* sp., 3, LV, sample 32; M – *Sclerochilus* sp. 2, RV, sample 36. LV – left valve; RV – right valve. All valves in external lateral view. Scale bar 100 µm.

samples 35, 33, 37, and 32 are dominated by *Coccolithus pelagicus*, which constitutes 85.7–90.7 % of the assemblage (Fig. 7; Supplement 3). Rare, reworked taxa were also observed throughout the section. These include Lower Miocene, Paleogene, and Cretaceous species represented by *Helicosphaera euphratis*, *Reticulofenestra lockeri*, *Triquetrorhabdulus carinatus*, *Watznaueria barnesiae*, *Micula staurophora*, *Prediscosphaera cretacea*, and *Cribrosphaerella ehrenbergii*. Samples in interval 37–11; (35.7–16.1 m) are characterized by the dominance of *Coccolithus pelagicus* in the lower part of the section (samples 37–30), accompanied by less abundant *Reticulofenestra haqii*, *R. pseudoumbilicus*, *Braarudosphaera bigelowii*, and *Helicosphaera car-teri*. Additional taxa recorded in this interval include *Cyclicargolithus floridanus*, *Rhabdosphaera sicca*, *Sphenolithus moriformis*, and *Syracosphaera pulchra*. In the samples 29–11, *Reticulofenestra pseudoumbilicus* becomes the dominant taxon, replacing *Coccolithus pelagicus*. Other commonly occurring taxa include *R. haqii*, *Braarudosphaera bigelowii*, *Rhabdosphaera sicca*, *Syracosphaera pulchra*, *Holodiscolithus macroporus*, *Umbilicosphaera jafari*, and *U. rotula*. The uppermost part of the well, samples 10-01; (15.9–07.7 m) is characterized by a marked decrease in assemblage diversity and abundance. *Reticulofenestra pseudoumbilicus* becomes rare or absent, whereas *Braarudosphaera bigelowii*, *B. bigelowii* ssp. *parvula*, and *Holodiscolithus macroporus* increase in abundance and become characteristic com-ponents of the assemblages. The uppermost sample yielded a poor nannoplankton assemblage and lacked characteristic taxa (Figs. 6, 7).

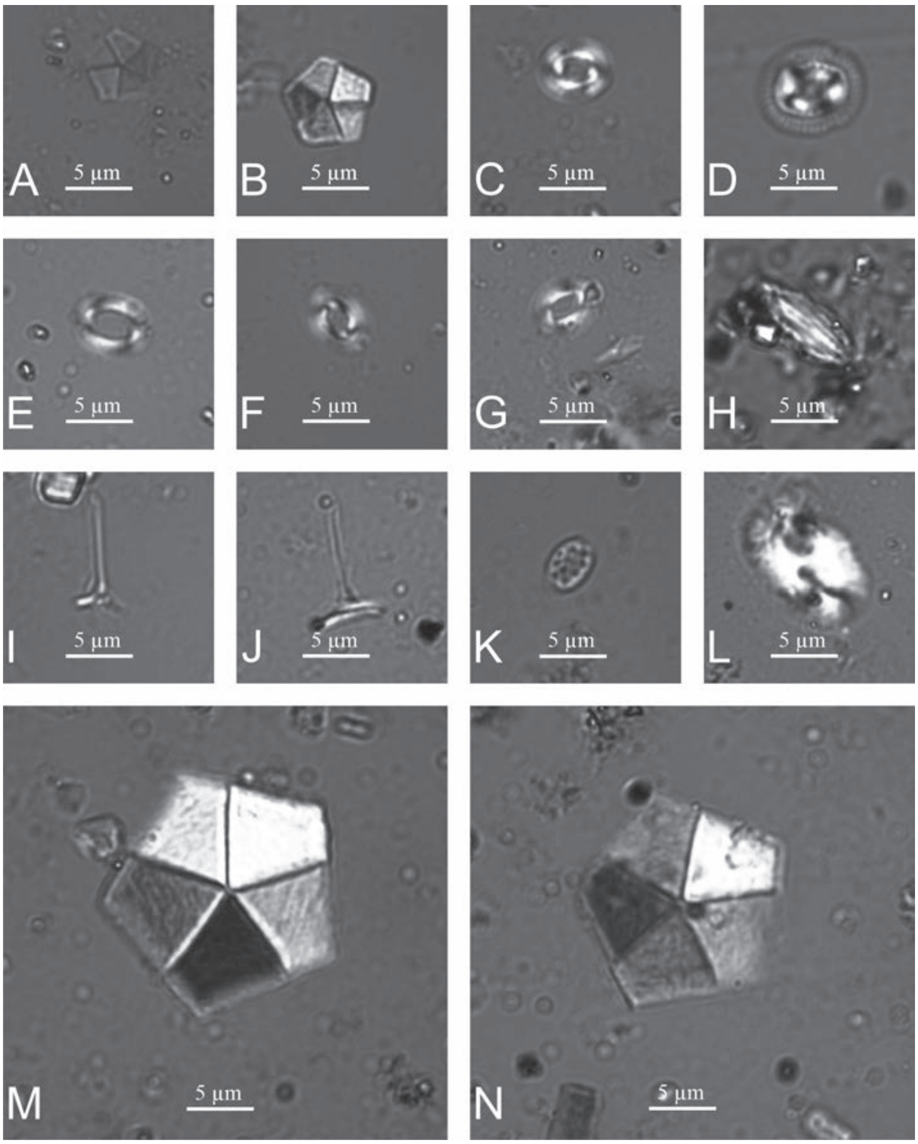

Fig. 6. Stratigraphically important calcareous nannoplankton in the samples studied.

A–B – *Braarudosphaera bigelowii* ssp. *parvula* Stradner, 1960 (samples 8, 37); C – *Cyclicargolithus floridanus* (Roth and Hay, in Hay et al., 1967) Bukry, 1971 (sample 36); D – *Coccolithus pelagicus* (Wallich, 1877) Schiller, 1930 (sample 16); E–F–G – *Reticulofenestra pseudoumbilicus* (Gartner, 1967) Gartner, 1969 (samples 11a, 12, 15); H – *Orthorhabdus rugosus* (Bramlette & Wilcoxon, 1967) Young & Bown 2014 (sample 27); I–J – *Rhabdosphaera sicca* (Stradner, 1963) Fuchs & Stradner 1977 (sample 18, 29); K – *Holodiscolithus macroporus* (Deflandre, in Deflandre and Fert, 1954) Roth, 1970 (sample 3); L – *Helicosphaera wallichii* (Lohmann, 1902) Okada and McIntyre, 1977 (sample 12); M–N – *Braarudosphaera bigelowii* (Gran and Braarud, 1935) Deflandre, 1947 (samples 4, 5).

Interpretation

The distribution of foraminifera, molluscs, and calcareous nannofossils reveals distinct changes in assemblage composition throughout the studied succession, particularly between the lower, middle, and upper intervals of the well. The high proportion of articulated carapaces (> 50 % of collected specimens) suggests limited post-mortem transport and relatively rapid burial. According to biostratigraphically important foraminifera species and calcareous nannoplankton (Figs. 3–7, Supplements 1–3), three stratigraphic units were identified in the studied material. The lower Konkian [samples 37–16, corresponding to 35.7–18.8 m, (Fig. 8)] is characterized by *Spiroloculina konkensis*, *Quinqueloculina minakovae minakovae*, *Q. minakovae ukrainica*, *Elphidium kudakoense*, and mollusc species *Limacina konkensis*, *L. andrussovi*. The upper Konkian [samples 15–11, corresponding to 18.1–16.1 m, (Fig. 8)] is characterized by benthic foraminifera *Elphidium horridum* and mollusc species *Obsoletiformes lithopodolicus ruthenicus* and *Musculus sarmaticus*. The Early Sarmatian [samples 10-01, corresponding to 15.9–07.7 m (Fig. 8)] is distinguished by the onset of foraminiferal species such as *Varidentella reussi, Articularia articulinoides, Articulina sarmatica*, and *Elphidium reginum* together with mollusc species including *Obsoletiformes lithopodolicus ruthenicus*,

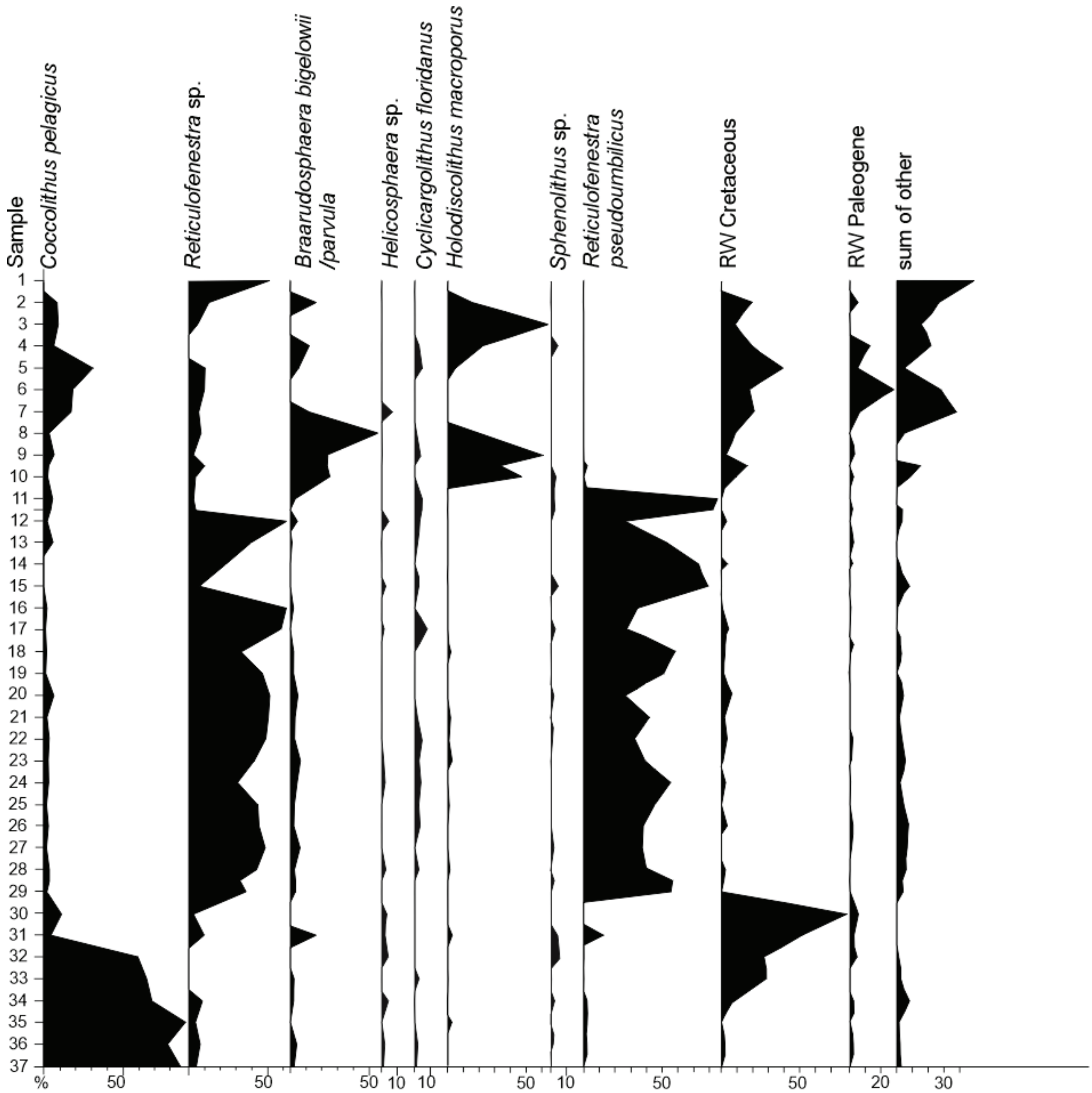

Fig. 7. Calcareous nannoplankton association with marked important and most abundant species.

and *Musculus sarmaticus*, as well as an abundance of calcareous nannofossils *Holodiscolithus macroporus*, *Braarudosphaera bigelowii*, *B. bigelowii* ssp. *parvula*. Planktic foraminifera are considered reworked. Only rare specimens of *Streptochilus subglobigerum*, *Catapsydrax unicavus* and *Trilobatus trilobus* can represent autochthonous planktic foraminifera of the Middle to Upper Miocene.

The ecological preferences of the identified ostracod genera indicate deposition in a shallow-water setting. *Aurila*, *Callistocythere*, *Loxoconcha*, *Loxocauda*, *Cytheridea*, *Cytherura*, *Sclerochilus*, and *Xestoleberis* are characteristic of littoral to shallow sublittoral marine environments, whereas *Euxinocythere* and *Leptocythere* are commonly associated with brackish conditions. The occurrence of two morphotypes of *Euxinocythere* may reflect either taxonomic differentiation or ecophenotypic variation related to environmental factors such as salinity, temperature, or carbonate availability.

The calcareous nannoplankton assemblages in lower and upper Konkian deposits contain common *Cyclicargolithus floridanus* and rare *Orthorhabdus rugosus*, whereas *Sphenolithus heteromorphus* is absent throughout the studied interval. The presence of *Orthorhabdus rugosus* together with the absence of *Sphenolithus heteromorphus* supports the assignment of the assemblages to the NN6 Zone of Martini (1971) (Young, 1998; Young et al., 2017). This interpretation is further supported by the occurrence of *Reticulofenestra pseudoumbilicus*, *Braarudosphaera bigelowii* ssp. *parvula*, *Helicosphaera wallichii*, *Holodiscolithus macroporus*, *Rhabdosphaera sicca*, *R. poculii*, *Syracosphaera pulchra*, *Umbilicosphaera jafari*, and *U. rotula*.

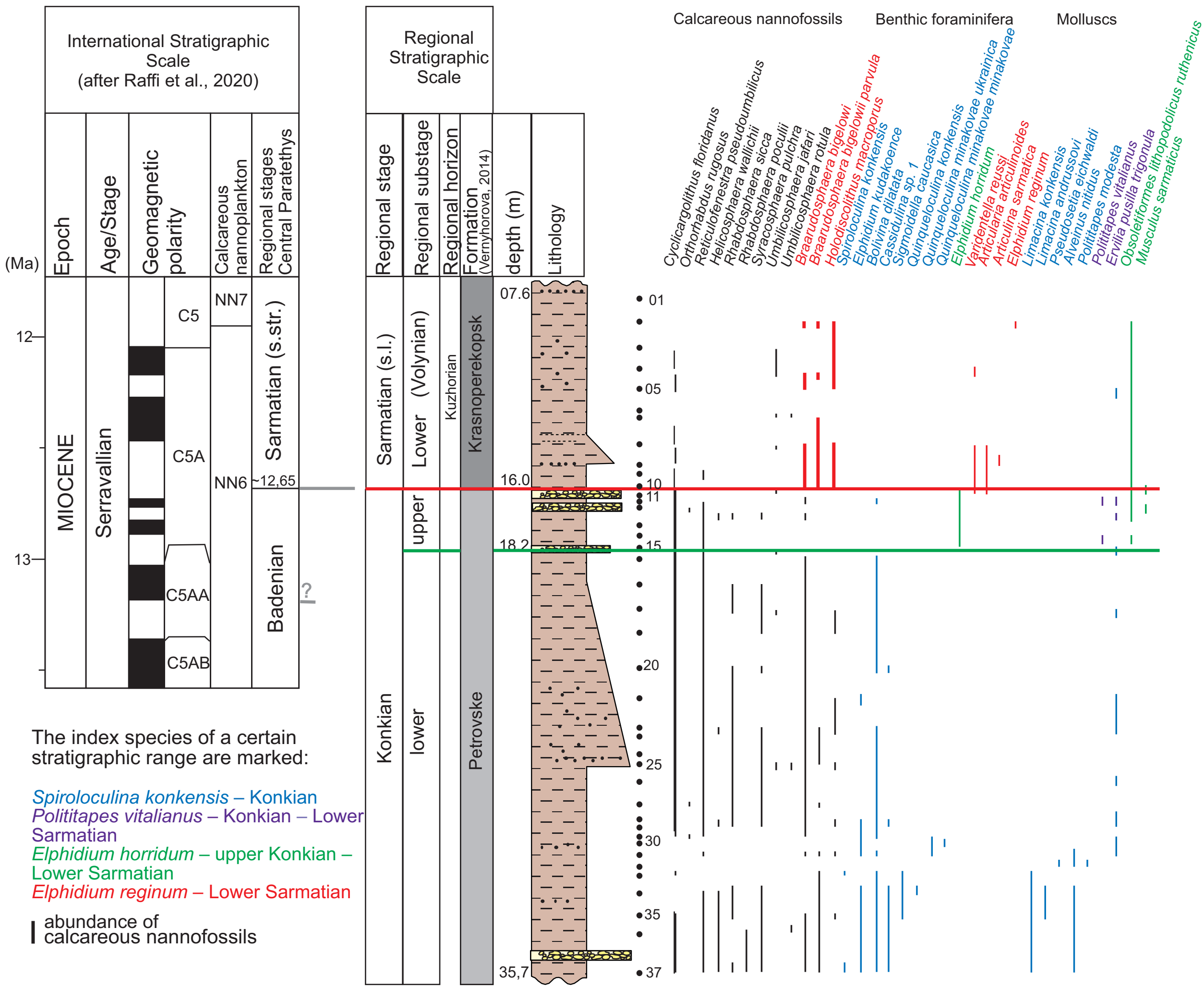

Fig. 8. Biostratigraphical synthesis of important biostratigraphical taxa with the position in the studied material from the well core samples.

The occurrence of common *Reticulofenestra pseudoumbilicus* (also > 7 µm) in the Konkian part of the section is consistent with an NN6 age and postdates its First Common Occurrence (FCO), calibrated at approximately 13.1 Ma (Abdul Aziz et al., 2008). Accordingly, the Konkian deposits penetrated by well #20 are assigned to the NN6 Zone and correlated with the middle Serravallian.

The upper Konkian is an important time interval, called the Konkian-Sarmatian Conversion Time (KSCT). It represents a key phase of the basin's gradual reorganization (Vernyhorova, 2015, 2018), during which mollusc and foraminiferal assemblages underwent a profound transformation from typically Konkian to Sarmatian types in the Eastern Paratethys. While earlier Konkian intervals also exhibit a sharp reduction or disappearance of stenohaline elements (e.g. Popov et al., 2016; Palcu et al., 2017), the late Konkian event is distinct. Here, the abrupt decline in stenohaline taxa occurs concurrently with the emergence of characteristic mollusc and benthic foraminiferal species whose stratigraphic ranges span from the late Konkian to the earliest Early Sarmatian (Sokolov, 1899; Liverovskaya, 1935, 1960; Bogdanovich, 1965; Nevesskaya et al., 1986; Krasheninnikov, 1959; Maissuradze, 1971; Bratishko et al., 2015). Nannoplankton data further constrain this interval, including the occurrence of *Reticulofenestra pseudoumbilicus* and correlation with calcareous nannoplankton zones CNM8–CNM11 (NN6–NN7) within the Serravallian (Andreyeva-Grigorovich & Nosovsky, 1976; Nevesskaya et al., 1986; Prisyazhnyuk et al., 2007; Radionova et al., 2012; Popov et al., 2016; Palcu et al., 2017; Raffi et al., 2020; Lazarev et al., 2025).

The overlying deposits are assigned to the early Sarmatian based on the presence and common occurrence of the foraminiferal species *Varidentella reussi*, *Articularia articulinoides*, *Articulina sarmatica*, and *Elphidium reginum* (Fig. 8), together with the mollusc assemblage containing *Obsoletiformes lithopodolicus ruthenicus* and *Musculus sarmaticus*. The marked reduction of *Reticulofenestra pseudoumbilicus* and the abundance of *Braarudosphaera bigelowii*, *B. bigelowii* ssp. *parvula*, and *Holodiscolithus macroporus* characterize the nannoplankton assemblages of this interval.

Conclusion

Integrated analyses of benthic foraminifera, calcareous nannoplankton, ostracods and molluscs from well #20 on the western Kerch Peninsula enabled recognition of the lower Konkian, upper Konkian and Lower Sarmatian deposits and refinement of the Konkian-Sarmatian transition.

Three successive assemblages were identified: (1) a lower Konkian assemblage characterized by *Spiroloculina konkensis*, *Quinqueloculina minakovae* group, *Elphidium kudakoense*, and the molluscs *Limacina konkensis* and *L. andrussovi*; (2) an upper Konkian assemblage dominated by *Elphidium horridum* and accompanied by *Obsoletiformes lithopodolicus ruthenicus* and *Musculus sarmaticus*; and (3) an Early Sarmatian assemblage marked by the appearance of *Varidentella reussi*, *Articularia articulinoides*, *Articulina sarmatica*, and *Elphidium reginum*.

Calcareous nannoplankton assemblages containing *Orthorhabdus rugosus*, *Cyclicargolithus floridanus*, and common *Reticulofenestra pseudoumbilicus*, together with the absence of *Sphenolithus heteromorphus*, indicate assignment of the Konkian deposits to the NN6 Zone of Martini (1971). The Early Sarmatian interval is characterized by abundant *Braarudosphaera bigelowii*, *B. bigelowii* ssp. *parvula*, and *Holodiscolithus macroporus*.

The Konkian-Sarmatian Conversion Time (KSCT) represents a transitional phase marked by a process of gradual basin reorganization during the late Konkian and the earliest Early Sarmatian in the Eastern Paratethys. This interval is characterized by a faunal turnover, where an abrupt decline in stenohaline elements occurs concurrently with the emergence of transitional mollusc and benthic foraminiferal species, which appear in the late Konkian and span into the early phase of the Early Sarmatian. Integrated nannoplankton data (*Reticulofenestra pseudoumbilicus*, zones CNM8–CNM11 or NN6–NN7) provide a robust biostratigraphic constraint for this event within the Serravallian.

The foraminifera and ostracod associations are typical of a shallow littoral environment with submerged macrophyte habitats and characterized by fluctuating salinity. Part of the association is probably transported from a very marginal, shallow water environment. The predominance of ostracod genera tolerant of brackish conditions supports this interpretation, while the occurrence of taxa typical of very shallow coastal settings suggests that part of the assemblage may have been transported over a short distance before burial.

The integrated microfossil and mollusc record documents a distinct faunal turnover across the Konkian-Sarmatian transition and provides a robust basis for regional stratigraphic correlation within the Eastern Paratethys.

Acknowledgments

The research was supported by the National Scholarship Programme of the Slovak Republic No. 52182 (2024–2025), VEGA 2/0012/24, VEGA 2/0106/23 and VEGA 2/0085/24. This study was prepared within the framework of the research project *Integrating Cenozoic stratigraphic data of Ukraine to solve geological mapping tasks* (State Registration No. 0126U000799). The authors are grateful to reviewers Olga Anistratenko, Andrej Ruman and Ondrej Pelech as handling editor whose insightful comments and suggestions improved the paper.

References

Abdul Aziz, H., Di Stefano, A., Foresi, L. M., Hilgen, F. J., Iaccarino, S. M., Kuiper, K. F., Lirer, F., Salvatorini, G. & Turco, E., 2008: Integrated stratigraphy and 40Ar/39Ar chronology of early Middle Miocene sediments from DSDP Leg 42A, Site 372 (Western Mediterranean). *Palaeogeography, Palaeoclimatology, Palaeoecology*, 257, 123–138. https://doi:10.1016/j.palaeo.2007.09.013.

Aze, T., Ezard, T. H. G., Purvis, A., Coxall, H. K., Stewart, D. R. M., Wade, B. S. & Pearson, P. N., 2011: A phylogeny of Cenozoic macroperforate planktonic foraminifera from fossil data. *Biological Reviews*, 86, 900–927. https://doi.org/10.1111/j.1469-185X.2011.00178.x.

Andrusov, N. I., 1893: Geotektonika Kerchenskogo Poluostrova [Geotectonics of the Kerch Peninsula]. Materialy dlya Geologii Rossii. *Edition by Imperatorskoy Akademii Nauk, St. Petersburg*, 16, 3–206 (in Russian).

Andrusov, N. I., 1899: Zametki o miotsene prikaspiiskikh stran [Notes on the Miocene of the Caspian countries]. *News of the Geological Committee*, 18, 7, 339–369 (in Russian).

Archangelsky, A. D. (ed.), 1940: Stratigraphiya SSSR. Tom 12: Neogen SSSR [Stratigraphy of the USSR. Vol. 12: Neogene USSR]. *AN SSSR, Moscow, Leningrad*, 680 p. (in Russian).

Arkhangelsky, A. D., Blokhin, A. A., Menner, V. V., Osipov, S. S., Sokolov, M. I. & Chepikov, K. R., 1930: Kratkiy ocherk geologicheskogo stroeniya I neftianykh mestorozhdeniy Kerchenskogo poluostrova [A Short Review of the Geological Structure and the Oil Deposits of the Kerch Peninsula]. *Transactions of the Geological and Prospecting Service of USSR, Moscow, Leningrad*, 13, 1–142 (in Russian).

Andreyeva-Grigorovich, A. S. & Nosovsky, M. F., 1976: O stratigraficheskikh analogakh konkskogo yarusa v Tsentralnom Paratetise [About stratigraphic equivalents of the Konkian stage in the Central Paratethys]. The stratigraphy of the Northern Black Sea region and the Crimea. *Dnepropetrovsk*, 72–77 (in Russian).

Barbot de Marny, N. P., 1862: O geologicheskom vozraste stepnogo izvestniaka v Rossii [On the geological age of the steppe limestone of southern Russia]. *Mining Journal*, 2, 77–85 (in Russian).

Barbot de Marny, N. P., 1866: Über die jüngeren Ablagerungen des südlichen Rußland (Mülfitgetheilt vom e. M. Ed. Suess in der Sitzung vom 26. April 1866). *Sitzungsberichte der Mathematisch-Naturwissenschaftlichen Classe der Kaiserlichen Akademie der Wissenschaften. Kl.*, Abt. 1, Bd. 13, 339–342.

Barbot de Marny, N. P., 1867: Sarmatskiy yarus miotsenovoi formatsii [Sarmatian stage of the Miocene formation]. *Mining Journal*, Part 7, 100–125 (in Russian).

Barg, I. M. & Stepaniak, Y. D., 2003: Stratigrafiya I Geologicheskoe Razvitie Ravninnogo Kryma I Kerchenskogo Poluostrova V Miotsenovuyu Epokhu [Stratigraphy and Geological Development of the Crimea and Kerch Peninsula in the Miocene Epoch]. *Monolit, Dnepropetrovsk*, 170 p. (in Russian).

Bogdanovich, A. K., 1952: Miliolidy I peneroplidy [Miliolidae and peneropliidae]. *Proc. VNIGRI*, 64 p. (in Russian).

Bogdanowicz, A. K., 1965: Stratigraficheskoe i fatsialnoe raspredelenie foraminifer v miotsene Zapadnoho Predkavkaz'ya i voprosy ikh genezisa [Stratigraphic and facies distribution of foraminifera in the Miocene of Western Ciscaucasia and questions of their genesis]. *Proceedings of the Krasnodar branch of the All-Union Oil and Gas Research Institute*, 16, 300–350 (in Russian).

Bonaduce, G., Ciampo, G. & Masoli, M., 1976: Distribution of Ostracoda in the Adriatic Sea. *Pubblicazioni della Stazione Zoologica di Napoli*, 40, 1–154.

Bown, P. R. & Young, J. R., 1998: Techniques. In: Bown, P. R. (ed.): Calcareous nannofossil biostratigraphy. British Micropalaeontological Society, Publications Series. *London, Chapman and Hall*, 16–28. https://doi.org/10.1007/978-94-011-4902-0_2.

Bratishko, A., Schwarzhans, W., Reichenbacher, B., Vernyhorova, Y. & Ćorić, S., 2015: Fish otoliths from the Konkian (Miocene, early Serravallian) of Mangyshlak (Kazakhstan): testimony to an early endemic evolution in the Eastern Paratethys. *Paläontologische Zeitschrift Scientific Contributions to Palaeontology*, 89, 839–889. https://doi.org/10.1007/s12542-015-0274-4.

Cernajsek, T., 1972: Zur Palökologie der Ostrakodenfaunen am Westrand des Wiener Beckens. *Verhandlungen der geologischen Bundesanstalt*, 2, 237–246.

Cicha, I., Rögl, F., Rupp, Ch. & Čtyroká, J. (eds.), 1998: Oligocene-Miocene foraminifera of the Central Paratethys. *Abhandlungen der Senckenbergischen Naturforschenden Gesellschaft*, 549, 325 p.

Didkovskiy, V. Ya., 1961: Miliolidy neogenovykh vidkladiv pivdenno-zakhidnoi chastyny rossiiskoi platformy. Tom 1 (Rody *Quinqueloqulina* ta *Triloculina* [Miliolidae of the Neogene deposits of the south-western part if the Russian platform. Volume 1 (Tom 1 genera of *Quinqueloqulina* and *Triloculina*)]. *Kyiv, Academy of sciences of Ukrainian SSR*, 172 p. (in Ukrainian).

Faranda, C., Gliozzi, E., Cipollari, P., Grossi, F., Darbaş, G., Gürbüz, K., Nazik, A., Gennari, R. & Cosentino, D., 2013: Messinian paleoenvironmental changes in the Easternmost Mediterranean Basin: Adana Basin, southern Turkey. *Turkish Journal of Earth Sciences*, 22, 839–863.

Gross, M., 2006: Mittelmiozäne Ostracoden aus dem Wiener Becken Badenium/Sarmatium, Österreich). *Wien, Österreichische Akademie der Wissenschaften, Schriftenreihe der Erdwissen-schaftlichen Kommissionen*, special volume, 1, 1–224.

Harzhauser, M. & Piller, W. E., 2004: Integrated stratigraphy of the Sarmatian (Upper Middle Miocene) in the western Central Paratethys. *Stratigraphy*, 1, 1, 65–86.

Harzhauser, M. & Piller, W. E., 2007: Benchmark data of a changing sea – Palaeogeography, palaeobiogeography and events in the Central Paratethys during the Miocene. *Palaeogeography, Palaeoclimatology, Palaeoecology*, 253, 8–31. https://doi.org/10.1016/ j.palaeo.2007.03.031.

Hayward, B. W., Le Coze, F., Vachard, D. & Gross, O., 2025: World Foraminifera Database. Accessed at https://www.marinespecies.org/foraminifera on 2025-09-23. https://doi.org/10.14284/305.

Holcová, K., 2008: Foraminiferal species diversity in the Central Paratethys – A reflection of global or local events? *Geologica Carpathica*, 59, 1, 71–85.

Ilyina, L. B., 1993: Opredelitel' morskih srednemiotsenovih gastropod Yugo-Zapadnoy Evrasii (Handbook for identification of the marine Middle Miocene gastropods of Southwestern Eurasia). *Trudy Paleontologicheskogo instituta*, 255, 1–151 (in Russian).

Kolesnikov, V. P., 1935: Sarmatskie molluski. Paleontologiia SSSR [The Sarmatian molluscs. Paleontology of the USSR]. *Leningrad, The Academy of Science USSR Press,* 507 pp. (in Russian).

Kováč, M., Hudáčková, N., Halásová, E., Kováčová, M., Holcová, K., Oszczypko-Clowes, M., Baldi, K., Less, G., Nagymarosy, A., Ruman, A., Klučiar, T. & Jamrich, M., 2017: The Central Paratethys palaeoceanography: a water circulation model based on microfossil proxies, climate, and changes of depositional environment. *Acta Geologica Slovaca*, 9, 2, 75–114.

Krasheninnikov, V. A., 1959: Foraminifery [Foraminifera]. In: Zhizhchenko, B. P. (ed.): Atlas Srednemiotsenovoi Fauny Severnogo Kavkaza I Kryma [Atlas of the Middle Miocene Fauna from North Caucasus and Crimea]. *Moscow, Gostoptekhizdat*, 15–103 (in Russian).

Laskarev, V., 1924: Sur les équivalents du Sarmatien supérieur en Serbie. *Recueil de traveaux offert à M. Jovan Cvijic par ses amis et collaborateurs*, 73–85.

Lazarev, S., Mandic, O., Stoica, M., Goĺdin, P., Ćorić, S., Harzhauser, M., Krijgsman, W., Kadirbek, D. & Vasilyan, D., 2025: Hydrological isolation of the Paratethys in the late Middle-Late Miocene: Integrated stratigraphy, palaeoenvironments and biotic record of the Caspian Basin, Karagiye, Kazakhstan. *Marine and Petroleum Geology*, 173, 107288. https://doi.org/10.1016/j.marpetgeo.2025.107288.

Liverovskaya, E. V., 1935: Fauna konkskogo gorizonta gory Dubrovoy (Severnyy Kavkaz) [Fauna of the Konkian horizon of mountain Dubrovaya (North Caucasus)]. *Proceedings of Petroleum Geological Prospecting Institute*, A/34, 35 p. (in Russian).

Liverovskaya, E. V., 1960: Tretichnyye otlozheniya Mangyshlaka [Tertiary sediments of Mangyshlak]. *Moscow, Gostoptehizdat*, 142 p. (in Russian).

Łuczkowska, E., 1972: Miliolidae (Foraminiferida) from Miocene of Poland Part I. Revision of the classification. *Acta Palaeontologica Polonica*, 17, 342–377.

Łuczkowska, E., 1974: Miliolidae (Foraminiferida) from the Miocene of Poland Part II. Biostratigraphy, palaeoecology, and systematics. *Acta Palaeontologica Polonica*, 19, 3–176.

Maissuradze, L. S., 1971: Sarmatskiye foraminifery Zapadnoi Gruzii [Sarmatian Foraminifera of Western Georgia]. *Tbilisi, Metsniereba*, 120 p. (in Russian).

Maissuradze, L. & Koiava, K., 2011: Biodiversity of Sarmatian Foraminifera of the Eastern Paratethys. *Bulletin of the Georgian National Academy of Sciences*, 5, 1, 143–151.

Maissuradze, L., Koiava, K., Kvaliashvili, L. & Spezzaferri, S., 2014: Biodiversity, evolution and biostratigrafic significance of Konkian foraminifers of Euxine-Caspian basin of Eastern Paratethys. *Proceedings of the Georgian National Museum, Natural Sciences and Prehistory Section*, 6, 9–22.

Martini, E., 1971: Standard Tertiary and Quaternary Calcareous Nannoplankton Zonation. In: Farinacci, A. (ed.): Proceedings of the II Planktonic Conference, *Roma, 1970. Edizioni Tecnoscienza*, 739–785.

Van Morkhoven, F. P. C. M., 1963: Post-Paleozoic Ostracoda, their Morphology, Taxonomy and Economic use. Vol. 2. Generic description. *Amsterdam – London – New York, Elsevier*, 478 p.

Muratov, M. V. & Nevesskaya, L. A. (eds.), 1986: Stratigrafiya SSSR. Neogenovaya sistema. Polutom 1 [Stratigraphy of the USSR. Neogene System Semivol. 1]. *Moscow, Nedra*, 420 pp. (in Russian).

Nevesskaya, L. A., Bogdanovich, A. K., Vyalov, O. S., Zhizhchenko, B. P., Iľina, L. B. & Nossovskiy, M. F., 1975: Yarusnaya shkala neogenovyih otlozheniy yuga SSSR [A stage stratigraphic scale of Neogene deposits for the South USSR]. In: Seneš, J. (ed.): Proceedings of the VIth Congress of the Regional Committee on Mediterranean Neogene Stratigraphy (RCMNS), *Bratislava*, 267–289.

Nevesskaya, L. A., Goncharova, I. A., Iľina, L. B., Paramonova, N. P., Popov, S. V., Bogdanovich, A. K., Gabuniya, L. K. & Nosovskiy, M. F., 1984: Regionalnaya stratigraficheskaya shkala neogena Vostochnogo Paratetisa [Regional stratigraphic scale of the Neogene of Eastern Paratethys]. *Soviet Geology*, 9, 37–49 (in Russian).

Nevesskaya, L. A., Goncharova, I. A., Iľina, L. B., Paramonova, N. P., Popov, S. V., Babak, E. V., Bagdasarian, K. G. & Voronina, A. A., 1986: Istoriya neogenovykh molluskov Paratetisa [The history of the Neogene mollusks of the Paratethys]. *Moscow, Nauka*, 208 pp. (in Russian).

Nevesskaya, L. A., Goncharova, I. A., Paramonova, N. P., Popov, S. V., Babak, E. V., Bagdasaryan, K. G. & Voronina, A. A., 1993: Opredeliteľ miotsenovih dvustvorchatih molluskov Yugo-Zapadnoy Evrazii [Handbook for identification of the bivalvia of Southwestern Eurasia]. *Trudy Paleontologicheskogo instituta*, 247, 1–412 (in Russian).

Osipov, S. S., 1927: O konkskom gorizonte Severnogo Kavkaza i Kerchenskogo poluostrova [About the Konkian horizon of the North Caucasus and the Kerch Peninsula]. *Bulletin of the Moscow Society of Naturalists, Department of Geology*, 5/3–4. New series, 35, 371–376 (in Russian).

Palcu, D. V., Golovina, L. A., Vernyhorova, Y. V., Popov, S. V. & Krijgsman, W., 2017: Middle Miocene paleoenvironmental crises in Central Eurasia caused by changes in marine gateway configuration. *Global and Planetary Change*, 158, 57–71. https://doi.org/10.1016/j.gloplacha.2017.09.013.

Paramonova, N. P. & Belokrys, L. S., 1972: Ob obyeme sarmatskogo yarusa [About the volume of the Sarmatian stage]. *Bulletin of the Moscow Society of Nature Testers*, 47, 3, 36–47 (in Russian).

Pipík, R. & Bodergat, A. M., 2004: *Euxinocythere* (Ostracoda, Cytheridae, Leptocytherinae) du Miocène supérieur du Bassin de Turiec (Slovaquie): taxonomie et paléoécologie. *Revue de Micropaléontologie*, 47, 36–52.

Popov, S. V., Rogl, F., Rozanov, A. Y., Steininger, F. F., Shcherba, I. G. & Kováč, M., 2004: Lithological-Paleogeographic maps of Paratethys. 10 Maps Late Eocene to Pliocene. *Courier Forschungsinstitut Senckenberg*, 250, 1–46.

Popov, S. V., Rostovtseva, Yu. V., Fillippova, N. Yu., Golovina, L. A., Radionova, E. P., Goncharova, I. A., Vernyhorova, Yu. V., Dykan, N. I., Pinchuk, T. N., Iljina, L. B., Koromyslova, A. V., Kozyrenko, T. M., Nikolaeva, I. A. & Viskova, L. A., 2016: Paleontology and stratigraphy of the Middle – Upper Miocene of Taman Peninsula. Part 1. Description of key-sections and benthic fossil groups. *Paleontological Journal*, 50, 1039–1206. https://doi.org/10.1134/S0031030116100014.

Prisyazhnyuk, V. A., Kovalenko, V. A. & Lyuleva, S. A., 2007: O konkskykh otlozhenyyakh yuga Ukrainy [About the Konkian sediments of the Southern Ukraine]. Paleontological research in Ukraine: history, current state and perspectives, *Kyiv*, 298–305 (in Russian).

Radionova, E. P., Golovina, L. A., Filippova, N. Y., Trubikhin, V. M., Popov, S. V., Goncharova, I. A., Vernigorova, Y. V. & Pinchuk, T. N., 2012: Middle-Upper Miocene stratigraphy of the Taman Peninsula, Eastern Paratethys. *Central European Journal of Geosciences*, 4, 1, 188–204.

Raffi, I., Wade, B. S., Palike, H., Beu, A. G., Cooper, R., Crundwell, M. P., Krijgsman, W., Moore, T., Raine, I., Sardella, R. & Vernyhorova, Y. V., 2020: The Neogene period. In: The Geologic Time Scale. *Elsevier*, 1141–1215. https://doi.org/10.1016/B978-0-12-824360-2.00029-2.

Rögl, F., 1998: Palaeogeographic considerations for Mediterranean and Paratethys seaways (Oligocene to Miocene). *Annalen des Naturhistorischen Museums in Wien, Serie A*, 99, 279–310.

Schornikov, E. I., 2011: Loxocaudinae: A new subfamily in the ostracod family Loxoconchidae. *Russian Journal of Marine Biology*, 37, 185–192.

Seko, M., 2019: Paleobiogeography of Middle Miocene marine ostracods (Ostracoda) of the Paratethys. Unpublished thesis. *Bratislava, Comenius University*, 213 pp.

Shnyukov, Y. F., Sheremetyev, V. M., Maslakov, N. A., Kutny, V. A., Gusakov, I. N. & Trofimov, V. V., 2006: Griazevye Vulkany Kerchensko-Tamanskogo Regiona [Mud Volcanoes of the Kerch-Taman Region]. *Krasnodar, GlavMedia*, 176 pp. (in Russian).

Smart, C. W. & Thomas, E., 2007: Emendation of the genus Streptochilus (Foraminifera) and new species from the lower Miocene of the Atlantic and Indian Oceans. *Micropaleontology*, 53, 73–103. https://doi.org/10.2113/gsmicropal.53.1-2.73.

Sokolow, N., 1899: Sloi s Venus konkensis na reke Konke [Venus konkensis beds at the Konka River]. *Memores du comite geologique*, 9, 5, 1–96 (in Russian).

Spezzaferri, S., Kucera, M., Pearson, P. N., Wade, B. S., Rappo, S., Poole, C. R., Morard, R. & Stalder, C., 2015: Fossil and Genetic Evidence for the Polyphyletic Nature of the Planktonic Foraminifera *"Globigerinoides"*, and Description of the New Genus *Trilobatus*. PLoS ONE10, 5, e0128108. https://doi:10.1371/journal.pone.0128108.

Suess, E., 1866: Untersuchungen über den Charakter der osterreichischen Tertiärablagerungen. 2. Uber die Bedeutung der sogenannten "brakischen Stufe" oder der "Cerithienschichten". *Sitzungsberichte der Mathematisch-Naturwissenschaftlichen Classe der Kaiserlichen Akademie der Wissenschaften*, 1, 54, 7, 218–260.

Ter Borgh, M., Stoica, M., Donselaar, M. E., Matenco, L. & Krijgsman, W., 2014: Miocene connectivity between the Central and Eastern Paratethys: Constraints from the western Dacian Basin. *Palaeogeography, Palaeoclimatology, Palaeoecology*, 412, 45–67. https://doi.org/10.1016/j.palaeo.2014.07.016.

Tunoğlu, C., 2002: Pontian Leptocytheridae and Cytherideidae (Ostracoda) species from the Eastern Black Sea region of Turkey. *Geologica Carpathica*, 53, 333–346.

Vernigorova, J. V., Fikolina, L. A. & Obsharskaya, N. N., 2012: Strukturno-fatsialnoye raionirovaniye neogenovykh otlozheniy Kerchenskogo poluostrova [Structural and facies zonation of the Neogene sediments of the Kerch Peninsula]. *Geological Journal*, 3, 74–94 (in Russian).

Vernyhorova, Yu. V., 2014: Lito- i biofatsialni osoblyvosti neogenovykh vidkladiv Kerchenskoho pivostrova [Litho- and biofacial features of the Neogene deposits of the Kerch Peninsula]. In: Proceedings of the Institute of Geological Sciences of the NAS of Ukraine. *Kyiv*, 7, 112–157 (in Ukrainian).

Vernyhorova, Yu. V., 2015: Kriterii stratigraficheskogo raschleneniya konkskikh otlozheniy Vostochnogo Paratetisa po mollyuskam i foraminiferam [The criteria of the Konkian deposits stratigraphy of the Eastern Paratethys based on mollusks and foraminifera – in Russian]. *Geological Journal*, 4, 77–86. https://doi.org/10.30836/igs.1025-6814.2015.4.139037. (in Russian).

Vernyhorova, Yu., 2018: Biostratigraphy of the Konkian (Middle Miocene of the Eastern Paratethys) deposits of Southern Ukraine based on foraminifera. *Geologia Croatica*, 71, 3, 135–146. https://doi.org/10.4154/gc.2018.18.

Wade, B. S., Olsson, R. K., Pearson, P. N., Huber, B. T. & Berggren, W. A., 2018: Atlas of Oligocene planktonic foraminifera. Cushman Foundation for Foraminiferal Research, Special Publication 46. *London, Cushman Foundation for Foraminiferal Research.*

Yoo, H., Huyen, P. T. M., Chae, J. & Karanovic, I., 2023: Three Loxocaudinae species (Ostracoda, Podocopida) from South Korea. *ZooKeys*, 1138, 183–209.

Young, J. R., 1998: Neogene, In: Bown P. R. (ed.): Calcareous nannofossil biostratigraphy. British Micropalaeontological Society, Publications Series. *London, Chapman and Hall*, 225–265.

Young, J. R., Bown, P. R. & Lees, J. A., 2017: Nannotax3 website. *International Nannoplankton Association*. http://www.mikrotax.org/ Nannotax3. Accessed 21 Apr 2017.

Benthic Foraminifera from the well #20

Benthic foraminifera species / samples	37	36	35	34	33	32	31	30	29	28a	28	27	26	25	24	23	22	21	20	19	18	17	16	15	14	13	12	11a	11	10	9a	9	8	7	6	5	4	3	2	1
Bolivina dilatata Reuss	32	18	59	64	23		1		20	1	18	8	5	35	5	6	1		5	1	7	9	27					1												
Bolivina scalprata Schwager	2		1	3																								1												
Bolivina sarmatica Didkowsky	10	8	14	11	8				1		1	2									1	1	2																	
Bolivina sp. 1	1	1	1				1					2																												
Bulimina ex gr. *elongata* d'Orbigny	67	35	60	88	29	7	6	2	22	5	32	12	1	62	4	11			3	3	6	11	40																	
Bulimina sp.1	1																																							
Angulogerina angulosa (Williamson)	12	12	48	39	8				5		5	3		1	1	2		1				3	7																	
Angulogerina sp. 1	4																																							
Cassidulina sp. 1	7	3	1	2					1										1																					
Globocassidulina subglobosa (Brady)	5	7	1	1	9				11	1	22		1	7	3	3			1				2																	
Guttulina communis (d'Orbigny)	2		2	3		2													1																					
Fursenkoina schreibersiana Cžjžek	4	2	7	13	1																																			
Stilostomella pyrula (d'Orbigny)	1		3	1																																				
Entosolenia sp.1	2	1	2								1	1	1	1					1																					
Quinqueloculina angustissima Bogdanowicz	2		1				15																																	
Quinqueloculina sp. dif. (poorly preserved)	1		9	3		5										2		3					1		1				11	1	1		1	1						
Varidentella sartaganica (Krasheninnikov in Maisuradze, 1971)	5		3	8		8	7	7	1								3		1										1	21	17	48								
Varidentella ex gr. *latelacunata* (Venglinsky)	30	18	36	21	1																					1														
Sinuloculina consobrina (d'Orbigny)	1					7															1									56	36	1	3							
Sinuloculina ex gr. *consobrina* (d'Orbigny)	1			8	2	1		1																																
Triloculina ebersini Didkowsky	1					7		1																																
Spiroloculina konkensis Bogdanowicz	1				1																																			
Sigmoilina sp.1	1																																							
Glabratella kartvelicus (Krasheninnikov)	4	4	5	5	4		1											1																						
Discorbis supinus Krasheninnikov	1	1	1	1	1				1																															
Epistominella sp.1	1	1																																						
Haynesina depressula (Walker & Jacob)	4				6	3	5				3			4		3		7		2	7		2					4												
Elphidium advenum Cushman	3		9	13																					6	1		5	6											
Elphidium ex gr. *joukovi* Serova	3																													1										
Elphidium kudakoence Bogdanowicz	4	2	3	9		2	5	8	6	4	4							2																						
Elphidium sp.1	5	1		2								2		2		3	1	2	30	1		1	7																	
Elphidium sp.2	6		15	9															42	6	3	11																		
Bulimina subulata Cushman & Parker		4	17	9																																				
Buliminella sp.1		1																																						
Miliolinella bonatiana luczlowska		1					2																																	
Discorbis squamulus (Reuss)		1																																						
Ammonia ex gr. *beccarii* (Linnaeus)		1			2				2	1	2	1	1	2	1			4	2	8	10	24	32						2	4	1						1			
Nonion sp.1		1	4	5	1	5	11	4			1																													

Benthic Foraminifera from the well #20 – continue

Benthic foraminifera species / samples	37	36	35	34	33	32	31	30	29	28a	28	27	26	25	24	23	22	21	20	19	18	17	16	15	14	13	12	11a	11	10	9a	9	8	7	6	5	4	3	2	1
Uvigerina sp. 1			2																																					
Uvigerina sp. 2			1																																					
Praeglobobulimina pupoides (d'Orbigny)			1																																					
Lotostomoides ex gr. *calomorpha* (Reuss)			1	2																																				
Sigmoidella caucasica Krasheninnikov			1	3	1																																			
Globulina gibba (d'Orbigny in Deshayes)			2	1	1																																			
Siphonodosaria sp.1			1																																					
Miliolinella selene (Karrer)			3	5	3						4												1						2											
Lenticulina inornata (d'Orbigny)			1	1	1																																			
Melonis pompilioides (Fitchtel & Moll)			1	2		1																																		
Bolivina plicatella Cushman				2																																				
Buliminella elegantissima (d'Orbigny)				1	1						1	1																												
Polymorphina sp.1				4																																				
Articulina sp. 1 (uniserial part)				2															1																					
Quinqueloculina sp. 1				1																																				
Quinqueloculina konkensis Bogdanowicz				1																																				
Quinqueloculina buchiana d'Orbigny				2		4		1			4																													
Cycloforina ex gr *gracilis* (Karrer)				2			1							2															6	5										
Nonoin commune (d'Orbigny)				3		1																																		
Elphidium ex gr. *macellum* (Fichtel & Moll)				9	2																																			
Quinqueloculina ex gr. *akneriana* d'Orbigny						7			1									4																						
Nodobaculariella ex gr. *konkemsis* Bogdanowicz						2																																		
Affinetrina ucrainica (Serova in Bogdanovich)						10	4						2	1																										
Porosononion granosum (D'Orbigny)						6	4	1											2	2					2		2			4	11	2	46	9	2	2	18	11	23	2
Nonion bogdanowiczi Voloshinova						3	16	23				1	1																											
Elphidium macellum (Fichtel & Moll)						111	47	19	1												1																10	1	2	
Elphidium sp.3						15																																		
Quinqueloculina fasseta Didkowski							1																																	
Quinqueloculina minakovae ukrainica Didkowski							9	1																																
Varidentella reussi sartaganica (Krasheninnikov)							1											1	1	1																				
Sigmoilina? sp.							4	5																																
Elphidium incertum (Williamson)							3													3	1	2																		
Haplophragmoides sp. 1								1					1				2	1							3				1											
Quinqueloculina minakovae minakovae Bogdanowicz								1																																
Ammonia tepida (Cushman)									2			1							2		1									1										
Cornuspira sp.1											1																													
Glabratella sp. 1											2												2																	
Nonion? exponense (Brady, Parker & Jones)											2																													
Haplophragmoides sp. 2																	1								2		2													

Benthic Foraminifera from the well #20 – continue

Benthic foraminifera species / samples	37	36	35	34	33	32	31	30	29	28a	28	27	26	25	24	23	22	21	20	19	18	17	16	15	14	13	12	11a	11	10	9a	9	8	7	6	5	4	3	2	1
Haynesina sp. 1																							6																	
Elphidium ex gr. *articulatum* (d'Orbigny)																							10																	
Elphidium horridum Bogdanowicz																									961	7		118	7	2										
Elohidium ex gr. *horridum* Bogdanowich																									28															
Elphidium aculeatum (d'Orbigny)																									4	7														
Ephidium crispum (Linne)																									1															
Quinqueloculina? sp. (abnormal form)																													1	2										
Varidentella ex gr. *reussi* (Bogdanowicz)																													1											
Elphidium hauerinum (d'Orbigny)																													1											
Varidentella reussi (Bogdanowicz)																														123	63	37	11				3			
Articularia articulinoides (Gerke & Issaeva)																														1	5	7	1							
Articularia articulinoides (Gerke & Issaeva) (uniserial part)																														9	10	28	2							
Sigmoilina? sp.																														6	4	7								
Flintina? sp.																														1										
Cibicides ex gr. *refulgens* (Fitchtel & Moll)																														1										
Elphidium subcarinatum (Egger)																														9	19	1	8				1	2		
Entosolenia sp. diff.																															1	2	13	8		3	13	12	56	
Spiroloculina sp. 1																															3									
Articulina sarmatica (Karrer) (uniserial part)																																7			1					
Elphidium reginum (d'Orbigny)																																							1	

Nannoplankton taxa from the well #20

Taxa/sample	*Braarudosphaera bigelowi*	*Braarudosphaera bigelowii parvula*	*Calcidiscus leptoporus*	*Calcidiscus pataecus*	*Calcidiscus* sp.	*Calcidiscus tropicus*	*Calciosolenia fossilis*	*Coccolithus pelagicus*	*Coronocyclus nitescens*	*Cyclicargolithus floridanus*	*Discoaster* sp.	*Helicosphaera carteri*	*Helicosphaera perch-nielseniae*	*Helicosphaera* sp.	*Helicosphaera wallichii*	*Holodiscolithus macroporus*	*Lithostromation obscurum*	*Lithostromation* sp.	*Micrantholithus* sp.	*Micrantholithus vesper*	*Orthorhabdus rugosus*	*Orthorhabdus serratus*	*Pontosphaera japonica*	*Pontosphaera multipora*	*Pontosphaera* sp.	*Reticulofenestra gelida*	*Reticulofenestra haqii*	*Reticulofenestra minuta*	*Reticulofenestra pseudoumbilicus*	*Reticulofenestra pseudoumbilicus* >7	*Reticulofenestra* sp.	*Rhabdosphaera poculii*	*Rhabdosphaera sicca*	*Rhabdosphaera* sp.	*Scyphosphaera*	*Sphenolithus moriformis*	*Sphenolithus* sp.	*Syracosphaera pulchra*	*Syracosphaera* sp.	*Triquetrorhabdulus milowii*	*Triquetrorhabdulus* sp.	*Umbilicosphaera jafari*	*Umbilicosphaera rotula*
1	0	0	0	0	0	0	0	0	0	0	1	0	0	0	0	0	0	0	0	0	0	0	0	0	0	0	1	0	0	0	0	0	0	0	0	0	0	0	0	0	0	0	0
2	1	3	0	0	0	0	0	2	0	0	0	0	0	0	0	4	0	0	0	0	0	0	2	5	0	0	3	0	0	0	0	0	0	0	0	0	0	0	0	0	0	0	0
3	0	0	0	0	0	0	0	5	0	0	0	0	0	0	0	39	0	0	0	0	0	0	0	5	0	0	0	3	0	0	0	0	0	0	0	0	0	0	0	1	0	4	0
4	3	1	2	0	0	0	0	2	0	1	0	0	0	0	0	7	0	0	1	0	0	0	0	1	2	0	0	0	0	0	0	0	0	0	0	0	1	0	0	0	0	1	0
5	1	0	0	0	0	0	0	7	0	1	0	0	0	0	0	1	0	0	0	0	0	0	0	1	0	0	2	0	0	0	0	0	0	0	0	0	0	0	0	0	0	0	0
6	0	0	0	0	0	0	0	2	0	0	0	0	0	0	0	0	0	0	0	0	0	0	0	0	0	0	0	1	0	0	0	0	0	0	0	0	0	0	0	0	0	3	0
7	0	2	0	0	2	0	0	3	0	0	0	0	0	1	0	0	2	0	0	0	0	0	0	1	0	0	0	0	0	0	1	0	0	0	0	0	0	0	0	0	1	0	1
8	49	26	0	2	0	0	1	4	0	1	0	0	0	0	0	26	0	0	0	0	0	0	1	0	1	1	1	7	0	0	0	0	0	0	0	0	0	0	0	0	0	1	0
9	3	5	0	0	0	0	0	2	0	1	0	0	0	0	0	20	0	0	0	0	0	0	0	0	0	1	0	0	0	0	0	0	0	0	0	0	0	0	0	0	0	0	0
9.5	6	3	0	1	0	0	0	1	0	0	0	0	0	0	0	13	0	0	0	0	0	0	4	0	0	2	1	1	1	0	0	0	0	0	0	0	0	0	0	1	0	0	0
10	10	10	0	0	0	0	0	1	0	1	0	0	0	0	0	36	0	0	0	0	0	0	2	1	0	0	1	2	0	0	0	0	0	1	0	2	0	0	0	0	1	1	0
11	1	0	0	0	0	0	0	3	0	3	0	0	0	0	0	0	0	0	0	0	0	0	0	0	0	0	2	0	36	20	0	0	0	0	0	0	1	0	0	0	0	0	0
11.5	0	0	0	0	0	0	0	5	0	7	0	0	0	0	0	0	0	2	0	0	1	0	0	0	0	0	6	0	129	0	0	0	0	0	0	3	0	0	1	1	0	0	0
12	7	0	0	1	0	0	0	4	0	7	0	0	0	0	1	0	0	0	0	0	0	0	0	0	0	0	133	10	56	0	0	0	3	0	0	0	0	3	0	0	0	0	0
13	0	0	0	0	0	0	0	4	0	1	0	0	0	0	0	0	0	0	0	0	0	0	0	0	0	0	31	0	41	0	0	0	0	0	0	0	0	0	0	0	0	0	0
14	0	0	0	0	0	0	0	0	0	1	0	0	0	0	0	0	0	0	0	0	0	1	0	0	0	1	19	2	49	24	0	0	0	0	0	0	0	0	0	0	0	0	0
15	0	0	0	0	0	0	0	0	0	1	1	1	0	0	0	0	0	0	0	0	0	0	0	0	0	0	2	0	22	11	0	0	0	0	1	2	0	0	0	0	0	1	0
16	1	0	0	0	1	0	0	3	0	6	0	0	0	0	0	0	0	0	0	0	0	0	0	0	0	0	195	2	105	0	0	0	0	0	0	0	0	1	0	0	0	0	0
17	1	0	0	0	0	0	0	3	0	51	0	1	1	0	0	1	0	0	0	0	0	0	0	0	0	0	348	3	168	0	0	0	3	0	0	1	0	1	0	0	0	0	0
18	3	0	0	0	0	0	0	3	1	4	0	0	0	0	0	2	0	0	0	0	0	0	0	0	0	1	75	7	100	47	0	0	2	0	0	0	0	1	0	0	1	1	0
19	2	0	0	0	0	0	0	2	0	1	1	0	0	0	0	0	0	0	0	0	0	0	0	0	0	0	120	2	86	46	0	0	0	0	0	0	0	0	0	0	0	0	0
20	4	0	0	0	0	0	0	5	0	4	1	0	0	0	0	0	0	0	0	0	0	0	0	0	0	0	52	2	28	0	0	0	1	0	0	1	0	1	0	1	0	0	0
21	5	0	0	0	0	0	0	1	0	3	0	0	0	0	0	1	0	0	0	0	0	0	0	0	0	1	96	5	84	0	0	0	3	0	0	0	1	0	0	0	0	0	0
22	3	1	0	0	0	0	0	4	0	8	0	0	0	0	0	1	0	0	0	0	0	0	0	0	0	0	82	4	58	0	0	0	2	0	0	2	0	2	0	0	1	0	0
23	12	1	0	1	0	0	0	6	0	6	1	0	0	0	1	4	0	0	0	0	0	0	0	0	0	0	108	6	104	0	0	0	12	0	0	0	0	2	0	0	0	0	0
24	11	2	0	0	0	0	0	6	0	13	0	4	0	0	0	0	0	0	0	0	0	0	0	0	0	2	87	7	114	57	0	0	3	0	0	0	0	2	0	0	0	0	0
25	6	2	0	0	0	1	0	4	0	11	0	2	0	0	0	1	0	0	0	0	0	0	0	0	0	3	171	6	126	63	0	0	10	0	0	0	0	4	0	0	0	0	1
26	5	0	0	0	0	0	0	3	0	7	1	0	0	1	0	0	0	0	0	0	0	0	0	0	0	0	90	10	87	0	0	0	6	0	0	1	0	9	0	0	0	0	0
27	15	1	0	3	0	0	0	4	0	3	1	0	0	0	0	0	0	0	0	0	1	0	0	0	0	0	156	3	120	0	0	0	13	0	0	2	1	3	0	0	0	1	0
28	6	0	0	2	0	0	0	6	0	5	0	0	0	0	1	1	0	0	0	0	0	0	0	0	0	0	84	1	81	0	0	0	4	0	0	0	0	5	0	0	0	0	0
28.5	5	0	0	0	0	0	0	5	0	1	0	0	0	0	0	0	0	0	0	0	0	0	0	0	0	0	60	1	72	36	0	0	3	0	0	0	1	4	0	0	0	0	0
29	5	1	2	0	0	0	0	5	0	2	0	0	0	0	0	0	0	0	0	0	1	0	0	0	0	0	117	5	189	0	0	0	7	0	0	0	0	1	0	0	0	0	0
30	0	0	0	0	0	0	0	4	0	0	0	1	0	0	0	0	0	0	0	0	0	0	0	0	0	0	1	0	0	0	0	0	0	0	0	0	0	0	0	0	0	0	0
31	8	0	0	0	0	0	0	2	0	0	0	1	0	0	0	1	0	0	0	0	0	0	0	0	0	0	5	0	6	0	0	0	0	0	0	1	1	0	0	0	0	0	0
32	0	0	0	0	0	0	0	36	0	0	0	2	0	0	0	0	0	0	0	0	0	0	0	0	0	0	0	0	0	0	0	0	0	0	0	2	1	0	0	0	1	0	0
33	0	1	0	0	0	0	0	29	0	1	0	0	0	0	0	0	0	0	0	1	0	0	0	0	0	0	0	0	0	0	0	0	0	0	0	0	0	0	0	0	0	0	0
34	0	1	0	0	1	0	0	46	1	0	0	0	0	0	2	0	0	0	0	0	0	0	0	0	0	0	5	0	1	0	0	0	2	0	0	1	0	2	0	0	0	0	0
35	3	5	0	0	0	0	0	1020	0	5	2	5	0	0	1	3	0	0	0	0	0	0	0	0	0	0	30	8	17	0	0	0	9	0	0	6	0	8	0	0	3	0	0
36	6	3	0	1	0	0	0	228	0	5	0	3	0	0	1	0	0	0	0	0	0	0	0	0	0	0	14	4	6	0	0	1	0	0	0	1	2	2	0	0	0	0	2
37	4	2	1	0	0	0	0	366	0	3	0	5	0	0	0	0	0	0	0	0	0	0	0	0	0	0	16	2	4	0	0	5	4	0	0	1	0	1	0	0	0	0	0

Ostracoda taxa from the well #20

	sample 1	sample 5	sample 9	sample 9a	sample 10	sample 11	sample 11a	sample 15	sample 17	sample 22	sample 28	sample 30	sample 31	sample 32	sample 34	sample 35	sample 36
Aurila sp.	1	0	1	0	0	1	0	1	0	0	0	1	1	0	0	0	0
Callistocythere sp. 3	0	1	0	1	0	0	0	0	0	0	0	0	0	0	0	0	0
Cytheridea sp. aff. *Cytheridea acuminata* Bosquet, 1852	0	0	0	0	0	0	0	0	0	1	1	0	1	0	0	0	0
Cytherura sp.	0	0	0	0	0	0	0	0	0	0	0	0	0	0	1	1	0
Euxinocythere sp. form A	0	0	0	0	0	0	0	0	0	0	0	1	1	0	1	0	1
Euxinocythere sp. form B	0	0	1	0	0	0	0	0	0	0	0	0	1	1	1	1	0
Euxinocythere sp. 2	0	0	0	0	0	0	0	1	1	0	1	0	0	0	0	0	0
Hiltermanicythere sp.	0	0	0	0	0	0	0	0	0	0	0	1	1	1	0	0	0
Leptocythere sp. 1	0	0	0	0	0	0	0	0	0	0	0	0	0	1	1	0	0
Leptocythere sp. 2	0	0	1	1	1	1	0	0	0	0	0	0	1	0	0	0	0
Leptocythere sp. 3	0	0	0	0	0	0	1	0	0	0	0	0	0	0	0	0	0
Loxocauda sp.	0	0	0	0	0	0	0	0	0	0	0	1	0	0	0	0	0
Loxoconcha sp. 1	0	0	0	0	0	1	0	0	0	0	0	1	1	0	0	0	0
Loxoconcha sp. 2	0	0	0	0	0	0	0	0	0	0	0	0	0	1	0	0	0
Sclerochilus sp. 2	0	0	0	0	0	0	0	0	0	0	0	0	0	0	0	0	1
Xestoleberis sp. 3	0	0	0	0	0	0	0	0	0	0	0	1	1	1	0	0	0

Biostratigrafický rámec konsko-sarmatského rozhrania na základe mikrofosílií z vrtu č. 20 Kerčský polostrov (Krym)

Táto práca sa zaoberá biostratigrafickým určením hranice stupňov konka a sarmat s. l. vo východnej Paratetýde na základe analýzy mikrofosílií z vrtu č. 20 (45° 15' 40,9" N, 35° 53' 49,2" E) na západnej časti Kerčského polostrova (Krym) (obr. 1, 2). Prechod medzi stupňom konka a sarmatským stupňom predstavuje obdobie významných paleoekologických zmien, sprevádzané výraznou prestavbou morských spoločenstiev (Harzhauser & Piller, 2004, 2007; Holcová, 2008; Ter Borgh et al., 2014). Cieľom štúdie bolo spresniť biostratigrafické členenie tejto hranice prostredníctvom integrovanej analýzy bentických dierkavcov, vápnitého nanoplanktónu, lastúrničiek, mäkkýšov a vzácnych planktonických dierkavcov (obr. 3 – 7).

Na základe výsledkov sme identifikovali tri po sebe nasledujúce spoločenstvá bentických dierkavcov, ktoré umožnili spoľahlivo rozlíšiť spodnú konku, vrchnú konku a spodný sarmat (obr. 2, 8). Spodná konka je charakterizovaná asociáciou s prevahou druhov *Spiroloculina konkensis, Quinqueloculina minakovae* a *Elphidium kudakoense* spolu s mäkkýšmi *Limacina konkensis* a *L. andrussovi*. Vrchná konka je typická dominanciou druhu *Elphidium horridum* a výskytom mäkkýšov *Obsoletiformes lithopodolicus ruthenicus* a *Musculus sarmaticus*. Spodný sarmat je definovaný prvým a početným výskytom druhov *Varidentella reussi, Articularia articulinoides, Articulina sarmatica* a *Elphidium reginum* (obr. 8). Analýza asociácie vápnitého nanoplanktónu potvrdila zaradenie sedimentov konky do biozóny NN6 na základe výskytu druhov *Orthorhabdus rugosus, Cyclicargolithus floridanus* a hojného *Reticulofenestra pseudoumbilicus* pri súčasnej absencii druhu *Sphenolithus heteromorphus*. Sedimenty spodného sarmatu sú charakterizované vysokým zastúpením druhov *Braarudosphaera bigelowii, B. bigelowii* ssp. *parvula* a *Holodiscolithus macroporus*. Planktonické dierkavce sa zistili len sporadicky a väčšina nájdených exemplárov predstavuje redeponované formy. Spoločenstvá lastúrničiek a bentických dierkavcov naznačujú sedimentáciu v plytkom prímorskom prostredí s premenlivou salinitou, pričom časť materiálu mohla byť transportovaná z veľmi plytkých pobrežných oblastí.

Výsledky mikropaleontologickej analýzy poukazujú na existenciu prechodného obdobia označovaného ako *Konkian-Sarmatian Conversion Time* (KSCT) (Vernyhorova, 2015, 2018), ktoré predstavuje postupnú reorganizáciu panvy počas neskorej konky a najstaršieho sarmatu. Pre toto obdobie je charakteristické prudké vymiznutie stenohalinných druhov (napr. Popov et al., 2016; Palcu et al., 2017) a súčasné objavenie sa euryhalinných foriem bentických dierkavcov a mäkkýšov (Sokolov, 1899; Liverovskaya, 1935, 1960; Bogdanovich, 1965; Nevesskaya et al., 1986; Krasheninnikov, 1959; Maisuradze, 1971; Bratishko et al., 2015), ktoré pretrvávajú aj v najstaršom sarmate. Naše výsledky potvrdzujú výsledky predchádzajúcich výskumov a identifikované zmeny asociácií dokumentujú postupnú adaptáciu spoločenstiev na meniace sa podmienky prostredia a kolísanie salinity.

Doručené / Received: 5. 6. 2026
Prijaté na publikovanie / Accepted: 15. 7. 2026

Mineralia Slovaca, Web ISSN 1338-3523, ISSN 0369-2086, https://doi.org/10.56623/ms.2026.58.1.5
58, 1 (2026), 87 – 96,

Biological iron removal and pigment recovery from acid mine drainage using native microbial consortia

ZUZANA BÁRTOVÁ[1,*], JAROSLAV BRIANČIN[1] and MARTIN FABIÁN[1]

[1] Institute of Geotechnics of the Slovak Academy of Sciences, Watsonova 45, 040 01 Košice, Slovak Republic;
* Corresponding author: bartova@saske.sk

Abstract: The biological removal and recovery of iron from actual mine water were carried out using mining influenced water (MIW) sourced from the Smolník mine site in Slovakia. The oxidation of ferrous iron was improved by utilizing native acidophilic microbial communities, resulting in more than 99 % iron removal within 30 hours under acidic conditions. A stepwise treatment process – incorporating aeration, microbial oxidation, and controlled pH adjustment – facilitated the formation of iron precipitates, including schwertmannite and ferrihydrite. Elemental and structural analyses showed that these biologically formed precipitates contained low levels of arsenic, complying with regulatory standards for pigment applications. Overall, the findings demonstrate a sustainable approach that not only removes contaminants but also enables the recovery of valuable materials.

Key words: acid mine drainage, pigments, Smolník, bacterial oxidation, mining influenced water, schwertmannite

Introduction

Iron occurs widely as a contaminant in both natural source waters and industrial wastewaters (Nordstrom, 2011). In particular, mining and metallurgical activities generate substantial volumes of effluents characterized by elevated iron concentrations (Johnson & Hallberg, 2005). The presence of iron in aquatic systems poses huge risks to ecosystems and technical infrastructure, thereby efficient and sustainable removal technologies are needed for such purposes (Kaksonen & Janneck, 2024; Stumm & Morgan, 1996).

At the same time, iron represents a valuable resource with diverse industrial applications, highlighting the importance of its recovery rather than mere disposal. Among other uses, the resulting products – often natural or synthetic iron oxides – can subsequently serve as mineral pigments in a wide range of applications, including paints, stains, ceramics, plastics, and building materials.

Microbial processes offer promising solutions for both iron removal and resource recovery. Among these, iron-oxidizing microorganisms promote the formation and precipitation of iron minerals such as jarosite, schwertmannite, ferrihydrite, and goethite (Bigham et al., 1990).

In nature, iron occurs mainly in two oxidation states, as ferrous (Fe^{2+}) and ferric (Fe^{3+}) ions. The prevailing form is dependent on pH, oxygen concentration, and redox conditions (Stumm & Morgan, 1996).

The oxidation of ferrous iron to ferric iron by dissolved oxygen is a complex and multi-step process. It involves the formation of transient, partially oxidized Fe^{2+}– Fe^{3+} intermediate phases, such as green rusts, which are metastable and challenging to characterize or predict. Over time, these intermediates undergo transformation into more thermodynamically stable iron oxide minerals, including hematite, magnetite, goethite, and lepidocrocite (Morgan & Lahav, 2007).

Mining influenced waters are commonly acidic due to the oxidation of sulfide minerals, such as pyrite, exposed during mining activities, which generates acidity and lowers the pH of the drainage waters (Johnson & Hallberg, 2005; Singer & Stumm, 1970; Wolkersdorfer, 2022).

In acidic environments, the abiotic oxidation of ferrous iron by dissolved oxygen is kinetically limited, as Fe^{2+} remains relatively stable at low pH (Morgan & Lahav, 2007). Consequently, spontaneous chemical oxidation proceeds slowly and is insufficient to account for the rapid iron cycling observed in acid mine drainage systems. Instead, this process is largely driven by the metabolic activity of acidophilic iron-oxidizing microorganisms, which catalyse the oxidation of ferrous to ferric iron at rates several orders of magnitude higher than abiotic reactions (Johnson et al., 2012).

The microbial oxidation of iron plays a central role in both natural and engineered systems, enabling efficient iron removal and influencing the formation of secondary iron minerals. Biohydrometallurgical studies have demonstrated that near-complete ferrous iron oxidation can be achieved at pH values as low as 1.5 without the need for chemical neutralization, highlighting the advantages of biological processes over conventional chemical treatments (Kaksonen et al., 2014). These processes promote the formation of iron precipitates such as schwertmannite, jarosite, and goethite, which are critical for the removal of iron and associated contaminants from mine waters.

This study focuses on iron removal regarding acid mine drainage from the historical mining site in Smolník, Slovakia. In the recent years, pH of the mining influenced water from the main drainage shaft Pech, ranges from 3.95 to 4.12 and produces a high volume of mine water (approximately 6.5–10 L/s). Concentration of metals analysed in the water ranges according to the weather conditions and rainfall volumes (Tabs. 1 and 2).

Tab. 1
Change in the composition of mine water over the years (the month number is in parentheses), mg/L, n.a.: not analysed, partly published in Bártová (2025)

Shaft Pech	SO_4^{2-}	Fe	Al	Mn	Zn	Mg	Ca
2011	2,082	272	57.9	22.6	8.4	n. a.	n.a.
2020	1,722	232	40.3	16.5	4.4	n. a.	n.a.
2024 (12)	n. a.	223	44.8	17.6	5.5	192	69.5
2025 (4)	1,766	229	44.1	17.1	5.4	210	153
2025 (10)	n. a.	192	34.0	11.9	4	153	115
2026 (1)	2,138	260	48.5	14.7	5.16	308	104
2026 (2)	2,871	238	40.7	12.9	50.3	275	111

Tab. 2
Change in the composition of mine water over the years (the month number is in parentheses), µg/L, n.a.: not analysed, partly published in Bártová (2025)

Shaft Pech	Cu	Li	Co	Pb	As	Cd	Sb	Cr	Ni
2011	1,710	312	861	20.8	22	16.4	–	2.9	n. a.
2020	498	253	308	36.4	73	3.8	11.2	0.4	n. a.
2024 (12)	1,140	250	390	10.5	34.6	0.43	< 0.1	< 0.1	140
2025 (4)	1,070	290	410	12.1	28.4	0.85	< 0.1	< 0.1	n. a.
2025 (10)	400	190	210	41	35.7	2.4	0.15	1	130
2026 (1)	2,580	310	460	41.7	63.9	6.2	0.1	0.8	150
2026 (2)	1,750	n. a.	360	47.1	39.4	5.8	< 0.1	0.6	90

This study uniquely integrates microbial iron oxidation with controlled pH-driven precipitation to simultaneously achieve iron removal, selective metal retention, and production of value-added pigment materials from real mine water. The primary objective was to optimize Fe^{2+} oxidation and to characterize iron precipitates generated from an actual mine water under controlled laboratory conditions. Mine water samples were either inoculated with pre-cultivated iron-oxidizing acidophiles (native strains) or left uninoculated, enabling comparison between products formed via biological and abiotic oxidation.

Methods

Bacterial strains and incubation conditions

Native microbial consortia were cultivated for experimental purposes in mine water from the outflow of the main discharge shaft (Pech), supplemented with 9K salts to promote growth: 1.6 mmol/L $MgSO_4 \cdot 7H_2O$, 0.76 mmol/L $(NH_4)_2SO_4$, 0.23 mmol/L K_2HPO_4, and 120 mmol/L $FeSO_4 \cdot 7H_2O$. The cultures were maintained in baffled, magnetically stirred and aerated vessels (working volume 0.5 L) at 25 °C and 240 rpm in a temperature-controlled incubator. Microbial culture was subcultured 5 times before the final inoculation used in the experiment.

Mine water parameters

Tab. 3
Parameters of the Smolník mine water (2026), n.a.: not analysed

pH	ORP	Conductivity	Temperature	Flow rate
–	mV	mS/cm	°C	L/s
3.95	286.4	2.53	11.7	n. a.

pH/ ORP analysis

A combined glass electrode (InLab Micro Mettler Toledo) was used for pH measurement. The oxidation-reduction potential (ORP) of the liquid phase during bacterial iron oxidation was measured with a combined Pt-Ag/AgCl redox electrode (InLab Redox Micro Mettler Toledo). In both cases, the Seven2Go S2 (Mettler Toledo) was used.

Iron speciation

Ferric iron was determined with a UV-spectrophotometric method at 300 nm (Basaran & Tuovinen, 1986). Ferrous iron concentrations were determined by a modified o-phenanthroline spectrophotometric method, insensitive to Fe^{3+} interference (Herrera et al., 1989).

Cell monitoring

Presence of microbial cells was confirmed by direct microscopic count using a Neubauer counting chamber with a depth of 0.01 mm.

Chemical analyses

Elemental analysis of the water was done using AAS (Varian AA240Z, AA240FS) and ICP-MS 7700 (Agilent). Sulfate concentration was analysed by ion chromatography (Dionex ICS 5000). Total iron was determined using AAS.

The microstructure and morphology

Iron powders were investigated by MIRA 3 FE-SEM scanning electron microscope (TESCAN GROUP, a. s.) with an EDX detector (Oxford Instruments).

XRPD patterns were obtained using a D8 Advance diffractometer (Bruker) operating with Cu Kα radiation in the Bragg-Brentano configuration.

Elemental composition was determined using a handheld X-ray fluorescence (XRF) analyzer (X-MET8000 Expert Geo, Hitachi High-Tech), equipped with a silicon drift detector (SDD) and an X-ray tube operating up to 50 kV.

Colour measurements

Colour measurements were performed using a Nix™ Spectro 2 Color Sensor with D50 2° settings. The sensor produces scan results in various colour systems (Stiglitz et al., 2016). For the purposes of this study, all data are expressed in the CIEL*a*b* colour space (Robertson, 1977).

Results and discussion

Water collected from the Smolník site was analysed and treated in order to remove dissolved iron and recover precipitates usable as mineral pigments in form of powders. Air-dried precipitates were then characterised using X-ray diffraction (XRD), X-ray fluorescence (XRF), scanning electron microscopy (SEM), energy-dispersive X-ray spectroscopy (EDX), and NIX™ colour determination instruments. Liquid samples and resulting mine water after Fe-precipitates removal were analysed using atomic absorption spectroscopy (AAS).

Initial composition of the mine water is given in the Tab. 1 and Tab. 2 in the last row [2026(2)]. During the experiment, concentrations of Fe, As, Al, Mg, Mn, Cu, Co and SO_4^{2-} were followed, as these elements either form a pigment structure (Fe, Al, S) or they are considered an unwanted impurity, often exhibiting toxic characteristics (As) or they are considered a valuable component of the water (Cu, Co, Mg, Mn) where leaving them in the water might lead to possibilities of their subsequent recovery from already iron-free solutions.

The formation of iron precipitates (pigments) in mine water was performed as a sequential process consisting of three main stages: (i) the initial aeration of MIW (30 hours) in order to lower pH and to oxidise and precipitate a small amount of Fe to remove a phase on which arsenic can be sorbed and which can be removed from the solution, (ii) the subsequent bacterial inoculation to accelerate ferrous iron oxidation, and (iii) pH adjustment in order to precipitate poorly crystalline iron phases such as ferrihydrite or schwertmannite. Subsequently, the gradual transformation of these metastable phases into more thermodynamically stable minerals, including goethite or hematite, can be achieved over time. Between individual stages, Fe-precipitates were filtered out from the solution using a PES filter with a pore size of 0.20 μm.

Iron oxidation

Enhanced ferrous iron oxidation is minor or negligible at pH below 4 (Jones et al., 2014; Morgan & Lahav, 2007). As the pH of Smolník MIW already oscillates around this value, and after several hours of aeration the value drops below 3.5, in order to accelerate iron oxidation, acidophilic microbial consortia need to be introduced into the process. Despite the genotypic differences, many acidophilic iron oxidisers share many common physiological traits (Kupka et al., 2023). For this reason, native microbial species were preferred over pure collection species, which can be costly and their purity needs to be confirmed over a longer period of time to ensure, that we are still working with the declared species. Native microbial consortia isolated directly from Smolník MIW were pre-cultivated and subsequently used for the process of iron oxidation.

2L of Smolník MIW was aerated for 30 hours and then filtrated to collect the first iron phase (A). The filtered water was transferred into a new flask (working volume 5 L), and 50 mL of an exponentially growing microbial culture (approximately 2.0×10^6 cells/mL) was added. Iron introduced with the growth medium was not taken into account.

Iron oxidation processes were monitored over an additional 30 hours, where already within first 21 hours the ferrous iron concentration dropped substantially. After 29 hours the Fe^{2+} concentration decreased below 2 mg/L (Fig. 1), corresponding to a removal efficiency exceeding 99 % (Fig. 2).

After iron oxidation was completed, the water was again filtered and iron precipitates were collected for the latter analyses (B).

After the filtration step, the water was divided into three flasks for the final step of the pH adjustment. The starting point for each of the adjustment was pH 2.6. From this point the pH was increased to values (i) 3.2 (optimal stability level to form schwertmannite), (ii) 4.1 (current

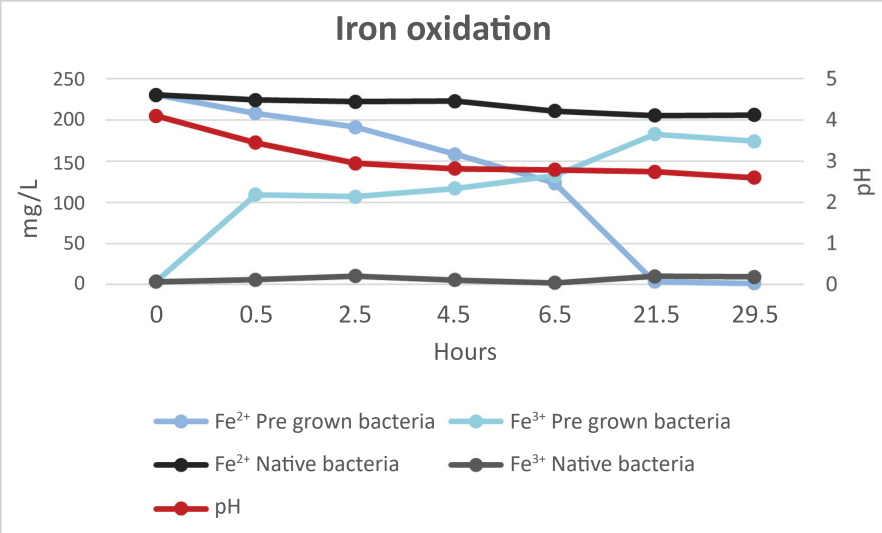

Fig. 1. Iron oxidation monitored via Fe^{2+} and Fe^{3+} concentration change over 30 h

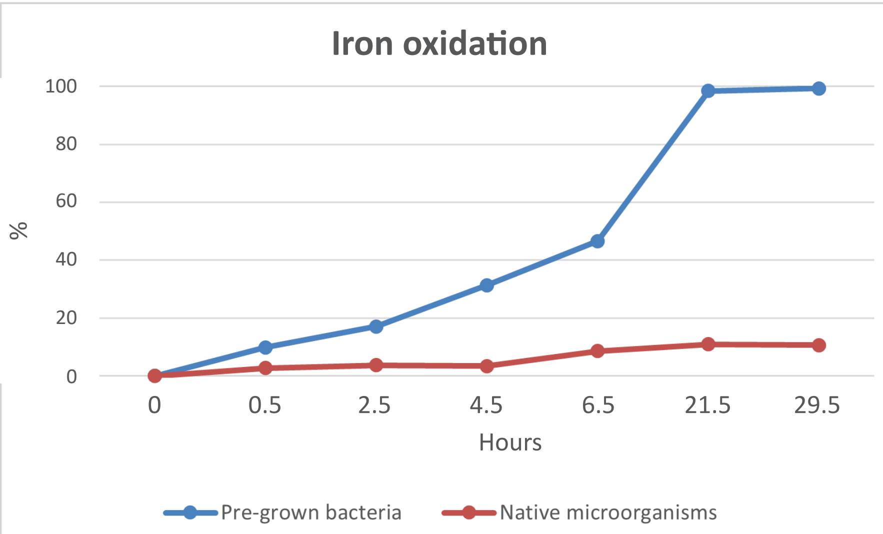

Fig. 2. Efficiency of Fe^{2+} removal/oxidation exceeding 99 %

Smolník MIW pH), (iii) 5.5 (high efficiency level for Al precipitation), and (iv) 6.2 (fast ferrihydrite formation + complete Al removal), using 20 % NaOH. After each adjustment step the precipitate was filtered out and the water either continued for another round of treatment or it was stabilised using concentrated HNO_3 and subsequently analysed using AAS (Tab. 4). It should be noted that, the pH of 5.5 was obtained by using the filtrate from water previously adjusted to pH 3.2, as a substantial iron concentration remained in this sample.

As table 4 shows, the majority of Fe was effectively removed during bacterial oxidation, without any further pH adjustments. Applying pH levels above 4.1, the Fe concentration complied with the Regulation No. 269/2010 Coll., for total iron in discharged wastewater, which is 2 mg/L. Aluminium was effectively removed from the solution at pH 5.5, as it was expected. Co, Cu, Mg, and Mn did not co-precipitate from the water at pH below 4.1

Tab. 4

Final elemental composition of mine water after the pH adjustment and precipitates removal

Name	Conditions	Fe [mg/L]	Al [mg/L]	Mn [mg/L]	Mg [mg/L]	Cu [µg/L]	As [µg/L]	Co [µg/L]
–	initial MIW	238.8	40.7	12.88	275.3	1750	39.4	359.9
A	30 hours aeration	196.5	40.9	13.12	277	1740	15.7	369.4
B	bacterial oxidation	15.68	42.2	13.22	273.1	1780	3.3	368.3
C	pH 3.2	8.39	38.8	13.18	246.3	1750	2.3	404.2
D	pH 4.1	0.21	32.7	13.03	236	1610	1.9	394.1
E	pH 5.5	0.05	0	11.7	216.3	210	1.8	400.2
F	pH 6.2	0.05	0	10.99	210.9	60	1.8	334.6

and such water may be used for their subsequent recovery. Most arsenic was removed during the initial aeration step. In the second step of the bacterial oxidation, the remaining arsenic concentration also complied with the Regulation No. 269/2010 Coll., for arsenic in discharged wastewater, which is 0.02 mg/L.

Pigments from the first two steps (i, ii) of the formation of iron precipitates were analysed using handheld X-ray fluorescence (XRF) analyser to confirm their elemental composition and to ensure that resulting products do not contain high concentrations of arsenic (or other potentially toxic elements). XRF analysis showed that product A (30-hour aeration) contained high concentrations of arsenic (384 mg/kg). In product B (bacterial oxidation) only minor arsenic traces were detected, 20 mg/kg. This value already complies with the European Commission criteria which claims, that pigments used shall not be based on Cd, Pb, Cr^{6+}, Hg, As, Se, Sb or Co, where the following impurities from any pigments used shall not be present in the final product formulation in quantities exceeding 100 mg/kg (Commission Decission 2025/2607). According to this definition, sample B could already be considered a usable product as a pigment. Remaining iron oxides resulting from the pH adjustment were not examined by XRF method since according to Tab. 2. As was not detected in the source water at sufficiently high concentration.

All samples were characterised using XRD. The obtained patterns of the iron precipitates show mostly broad and low-intensity reflections, indicating that all solids are poorly crystalline. Considering the low pH and high sulfate concentrations of the mine water, samples formed at pH < 4.1 are most consistent with schwertmannite-type Fe(III), oxyhydroxysulfate precipitates. At higher pH (5.5–6.2), the precipitates likely shift toward poorly crystalline ferrihydrite-like Fe oxyhydroxides. No sharp reflections characteristic of well-crystallized hematite or goethite are observed, indicating that the solids are freshly formed and structurally disordered (Fig. 3).

Elemental composition of precipitates was analysed by scanning electron microscopy (SEM) coupled with energy-dispersive X-ray (EDX) detection (Tab. 5).

EDS analysis revealed a transition from Fe-rich oxyhydroxysulfate phases (schwertmannite-like) at low pH (Fig.4) to Al-rich hydroxide phases at higher pH (Fig. 5), confirming a sequential precipitation mechanism controlled by microbial oxidation and pH adjustment.

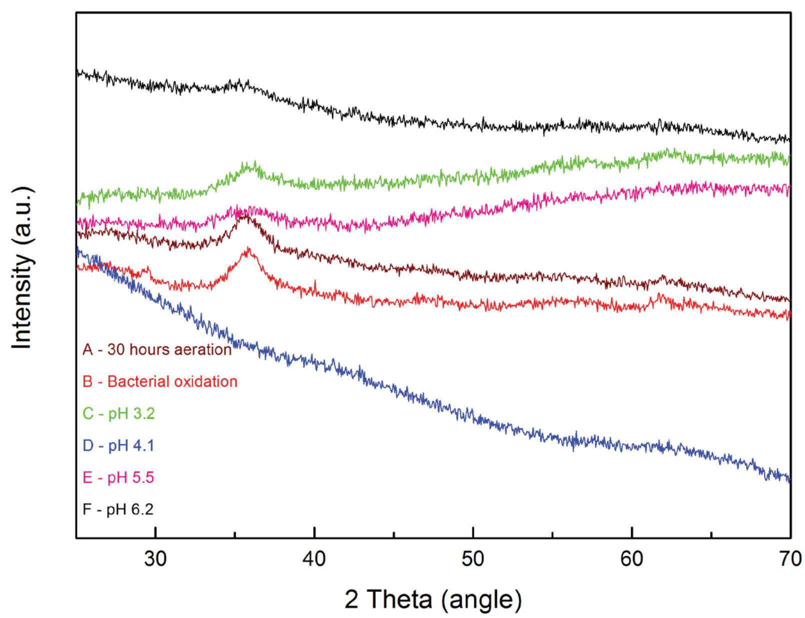

Fig. 3. XRD patterns of precipitates: A, B – without pH adjustment; C, D, E, F – with pH adjustment

Tab. 5
Elemental composition of precipitates according to SEM-EDS analyses (all values are expressed in At %)

Name	Conditions	O	Fe	S	Al	Si	K	Cu	Co	Mg	Mn	Zn	As
–	**30 hours aeration**	75.4	18.9	3.8	1.4	–	–	0.2	0.2	0.1	0.0	–	0.0
A	**Bacterial oxidation**	70.8	23.8	5.0	–	–	–	0.3	0.1	0.0	0.0	–	0.0
B	**pH 3.2**	68.2	20.6	5.2	5.2	–	0.3	0.2	0.1	0.1	0.1	–	0.0
C	**pH 4.1**	69.8	21.5	5.4	2.3	–	0.3	0.1	0.1	0.2	0.2	–	0.0
D	**pH 5.5**	70.0	2.9	3.6	19.0	3.1	0.2	0.6	0.0	0.0	0.3	0.3	0.0
E	**pH 6.2**	72.1	13.9	2.8	8.0	2.2	0.6	0.2	0.0	0.1	0.0	–	0.0

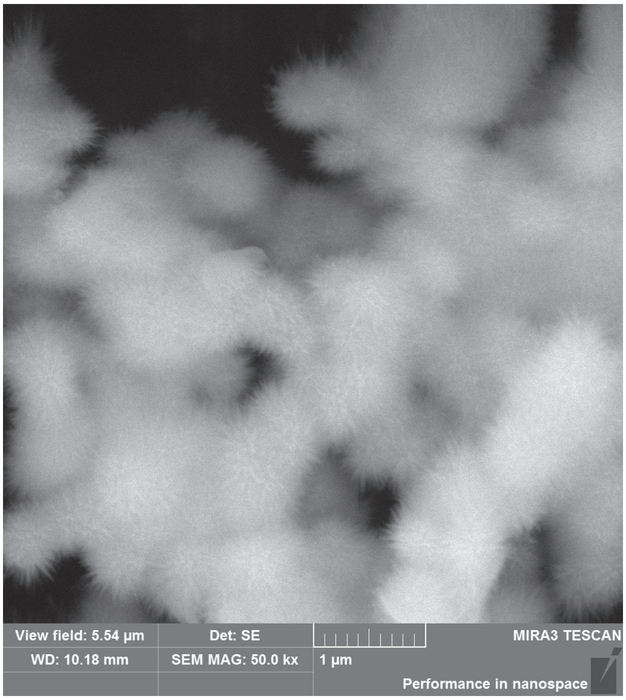

Fig. 4. Morphology of the surface of Fe-rich oxyhydroxysulfate phases (schwertmannite-like) at low pH 2.6 after bacterial iron oxidation

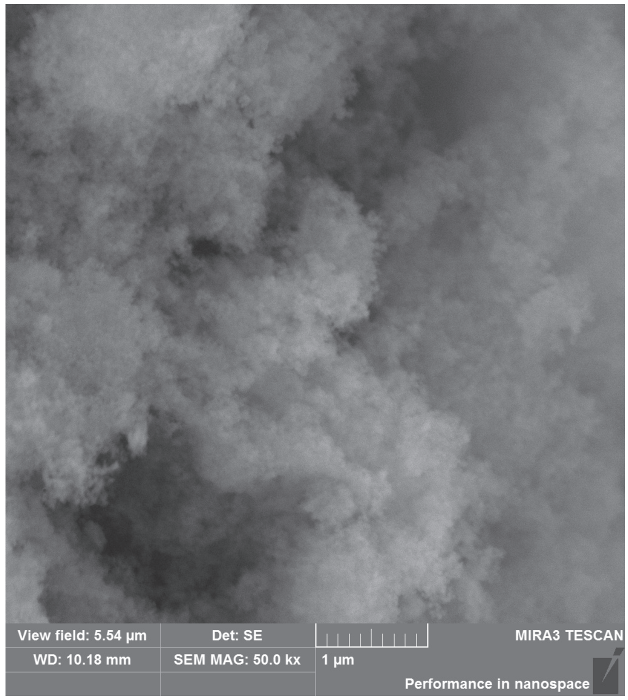

Fig. 5. Morphology of poorly crystalline ferrihydrite-like Fe oxyhydroxides following adjustment to pH 6.2

Tab. 6
Precipitates characterisation according to XRD and SEM-EDS analyses

Name	Conditions	Description
A	**30 hours aeration**	Predominantly amorphous to poorly crystalline Fe-rich sulfate-bearing oxyhydroxide, likely ferrihydrite- to schwertmannite-like, with minor Al-silicate traces.
B	**Bacterial oxidation**	Amorphous to poorly crystalline Fe-rich oxyhydroxide with significant sulfate association (schwertmannite-like) and minor trace metals.
C	**pH 3.2**	Mixed Fe-Al oxyhydroxide phase with minor sulfate and trace metal components; poorly crystalline.
D	**pH 4.1**	Fe-rich oxyhydroxide with notable sulfate association (possibly schwertmannite-like) and minor Al and trace metals; low crystallinity.
E	**pH 5.5**	Al-rich hydroxide/hydroxysulfate phase (basaluminite- or hydrobasaluminite-like) with minor Fe oxyhydroxide and silicates.
F	**pH 6.2**	Al-rich hydroxide/hydroxysulfate phase (basaluminite- or hydrobasaluminite-like) with minor Fe oxyhydroxide and silicate components.

Tab. 7
Colour characterisation of prepared precipitates/pigments

→		CIE L*a*b*	Nix Color
A	30 hours aeration	CIELAB: 32.84, 16.42, 34.09	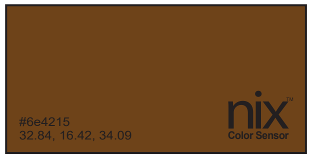
B	bacterial oxidation	CIELAB: 46.63, 18.09, 47.59	
C	pH 3.2	CIELAB: 34.16, 14.59, 26.14	
D	pH 4.1	CIELAB: 14.81, 5.94, 10.97	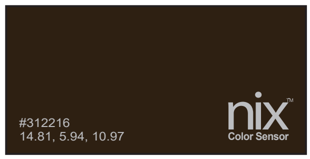
E	pH 5.5	CIELAB: 48.80, 8.82, 26.42	
F	pH 6.2	CIELAB: 18.80, 6.78, 11.48	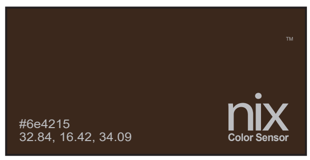

Mineralogical and compositional characteristics of the precipitates obtained under different experimental conditions determined by XRD and SEM-EDS analyses reflect the progressive removal of iron and the increasing influence of aluminium precipitation as pH increases. The presence of sulfate and minor trace elements across several samples suggests their incorporation into poorly crystalline phases, such as ferrihydrite- or schwertmannite-like materials at acidic conditions, and basaluminite-type phases at near-neutral pH. Overall, the observed mineral transformations highlight the strong dependence of precipitate composition and structure on pH and oxidation conditions (Tab. 6).

The colour of iron precipitates is a critical parameter for their potential application as pigments, as it directly influences both their aesthetic appeal and commercial value. Colour variations are strongly governed by mineral phase, degree of crystallinity, particle size, and chemical composition, all of which affect optical properties such as light absorption and scattering (Cornell & Schwertmann, 2003). In addition, impurities and substitutions (e.g., Al, sulfate, or trace metals) can modify hue and stability, affecting pigment performance (Bigham et al., 1990; Schwertmann & Cornell, 2000). To quantitatively evaluate these properties, it is convenient to express colour values in the CIE L*a*b* colour space system, which provides a standardized, device-independent framework based on lightness (L*) and chromatic coordinates (a*, b*). This system correlates well with human visual perception and enables precise comparison between samples, including the calculation of colour differences (ΔE), making it particularly suitable for pigment characterization and quality control (Mclaren, 1976; Robertson, 1977).

To determine colour, Nix™ Spectro 2 Color Sensor was used. The Nix Pro Color Sensor is able to determine the true colour of a soil sample regardless of moisture content, which is based on positive correlations between Nix Pro Color Sensor scans for samples in dry and moist conditions (Stiglitz et al., 2016).

The synthesized iron precipitates exhibited a wide range of colour coordinates in the CIE L*a*b* space (L* = 14.81–48.80, a* = 5.94–18.09, b* = 10.97–47.59), corresponding to dark brown, brown, and yellow- to orange-brown (ochre-like) hues typical of iron-based pigments (Tab. 7). The consistently positive a* and b* values indicate the predominance of red and yellow chromatic components, while variations in L* reflect differences in lightness among the samples. These colour differences can be related to the identified mineral phases and compositions, where Fe-rich oxyhydroxides (ferrihydrite- to schwertmannite-like) tend to produce darker brown to orange-brown hues, while Al-rich hydroxide/hydroxysulfate phases are associated with lighter, more yellowish tones (Cornell & Schwertmann, 2003; Schwertmann & Cornell, 2000). In addition, sulfate incorporation and the presence of trace elements can influence colour intensity and saturation, particularly in poorly crystalline Fe-phases such as schwertmannite (Bigham et al., 1990). From an application perspective, this variability is advantageous, as it enables the production of a range of earth-tone pigments from a single secondary raw material. Such pigments are suitable for use in construction materials, coatings, ceramics, and decorative applications. Overall, these findings demonstrate that mine water can serve not only as a source of iron-rich precipitates but also as a promising feedstock for the sustainable production of inorganic pigments with tunable colour properties.

Conclusions

Despite extensive research on acid mine drainage (AMD) treatment, most studies have focused on iron removal, microbial oxidation, or mineral formation separately. The integration of biological oxidation with controlled precipitation for simultaneous contaminant removal and resource recovery remains limited, particularly in real AMD systems. In addition, the role and performance of native microbial consortia under field-relevant conditions have not been adequately addressed.

This study demonstrates that coupling microbial Fe^{2+} oxidation with staged pH adjustment enables efficient iron removal from authentic mine water while generating iron-rich precipitates with properties suitable for pigment applications. Native acidophilic microorganisms showed high activity under acidic conditions, eliminating the need for intensive chemical inputs and highlighting their practical applicability.

Importantly, the process allows selective iron removal while retaining dissolved metals such as Cu, Co, Mn, and Mg in solution, creating opportunities for their downstream recovery. These metals could be recovered in subsequent treatment steps, such as selective precipitation, adsorption, or solvent extraction, depending on their chemical speciation. The combined treatment and valorization approach enhances both environmental and economic performance.

Overall, this work presents an integrated and sustainable strategy that advances AMD treatment beyond remediation toward resource recovery, supporting the development of circular and value-driven water management solutions. The results are directly applicable to the treatment of mining-influenced waters at the Smolník site and similar AMD-affected localities.

Acknowledgements

This study was funded by the EU NextGenerationEU through the Recovery and Resilience Plan for Slovakia under the projects No. 09I03-03-V04-00697. Authors would like to thank reviewers Alexandra Bekényiová and an anonymous reviewer for their valuable comments.

References

Bártová, Z., 2025: The Smolník Mining Site in Slovakia: its Potential Use for the Production of Mineral Pigments. In: Valente, T., Mühlbauer, R., Ordóñez, A. & Wolkersdorfer, Ch. (eds.): *IMWA 2025 – International Mine Water Association Conference, Braga, Portugal*, 102–106.

Basaran, A. H. & Tuovinen, O. H., 1986: An ultraviolet spectrophotometric method for the determination of pyrite and ferrous ion oxidation by Thiobacillus ferrooxidans. *Applied Microbiology and Biotechnology*, 24, 4, 338–341. https://doi.org/10.1007/BF00257060.

Bigham, J. M., Schwertmann, U., Carlson, L. & Murad, E., 1990: A poorly crystallized oxyhydroxysulfate of iron formed by bacterial oxidation of Fe(II) in acid mine waters. *Geochimica et Cosmochimica Acta*, 54, 10, 2743–2758. https://doi.org/10.1016/0016-7037(90)90009-A.

Cornell, R. M. & Schwertmann, U., 2003: The Iron Oxides: Structure, Properties, Reactions, Occurrences and Uses. *Weinheim, Wiley-VCH*. https://doi.org/10.1002/3527602097.

Commission Decision (EU) 2025/2607 establishing EU Ecolabel criteria. *Brussels, European Commission*. http://data.europa.eu/eli/dec/2025/2607/oj.

Regulation No. 269/2010 Coll. laying down requirements for achieving good water status. Collection of Laws of the Slovak Republic.

Herrera, L., Ruiz, P., Aguillon, J. C. & Fehrmann, A., 1989: A new spectrophotometric method for the determination of ferrous iron in the presence of ferric iron. *Journal of Chemical Technology & Biotechnology*, 44, 3, 171–181. https://doi.org/10.1002/jctb.280440302.

Johnson, D., Kanao, T. & Hedrich, S., 2012: Redox Transformations of Iron at Extremely Low pH: Fundamental and Applied Aspects. *Frontiers in Microbiology*, 3, 96, https://doi.org/10.3389/fmicb.2012.00096.

Johnson, D. B. & Hallberg, K. B., 2005: Acid mine drainage remediation options: a review. *Science of The Total Environment*, 338, 1, 3–14. https://doi.org/10.1016/j.scitotenv.2004.09.002.

Jones, A. M., Griffin, P. J., Collins, R. N. & Waite, T. D., 2014: Ferrous iron oxidation under acidic conditions – The effect of ferric oxide surfaces. *Geochimica et Cosmochimica Acta*, 145, 1 – 12. https://doi.org/10.1016/j.gca.2014.09.020.

Kaksonen, A. H. & Janneck, E., 2024: Biological Iron Removal and Recovery from Water and Wastewater. In: Hedrich, S. & Wiche, O. (ed.): Biological Metal Recovery from Wastewaters. *Springer Nature, Cham*, 31–88. https://doi.org/10.1007/10_2024_255.

Kaksonen, A. H., Morris, C., Rea, S., Li, J., Wylie, J., Usher, K. M., Ginige, M. P., Cheng, K. Y., Hilario, F. & du Plessis, C. A., 2014: Biohydrometallurgical iron oxidation and precipitation: Part I – Effect of pH on process performance. Hydrometallurgy, 147–148, 255–263. https://doi.org/10.1016/j.hydromet.2014.04.016.

Kupka, D., Bártová, Z. & Hagarová, L., 2023: Kinetics study comparing bacterial growth and iron oxidation kinetics over a range of temperatures 5–45 °C. *Hydrometallurgy*, 222, 106181. https://doi.org/10.1016/j.hydromet.2023.106181.

Mclaren, K., 1976: XIII – The Development of the CIE 1976 (L* a* b*) Uniform Colour Space and Colour-difference Formula. *Journal of the Society of Dyers and Colourists*, 92, 9, 338–341. https://doi.org/10.1111/j.1478-4408.1976.tb03301.x.

Morgan, B. & Lahav, O., 2007: The effect of pH on the kinetics of spontaneous Fe(II) oxidation by O_2 in aqueous solution – basic principles and a simple heuristic description. *Chemosphere*, 68, 11, 2080–2084. https://doi.org/10.1016/j.chemosphere.2007.02.015.

Nordstrom, D. K., 2011: Mine Waters: Acidic to Circmneutral. *Elements*, 7, 6, 393–398. https://doi.org/10.2113/gselements.7.6.393.

Robertson, A. R., 1977: The CIE 1976 Color-Difference Formulae. *Color Research & Application*, 2, 1, 7–11. https://doi.org/10.1002/j.1520-6378.1977.tb00104.x.

Schwertmann, U. & Cornell, R. M., 2000: Iron Oxides in the Laboratory: Preparation and Characterization. *Wiley-VCH, Weinheim*. https://doi.org/10.1002/9783527613229.

Singer, P. C. & Stumm, W., 1970: Acidic Mine Drainage: The Rate-Determining Step. *Science*, 167, 3921, 1121–1123. https://doi.org/10.1126/science.167.3921.1121.

Stiglitz, R., Mikhailova, E., Post, C., Schlautman, M. & Sharp, J., 2016: Evaluation of an inexpensive sensor to measure soil color. *Computers and Electronics in Agriculture*, 121, 141–148. https://doi.org/10.1016/j.compag.2015.11.014.

Stumm, W. & Morgan, J. J., 1996: Aquatic Chemistry: Chemical Equilibria and Rates in Natural Waters. 3rd ed. *New York, John Wiley*, 1040 pp.

Wolkersdorfer, C., 2022: Mine Water Treatment – Active and Passive Methods. *Berlin – Heidelberg, Springer*, 328 pp. https://doi.org/10.1007/978-3-662-65770-6.

Biologické odstránenie železa a súčasné získavanie pigmentov z kyslých banských vôd s využitím prirodzene sa vyskytujúcich mikrobiálnych spoločenstiev

Táto práca sa zaoberá biologickým odstraňovaním a súčasným získavaním železa z reálnej banskej vody (*mining influenced water*, MIW) z lokality Smolník. Vzhľadom na vysokú koncentráciu železa a prítomnosť sprievodných prvkov predstavuje takáto voda environmentálny problém, ale zároveň potenciálny zdroj sekundárnych surovín. Cieľom práce bolo optimalizovať proces oxidácie Fe^{2+} pomocou natívnych acidofilných mikroorganizmov a charakterizovať vzniknuté zrazeniny z hľadiska ich potenciálneho využitia ako minerálnych pigmentov.

Proces odstránenia železa a jeho následné získavanie vo forme pigmentov pozostával z troch hlavných krokov: (i) počiatočnej aerácie banskej vody, (ii) biologickej oxidácie železa pomocou natívnych mikrobiálnych konzorcií izolovaných priamo z lokality Smolník a (iii) postupnej úpravy pH s cieľom tvorby pevných fáz. Výsledky ukázali, že biologická oxidácia Fe^{2+} výrazne urýchľuje proces oxidácie železa aj pri nízkych hodnotách pH, pričom účinnosť odstránenia železa presiahla 99 % v priebehu 30 hodín.

Mineralogická charakterizácia (XRD) a chemická analýza (SEM-EDS, XRF) preukázali, že pri nižších hodnotách pH vznikajú prevažne slabo kryštalické Fe-oxyhydroxysulfátové fázy typu schwertmannit, zatiaľ čo pri vyšších hodnotách pH sa tvorí ferrihydrit a hydroxidové fázy bohaté na Al. Výsledky potvrdzujú, že zloženie a štruktúra precipitátov sú silne závislé od pH a oxidačných podmienok.

Z hľadiska chemického zloženia sa preukázalo, že väčšina železa je odstránená už počas biologickej oxidácie, zatiaľ čo ďalšie prvky ako Cu, Co, Mn a Mg zostávajú v roztoku. To vytvára predpoklady na ich následné získanie. Arzén bol účinne odstránený už v počiatočnej fáze aerácie a jeho koncentrácia v produktoch spĺňala legislatívne limity na využitie pigmentov.

Farebná charakterizácia (CIELab*) ukázala, že pripravené materiály vykazujú široké spektrum odtieňov od tmavohnedej po žltooranžovú, typických pre železité pigmenty. Tieto vlastnosti spolu s ich chemickým zložením naznačujú možnosť ich využitia v stavebných materiáloch, farbách alebo keramike.

Výsledky práce ukazujú, že kombinácia biologickej oxidácie železa a riadenej úpravy pH predstavuje efektívny a prakticky aplikovateľný spôsob úpravy banských vôd. Zároveň umožňuje nielen odstránenie kontaminantov, ale aj získanie hodnotných produktov. Tým prispieva k efektívnejšiemu využívaniu zdrojov v oblastiach ovplyvnených banskou činnosťou.

Doručené / Received: 4. 5. 2026
Prijaté na publikovanie / Accepted: 15. 7. 2026

Inštrukcie autorom

www.geology.sk/mineralia položka *Inštrukcie autorom*

1. Manuskripty sa do redakcie zasielajú e-mailom (editovateľné súbory formátu .doc, .docx alebo .odt a verzia v PDF formáte) na adresu vedeckého redaktora alebo mineralia.slovaca@geology.sk.
2. **Súčasne s manuskriptom je potrebné redakcii poslať autorské vyhlásenie o originalite textu a obrázkov. Kópie obrázkov z iných publikácií musia byť legalizované získaním práva na publikovanie. Vyhlásenie musí obsahovať meno autora (autorov), akademický titul** a tr**valé bydlisko.** Články sú uverejnené pod licenciou *Creative Commons Attribution (CC BY)*. Autori článkov majú možnosť požiadať aj o iný typ licencie *Creative Commons*.
3. Rozsah manuskriptu na publikovanie je štandardne do 40 rukopisných strán (font Times New Roman, veľkosť písmen 12 bodov, riadkovanie 1,5) vrátane literatúry, obrázkov, popisov obrázkov a tabuliek. V prípade veľkého odborného prínosu sú v ojedinelých prípadoch povolené aj dlhšie články. Rozsiahlejšie doplňujúce materiály v prípade potreby je možné publikovať ako prílohu online.
4. Články sú publikované v angličtine, výnimočne aj v slovenčine. Články písané v angličtine musia obsahovať slovenské resumé. Články v slovenčine musia obsahovať anglický preklad názvu, abstraktu, kľúčových slov, resumé a popisov k obrázkom a tabuľkám.

Text

Úprava textu aj zoznamu literatúry musí korešpondovať so súčasnou úpravou článkov v časopise. Predkladaný manuskript musí spĺňať tieto požiadavky:

1. Text manuskriptu musí mať priebežne číslované riadky.
2. Na začiatku manuskriptu je uvedený názov, ktorý by mal byť stručný a informatívny.
3. Meno a priezvisko autora alebo autorov musí byť uvedené spolu s názvom pracoviska a adresou (mesto, krajina). Korešpondujúci autor musí byť riadne označený a musí byť uvedená jeho e-mailová adresa. Ak je k dispozícii aj ORCID autorov, treba ho uvádzať.
4. Abstrakt stručne sumarizuje článok. Môže mať najviac 200 slov a nemá obsahovať citácie. Počet kľúčových slov je maximálne 6.
5. Text má takéto členenie: úvod, charakteristika (stav) skúmaného problému vrátane prehľadu dôležitých starších výskumov, použitá metodika, nové zistenia (výsledky), ich interpretácia, diskusia, záver, poďakovanie, zoznam literatúry a resumé v slovenskom, resp. anglickom jazyku (pri článku v slovenčine). Východiskové údaje musia byť zreteľne odlíšené od interpretácií. V texte musia byť odvolávky na všetky použité obrázky a tabuľky.
6. V texte je možné použiť maximálne 3 hierarchické úrovne podnadpisov.
7. V texte sa uprednostňuje citácia v zátvorke, napr. (Dubčák, 1987; Hrubý et al., 1988), pred formou napr. podľa Dubčáka (1987).
8. Manuskript odporúčame zasielať s obrázkami vloženými v texte alebo na konci manuskriptu.
9. V texte treba prednostne používať platné jednotky SI, napr. s (sekunda, nie sec), m (meter), kg (kilogram). V oprávnených prípadoch možno použiť aj iné miery zaužívané v odbornej literatúre a v zátvorke uviesť ich ekvivalent v jednotkách SI, napr. 3 kbar (300 MPa, resp. 0,3 GPa), 30 kt, resp. 30 000 t (3,107 kg), 800 K (527 °C), 4,26 Å (4,26 . 10^{-10} m).
10. V texte sa môžu používať len názvy minerálov oficiálne schválené Komisiou pre nové minerály a nomenklatúra schválená Medzinárodnou mineralogickou asociáciou (CNMNC IMA). Ich zoznam (inovovaný každé dva mesiace) je prístupný na stránke https://cnmnc.units.it/ (*IMA-CNMNC List of Mineral Names*). Rovnako sa môžu používať len odporúčané skratky minerálov (*Updated list of IMA-CNMNC mineral symbols*). Pokiaľ autori disponujú chemickou analýzou minerálu, treba napísať jeho celý platný názov, napr. fluórapatit (nie apatit), monazit-(Ce) (nie monazit). Neúplné názvy minerálov (napr. apatit, monazit) možno použiť pri petrografickom opise hornín alebo názve metódy (napr. monazitové datovanie). Použitie názvov izomorfných sérií minerálov zaužívaných v geologickej literatúre (napr. biotit, zinnwaldit, olivín) alebo skupinových názvov minerálov (napr. granáty, turmalíny, amfiboly, spinely) je akceptované. V prípade nejasností sa autori môžu písomne obrátiť na redakčnú radu.

Obrázky, ilustrácie a tabuľky

1. Ilustrácie a tabuľky vysokej kvality bývajú publikované buď **na šírku stĺpca** (81 mm)**, alebo strany (170 mm)**. Optimálna veľkosť písma a čísiel v publikovaných obrázkoch je 2 mm. Články v angličtine majú všetky texty v angličtine. Články v slovenčine musia mať popisy v obrázkoch a tabuľkách v slovenčine, záhlavie tabuliek a texty pod obrázkami a tabuľkami sú v slovenčine a angličtine. **Maximálny rozmer ilustrácie a tabuľky vytlačený v časopise je 170 x 230 mm**. Väčšie (skladané) ilustrácie sú publikované len v ojedinelých prípadoch.
2. Ilustrácie vrátane fotografií musia obsahovať **grafickú mierku** v centimetrovej či metrovej škále, prípadne sa rozmer zobrazených objektov vyjadrí v popise obrázka. Mapy a profily musia mať aj **azimutálnu orientáciu** a jednotné vysvetlivky, ktoré sa uvedú pri prvom obrázku. Zoskupené obrázky, napr. fotografie a diagramy, sa uvádzajú ako jeden obrázok s jednotlivými časťami označenými písmenami (a, b, c atď.).
3. **Ilustrácie, mapy a fotografie je nutné uložiť vo formátoch JPG, PNG alebo TIF v rozlíšení minimálne 600 dpi, vektorovú grafiku vo formátoch EPS, PDF, AI alebo COR.**

Redakcia si vyhradzuje právo vrátiť autorovi grafické prílohy na opravu po jazykovej úprave, resp. požiadať o ich nahradenie za prílohy v požadovanej kvalite.

Literatúra

Zoznam použitej literatúry musí obsahovať iba publikované alebo akceptované práce. Pri jednom autorovi sú práce v zozname zoradené abecedne podľa priezviska autora každého diela. Pri dvoch autoroch sa práce uvádzajú abecedne najprv podľa priezviska prvého autora, potom podľa priezviska spoluautora a potom chronologicky. Pri viac ako dvoch autoroch sa práce zoradia abecedne iba podľa priezviska prvého autora, potom chronologicky. Ak má publikácia DOI, vždy sa uvádza za číslom citovaných strán vo forme https://doi.org/číslo.

Spôsob uvádzania literatúry v zozname literatúry:

Knižná publikácia: Gazda, L. & Čech, M., 1988: Paleozoikum medzevského príkrovu. Bratislava, Alfa, 155 s.

Časopis: Hók, J. & Olšavský, M., 2023: Vernaricum – regional distribution, lithostratigraphy, tectonics and paleogeography. Mineralia Slovaca, 55, 1, 3 – 12. https://doi.org/10.56623/ms.2023.55.1.1.

Zborník: Návesný, D., 1987: Vysokodraselné ryolity. In: Romanov, V. (ed.): Stratiformné ložiská gemerika. Špec. publ. Košice, Slovenská geologická spoločnosť, 203 – 215.

Manuskript: Tulis, J. & Novotný, L., 1998: Zhodnotenie geologických prác na U rudy v mladšom paleozoiku hronika v severnej časti Nízkych Tatier a Kozích chrbtov. Manuskript. Bratislava, archív Štátny geologický ústav Dionýza Štúra (arch. č. 82752), 144 s.

Instructions to authors

www.geology.sk/mineralia item *Instructions to authors*

1. The manuscripts must be sent to Editorial Office by e-mail (editable files in .doc, .docx or .odt format, plus complete preview version in PDF format) to the Scientific Editor or mineralia.slovaca@geology.sk.
2. **Simultaneously with the manuscript the Editorial Office must receive the author´s proclamation that no part of the manuscript was already published and figures and tables are original as well. Copied illustrations from other publications must contain a copyright.** The articles are published under a Creative Commons Attribution (CC BY) license. Authors have the option to apply for other types of Creative Commons licenses.
3. The extent of the manuscript for publishing is limited to 40 manuscript pages (12 points Times New Roman font, line spacing 1.5) including figures, tables, explanations and references. In the case of contribution with a high scientific value, the longer manuscripts for publishing are exceptionally permitted. More extensive supplementary material can be published as an online annex if required.
4. Articles are published in English (preferably) or Slovak languages. The title, abstract, key words, shortened text (summary), as well as description to figures and tables in Slovak articles are published also in English. Articles published in English contain Slovak resumé.

Text

The format of the text and the reference list must correspond to the current format of the papers in the journal. The submitted manuscript must meet the following requirements:

1. The text of the manuscript must have continuously numbered lines.
2. The title at the beginning of the manuscript should be brief and informative.
3. The name and surname of the author(s) must be given together with affiliation(s) to the institutions and the address (city, country). The corresponding author must be properly marked and his/her e-mail address must be given. If the ORCID of the authors is also available, it should be provided.
4. Abstract briefly summarizing the manuscript is limited to 200 words, no references are allowed. The maximum number of key words is 6.
5. The text must be structured as follows: the introduction, characterization (state) of investigated problem, applied methodology, obtained new findings (results), interpretation, discussion, conclusion, acknowledgements and references. The obtained data must be distinctly separated from interpretations. All applied figures and tables must be referred in the text.
6. A maximum of 3 hierarchical levels of headings may be used in the text.
7. In the case of references in the text the parentheses are preferred, e.g. (Dubčák, 1987; Hrubý et al., 1988). The form “according to Dubčák (1987)” should be used only exceptionally.
8. We recommend submitting the manuscript with figures inserted in the text or at the end of the manuscript.
9. Valid SI units ought to be used in the text, preferably, e.g. s (second, not sec), m (metre), kg (kilogram). Where justified, other units used in the literature may be used and their equivalent in SI units may be given in brackets, e.g. 3 kbar (300 MPa or 0.3 GPa), 30 kt or 30 000 t (3.10^{7} kg), 800 K (527 °C), 4.26 Å (4.26 . 10^{-10} m).
10. Only mineral names officially approved by the Commission for New Minerals and nomenclature approved by the International Mineralogical Association (CNMNC IMA) may be used in the text. A list of these (updated every two months) is available at https://cnmnc.units.it/ (IMA-CNMNC List of Mineral Names). Also, only recommended mineral abbreviations may be used (Updated list of IMA-CNMNC mineral symbols). If the authors have a chemical analysis of the mineral, its full valid name should be written, e.g. fluorapatite (not apatite), monazite-(Ce) (not monazite). Incomplete mineral names (e.g. apatite, monazite) may be used in the petrographic description of the rocks or the name of the method (e.g. monazite dating). The use of isomorphic mineral series names established in the geological literature (e.g. biotite, zinnwaldite, olivine) or mineral group names (e.g. garnets, tourmalines, amphiboles, spinels) is accepted. It is recommended to contact the Editorial Board in unclear cases.

Figures and tables

1. The high-quality figures and tables can be published either in **maximum width of column (81 mm) or page (170 mm)**. The optimum size of letters and numbers in the printed figure is 2 mm. Manuscripts published in Slovak contain the Slovak descriptions in figures and tables, the tables headings and descriptions beneath figures and tables are in Slovak and English. English manuscripts contain all texts in English. **Maximum dimension of figures and tables in the journal is 170 x 230 mm. Larger (folded)** illustrations are published only exceptionally.
2. Illustrations including photographs must contain graphic (metric) scale, eventually the dimensions of visualized objects have to be stated in the describing text to figure. Maps and profiles must contain also the azimuth orientation; their unified explanations are stated at the first figure. Grouped figures, e.g. photographs and diagrams, are compiled as one figure with separate parts designated by letters (a, b, c, etc.).
3. **Illustrations, maps and photographs must be saved in JPG, PNG or TIFF formats with a resolution of at least 600 dpi, vector graphics in EPS, PDF, AI or COR formats.**

The editors reserve the right to return illustrations to the author for correction after language editing, or to request their replacement with illustrations of the required quality.

References

The list of references used must include only published or accepted works. Single-authored works are listed alphabetically by the surname of the author of each work. For two authors, the works are listed alphabetically first by the surname of the first author, then by the surname of the co-author, and then chronologically. For more than two authors, the works are listed alphabetically only by the surname of the first author, then chronologically. If a publication has a DOI, it is always listed after the citation page number in the form https://doi.org/number.

References examples:

Book: Gazda, L. & Čech, M., 1988: Paleozoikum medzevského príkrovu [Paleozoic of the Medzev nappe]. Bratislava, Alfa, 155 pp.

Journal: Hók, J. & Olšavský, M., 2023: Vernaricum – regional distribution, lithostratigraphy, tectonics and paleogeography. Mineralia Slovaca, 55, 1, 3 – 12. https://doi.org/10.56623/ms.2023.55.1.1.

Proceedings contribution: Návesný, D., 1987: Vysokodraselné ryolity. In: Romanov, V. (ed.): Stratiformné ložiská gemerika [High-potassium rhyolites. In: Romanov, V. (ed.): Stratiform deposits of Gemericum]. Spec. publ. Košice, Slov. geol. soc., 203 – 215.

Manuscript: Tulis, J. & Novotný, L., 1998: Zhodnotenie geologických prác na U rudy v mladšom paleozoiku hronika v severnej časti Nízkych Tatier a Kozích chrbtov. [Assessment of geological works on U ore in the Late Paleozoic of Hronicum in the northern part of the Nízke Tatry and Kozie chrbty Mts.] Manuscript. Bratislava, Archive of State Geological Institute of Dionýz Štúr (arch. no. 82752), 144 pp. (in Slovak).

Ďalšie informácie / Further information: mineralia.slovaca@geology.sk**;** ondrej.pelech@geology.sk

Indexed / Abstracted / Accessed by SCOPUS, WEB OF SCIENCE and EBSCO
Indexované / abstraktované / sprístupňované databázami SCOPUS, WEB OF SCIENCE a EBSCO

www.geology.sk/mineralia